STUDY THE EFFECTS OF CORE ORIENTATION AND DIFFERENT FACE THICKNESSES ON MECHANICAL BEHAVIOR OF HONEYCOMB SANDWICH STRUCTURES UNDER THREE POINT BENDING

A Thesis Presented to

The Faculty of California Polytechnic State University

San Luis Obispo

In Partial Fulfillment

Of the Requirements for the Degree of

Masters of Science in Aerospace Engineering

By

Joshua M. Lister

February 2014

COMMITTEE MEMBERSHIP

TITLE:	Study the Effect of Core Orientation and Different Face Thicknesses on Mechanical Behavior of Honeycomb Sandwich Structures Under Three Point Bending
AUTHOR:	Joshua Martyn Lister
DATE SUBMITTED:	February 2013

COMMITTEE CHAIR:	Faysal Kolkailah, PhD Professor of Aerospace Engineering
COMMITTEE MEMBER:	Eltahry Elghandour, PhD Professor of Aerospace Engineering
COMMITTEE MEMBER:	Eric Mehiel, PhD Associate Professor of Aerospace Engineering
COMMITTEE MEMBER:	Andrew Davol, PhD Professor of Mechanical Engineering

ABSTRACT

Study the Effect of Core Orientation and Different Face Thicknesses on Mechanical Behavior of Honeycomb Sandwich Structures Under Three Point Bending

Joshua M. Lister[1]
California Polytechnic State University, San Luis Obispo, CA, 93407

This study will present the Experimental, numerical and analytical characterizations of composite sandwich structures needed to optimize structure design. In this study, the effects of varying honeycomb core ribbon orientation and varying face sheet thickness's have on the flexural behavior of honeycomb sandwich structures was investigated. Honeycomb sandwich panels were constructed using Hexcel 6367 A250-5H carbon fiber face sheets and Hexcel Nomex HRH-10-1/8-5 honeycomb cores. The mechanical properties of the constituent materials were discovered experimentally using ASTM standards and theoretical models using honeycomb mechanics and classical beam and plate theory are described. A failure mode map for loading under three point bending is developed from previous works by Triantafillou and Gibson[26], showing the dependence of failure mode on face sheet to core thickness and honeycomb core ribbon orientation. Beam specimens are tested with the effects of Honeycomb core ribbon orientation and unequal face sheet thickness's examined. Experimental data sufficiently agrees with theoretical predictions. A finite element model was developed in ABAQUS/CAE to validate experimental and analytical analysis and produced agreeable results. Optimal bending stiffness and strength with respect to minimum weight was analyzed. The results reveal an important role core ribbon orientation has in a sandwich beam's bending behavior, and design of unequal ply count face sheets can produce higher stiffness to weight ratios than conventional symmetric sandwich structures of similar weight when subjected to a single static load.

ACKNOWLEDGMENTS

I would like to thank my advisor Dr. Kolkailah and co-advisors Dr. Elghandour, Dr. Mehiel and Dr. Davol for their help and guidance through this project, which was greatly appreciated. A special thank you goes out to Dr. Elghandour for his endurance with helping me in the experimental testing. Also a great thank you to my two good friends and co-workers Jeff Carter and Justin Tafoya on their help and friendship throughout this thesis. I wouldn't have been able to complete this project without them. To my parents for their guidance, love and support throughout this long college career, I know it's been tough, but we are finally through. I'd also like to thank Hexcel inc. for donating the carbon fiber and Nomex honeycomb used in this thesis.

TABLE OF CONTENTS

LIST OF TABLES

Over 50% composite commercial plane - Boeing's 787 Dreamliner. 20

LIST OF FIGURES

LIST OF MATLAB CODE

Nomenclature

A = *area (in^2)*
ASTM = *American Society for Testing and Materials*
b = *specimen width (in)*
D = *flexural rigidity (lb*in^2)*
d = *depth (in)*
E = *elastic modulus (psi)*
h = *specimen height (in)*
I = *moment of inertia (in^4)*
L = *specimen length (in)*
m = *mass (lbf)*
m = *slope*
P = *load (lbf)*
R = *load rate (lbf/min)*
t = *thickness (in)*
V = *volume fraction*
W1 = *weight of specimen (lb)*
W2 = *weight of residue (lb)*
Δ = *change in given variable*
δ = *homogenous beam deflection (in)*
ϵ = *strain*
ν = *Poisson's ratio*
ρ = *density (lbm/in^3)*
σ = *normal stress (psi)*

Subscripts

C = *Compression*
hc = *HoneycombCore*
fibers = *relating to the fibers*
fs = *face sheets*
L = *Longitudinal*
Matrix = *relating to the matrix*
Max = *maximum*
Min = *minimum*
T = *Transverse*
Y = *y-direction*
X = *x-direction*

1.0 Introduction

1.1 Introduction to Composites

Composites have been integrated into just about every field of today's engineering world. As technology advances, so too has the demand for lighter materials with an increase in performance capabilities. Composites have come a long way from mud and straw used by our ancestors to the integration into advanced systems including the aerospace and sporting industries shown in Figure 1.1.

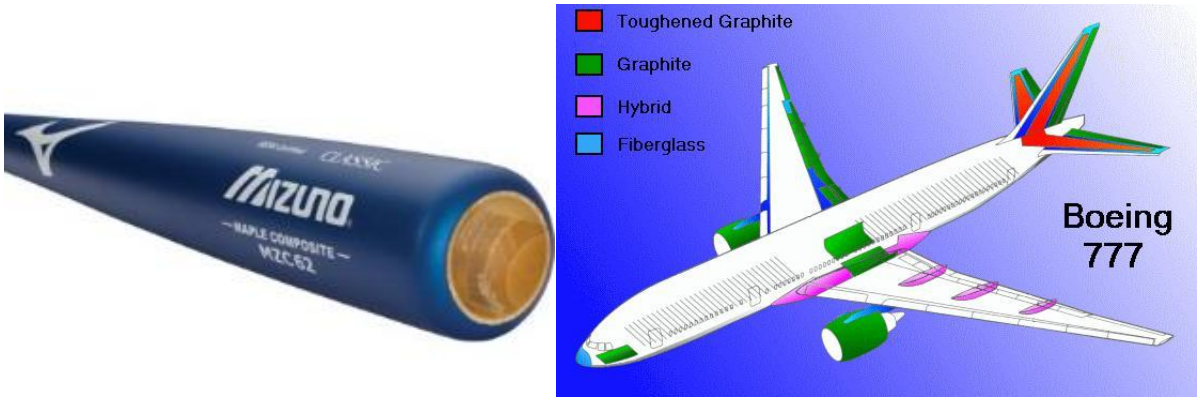

Figure 1.1. Composite Baseball bat (left) and Boeing 777 (right) are examples of recent technology using various composites[1]

A composite material consists of two or more materials, with an interface between them. The composite consists of strong fibrous materials surrounded by a weaker matrix material, which distributes the load to the fibers. Principal fiber materials include but not limited to, aramid or Kevlar (very light), glass, Carbon or Boron (high strength), and Silicon carbide (high temperature resistance). Most matrix materials include but are not limited to; Polymeric matrix's (thermoplastic and thermoset resins), Mineral matrix's (silicon carbide, carbon), and metallic matrix's (aluminum alloys, titanium alloys, and orientated eutectics).[2]

Composites are used because of their structural properties and their electrical, thermal, and environmental applications. Creating a composite does not increase all mechanical properties of its

[1] Graduate, Aerospace Engineering, 1 Grand Avenue San Luis Obispo, California 93407

constituent materials; however, a composite can be optimized to meet the property needs of an application. Composites emphasize those materials that contain a continuous matrix that binds together with an array of stronger reinforcing material. The integration of the two result in structural properties that are superior to its' make up materials. The improved structural properties generally result from a load-sharing mechanism. Composites typically have a fiber that is stiff and strong whilst the matrix is more ductile. Many types of reinforcements also often have good thermal and electrical conductivity with a coefficient of thermal expansion (CTE) that is less than the matrix, and/or has good wear resistance. Composites allow for a weight reduction of 10-50% with equal or greater performance with a 10-20% decrease in material and manufacturing cost when compared with the same piece of the conventional metal material previously used. In an aircraft the saving in mass of using composites in turn leads to reduced fuel mass which results in increased payload mass or performance. Also composites have a good fatigue and corrosion resistance which leads to long term savings and a reduction in maintenance costs of the part.[2] When the requirements for the application have been determined, the engineer can then decide on material choice, fiber and matrix combination, number of laminates and direction, and layup/curing technique needed to produce a composite that meets all design requirements.

1.2 Types of Composites

There are three types of composite materials: fibrous, laminated and particulate composites. Fibrous composites contain fibers that are held together by a matrix shown in Figure 1.2. Laminated composites consist of two or more layers of a material that are bonded together. Particulate composites are made up of fibrous particles with a matrix such as concrete or a cake.

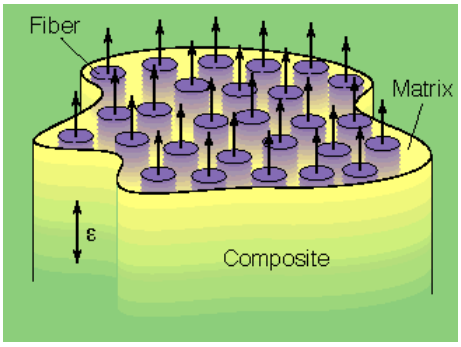

Figure 1.2. Fibrous Composite[3]

Laminated composites are created by layering different materials to create a new macroscopic structure that combines different aspects of the constituent materials. Laminated composites can be broken up into 5 categories: laminated fibrous composites, plastic based laminates, clad metals, laminated glass and bimetals. Bimetals, shown in Figure 1.3, are made up of two materials with different thermal expansion coefficients. When a significant temperature change is induced on the bimetal; the

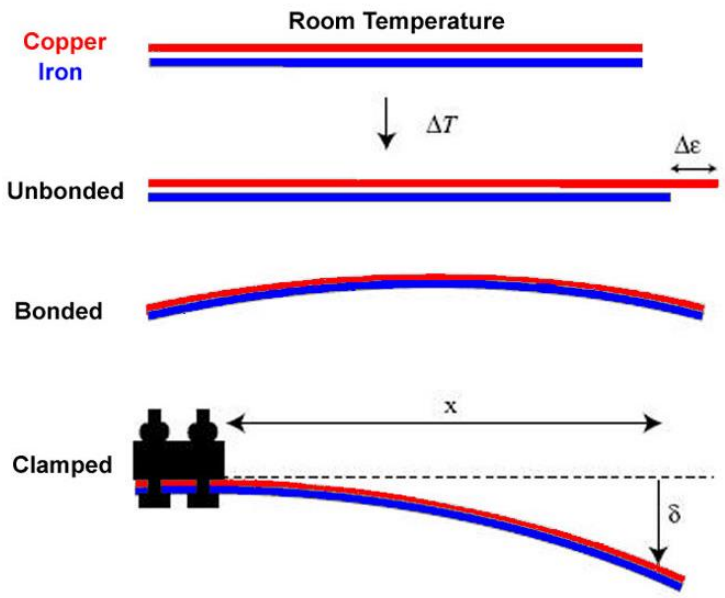

Figure 1.3. Bimetal Interaction[4]

change results in a deflection of the bimetal due to each metal expanding or retracting at different rates.

Clad metal composites is the bonding together of dissimilar metals to obtain the properties of the constitutent metals. An example is galvanizing metal parts to obtain non-corrosive qualities. Laminated glass can tolerate higher strains than traditional glass and often have scratch resistive qualities. An example of laminated glass is saftey glass.

Plastic based laminates are layers of different materials that are saturated with other materials and then treated for many purposes. An example of a plastic based laminate is Arborite, which consists

of layers of phenolic resin impregnated paper overlaid by plastic saturated sheets, which is then overlaid with a plastic cellulose mat. The layers are then fused together with heat and pressure.[5]

Laminated fibrous composites are a mixture of laminated composites and fibrous composites. Each layer is composed of fibers and a matrix and then stacked or laminated with other layers in varied orientations so that the whole composite will have more or less stiffness in the required loading direction shown in Figure 1.4. This category is widely used in industry to meet specific design requirements.

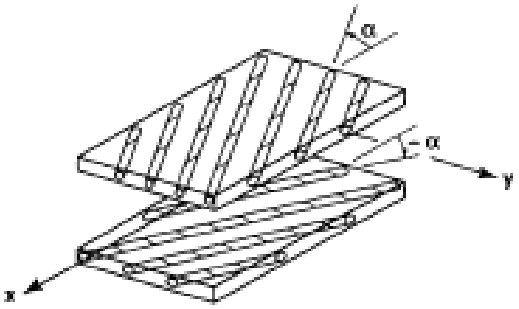

Figure 1.4. Laminated Fibrous composites[6]

The idea behind fibrous composites is fairly simple; a matrix that supports protects and distributes the load evenly to the fibers. The bonded materials produce improved mechanical properties over the properties of the materials by themselves. The key to the improved strength of the composite is because of the orientation and geometry of the fibers. By optimizing the fibers direction and by aligning the fibers with the load direction, the composite will be lighter whilst maintaining the needed strength. The matrix binds the fibers, giving protection from damage and corrosion whilst distributing the load between the fibers. The matrix often puts limitations on the composite, such as operational temperature ranges. Often polymers and plastics are used as composite matrices due to easy production, low cost, high availability, low specific gravity and high chemical resistance. The

disadvantages of polymer matrices are that they have low moduli, strength and operational temperature ranges. Other materials can be used for matrices, including metal that provide higher moduli larger operable temperature ranges and high impact strength, but with higher density, subject to corrosion and higher fabrication cost.[7]

Fibrous composites have been used for applications in aircraft from the first flight of the Wright Brothers' Flyer I, in North Carolina on December 17, 1903, to the many applications now used in military and civil aircraft, satellites, launch vehicles and even automobiles and sports equipment. In the early days, aircraft structure was primarily composites made of wood, wire and fabric. It wasn't until the 1930's that aluminum alloys became the predominant aircraft structure material, although wooden structures were still used until World War II. Recent military and civil aircraft have worked on replacing the secondary structure with fibrous composites made up of carbon, Kevlar, glass or a hybrid of the three. The reason behind the influx of fibrous composites in manufacturing of parts is due to their high specific stiffness and strength, as well as the ability to shape and manufacture the composite to produce a greater aerodynamic structure than its metal counterpart.[8]

Particulate composites tend to be much weaker and less stiff than continuous fibrous composites, but that is countered by the decrease in manufacturing and material costs. Particulate composites usually contain less reinforcement due to processing difficulties and brittleness. An example of particulate composites is asphalt or concrete. The stones and small pebbles act as the particulate and the cement acts as the matrix. This study does not involve particulate composites and thus will not be talked upon further.

1.3 Methods of Composite Fabrication

In creating polymeric composites, there are currently four different types of layups that are most commonly used in industry. The most favored method is known as "Pre-preg" layup, which is a composite that has had the resin pre-impregnated into the composite when it is initially created. The

advantages include a consistent fiber-to-resin ratio, which allows for the strongest part by layer possible when cured. Disadvantages of pre-preg include high material costs, very specific curing cycles, expensive machines for curing (Autoclaves or heat presses), and storage at temperatures for the pre-preg close to 0°F to insure the epoxy resin does not cure.[10]

The second method is known as the "wet-layup" as seen in Figure 1.5, which involves taking dry fibers and ingraining resin by hand, before curing. Advantages include low cost, simple process, no

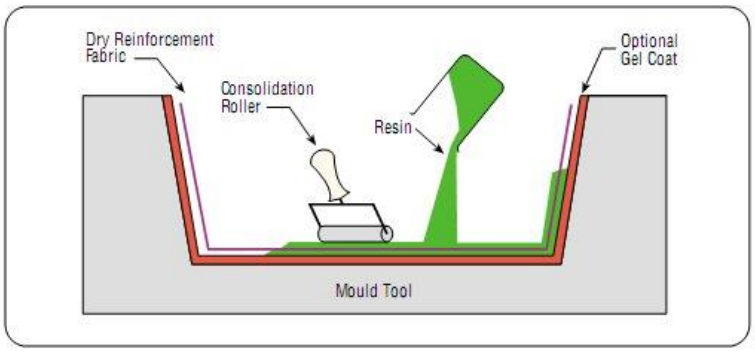

Figure 1.5. Wet Lay-up Method[9]

machines needed for curing, no stringent curing cycles. Disadvantages include inconsistencies in fiber-to-resin ration, and damage to fibers can occur during resin integration.[10]

The third method is known as resin infusion or vacuum assisted transfer-molding system (VARTM), shown in Figure 1.6. This method uses a vacuum to pull resin across a composite part, whilst

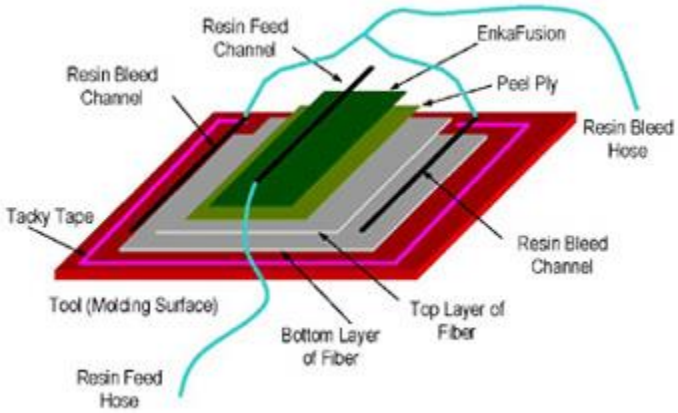

Figure 1.6. Vacuum Resin Infusion Lay-up Method[11]

also infusing the fibers with the resin. Advantages include a balance between quality and cost, potentially minimal damage to fibers due to any handling of the fibers, and fairly consistent fiber-to-resin ratio. Disadvantages include limited working time reliant on resin setting rate and limited part size due to resin being sucked across part by vacuum. Big parts tend to prove troublesome with fiber-to resin ratio inconsistencies. This method is a happy medium between wet-layup and pre-preg; it's quick, not as costly as pre-preg and better fiber-to-resin ratios as wet-layup.[10]

The last main method is known as filament winding, where, as shown in Figure 1.7, fibers and resin are tension-wound together over a mold or mandrel and, after curing, the mold or mandrel is removed. This process is usually used for composite tubing, is relatively new and has had many improvements since its inception.

As the integration of composite materials, specifically in military aircraft, increased from the 1960's onward, improvements in fibers and matrix materials resulted in carbon fiber reinforced plastics (CFRP) composites. With improved mechanical properties, CFRP's replaced the more conventional

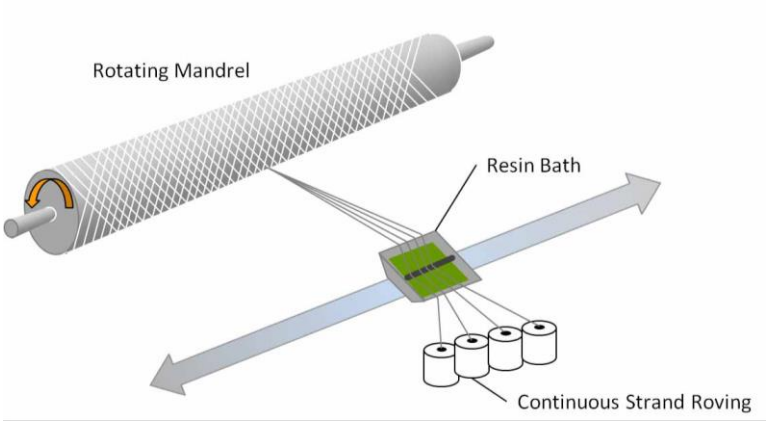

Figure 1.7. Filament Winding Method[12]

titanium alloys and aluminum for primary aircraft structures. The main advantages of CFRP include complex shape manufacture, improved fatigue life, design optimization, reduction in excess material, significant part mass reduction and improved corrosion resistance. The disadvantages include high material and processing costs, susceptibility to impact damage[13], more advanced repairs and

inspections, and size effects on strength. Innovation is paramount in making composites as affordable as, or as close to the affordability of, the conventional material counterparts.

1.4 Composite Sandwich Panels

In the aircraft industry every extra kilogram of structural mass taken off, means an increase in payload mass as well as a decrease in fuel mass, which trickles down to an increase in profit. Thus honeycomb sandwich panels were one of the outcomes of research into decreasing structural mass. Sandwich panel structures consist of two thin face sheets on the top and bottom of a shear resistant lightweight core as shown in Figure 1.8.

The relative separation of the stable face sheets result in high stiffness to weight ratios. Essentially the honeycomb was used as a shear web between two upper and lower skins, with the early honeycomb sandwiches made of balsa wood as the core and plywood as the skins. With the

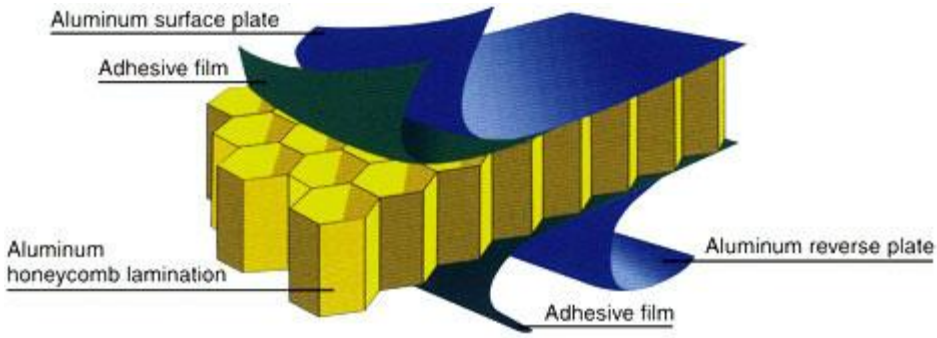

Figure 1.8. Schematic of Honeycomb Sandwich Structure[14]

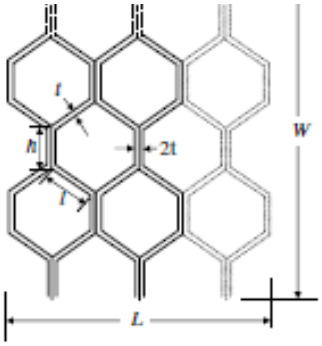

Figure 1.9. Geometrical Parameters of a Nomex honeycomb structure[14]

development of Epoxy resin, it was possible to bond aluminum skins to an aluminum honeycomb core, which occurred in 1954.[15] Since then, many advancements have been made in honeycomb studies, with the most commonly used honeycomb for aircraft structures being Nomex Honeycomb.[16] Figure 1.9 shows the honeycomb structure of Nomex, which is used extensively in this thesis. Nomex is constructed from ribbons of aramid fibers running in the longitudinal direction that are fused together with glue at sections along the ribbon. By pulling on the ribbons in the direction perpendicular to the longitudinal direction, the ribbons expand to form a honeycomb structure. The fiber structure is then dipped into phenolic resin to strengthen the walls of the honeycomb, which makes the honeycomb anisotropic with respect to out-of-plane shear stiffness and strength. Choo. F., et al. observed that honeycomb structures under tensile tests produced higher ultimate loads when the load was applied in the longitudinal (fiber) direction than in the direction perpendicular to the longitudinal direction.[17]

1.4.1 Advantages and Disadvantages of Sandwich Composites

Sandwich structures utilize each of its constituent materials' properties. The thin face sheets' high stiffness combined with low-density cores give a sandwich structure of high stiffness to weight ratio when compared with a face sheet beam of same weight, and a high bending strength to weight ratio. In addition to the efficiency between stiffness and strength, honeycomb sandwich panels are fairly fatigue resistant, great insulators or radiators depending on the core material selection, highly serviceable and have smooth aesthetically pleasing surfaces.[18] Honeycomb sandwich panels are analogous to beams or plates. The use of honeycomb prevents buckling of the thin skins by providing the amount of shear strength to do so. Honeycomb panels are lightweight, easy to work with, and not labor intensive. By increasing the thickness of the core, the composite panel's strength and flexural stiffness increases much like increasing the height of a beam, but without the weight increase shown in Table 1.[19] This is due to an increase in the panels' moment of inertia. Composite panels are designed such that failure occurs in the core of the panel, thus shear strength is the main factor in design, which is the core's predominant material property. Composite panels are designed to meet the application requirements. They have the same normal strengths that composites

have, due to the face sheets being constructed from materials of high modulus of elasticity's (when compared with the core) like fiber-resin mixtures, metal alloys and plastics. The cores have low elastic moduli that yield without failure in the high deflection regimes. Cores usually consist of metallic and fibrous honeycomb structures to opened and closed cell structured foams seen in Figure 1.10.[19]

Table 1.1. An example of sandwich panel structural efficiency with respect to weight[19]

	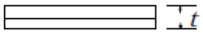	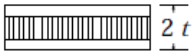	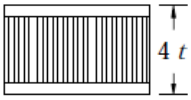
Relative Bending Stiffness	1	7.0	37
Relative Bending Strength	1	3.5	9.2
Relative Weight	1	1.03	1.06

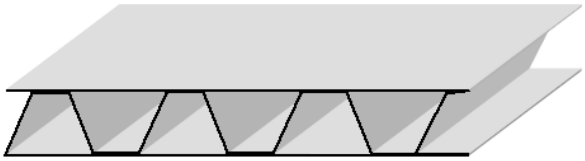

(a)

(b)

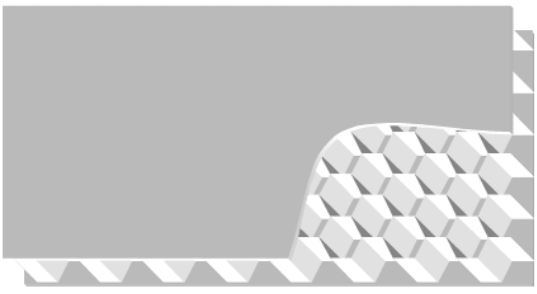

(c)

Figure 1.10. Sandwich panels with (a) corrugated (b) foam and (c) honeycomb core[19]

There are many standards, manufacturing techniques and accepted methods for constructing and testing materials such as metals. As sandwich composite structures are relatively new, there are not nearly as many standards for manufacturing and testing, particularly with the inclusion of honeycomb. Quality control thus is difficult to ensure correct integration into the strict design requirements of the aerospace industry. This results in a much higher safety factor when constructing the sandwich design, which is counterproductive to the main goal of reducing weight.

1.4.2 Aerospace Industrial Application

The application of composites is in high demand due to their favorable mechanical characteristics and material properties to current materials used, especially in the aerospace industry. Composite sandwich structures have revolutionized the aerospace industry because of their high stiffness and lightweight attributes when compared with aluminum, the aviation standard. Sandwich structures have proven particular advancements in the latest spacecraft, automobiles, airplanes and racing yachts to name a few. In the civil industry, sandwich composites have revolutionized bridge and flooring structures. In the auto industry, companies have shifted to the use of fiberglass and carbon fiber

Figure 1.11. Over 50% composite commercial plane - Boeing's 787 Dreamliner.[20]

to dramatically decrease weight, and thus directly increase performance. These advancements are accounted mostly to the large weight reduction sandwich structures and composites offer over traditional materials. The aerospace and military industry has had the most dramatic advancements due to the use of sandwich composites. Aircraft performance, for the most part is directly affected by weight. Sandwich structures can be almost as stiff as steel whilst the low core density maintains the sandwich structure weight at a fraction of that compared with a comparable steel beam. Sandwich structures can be integrated into such aircraft parts as the wings, floor, ceiling, fuselage and cargo compartment paneling, and even control surfaces. Figure 1.11 shows the Boeing 787: the most recent aircraft to be constructed out of mostly composite materials, allowing for a 20% increase in fuel efficiency and 40% increase in engine efficiency over its' replacement, the Boeing 767.[21]

1.5 Previous Work

Reviewing previous works is vital in preventing time wasted by conducting redundant work. Reviewing past materials can help the researcher see what methods have been successes and failures, which prove invaluable to producing progressive works. All the previous works reviewed in this thesis have been published and peer reviewed. The most helpful works have been Frostig et al. Bending of Nonsymmetrical Sandwich Beams with Transversely Flexible Core[22], Lim, T.S., Lee, C.S. and Lee. D.G. Failure Modes of Foam Core Sandwich Beams under Static and Impact Loads[23], Foo. C., Chai. G., Seah. L., Mechanical Properties of Nomex Material and Nomex Honeycomb Structure[17], Whitney, J. A Local Model for Bending of Weak Core Sandwich Plates[44], Khan, S. Bonding of Sandwich Structures – The Face sheet/Honeycomb Interface[14] and Allen, H. G., Analysis and Design of Structural Sandwich Panels.[25]

The bending of unsymmetrical sandwich beams with flexible, foam or honeycomb cores has been investigated analytically by Frostig et al[22]. Beams consisting of different upper and lower skins, with a soft core were tested, analyzing the effects of the flexibility of the core in the vertical direction, the bending behavior of the face sheets, and the overall panel behavior. Fibrous composite, and metallic

face sheets have, as a rule of thumb approximately twice the tensile strength as compressive strength. By having a thicker face sheet at load application, it can prove beneficial to overall panel performance[22].

Khan's paper discusses that the most occurring failure of composite sandwich panels occurs at the de-bonding of the composite face sheets from the core, which is usually initiated by impact damage on the surface, which is then propagated by flexural load on the damaged portion subjected to cyclic fatigue or compression. Due to a difference in moduli between the face sheets and the honeycomb core, if a bending load is applied, a large shear stress generates at the interface. If a flaw is present at the face sheet-core interface, this shear stress can separate the face sheet from the honeycomb core. The quality of the adhesion between face sheet and core determines how much force a sandwich structure can hold and so it is crucial that the quality of this bond is a major design factor of honeycomb sandwich panels.[24]

There are two methods to bonding the composite face sheets and the honeycomb. The first, an adhesive film is placed on the bottom and top faces of the honeycomb, where the cured or uncured face sheets are placed. The whole piece is then cured in an autoclave. This process melts the adhesive resin, which creates a bond between the composite face sheet and the honeycomb wall. The second method has uncured pre-preg face sheets placed on the top and bottom surfaces of the honeycomb and the whole panel is cured in an autoclave, whereupon the resin from the pre-preg melts and creates a bond between face sheets and honeycomb walls. An optimal bond is formed between face sheet and honeycomb wall when the resin flows to form a symmetric fillet on the honeycomb wall as seen in Figure 1.12. The edge of the honeycomb wall should be

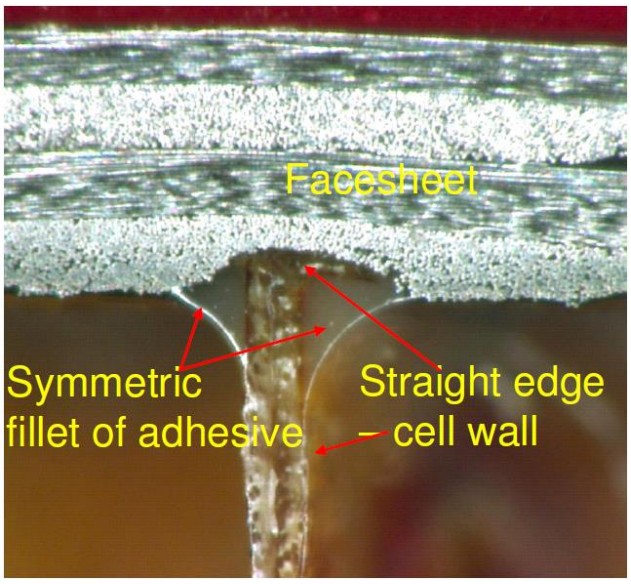

Figure 1.12. Schematic of facesheet/Honeycomb Interface.[24]

perpendicular to face sheet and should indent the face sheet marginally to make an ideal interface bond.

During the bonding process, the honeycomb does not melt or flow and thus the surface quality of the honeycomb plays a role in bond quality. It is paramount that the honeycomb-bonding surface is clean of fibers so that delamination failure will not occur as a result of damaged fibers. A clean surface can be achieved through wet sanding.[24]

Lim, Lee and Lee[23] investigated the static failure modes of foam core sandwich panels experimentally using the static three point bending test with respect to face sheet thickness, span and core density. Triantafillou and Gibson[26] developed failure equations to describe the failure load for face yielding, face wrinkling and core shear from which the failure mode map was constructed. Analytical failure loads and modes were obtained from the theory of sandwich beams on elastic foundation. The results were compared and showed good agreement with each other. Three transition equations were made using non-dimensional parameters, including strength ratio, moduli ratio, and normalized thickness and span. Using the transition equations, the general static failure mode map could be developed considering local deflection.[23] There has been much analysis of panels, beams and struts of sandwich panels summarized by Allen[25] and Plantema[27]. Allen[25] modeled sandwich panels as a beam, with the assumptions that the core is homogenous, of much lower stiffness when compared with the face sheet material and the skin is relatively thin when compared with the core and later Ashby and Gibson[28] further developed this model. Optimization of skin and core thickness that satisfy stiffness constraints at minimum weight have been developed by Gibson and Triantafillou[29]. Some buckling and wrinkling behavior of sandwich panels under in-plane compression has been conducted by Kwon and Pearce[45].

1.6 Main Objective and Scope of Research

The main objective of this study is to investigate the effects of varying the Honeycomb core orientation on flexural characteristics of composite sandwich structures with constant face sheet thickness. Once the optimal core orientation is determined the objective is to investigate the effects of varying top and bottom face sheet ply count (thickness) with a constant honeycomb Nomex core. Typically, symmetry is used in composite sandwich design to account for multiple loading conditions. For example, an aircraft wing experiences torsion, compression and tension from its environment during flight. If the wing were simplified to a single composite sandwich, it can be seen that symmetry in construction is necessary as the loading direction could be in compression, tension or torsion at any given point. Composite sandwich structures in other sections of aircraft experience loading in only one direction for example, floor paneling for the most part, experience only static loading in one direction, and knowing that fibrous composites can take, depending on material selection, twice as much load in tension as compression, by adding extra layers to the side of the sandwich under the loading force, and/or subtracting layers on the opposite side, we can obtain two things: either increase performance in bending stiffness and/or strength whilst keeping weight constant or in the case of aerospace design; decreasing weight whilst maintaining or increasing performance.

Chapter 1 goes over the introduction of composite materials, from the varying composite types to different fabrication methods. The background and advantages of composite sandwich panels are discussed as well as their aerospace industrial applications. Previous honeycomb sandwich works are discussed and the main objective and scope of this research is explained. Chapter 2 outlines the manufacturing, procedure and experimental set-up for obtaining the mechanical properties of the composite sandwich structure's constituent materials and the sandwich structure as a whole using available ASTM standards. Chapter 3 entails the analytical analysis conducted using classical beam and plate theory for sandwiches with varying core ribbon orientation and varying face sheet thickness. A

study into the necessity of adding an adhesive layer between carbon fiber pre-impregnated face sheets and Nomex honeycomb core is also conducted. Failure mode analysis for panels with equal face sheet thicknesses is conducted using carbon fiber and Nomex honeycomb with respect to core ribbon orientation. Optimization of bending stiffness and strength with respect to minimum weight is looked at. Chapter 4 discusses and analyzes the experimental data of specimens with varying core orientation and varying face sheet thickness. A Finite element model is developed in chapter 5 and FEA analysis is compared with experimental and analytical results and obtains good agreement with both. Chapter 6 concludes the study.

2.0 Manufacturing, Procedure and Experimental set-up

This section covers the manufacturing and testing procedures for obtaining the mechanical properties of the carbon fiber face sheets, honeycomb core and sandwich structure as a whole. Composite materials have few ASTM standards to guide the tester with a proven method. There are some general guidelines that must be followed when testing composite specimens, however. It is paramount that extra precautions must be taken to prevent notches, uneven surfaces, and delamination when machining specimens. Caution must be taken when cutting sandwich panels to ensure the core does net get compromised due to low heat resistance. The testing of all specimen mechanical properties followed their respective ASTM standards shown in Table 2.1 below.

Table 2.1. ASTM Standards used in this experiment

Material	Mechanical Property	ASTM Standard
Carbon Fiber	Tensile/Compressive stress/strength	D3039/D3410
	Tensile/Compressive Modulus of Elasticity	D3039/D3410
	Volume Fraction	D2584
	Poisson's Ratio	E132
Honeycomb	Poisson's Ratio	D6790
	Core Shear Ultimate strength	C0393
	Core Shear Modulus	D7250
Sandwich structure	Flexural stiffness	D7250
	Shear Rigidity	D7250
	Facing Stress	C0393/D7249

All specimens were cured in a tetrahedral press seen figure 2.1. All three-point bending tests were performed in an Instron 8801 universal test machine with a 100 kN cell seen figure 2.2. Load and deflection were taken from the tests and results were obtained by applying the simplified beam theory.[25]

Figure 2.1. Tetrahedral Press

Figure 2.2. Instron 8801.

2.1 Carbon Fiber Face Sheet Mechanical Properties

The face sheet material used in the composite sandwich structures was Hexcel's pre-impregnated Hexply 6376 matrix with A280-5H bidirectional woven carbon fiber seen. There are several ways to cure pre-impregnated carbon fiber, but the chosen method was in a tetrahedron press, located in the Cal Poly Aerospace Structures/Composites Lab.

2.1.1 Tensile Mechanical Properties

To determine the tensile properties of the face sheets of HexPly 6376 pre-preg, 12x12 inch plates were cut out and cured in a Tetrahedron heat press. HexPly 6376's curing cycle in a heat press can be seen below in Figure 2.2. The specimen is heated at a rate of 5°/min up to 225°F and held at that temperature for 1 hour. The temperature is then ramped at 5°/min up to 350°F and held at that temperature for 2 hours. The Temperature is then ramped down at a rate of 5°/min down to 75°F and cycle is then terminated.

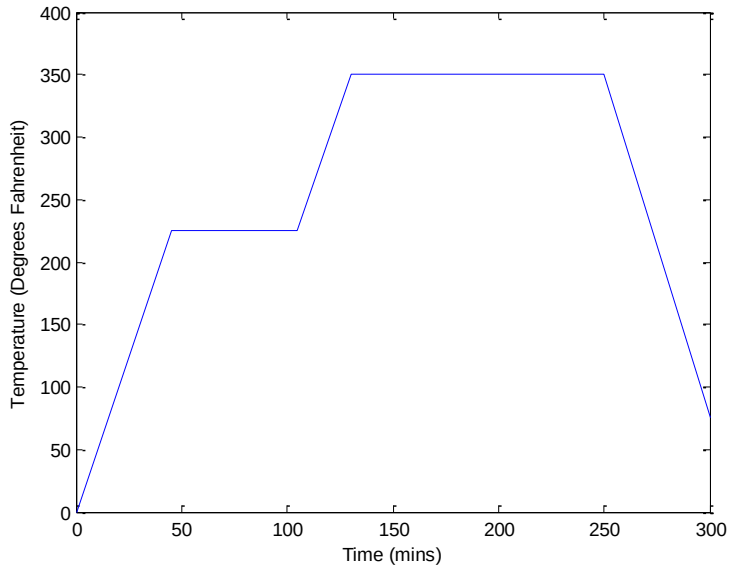

Figure 2.3 Curing Cycle for Hexply 6376 A280-5H

The carbon fiber was cured with pressure set at 2 psi to allow the honeycomb to indent into the carbon fiber during cure to increase bonding surface area between core and face sheet. The pre-preg is cut into 12"x 12" squares and placed between two layers of non-porous material. The stacking of the layers is as follows: non-porous material, six layers of bi-directional A280-5H pre-preg carbon fiber, and non-porous material. The non-porous material is essential to keep the heating press clean from resin and to allow for easy removal of the cured carbon fiber plate. It is imperative that the carbon fiber sheets be layered on each other at right angles. Small changes in ply orientation can result in

unsymmetrical laminates and subsequently skewed results in mechanical tests. The carbon fiber plate was then cut into 10 inch long by 1 inch wide by 0.1 inch thick or wider inch strips to comply with ASTM D3039 tensile testing.[30] Cutting specimens to the required dimensions required a tile saw with accurate measuring device to ensure repeatability between samples. In accordance with ASTM standard, aluminum tabs, also known as grips, measuring 1”x1” are used for the tensile testing shown in Figure 2.3.

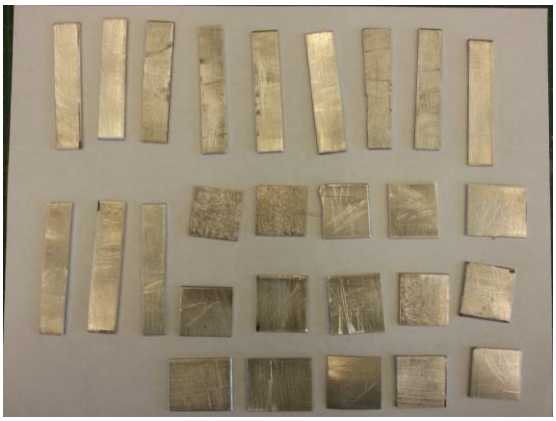

Figure 2.4. Scored aluminum tabs used for tensile tests.

The tabs were scored to allow for better grip between the carbon fiber surface and aluminum tab. Scoring the aluminum increases the bonded surface and thus bonding strength. The tabs were cleaned and attached to the carbon fiber samples with a resin-epoxy adhesive shown Figure 2.4. The curing cycle for the structural adhesive can be seen in figure 2.5. Temperature is ramped at 5^{o}/min up to 120^{o}F, held at that temperature for 1 hour and then ramped down at a rate of 5^{o}/min back to room temperature.

Grips apply sufficient lateral pressure to prevent slippage between the grip face and the test specimen. A strain transducer in the lateral direction of the test samples is needed to determine poisons ratio. The Longitudinal strain is calculated in the Instron testing machine and thus a strain gage was not necessary in the longitudinal direction, shown in Figure 2.7. Strain gauges should be placed in the middle of the test sample. Consideration of temperature compensation is recommended for non-ambient temperature environments.

Figure 2.5. 1614 A&B Structural adhesive from 3M used on tensile testing tabs

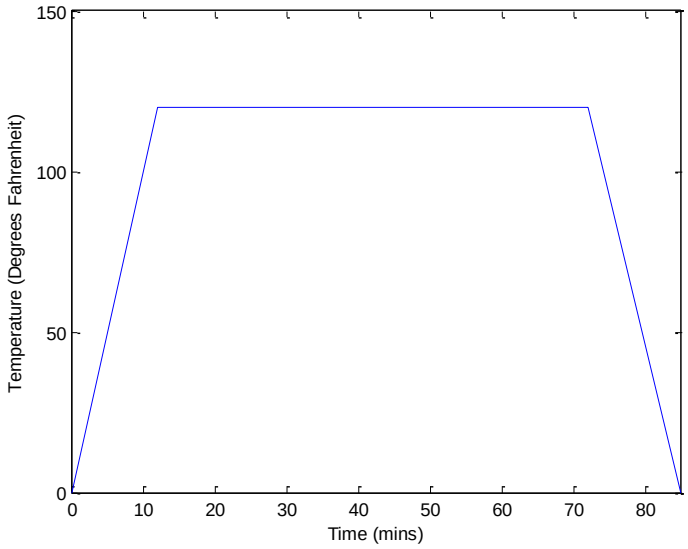

Figure 2.6. Cure Cycle for Structural Adhesive

To meet ASTM standards at least six samples were needed for testing. Each sample strip is first fed into the top fixture of the Instron 8801 machine and clamped down while being positioned perfectly vertical. The bottom fixture is moved into position to reach the bottom tab of the sample and then allowed to clamp down. Care must be taken to make sure there is no twist to the sample strips as it will induce a bending moment during the test and will greatly affect results, shown in Figure 2.8.

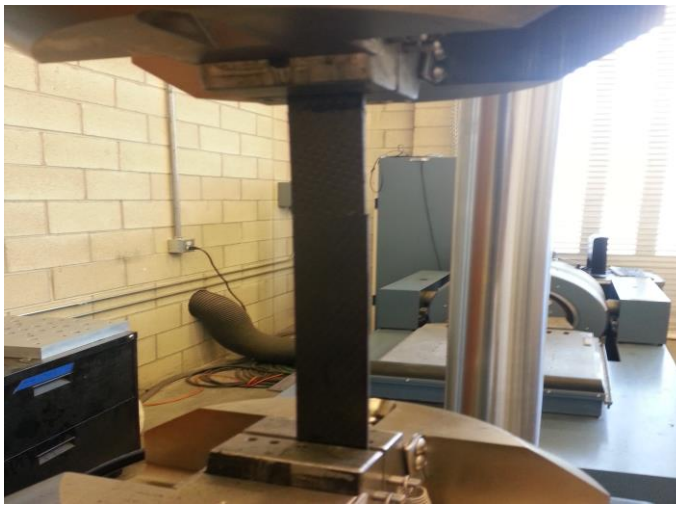

Figure 2.7. Tensile Testing of Carbon Fiber

As per ASTM D3039, A standard head displacement rate of 0.05 in./min was applied to specimens until failure. The Instron machine records all testing data: elongation, load, stress, strain, and ultimate stress. Test specimens that failed near the grip fixture were discarded from results.

The raw data is then analyzed to obtain ultimate tensile strength and Young's modulus. Calculation of the ultimate tensile strength is executed through Eq 2.1. Determination of the tensile stress at each required data point is executed through Eq 2.2.

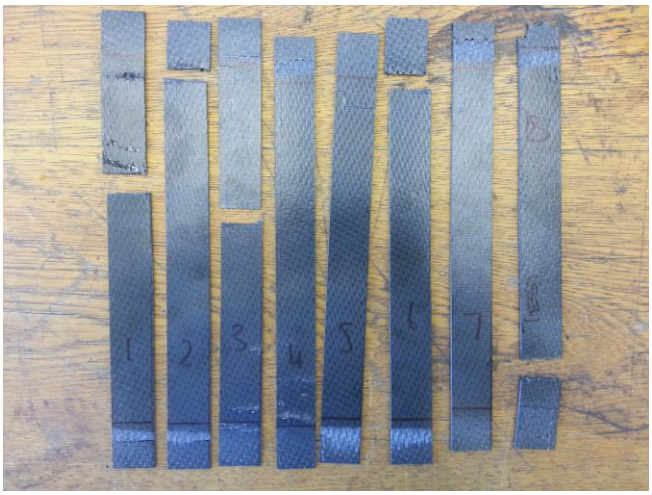

Figure 2.8. Samples failing at or near grip fixture are discarded

$$F^{ult} = \frac{P^{max}}{A} \tag{2.1}$$

$$\sigma_i = \frac{P_i}{A} \tag{2.2}$$

Where F^{ult}= ultimate tensile strength, [Mpa [psi]; P^{max}= maximum force before failure, N [lbf]; σ_i= tensile stress at ith data point, Mpa [psi]; P_i = force at ith data point, N [lbf]; and A = average cross-sectional area, mm^2 [in.^{2}].

$$E = \varepsilon/\sigma \tag{2.3}$$

The elastic modulus is calculated in the linear elastic region between 10-25% of ultimate load for each specimen and then averaged resulting in an elastic modulus. In addition to the elastic moduli, the ultimate stress values were also recorded for each sample. Ultimate stress is needed for theoretical calculations for the sandwich structure. Table 2.2 shows the tensile mechanical properties found experimentally. Experimental tensile data can be found in the appendix. A total of 12 tensile specimens were tested with 7 acceptable failure modes.

Table 2.2. Tensile mechanical properties of Hexply 6376 A280-5H carbon fiber pre-preg

	Young's Modulus (Msi)	**Ultimate Tensile Strength (ksi)**
Experimental	12.934±.263	163.3±5.22
Data Sheet	9.7	127
Error (%)	-33.3%	-28.6%

The tensile tests produce conflicting results with the data sheet values, which leads me to believe the material may have been labelled wrongly.

2.1.2 Compressive Mechanical Properties

As per ASTM D6641 the composite face sheets are cut into strips 5.5 inches long by 0.5 inches wide by approximately 0.1 in thick, equivalent to 7 plies of HexPly 6367, to obtain compressive property data. Laminate compressive strength and modulus can be calculated as follows:

$$h \geq \frac{l_g}{0.9069\sqrt{\left(\left(1-\frac{1.2F^{cu}}{G_{xz}}\right)\left(\frac{E^c}{F^{cu}}\right)\right)}} \tag{2.5}$$

$$F^{cu} = \frac{P_f}{wh} \tag{2.6}$$

$$E^c = \frac{P_2 - P_1}{(\varepsilon_{x2} - \varepsilon_{x1})wh} \tag{2.7}$$

Where: F^{cu}=laminate compressive strength, psi, l_g= length of gage section, 0.5 in, G_{xz} = through thickness shear modulus, psi, P_f = maximum load to failure, lbf, w = specimen gage width, in, h = specimen gage thickness, in, E^c = compressive modulus, psi, P_2, P_1 = load at $\varepsilon_{x2}, \varepsilon_{x1}$, lbf, $\varepsilon_{x2}, \varepsilon_{x1}$= actual strain nearest upper, lower end of strain range used. Results of compressive tensile testing can be seen

Figure 2.9. Compressive specimen in the Instron Machine.

Figure 2.10. Broken Compressive Specimens.

in table 2.3. An example of the experimental test set-up can be seen in Figure 2.9. A total of 12 specimens were tested, 8 had acceptable failure modes which can be seen in Figure 2.10. Experimental data can be seen in the appendix.

Table 2.3. Compressive Mechanical properties of Hexply 6376 A280-5H Carbon Fiber.

	Compression Young's Modulus (Msi)	Compressive Ultimate Strength (ksi)
Experimental	4.48±0.4	127.7±3.4
Datasheet	9.5	134
Error (%)	52.8%	4.93%

It must be noted that compressive and tensile data found experimentally are off by a large margin and have produced results not typical of a bi-weave carbon fiber. For analysis purposes, experimental mechanical properties shall be used.

2.1.3 Poisson's Ratio of Face Sheets

To determine the Poisson's ratio of the face sheets ASTM E132 is used.[31] ASTM E132 is used in conjunction with ASTM D3039 and follows the same fabrication and test method. The only difference is that strain gages are added to the test specimens to obtain the two-dimensional behavior of the lamina. To do so, an M-Bond 200 Adhesive kit is used to adhere the gage to the specimen. The surface of the composite sample needs to be cleaned with acetone before gage application for optimal adhesion. The resin from the kit is applied to the composite surface and allowed to dry for a few seconds. The hardener is applied to the gage and applied to the composite sample on the catalyst

Figure 2.11. Placement of transverse strain gage

surface. Pressure is applied over the work area for a few minutes for the epoxy to cure. Once cured the strain gage must be soldered and resistance verified with requirements. The gage system is shown in

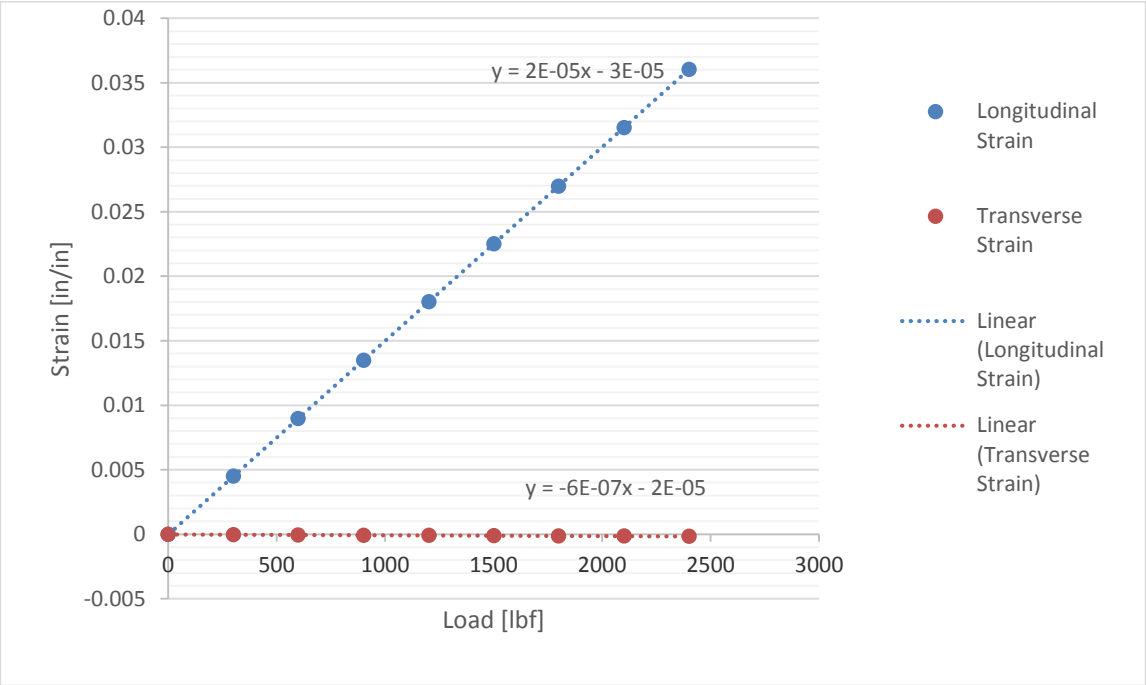

Figure 2.12. Strain versus Load in longitudinal and transverse directions of the Carbon Fiber

Figure 2.8. To obtain values for Poisson's ratio, a plot of the average strain versus load was created for both longitudinal and transverse directions as shown in Figure 2.12.

The derivative of the strain in the transverse direction is divided by the derivative of the strain in the longitudinal direction as seen in Eq. 2.4.

$$v = \frac{-\frac{\partial \varepsilon_T}{\partial P}}{\frac{\partial \varepsilon_L}{\partial P}} = -\frac{\varepsilon_T}{\varepsilon_L} \tag{2.4}$$

Where v is the Poisson's ratio, P is the applied load and ε_T and ε_L are the transverse and longitudinal strains respectively. A plot of the strain versus load curve for the average transverse and longitudinal directions can be seen in Figure 19. Poisson's ratio for Hexply 6367 A280-5H was found to be 0.03, which is a little low for bi-directional carbon fiber sheet, but not terrible. Hexcel does not provide Poisson's ratio for Hexply 6367 A280-5H carbon fiber and is thus not shown.

2.1.4 Weight Fraction and Density of Face Sheets

The density of the face sheet is required in this research particularly for theoretical and finite element analysis. Experimental density values are found by measuring the dimensions of a sample and the samples weight. To find the density of the HexPly 6376 A280-5H carbon fiber face sheets, cured samples of 4, 6 and 8 layers were cut into 4" x 1" rectangles and measured with a micrometer along with the samples' weight. Each configuration contained 6 samples for statistical accuracy. The density is calculated by dividing the mass sample in lbs. by the mass volume in in^3. Validation of experimental density, the theoretical value was calculated using the densities of the fibers and matrix along with the volume fraction of the laminate. The weight fraction requires the measured weights of the specimen before and after ignition loss. The weight fraction is defined as W and subscripts are dependent on constituent material, f for fiber, m for epoxy. The weight ratio is the ratio of component to the whole structure and is defined as follows:

$$W_{total} = w_f + w_m \tag{2.12}$$

$$W_m = \frac{(w_{total} - w_f)}{w_{tot}} \tag{2.13}$$

$$W_f = \frac{w_f}{w_{tot}} \tag{2.14}$$

The volumetric fractions require the density of each constituent material. The volume fraction is defined as V and is as follows:

$$v_{total} = v_f + v_m \tag{2.15}$$

$$V_m = \frac{(v_{total} - v_f)}{v_{tot}} \tag{2.16}$$

$$V_f = \frac{v_f}{v_{tot}} \tag{2.17}$$

The relationship between volumetric fraction and weight fraction is dependent on the density of the constituent materials and structure as a whole. The proportional relationship of the weight fractions to volumetric fractions is as follows:

$$V_f = \frac{\rho_{total}}{\rho_f} W_f \tag{2.18}$$

$$V_f = \frac{\rho_{total}}{\rho_m} W_m \tag{2.19}$$

If the density of the structure is unknown, the volumetric fractions can be determined with the weight of the constituent materials only as follows:

$$V_f = \frac{\rho_m W_f}{\rho_f W_m + \rho_m W_f} \tag{2.20}$$

$$V_m = 1 - V_f \tag{2.21}$$

The density of the Hexply 6376 matrix epoxy and A280-5H Fibers are given by Hexcel and are 0.0473 and 0.0648 lbs./in^3 respectively. Using the 55.29% fiber volume fraction stated on the Hexcel data sheet, Eq. 2.22 can be used to determine the density of the laminate:

$$\rho_{laminate} = V_{fibers} * \rho_{fibers} + V_{matrix} * \rho_{matrix} \tag{2.22}$$

Table 2.4 shows the results of the density calculations.

Table 2.4. Density Calculations of cCrbon Fiber

Configuration	Density (lbs/in^3)	Standard Deviation (lbs/in^3)
4 Layers	0.0562	0.0013
6 Layers	0.0542	0.0011
8 Layers	0.056	0.0011
Average	**0.0555**	0.0014
Theoretical	**0.057**	-
Error (%)	2.63%	

Experimental volumetric fiber burning density calculations showed favorable results with data sheet values.

Figure 2.13. Crucible used for ignition loss testing.

Figure 2.14. Carbon fiber samples after ignition

To validate the 55.29% fiber volume fraction stated by Hexcel, ASTM D2584[34] is used to measure the ignition loss of a cured reinforced resin sample. The 4" by 1" samples used for density calculations were cut into 1" x 1" squares and reweighed. One sample consisted of 4, 1" x 1" squares and were placed into a crucible shown Figure 2.13 and maintained at a temperature of 1050±50°F for approximately one hour to completely burn off the epoxy, leaving only the carbon fibers shown Figure 2.14.

The ignition loss of the specimen in weight percent is calculated as follows:

$$Ignition\ loss, weight\ \% = \left[\frac{W_1 - W_2}{W_1}\right] * 100 \tag{2.23}$$

Where: W_1 = weight of specimen, lbs and W_2 = weight of residue, lbs.

The fiber volume fraction of the samples can be calculated as follows:

$$V_{fiber} = \frac{\frac{w_{laminate}}{\rho_{laminate}} - \frac{w_{matrix}}{\rho_{lmatrix}}}{\frac{w_{laminate}}{\rho_{laminate}}} \tag{2.24}$$

Where m donates mass of constituent in lbs. The results can be seen in Table 2.5.

Table 2.5. Weight fiber fractions calculated experimentally and theoretically

	Volumetric Fiber Fraction
Experimental	0.5571±9.4%
Theoretical	0.5529
Error (%)	0.759%

2.2 Honeycomb Core Mechanical Properties

Determination Honeycomb core mechanical properties proved difficult due to not having access to the required test apparatus's for testing under ASTM C273[37], and tests to determine Young's moduli. Although core shear strength, and core shear modulus could not be obtained experimentally and from the limited experimental mechanical properties, the required mechanical properties were obtained theoretically.

2.2.1 Poisson's ratio

ASTM standard D6790 – 02[38] was used for determination of honeycomb Poisson's ratio in both longitudinal and transvers core orientations from the anticlastic curvature radii shown in Figure 2.1.

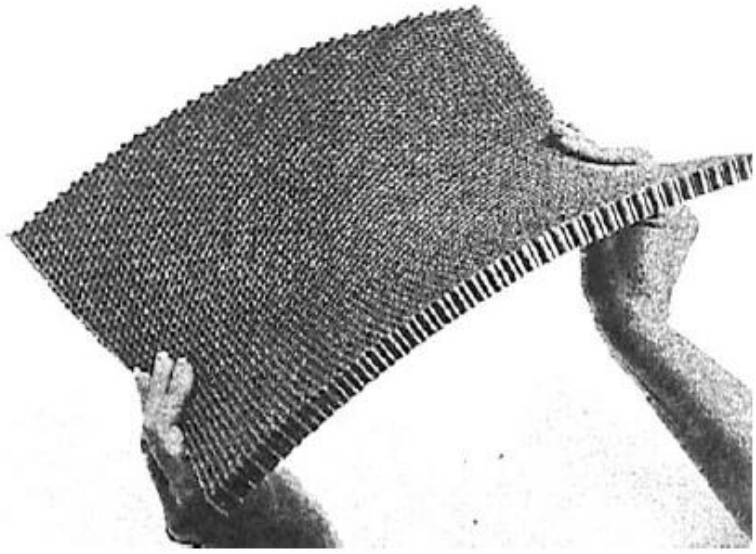

Figure 2.15 Anticlastic Curvature[38]

Certain sandwich panel finite element programs require the Poisson's ratio of the honeycomb core. As it is not possible to measure honeycomb's Poisson's ratio by standard method, the test method ASTM D6790 is on means of obtaining the Poisson's ratio of honeycomb, however this test method is not widely used and is in its conceptual stage. A specimen of 12 by 12 inches is bent in both directions, as shown in Figure 2.16 around a 24-inch drum and the anticlastic curvature radius is calculated as follows.

$$R_a = \frac{4d^2+c^2}{8d} \tag{2.25}$$

$$\mu = \frac{R_c}{R_a} \tag{2.26}$$

Where: μ = Poisson's ratio, R_a = anticlastic curvature radius, R_c = cylinder radius, c = chord measurement, and d = depth measurement.

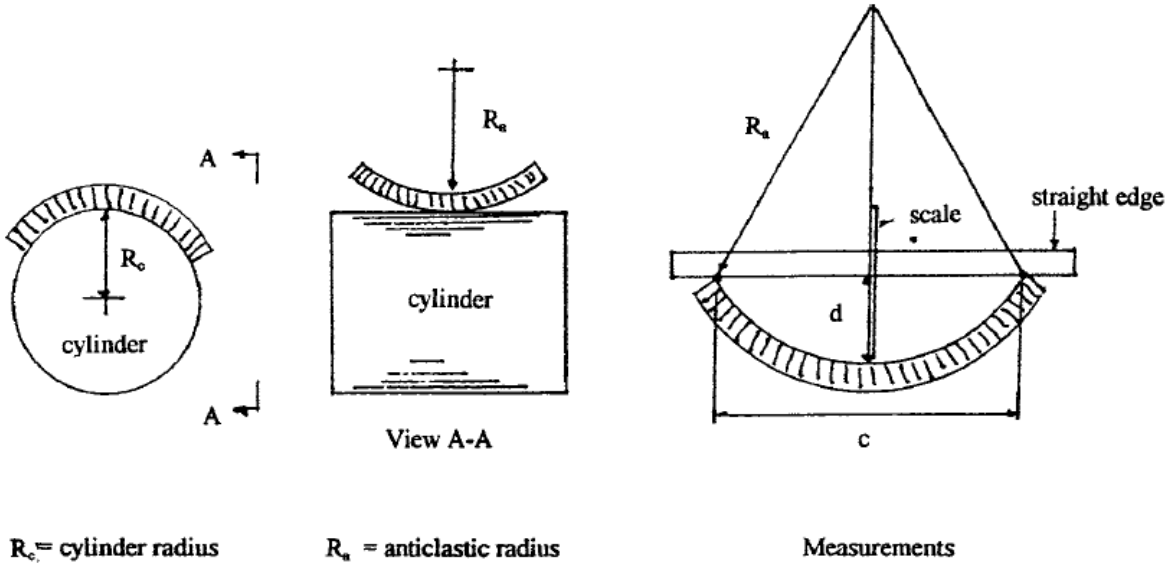

Figure 2.16. Measurements for ASTM D6790[38]

From the Poisson's ratio and shear modulus given by Hexcel, Young's moduli in the transverse and longitudinal directions can be determined as follows:

$$E_{L,T} = G_{L,T}\left(2\left(1 + v_{L,T}\right)\right) \tag{2.27}$$

In total 8 specimens were tested in both longitudinal and transverse directions. Table 2.6 shows the results of the testing.

Table 2.6. Experimental Mechanical Properties of Hexcel HRH-10-1/3-5 Honeycomb

Direction	Poisson's	Young's Moduli (psi)	Shear Modulus (psi)
Longitudinal	0.8036 ±0.033	37669 ±719	10442.7
Transverse	0.4114 ±0.0066	16375 ±76.6	5801.5

Experimental values cannot be compared to data sheet values, as Hexcel has not supplied them.

2.3 Composite Sandwich panels

This section covers the mechanical behaviors of the composite sandwich specimens. The mechanical properties found in this section are determined using equations presented in relevant ASTM standards using experimental data.

2.3.1 Necessity of Adhesive Layer between Core and Face Sheet

A similar method to the face sheets is used to determine the mechanical properties of the adhesive. An adhesive with similar curing cycles to the carbon fiber face sheets was used to prevent shock, or over cure of the adhesive. The adhesive chosen was 3M's Scotch-Weld Structural Adhesive Film 163-2OST. The adhesive is green in color weighing 0.03 lb/ft^2 with a nominal thickness of 5.5 mils.[35] The 163-2OST has a range of cure cycles from 225^{o}F at 90 minutes to 300^{o}F at 60 minutes. To minimize error caused by different cure cycles, the whole panel cure cycle was set to the carbon fiber face sheet cure cycle seen in the above section 2.1.

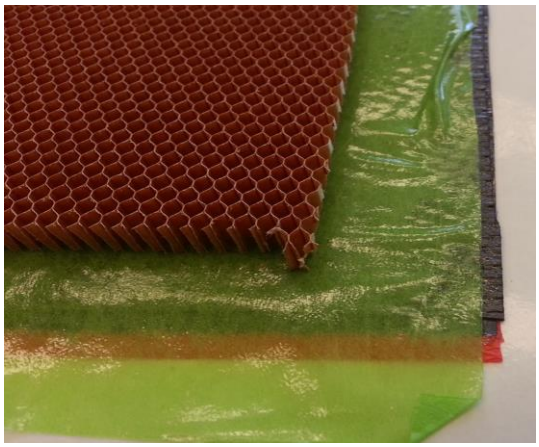

Figure 2.17. Viscid side of adhesive placed against honeycomb core.

The manufacture of test specimens follows ASTM D638 standards.[36] When making the sandwich; the viscid side of adhesive is placed against the honeycomb so to prevent face sheet slipping if pre-cured sandwich is to be stored before curing as shown in Figure 2.17.

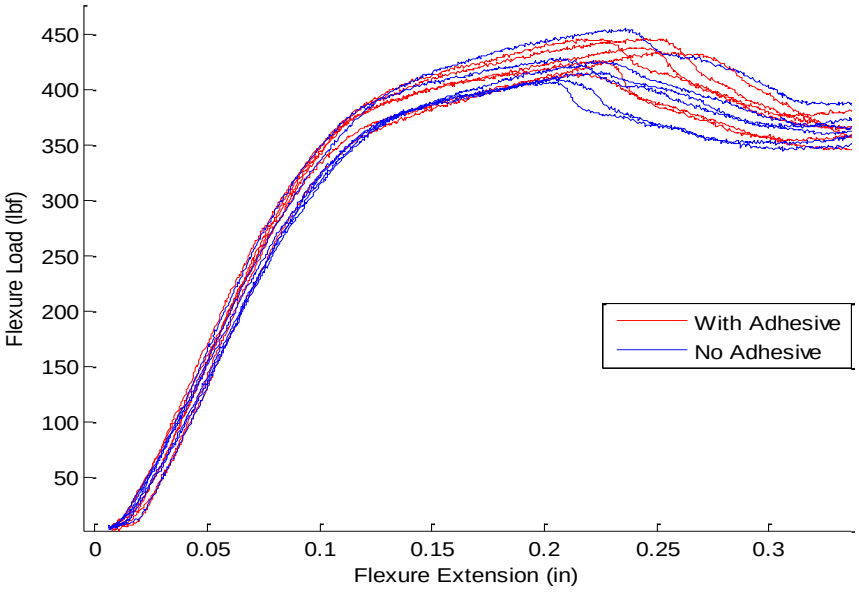

Figure 2.18. Load versus Extension plot for 3 ply Sandwich structures with and without adhesive layers

To test the effects of an adhesive layer between the face sheets of the sandwich and the honeycomb core, 6 sandwiches with an adhesive layer between core and face sheets and 6 sandwiches without an adhesive layer were constructed and tested under three-point bending. Figure 2.18 and Table 2.7 show that sandwich structures with the adhesive layers exhibited marginally lower ultimate loads than sandwich structures without adhesive whilst incurring a small weight increase. For the purposes of optimization in this thesis, it was determined that the adhesive layer does nothing to increase the performance of the sandwich structure.

Table 2.7. Effect of adhesive layer on the ultimate load at initial failure

	Ultimate Load (lbs)	Standard Deviation (lbs)
With Adhesive	424.37	17.502
Without Adhesive	434.44	12.263

2.3.2 Core Shear Properties of Sandwich Constructions by Beam Flexure

This test covers determination of the core shear properties of flat sandwich constructions subjected to flexure, such that the applied moments produce curvature of the sandwich facing planes. All specimens should be 3 inches wide, 8 inches long and face sheet to core thickness less than 0.1 to

Figure 2.19. Panel placement for testing

follow ASTM C393 standards.[39] All bending tests were conducted in the Instron 8801 machine at Cal Poly SLO Aero structures/composites Lab.

All specimens shall have dimensions recorded. Measure and record the length of the support and loading spans being 6 and 0 inches respectively. The speed of the testing set is to be set to 0.25 in per minute. Arrange the loading fixture as seen in Figure 2.19 and place in testing fixture. Place the specimen into the test fixture aligning the longitudinal axis perpendicular to the longitudinal axis of the loading bars. Apply the compressive force to the specimen at the specified rate of 0.25 in/min. Load the specimen until failure or until the deflection equals the specimen thickness.[39] Core shear ultimate stress can be calculated as follows:

$$F_s^{ult} = \frac{P_{max}}{(d+c)b} \tag{2.28}$$

Where: F_s^{ult}= core shear ultimate strength, psi, P_{max}= maximum force prior to failure, lb, t = nominal facing thickness, in, d = sandwich thickness, in, c = core thickness, in and b = sandwich width, in.

Facing stress can be calculated using Eq. 2.29. It must be noted that Eq. 2.29 can only be used for sandwich structures with facings of equal thickness:

$$\sigma = \frac{P_{max}S}{2t(d+c)b} \tag{2.29}$$

Where: σ= facing stress, psi, t = facing thickness, in, and S = support span length, in.

For sandwich structures of unequal facing thickness, in accordance with ASTM D7249[40], the upper and lower facing stresses can be calculated as follows.

$$F_{upper} = \frac{P(S-L)}{2(d+c)bt_1} \tag{2.30}$$

$$F_{lower} = \frac{P(S-L)}{2(d+c)bt_2} \tag{2.31}$$

Where: F_{upper}= facing 1 stress, psi, F_{lower}= facing 2 stress, psi, t_1 = upper facing thickness, in, t_2 = lower facing thickness, in, and L = loading span length, in. L = 0 for 3-point loading.

2.3.3 Determination of Sandwich Beam Flexural and Shear Stiffness

Testing under ASTM D7250[41] determines the flexural and transverse shear stiffness properties of flat sandwich constructions that have equal top and bottom facing thicknesses subjected to flexure such that the applied moments produce curvature of sandwich facing planes. Flexural stiffness, shear rigidity, and core shear modulus can be calculated as follows:

$$D = \frac{E_f(d^3-c^3)b}{12} \tag{2.32}$$

$$U = \frac{P(S-L)}{4\left(\Delta-\left(\frac{P(2S^3-3SL^2+L^3)}{96D}\right)\right)} \tag{2.33}$$

Where: D = flexural stiffness, lb-in^2, U = transverse shear rigidity, lbs., Δ = beammid-span deflection, in, P = total applied force, lbf.

Equation 2.33 can then be substituted into Eq.2.34 to obtain the core shear modulus, G, as shown:

$$G = \frac{U(d-2t)}{(d-t)^2 b} \tag{2.34}$$

3.0 Theoretical Analysis

This section focuses on the development of simplified expressions for shear and flexural stiffness' in the longitudinal orientation in order to estimate deflections to reasonable accuracy. Equations using Classical beam and plate theory are compared with the more in-depth orthotropic composites approach and then compared with the FEA solver Abaqus. The comparisons of equations are shown for a better understanding of how the solver functioned and which approach is more accurate when compared to the experimental results.

A sandwich beam can be predicted rather well with the classical theory. To study local effects on the other hand, higher-order theories have to be used. The examples show that the higher-order theory gives the best descriptions, since it takes influences through the thickness of the sandwich into account. From this point of view the higher-order theory is preferable. The only disadvantage is that the derivations are more complex than those for the superposition approach. But since general numerical procedures are developed to solve the boundary value problem easily, the higher-order theory is preferable. A simple analytical expression to estimate the flexural rigidity (EI or D) and Shear stiffness (GA or U) for the sandwich structures in the longitudinal orientation is needed to predict the overall response as a ball park reference before more time and computational costly finite element analysis is conducted. This expression would act as a guide to predict the structure's stiffness without implementing all needed material properties at the lowest level required by the orthotropic composite approach.

The following assumptions are made in regards to the face sheets:

1. Orthotropic, homogenous face sheets of thickness t_t (top face sheet) and t_b (bottom face sheet).
2. Transverse normal stresses σ_z are neglected in face sheets.
3. Transverse displacements in face sheets are independent of z coordinate, such that

$w_t = w_t^0(x,y)$, $w_b = w_b^0(x,y)$

4. In z coordinate in the face sheets, in plane stresses,σ_x,σ_y, τ_{xy} are assumed to be linear functions.
5. In plane stresses σ_x, σ_y, τ_{xy} are neglected in the core.
6. The material properties for the face elements are known from experimental testing, including Young's modulus and shear modulus derived from Eq. 2.27
7. The cross section of the structure can be idealized as the cross section of an I-Beam.
8. Both core and face laminates contribute to the flexural stiffness (EI or D). Only the core is accounted for in the shear stiffness (GA or U), due to the fact that shear deformation in the faces is negligible.

3.1 Analytical Formulation for Mechanical Properties

Using the simplified beam theory as proposed by Allen[25] the Core Shear Stress (3 point loading):

$$\tau = \frac{P_{max}}{(d+c)b} \tag{3.1}$$

Where τ is the core strength or shear yield stress [psi], P is the load [lb], d is the sandwich thickness, c is the thickness of the core and b is the width of the specimen. The effective area of transverse shear stress is the core thickness + half of each face sheet thickness, thus, $\frac{(d+c)}{2} = c + \frac{t_t}{2} + \frac{t_b}{2}$. The sandwich beam deflection for a three-point bend test is as follows:

$$\Delta = \frac{PL^3}{96D} + \frac{PL}{4U} \tag{3.2}$$

Where Δ is total mid-point deflection, D is the panel bending stiffness, U is the panel shear rigidity and L is the panel length. If the facing modulus is known and the top and bottom face sheets are identical and symmetric, the panel flexural rigidity is as follows:

$$D = 2\frac{E_f t_f^3}{12} + \frac{E_f t_f d^2}{2} + \frac{E_c t_c^3}{12} = 2D_f + D_o + D_c \tag{3.3}$$

Where E_f and E_c are the facing and core moduli, t_f and t_c are the facing and core thicknesses, and d is the distance between the centroids of the faces (d=$\frac{(t_f+t_c)}{2}+c$). D_f,D_o, and D_c are the bending stiffness's of the faces about their individual axes, faces about the middle axis, and core, respectively.[23] The panel shear rigidity is as follows:

$$U = \frac{G_c(d+c)^2 b}{4c} \tag{3.4}$$

Where $G_c$the core shear modulus is calculated using Eq. 3.5.

$$G_c = \frac{E_c}{2(1+v_{c12})} \tag{3.5}$$

In the case of uneven face thickness' a different approach based on the assumptions in section 3, can be utilized to obtain bending and shear stiffness'.

$$EI = bD = \sum_{i=1}^{n} E_i I_{total,part,i} \tag{3.6}$$

$$GA = U = \sum_{i=1}^{m} G_{core} A_{total,core,i} \tag{3.7}$$

Where n is the total number of sub sections; m is the number of core subsections; $I_{total,part,i}$ is the moment of inertia of the ith subsection about the neutral axis of the whole structure and $A_{total,core,i}$ is the are of the core ith subsection.

In order to obtain $I_{total,part,i}$ the centre of gravity of the whole section is needed and is calculated as follows:

$$C_g = \frac{\sum A_i y_{c,i}}{A_{total}} \tag{3.8}$$

Where $y_{c,i}$is the distance from the bottom of the whole section to subsection centre. The moment of inertia of the whole section is equal to sum of the subsections about their own axis and using the parallel axis theorem.

$$I_i = \frac{1}{12} bh^3 \text{ (Beam Element)} \tag{3.9}$$

$$I_i = \frac{1}{12(1-v_{12}^2)} bh^3 \text{ (Plate Element)} \tag{3.10}$$

$$I_{total,part,i} = \sum_i I_i + \sum_i (y_i - C_g)^2 A_i \tag{3.11}$$

By substituting Eq. 3.5-11 into 3.2 theoretical midspan beam deflection can be estimated. The above equations assume symmetry about the panels' middle axis and thus deflection to the extensional bending coupling or B matrix is assumed to be 0. As the top to bottom face sheet thickness becomes too small or large, the extensional-bending coupling cannot be neglected and can be calculated as follows. Starting with the three dimensional thermoelastic strain-stress relation for anisotropic material, this is given as:

$$\varepsilon_i = S_{ij}\, \sigma_{ij} \tag{3.7}$$

Where the total strain, ε_i , is the sum of the mechanical strain, $S_{ij}\, \sigma_{ij}$. For an orthotropic lamina, the plane stresses in the principle material orientation is defined below by Eq.3.8

$$\begin{Bmatrix} \sigma_1 \\ \sigma_2 \\ \sigma_3 \end{Bmatrix} = \begin{bmatrix} Q_{11} & Q_{12} & 0 \\ Q_{11} & Q_{22} & 0 \\ 0 & 0 & Q_{66} \end{bmatrix} \begin{Bmatrix} \epsilon_1 \\ \epsilon_2 \\ \gamma_{12} \end{Bmatrix} \tag{3.8}$$

In the above equation, Q_{ij} represents the reduced stiffness matrix, where the components of Q_{ij} are defined below in Eq. 3.9, 3.10, 3.11, and 3.12.

$$Q_{11} = \frac{E_1}{1 - v_{12}\, v_{21}} \tag{3.9}$$

$$Q_{22} = \frac{E_2}{1 - v_{12}\, v_{21}} \tag{3.10}$$

$$Q_{12} = \frac{E_1\, v_{21}}{1 - v_{12}\, v_{21}} = \frac{E_2 v_{12}}{1 - v_{12}\, v_{21}} \tag{3.11}$$

$$Q_{66} = G_{12} \tag{3.12}$$

Using the above Eq 3.9-3.12, The magnitudes of the extension in each respective principle material orientation under normal stress are applied in an orthogonal orientation. An orthotropic

material has a different response to loading depending on the orientation, and different moduli and Poisson's ratios exist in the principle material orientation.

$$A_{ij} = \sum_{k=1}^{\infty} \left(\bar{Q}_{ij}\right)_k (h_k - h_{k-1}) \tag{3.13}$$

A_{ij} in Equation 3.13 represents the extensional stiffness.

$$2B_{ij} = \sum_{k=1}^{\infty} \left(\bar{Q}_{ij}\right)_k ({h^2}_k - {h^2}_{k-1}) \tag{3.14}$$

B_{ij} in Equation 3.14 represents the coupling stiffness, for simplicity the panels in this thesis are close to symmetric and thus, B_{ij} will be assumed to equal to zero.

$$D_{ij} = \frac{1}{3}\sum_{k=1}^{\infty} \left(\bar{Q}_{ij}\right)_k ({h^3}_k - {h^3}_{k-1}) \tag{3.15}$$

D_{ij} in Equation 3.15 represents the bending stiffness.

3.2 Honeycomb Mechanics

The stiffness and strength properties of the honeycomb core are required to evaluate the failure mechanisms of the honeycomb panel. Poisson's ratio of honeycomb which is required for failure analysis is defined as v_{13} or v_{23} for in-plane Poisson strains due to out-of plane loading in the three orientation. The elastic modulus of honeycomb in the out-of plane three directions is given by the rule of mixtures expression defined as given in Equation 3.16.

$$\frac{E_3}{E_s} = \frac{\rho_c}{\rho_s} \tag{3.16}$$

Where subscripts, c and s, represent core as a whole and constituent material making up the core. The failure of honeycomb occurs due to the fracture of the cell walls under a buckling load. Using the rule of mixtures, one can estimate the relevant collapse strength and stress. Common honeycomb is

created as arrayed hexagonal cells. The prediction of collapse strength, shear strength, and shear moduli can be found using Equations 3.17, 3.18, 3.19, 3.20 below.[19]

$$\sigma_c = 3.25\sigma_s \left(\frac{\rho_c}{\rho_s}\right)^{5/3} \tag{3.17}$$

$$\frac{\tau_{31}}{E_s} = 1.7 \left(\frac{\rho_c}{\rho_s}\right)^{3} \tag{3.18}$$

$$\frac{G_{31}}{G_s} = 0.375 \left(\frac{\rho_c}{\rho_s}\right) \tag{3.19}$$

$$\frac{G_{32}}{G_s} = 0.6 \left(\frac{\rho_c}{\rho_s}\right) \tag{3.20}$$

Where E_3 is the compressive Young's modulus for the core and ρ_c and ρ_s are the density of the core and face sheet, respectively. The anisotropy of the honeycomb leads to a dependence of skin failure loads on the orientation of the honeycomb. Similarly, the shear strength of the core depends on the orientation of the cells within the honeycomb. See Table 5.2 for values produced by Eq. (3.17)-(3.20).[19]

3.3 Failure Mode Analysis

Currently, a reliable ultimate failure criterion has only been partially successful. The issue is that sandwich structures generally fail by series of local failures at internal stress concentrations such as loading points or defects which in turn leads to global failure and so must be accounted. The effect of these localized failures for the most part is greater in larger sections, where the face sheets are comparable small when compared to the core. Manufacturing process's play a key role on the structures efficiency, see section 2.

Understanding failure modes allow the designer to ensure that no component of their composite sandwich is over-designed when compared to other components and can assist in weight optimization with respect to the static test requirements. Subjecting composite sandwiches to 3-point bending results in multiple types of failures, such as face fracture, face wrinkling, core shear yield, core compressive yield, and interfacial failure between the core and the faces.[23] The failure mode analysis in this report developed on by the works of Triantafillou and Gibson[26] will investigate face failure, core compressive yield, and core shear yield, which are the three most typical failures from the experimentation. Sufficient analysis of sandwich structures require a thorough knowledge of the mechanical behavior of the face sheets and the core. The face sheets act in a relatively predictable manner, as modelled by laminated plate theory. The mechanical modelling of the core is not so straight forward, particularly for honeycomb. The addition of core behavior of core to shear loading from the face sheets or loading perpendicular to the face sheet planes is needed. This response is affected by the core relative density which is a ratio of the core density as a whole to the density of the materials making up the core.

Considering a constant core and face sheet thickness and constant face sheet orientation, analysis was then done with varying core angles. This resulted in varying core Young's moduli and core shear yield strength with respect to core angle of the honeycomb. Using this, bending stiffness and flexural rigidity of the beam where then calculated at specific core angles using Eq. 3.4.[23] The bending stiffness of the face about its individual axis was beneficial in solving for the core's shear and compressive stress and the face's compressive stress as well as the failure loads per unit width due to the three types of failures mentioned earlier. The local bending moment and deflection could also be calculated using this value.

The face compressive stress in the beam is calculated using the equation below:

$$\sigma_{f,total} = \sigma_{f,overall} + \sigma_{f,local} = \frac{PL}{4t_f d} + \frac{6P}{4t_f^2 \beta} \quad (3.20)$$

Where P is the central load per unit width, L is the length of the beam, and β is a variable that is defined by $\beta = \sqrt[4]{k/4D_f}$ with $k = E_c/t_c$. The β term is dependent on the face bending stiffness defined earlier.

To understand how the beam theoretically should fail due to the five main types of failure mentioned earlier, maximum loads per unit width were calculated for each failure condition using the equations below:

$$P_{max} = \frac{X_f}{((L/4t_f d)+(6/4t_f^2 \beta))} \quad \text{(Face Compressive Failure)} \quad (3.21)$$

$$P_{max} = 2S_c d \quad \text{(Core Shear Yield)} \quad (3.22)$$

$$P_{max} = \frac{2X_c}{\beta} \quad \text{(Core Compressive Yield)} \quad (3.23)$$

$$P_{max} = \frac{t_f(\pi^2 E_f c d)^{\frac{1}{3}}}{3L} \quad \text{(Indentation with Face Elastic Buckling)} \quad (3.24)$$

$$P_{max} = \frac{4t_f d X_f}{L} \quad \text{(Micro buckling)} \quad (3.25)$$

Where X_f, S_c, and X_c are the the face compressive strength, core shear yield strength, and core compressive yield strength, respectively. This report investigates the effects of changing core angle, so the Young's modulus of the core and the core shear yield strength will be varied with the varying core angle. Eq. 3.21 above varies with core angle due to the core shear yield strength value and Eq. 3.21-23 vary due to the β term, which is dependent on the core Young's modulus value. Micro buckling, is not an

active constraint, when $\frac{X_f}{X_c}$ is large or L is small, in which case Eq 3.22-23 become the active constraints as is the case with the materials in this thesis. Indentation with face elastic buckling only tends to become active when face sheet thickness is much less than core thickness. The inclusion of the indentation failure mode departs from classical theory due to the inclusion of plastic collapse of the core material and a strong interaction of between the face loading and displacement of the core. These five maximum failure loads where plotted against each other, shown in Figure 3.1, to show where the beam will likely fail due to the five failure conditions with respect to core orientation mentioned earlier.

From Figure 3.1, the yielding loads for the three types of failures using experimental mechanical properties can be seen. For a core angle of 0°-30°, the sandwich will yield due to core compression and for a core angle of 30°-90°, the sandwich will yield due to shearing of the core. According to the plot, the

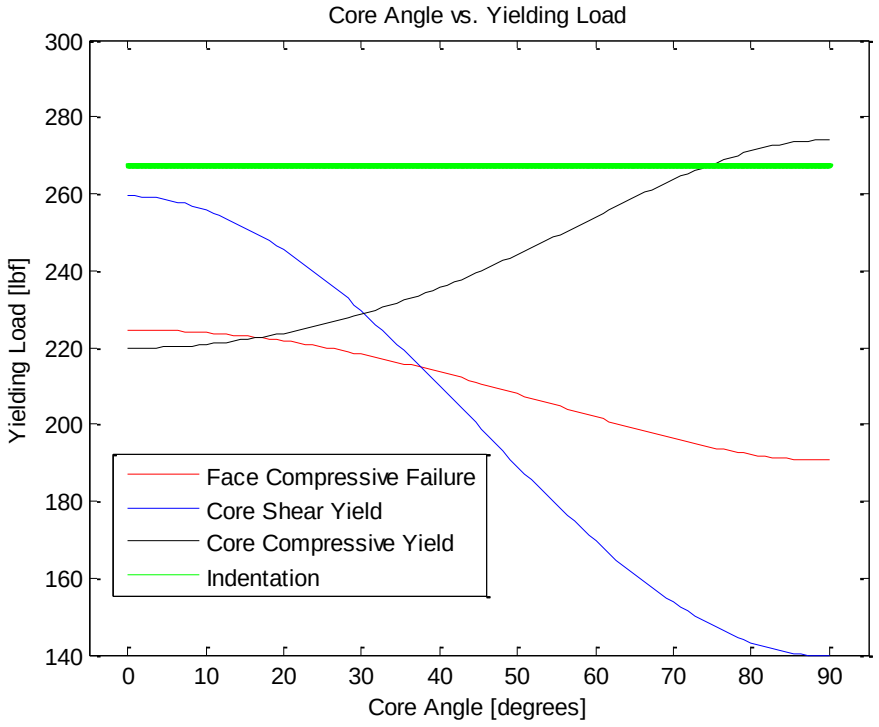

Figure 3.1. Core angle vs. yielding loads for three main types of failure

sandwich will fail due to compression of the face after yielding; however, this does not take into account

failure of the beam due to core shear or compression because these values were not able to be experimentally gathered for honeycomb.

These failure mode loads can be manipulated to estimate failure loads for specimens with varying face sheet thicknesses, but can be used only as a guide because all the above equations are simplified with the assumption of symmetric panels with face sheet to core thickness ratio's less than 0.1, particularly with the core shear failure mode. The analytical model for failure due to core shear slightly under predicts failure load due to the exclusion of the effects the face sheets have on bending strength, Thus for higher face sheet thickness's (>0.036) core shear estimates become less accurate. For specimens used in this thesis, specimens with a total layer count over 6 layers violates the face sheet to core thickness ratio of less than 0.1, and thus predicted failure loads should be taken strictly as a guide to estimate which failure mode will occur first. Figure 3.2 shows the failure loads for specimens with

constant bottom face sheet thickness set at 0.012. All other configuration maps can be viewed in the appendix.

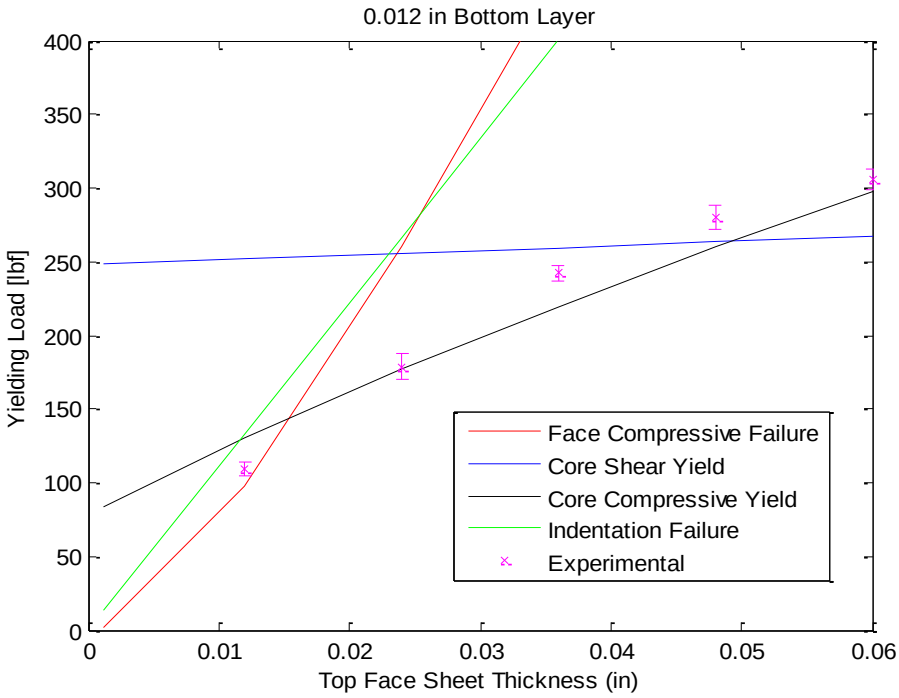

Figure 3.2. Failure Loads for Specimens with Varying Top Face Sheet thickness and Bottom Layer Constant at 0.012 in

The main focus of this analysis, however, was the creation of static failure mode maps. To do this, transition equations between the failure modes had to be used to create a visual of how they interact with each other. The three equations used are shown below:

$$\frac{L^*}{2s^*\sigma^*t^*} + \frac{3(1+t^*)}{s^*\sigma^*t^*}\sqrt[4]{\frac{E^*}{3t^*}} = 1 \quad (Face\ and Core\ Shear) \tag{3.25}$$

$$\frac{L^*}{2\sigma^*(1+t^*)}\sqrt[4]{\frac{E^*}{3t^*}} + \frac{1}{\sigma^*}\sqrt{\frac{3E^*}{t^*}} = 1 \quad (Face\ and\ Core\ Compressive) \tag{3.26}$$

$$\frac{s^*t^*}{(1+t^*)}\sqrt[4]{\frac{E^*}{3t^*}} = 1 \quad (Core\ Shear\ and\ Core\ Compressive) \tag{3.27}$$

These three equations use non-dimensional parameters that are defined as $t^* = t_f/t_c, L^* = L/t_c, E^* = E_f/E_c, \sigma^* = X_f/X_c, s^* = X_c/S_c$. Solving these three equations for t^* and L^* allowed for a plot

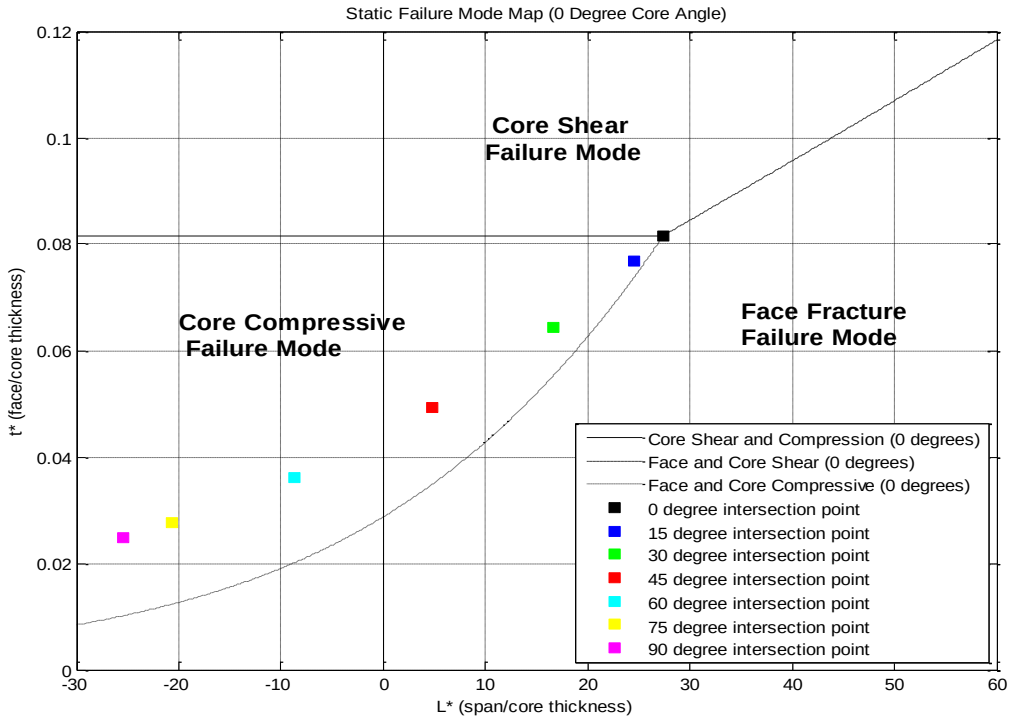

Figure 3.3. Static failure mode map for 0 degree core angle, where s* = 2.154 E* = 350.638 σ*= 191.428

of L^* vs. t^* to be created. Figure 3.3 shows this plot and describes the areas where each failure will occur. It can be seen from the plot that the failure modes occur between the transition lines that account for that certain failure mode. For example, the core compressive failure mode occurs between the core shear and core compressive line and the face and core compressive line. The interaction points show, in general, that as the core changes from 0° to 90°, the core compressive failure mode decreases while the other modes increase. For example, for a constant span length, the core thickness would have to be increased and/or the face thickness would have to be decreased to create a better likelihood of core compressive failure. A decrease in core thickness would be more likely to result in face fracture failure and an increase in face thickness would be more likely to result in core shear failure.

Understanding how this plot works allows for optimization of beam design depending on type of failure desired and beam dimensions. Failure mode maps for the other six core angles can be seen in the Appendix section at the end of this report. Our experimental specimens had $t^* = 0.0640$ and $L^* = 16$ to ensure failure was due to core compression or shear only. Core shear and compression failure is needed to determine the effect of core ribbon orientation on the composite sandwich. Had experimental parameters been chosen that failure occurred in the face fracture regime; there would be little difference in failure loads.

3.4 Theoretical Midspan Deflections of Varying Core Ribbon Orientation

Using Classical beam and plate theory from section 3.1, theoretical midpsan deflections at 100 lbf applied load were calculated for test specimens shown in table 3.1

Table 3.1. Beam and Plate Theory midspan deflections for varying core angle specimens at 100 lbf

Core Orientation	Beam Theory Deflection (in)	Plate Theory Deflection (in)	Difference (%)
0	0.03517	0.0350	0.403
15	0.035927	0.0358	0.316
30	0.038264	0.0382	0.169
45	0.042303	0.0423	0.074
60	0.047805	0.0478	0.031
75	.0532900	0.0533	0.015
90	0.055746	0.0577	0.012

As can be seen these specimens have little difference between beam and plate theory. The specimens' width is comparatively small compared to its length and so falls under the beam theory regime.

3.5 Theoretical Midspan Deflections of Varying Face Sheet Thickness's

Using Classical beam and plate theory from section 3.1, theoretical midpsan deflections at 100 lbf applied load were calculated for test specimens shown in tables 3.2-4.

Table 3.2. Beam Theory midspan deflections for varying Face sheet thickness specimens at 100 lbf

		Top Face Sheet Thickness (in)				
		0.012 (1 Layer)	**0.024 (2 Layers)**	**0.036 (3 Layers)**	**0.048 (4 Layers)**	**0.06 (5 Layers)**
Bottom Face Sheet Thickness (in)	**0.012 (1 Layer)**	0.025	0.0202	0.0177	0.0161	0.0150
	0.024 (2 Layers)	0.0202	0.0176	0.0159	0.0147	0.0138
	0.036 (3 Layers)	0.0177	0.0159	0.0147	00137	0.0130
	0.048 (4 Layers)	0.0161	0.0147	0.0137	0.0130	0.0123
	0.06 (5 Layers)	0.0150	0.0138	0.0130	0.0123	0.0117

Table 3.3 Plate Theory deflections for varying Face sheet thickness specimens at 100 lbf

		Top Face Sheet Thickness (in)				
		0.012 (1 Layer)	**0.024 (2 Layers)**	**0.036 (3 Layers)**	**0.048 (4 Layers)**	**0.06 (5 Layers)**
Bottom Face Sheet Thickness (in)	**0.012 (1 Layer)**	0.0247	0.0201	0.0177	0.0161	0.0149
	0.024 (2 Layers)	0.0201	0.0175	0.0159	0.0147	0.0138
	0.036 (3 Layers)	0.0177	0.0159	0.0146	00137	0.0130
	0.048 (4 Layers)	0.0161	0.0147	0.0137	0.0129	0.0123
	0.06 (5 Layers)	0.0149	0.0138	0.0130	0.0123	0.0117

Table 3.4 Differences between Beam and Plate Theory midspan deflections for varying Face sheet thickness specimens at 100 lbf

		Top Face Sheet Thickness (in)				
		0.012 (1 Layer)	**0.024 (2 Layers)**	**0.036 (3 Layers)**	**0.048 (4 Layers)**	**0.06 (5 Layers)**
Bottom Face Sheet Thickness (in)	**0.012 (1 Layer)**	1.24 %	0.66 %	0.42 %	0.29 %	0.22 %
	0.024 (2 Layers)	0.66 %	0.40 %	0.27 %	0.20 %	0.15 %
	0.036 (3 Layers)	0.42 %	0.27 %	0.19 %	0.14 %	0.11 %
	0.048 (4 Layers)	0.29 %	0.19 %	0.14 %	0.11 %	0.09 %
	0.06 (5 Layers)	0.21 %	0.15 %	0.11 %	0.09 %	0.07 %

Again we can see that there is little difference between theoretical beam and plate theory midpsan deflections. The specimens used for varying face sheet thickness were double the width than the specimens manufactured for varying core orientation giving a width to span ratio of 0.5. As the width increases the structure moves away from being classified as a beam and closer into the plate regime. The Plate theory deflections shall be used for later comparisons with experimental and numerical data.

3.6 Bending Stiffness and Strength Optimization

Sandwich construction involves mating high modulus face sheets with thick, and relatively light core. Through design maximum stiffness and strength can be obtained through minimum weight combinations. Optimization of face sheet to core thickness ratios are crucial in minimizing cost in design. Design optimization of sandwich structures with respect to weight is presented by Froud.[47] Froud optimizes face sheet to core weight analytically for maximizing bending stiffness and bending strength. Johnson and Sims[48] reviewed the method for optimum design with respect to minimum weight, improving the design of sandwich construction.

3.6.1 Bending Stiffness

By using the equation for flexural rigidity, derived from equations 3.9-12, the main contribution to bending resistance is the middle term and may be written as:

$$D = E_f(t_b + t_t)\left(\frac{\left(d + \frac{t_b + t_t}{2}\right)}{2}\right)^2$$

As well as the combined weight of the face sheets and core given by:

$$W = \rho_c d + t_t\rho_f + t_b\rho_f \tag{3.28}$$

Where ρ_c and ρ_f are the densities of the core and face sheet materials respectively.

$$\text{If } \varphi = \frac{\rho_c d}{W} \text{ and } (1 - \varphi) = \frac{\rho_f(t_t + t_b)}{W}$$

t_t, t_b and c can be expressed in terms of φ. The maximum flexural rigidity will occur when

$$\frac{dD}{d\varphi} = 0$$

Solving for φ the minimum and maximum values are obtained.

$$\varphi_{minimum} = \frac{\rho_c}{\rho_c - 2\rho_f} \tag{3.29}$$

$$\varphi_{maximum} = \frac{3\rho_c - 4\rho_f}{3\rho_c - 6\rho_f} \tag{3.30}$$

For the materials used in this thesis,

$$\varphi_{minimum} = 0$$

$$\varphi_{maximum} = 0.658$$

Which means that the minimum flexural rigidity occurs when there is no core present, which makes sense and the maximum theoretical flexural rigidity occurs when

$$\frac{\rho_c d}{\rho_c d + 2\rho_f t} = 0.658 \tag{3.31}$$

Substituting the material values for this thesis,

$$total\ face\ thickness = \ 0.04\ in = 3.33\ layers$$

For a symmetrical sandwich panel this would mean a sandwich structure with 1.665 layers on the top and bottom face sheet. Due to geometric constraint on the carbon fiber, this is not possible. Thus the optimum sandwich configuration lies somewhere between the 2/1 and 2/2 configuration. If the stiffness is divided by the weight and then normalized to the minimum value, the optimum stiffness to weight sandwich structure can be obtained.

3.6.2 Bending Strength

Using Eq. 3.21-25, theoretical maximum loads for all failure modes can be determined, for all face structure combinations. By dividing the minimum predicted failure load by the structures weight and applying geometric constraints being a minimum of 1 layer for top and bottom face sheets, and a maximum of 6 layers for top and bottom face sheets, the optimal bending strength with respect to minimum weight can be determined shown figure 3.4

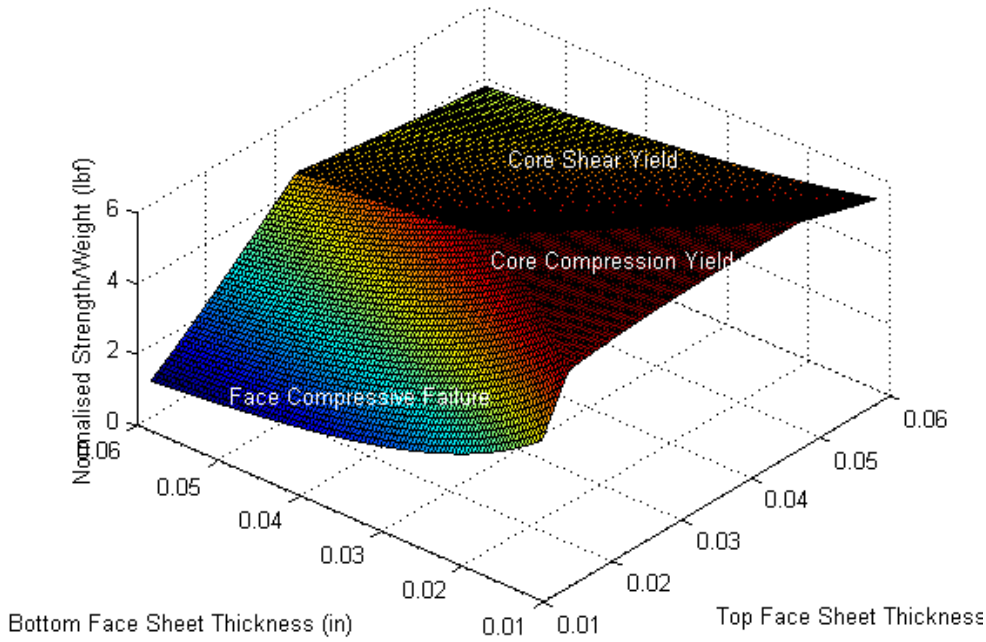

Figure 3.4. Normalized strength to weight ratio with respect to top and bottom face sheet thickness.

The theoretical total face sheet thickness for optimal bending stiffness with respect to minimum weight was calculated to be 0.05698 in (4.741 layers). Examples of calculations can be viewed in the MATLAB code section of the appendix.

4.0 Experimental Results, Analysis and Discussion

This section presents the results of the experimental tests of static 3-point bending specimens.

For each series of tests, the average value, standard deviation and coefficient of variation, %, were calculated for ultimate strength:

$$\bar{x} = \frac{\sum_{i-1}^{n} X_i}{n} \tag{4.1}$$

$$S_{n-1} = \sqrt{\frac{\sum_{i-1}^{n} x_i^2 - n\overline{x^2}}{n-1}} \tag{4.2}$$

$$CV = 100 * \frac{S_{n-1}}{x} \tag{4.3}$$

Where x is sample mean (average), S_{n-1} is the sample standard deviation, CV is the sample coefficient of variation, %, n is the number of tested specimens, and X_i is the measured or derived property.

4.1 Toe Compensation

In a typical force versus displacement curve (see Figure. 4.1) there is a toe region, AC, which does not represent a property of the material. It is caused by the take up of slack and alignment of the test

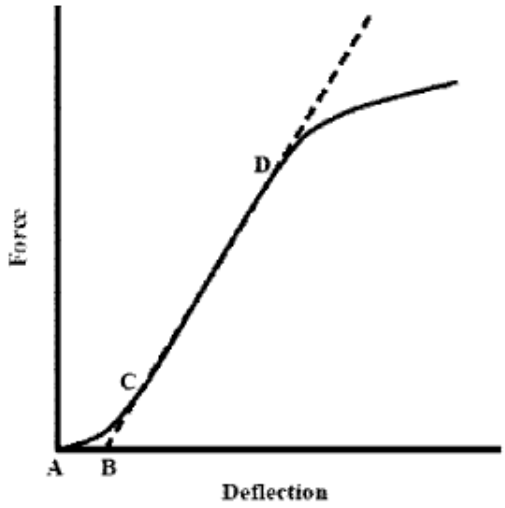

Figure 4.1. Sandwich Material with Hookean Response Region

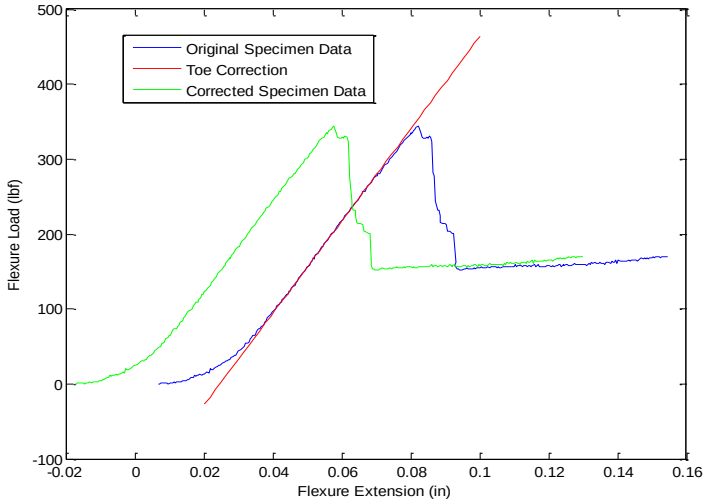

Figure 4.2. Toe correction Example

specimen. To extract correct data, the AC portion must be compensated to get the correct zero displacement point. By continuing the linear Hookean region (CD) of the curve will give the correct zero displacement point (B) where $\delta = 0.0$ and all displacements are then measured from that point (B).

4.2 Experimental Analysis of sandwiches with varying core orientation

For Sandwich structure optimization, it is critical to determine the effects of varying the honeycomb core orientation. Varying core orientation effects ultimate core strength, sandwich stiffness, sandwich ultimate load at failure, and sandwich extension at failure. For the purposes of this paper, the longitudinal orientation of the honeycomb shall be considered 0 degrees orientation and the transverse orientation being 90 degrees of orientation. Table 3.1 shows how varying the orientation of the honeycomb within the composite sandwich affects the structural properties of the sandwich when subjected to 3-point bending.

Table 4.1. Effects of core angle on composite sandwich structural properties

Core Orientation	Ultimate Load (lbf)	D (lbf/in^3)	U (lbf)	G (lbf/in^2)	Extension at failure (in)	Core Shear Ultimate Stress (psi)
0	301.61 ±5.051	3.725e4	6.49e3	10.2e3	0.1016 ±0.0281	262.27 ±4.392
15	274.9 ±10.00	3.7243e4	6.29e3	9.87e3	0.1007 ±0.0032	237.80 ±8.65
30	264.71 ±5.77	3.7213e4	5.73e3	9e3	0.1042 ±0.000286	228.86 ±4.984
45	248.16 ±9.09	3.7176e4	4.96e3	7.8e3	0.1170 ±0.00052	214.67 ±7.867
60	246.02 ±4.29	3.7142e4	4.2e3	6.6e3	0.1336 ±0.000517	213.09 ± 3.72

75	238.13 ±5.10	3.7119e4	3.64e3	5.72e3	0.1425 ±0.000213	207.19 ±4.44
90	240.73 ±9.23	3.7112e4	3.44e3	5.4e3	0.1450 ±0.000269	205.93 ±7.897

The figures produced below present the core orientation on the horizontal axis while the vertical axis is varying from the maximum extension at failure, maximum facing stress, and maximum force. Each figure's data was found to represent a sinusoidal curve varying over the orientation of the core.

In Figure 4.3, the left vertical axis shows the Failure Load with right vertical axis showing the Failure Extension. The maximum extension at a given load occurs when the core is in the transverse position which is defined as 90° from the longitudinal core ribbon orientation.

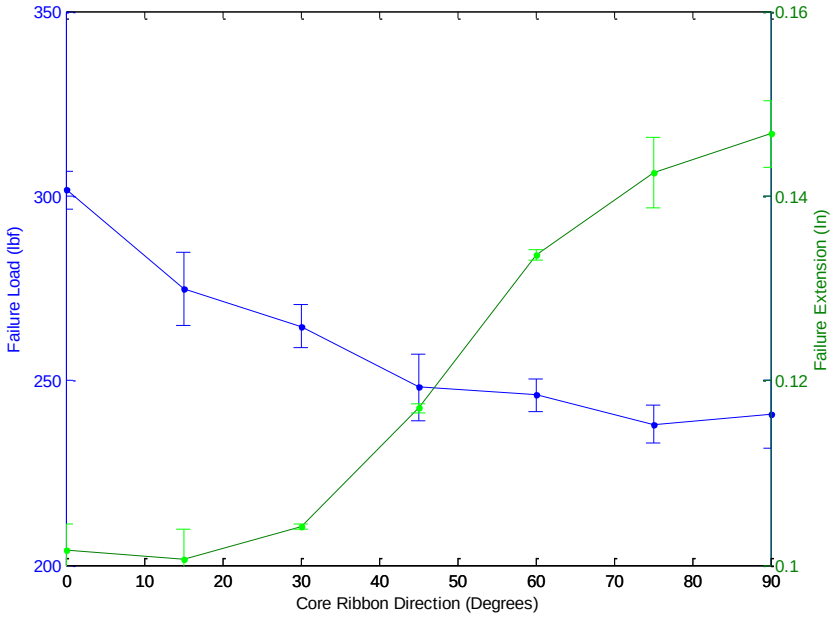

Figure 4.3. Failure Load and Extension vs core orientation

The maximum force that the specimen can withhold before failure occurs at approximately 300 lbf when the core is in the longitudinal orientation. Similar to the maximum facing stress plot, the trend follows a sinusoidal curve. The minimum force occurs at the transverse position of 90°, which is

approximately 240 lbf. The reason for this variation in maximum load with core ribbon value is due to the fact that the longitudinal core ribbon orientation has a much higher Young's modulus value than the transverse orientation. Failure, again, is occurring in the core so this variation in the longitudinal and transverse Young's moduli directly correlate to the variation in failure load values. This lower value of force indicates that depending on the application, the ideal core orientation for minimal extension and higher loading is the longitudinal 0° orientation. If more extension is desired in the application with lower stress, then the transverse core orientation is ideal. The most compliant core ribbon orientation is the transverse orientation, at 90°, where the max extension value in inches is approximately 0.145. Whereas, the stiffest ribbon orientation is at 0°, or the longitudinal orientation, where the smallest maximum extension occurs and is approximately 0.1 inches. This lower value of extension shows that the longitudinal orientation of core has a higher flexural rigidity than the transverse orientation.

In Figure 4.4, the vertical axis represents the maximum facing stress of the specimens at their failure loads. These values were calculated from Eq. 3.2, which is a function strictly of the load. The maximum facing stress occurs when the core is in the longitudinal orientation and the facing stresses vary with core angle, which shows that the failure is occurring in the core. If failure was to occur within the face sheets, the maximum facing stress values would be roughly the same for varying core angles due to the fact that the structure of the faces does not change between specimens.

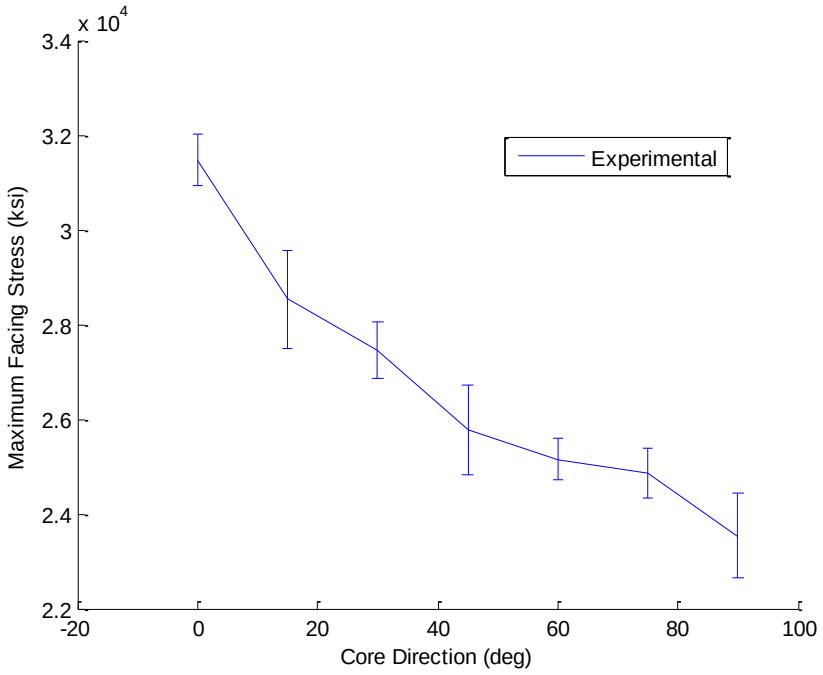

Figure 4.4. Theoretical maximum facing stress at failure vs. core orientation

Figure 4.5 shows the normalized stiffness with respect to core ribbon orientation.

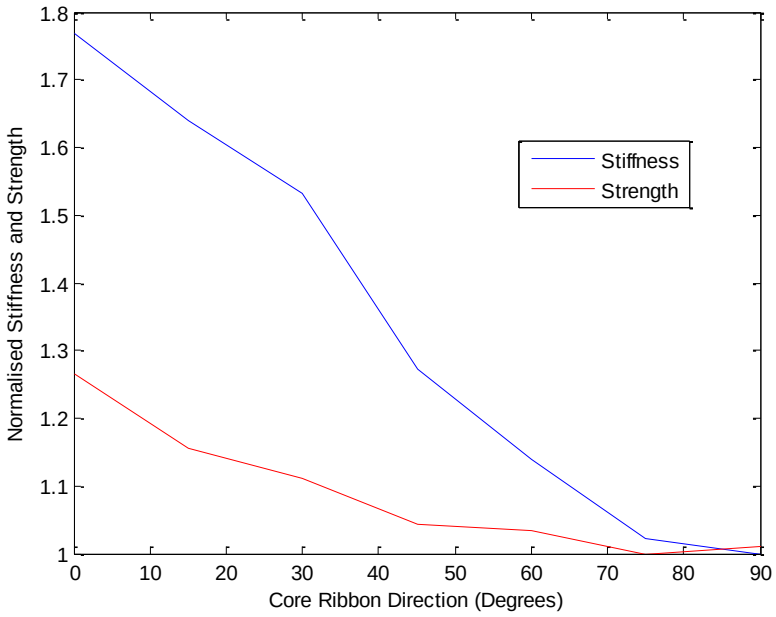

Figure 4.5. Normalised Stiffness and Strength with respect to Core Ribbon Orientation

As can be seen the 0^{o} degree core ribbon orientation specimen produced the stiffest behavior with approximately 80% increase in stiffness from the 90^{o} degree core ribbon orientation. This is due to stiffness being a function of Young's moduli and the longitudinal Young's moduli of the honeycomb is twice that of its transverse orientation. The bending strength of the specimen decreased with the increase of core direction.

Table 4.2. Theoretical and Experimental mid-span Deflection comparison with respect to Core Ribbon Orientation at 100lb Load

Core Ribbon Orientation (Degrees)	Theoretical Deflection at 100lb (in)	Experimental Deflection at 100lb (in)	Error (%)
0	0.03517	0.0337 ±0.00078	4.179%
15	0.03592	0.0363 ±0.0011	1.058%
30	0.03826	0.038 ±0.0012	0.679%
45	0.0423	0.0453 ±0.0013	7.09%
60	0.04781	0.0486 ±9.13e-4	1.652%
75	0.05329	0.0555 ±0.0022	3.771%
90	0.05575	0.0558 ±0.0019	0.089%

Using a deflection equation that takes into account shear rigidity and bending stiffness values, theoretical deflection values were calculated that compare quite well to experimental values. Typically the deflection due to shear rigidity is significantly lower than the deflection due to bending stiffness so it is often neglected; however, when the core's Young's moduli is significantly lower than face Young's moduli, the deflection due to shear rigidity cannot be neglected. The shear rigidity decreased with a decrease in core Young's moduli, which resulted in an increase in the deflection due to shear rigidity as can be seen with the deflection increase from 0°- 90° core ribbon angle. The slight difference in deflection

values between theoretical and experimental could be due to multiple variables throughout the experiment such as layup quality, material quality, the assumption of 0.012 in per layer varying with layup thickness and/or discrepancies in tolerances within the 3-point bend machine. Fiber volumes for the carbon fiber face sheets were very close to theoretical values, which tells us that the material's resin content is still intact and probably not much of a factor in the deflection error. Overall, however, the low error percentages give numerical proof of a well-designed and executed 3-point bend experiment of the composite sandwiches.

4.3 Experimental Analysis of sandwiches with varying face sheet thicknesses

Three inch wide Specimens with top and bottom face sheet thickness's ranging from 0.012 in to 0.06 in were tested under a three point bend test with a 6 in support span. Deflections and extensions can be seen in the below tables and figures below.

Table 4.3 Experimental Failure Loads for varying Face sheet thickness specimens (lbf)

		Top Face Sheet Thickness (in)				
		0.012 (1 Layer)	**0.024 (2 Layers)**	**0.036 (3 Layers)**	**0.048 (4 Layers)**	**0.06 (5 Layers)**
Bottom Face Sheet Thickness (in)	**0.012 (1 Layer)**	328.11 ±14.74	536.49 ±26.64	726.65 ±17.08	840.122 ±23.72	917.07 ±21.12
	0.024 (2 Layers)	312.82 ±15.48	556.10 ±20.72	730.85 ±7.23	960.04 ±23.43	1050.4 ±13.01
	0.036 (3 Layers)	308.69 ±8.65	530.77 ±8.34	747.91 ±11.07	934.67 ±25.8	1154.7 ±27.68
	0.048 (4 Layers)	326.69 ±18.78	510.00 ±9.91	750.15 ±29.07	987.41 ±58.06	1134.1 ±31.36
	0.06 (5 Layers)	337.72 ±8.18	533.69 ±18.39	835.97 ±25.71	995.21 ±30.99	1166.0 ±43.24

Figure 4.6 shows that adding layers on the bottom face sheet has little to no increase in failure load unless the top face sheet to bottom face sheet ratio was greater than two as indicated by constant top layer counts 4 and 5. Constant top layer count 1, 2 and to an extent 3 show no increase failure load indicating that the top face sheet yield load exceeds bottom face sheet yield load. Figure 4.7 shows the

effect of increasing the top face sheet thickness. A three dimensional representation of the failure loads for all specimen configurations shows the overall behavior of all specimens, with little increase in failure load along constant top face sheet lines and roughly 200 lbf increment increases along constant bottom face sheet lines. Adding a second layer to the top face sheet increases failure load by approximately 64%. Adding a third layer increases failure load by 68% from the two layer specimens. When a fourth layer is added the average failure load increase is slightly less at 56%. A fifth layer results in a smaller increase yet at 43%. Figure 4.7 shows that increasing the top to bottom face sheet ratio past 2.5 results in less of an increase in failure load from previous increments.

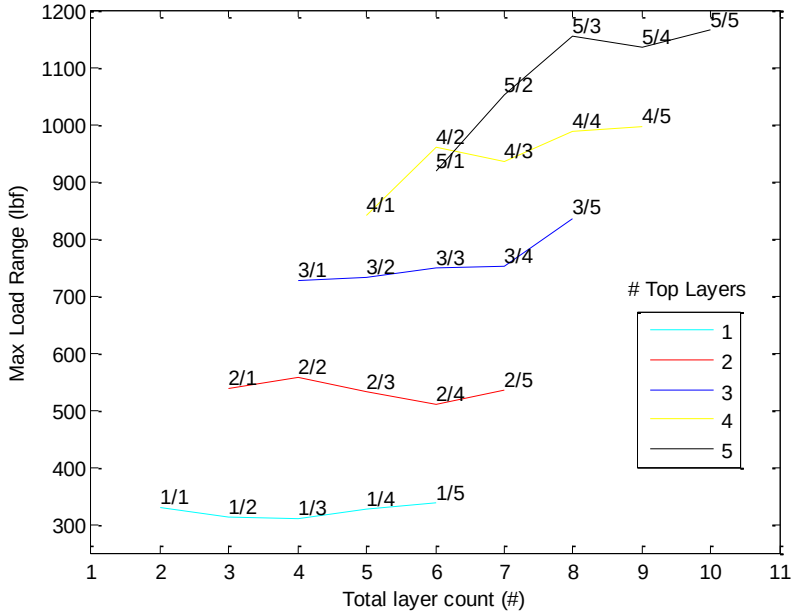

Figure 4.6. Failure Load for varying face sheet thickness, Constant top layer.
#/# indicates Top face layers/Bottom face layers

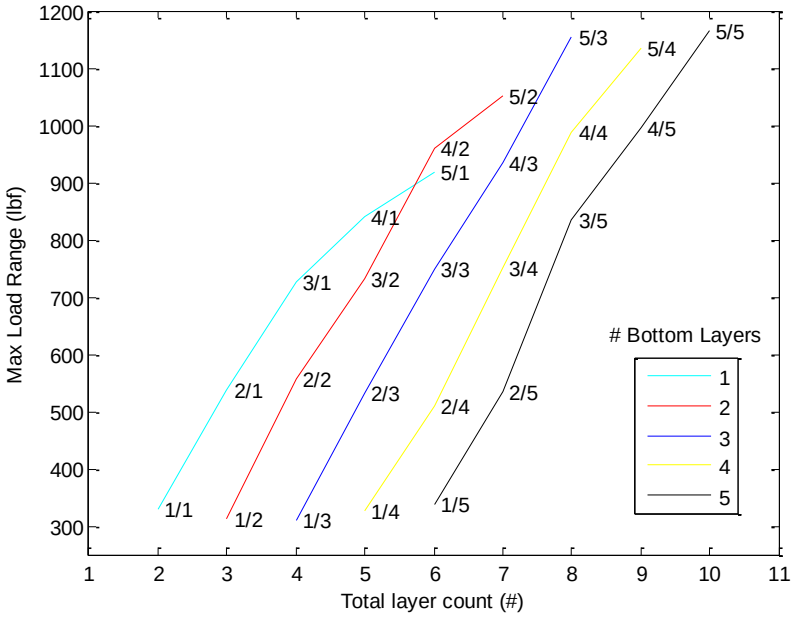

Figure 4.7. Failure Load for varying Face Sheet Thickness, Constant Bottom Layer

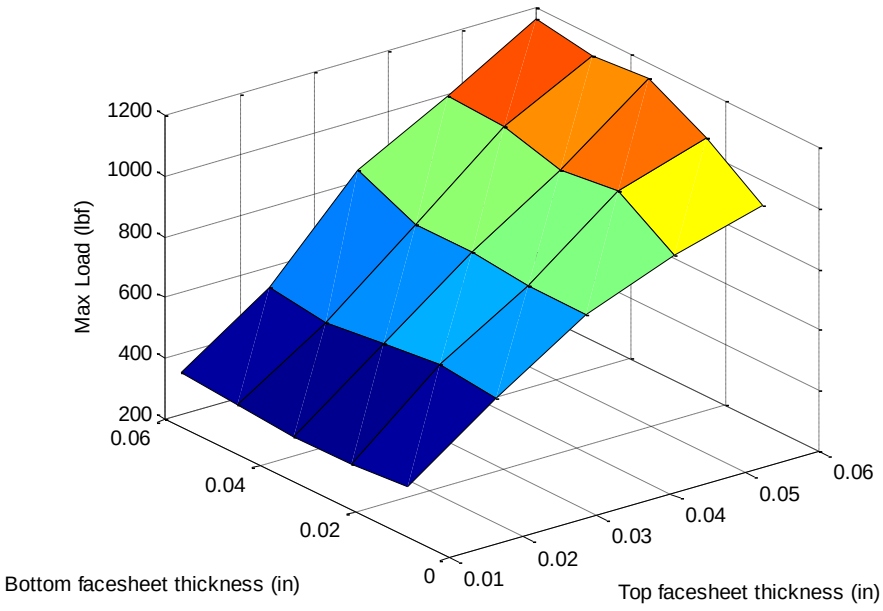

Figure 4.8. Three Dimensional Perspective of Failure Loads for varying Face Sheet Thickness's

Table 4.4 and Figures show the experimental midspan failure extensions. The specimen with 0.012 in top face sheet and 0.06 in bottom face sheet had the minimum failure extension, but with a comparatively large weight and low failure load, it was the least efficient sandwich structure. Increasing bottom face sheet thickness along constant top face sheet lines, decreases maximum failure extension by approximately 30%, but with increased weight. Increasing top face sheet thickness increases Failure extension by approximately 100% from 0.012 to 0.06 along constant bottom face sheet thickness lines. Figure 4.9 shows a three dimensional perspective on the overall effects on failure extension for all specimen configurations.

Table 4.4 Experimental Midspan Failure Extensions varying Face sheet thickness (in)

	Top Face Sheet Thickness (in)					
		0.012 (1 Layer)	**0.024 (2 Layers)**	**0.036 (3 Layers)**	**0.048 (4 Layers)**	**0.06 (5 Layers)**
Bottom Face Sheet Thickness (in)	**0.012 (1 Layer)**	0.0873 ±4.7e-4	0.1081 ±0.1e-3	0.1462 ±3.6e-4	0.1611 ±1.7e-3	0.1644 ±8.7e-4
	0.024 (2 Layers)	0.0715 ±3.9e-4	0.0928 ±5.5e-4	0.1124 ±6.2e-4	0.1313 ±73.e-4	0.1419 ±6.9e-4
	0.036 (3 Layers)	0.0628 ±5.9e-4	0.0804 ±2.3e-4	0.1054 ±3.4e-4	0.1232 ±7.4e-4	0.1436 ±6.2e-4
	0.048 (4 Layers)	0.06061 ±3.3e-4	0.070 ±2.1e-4	0.098 ±4.7e-4	0.1151 ±6.0e-4	0.1296 ±5.5e-4
	0.06 (5 Layers)	0.0606 ±1.7e-4	0.701 3.8e-4	0.0927 ±6.5e-4	0.1093 ±3.6e-4	0.1251 ±3.9e-4

Figure 4.10 shows normalized bending stiffness with respect to minimum weight. Each specimens normalized stiffness value can by divided by its weight to obtain a stiffness to weight ratio, of which each specimen configuration can then be compared. The specimen configurations of 2/2 and 2/1 had the highest stiffness to weight ratio, which agrees with the predicted highest bending stiffness to minimum weight ratio of total layer count 3.33, which lies between the two experimental data points.

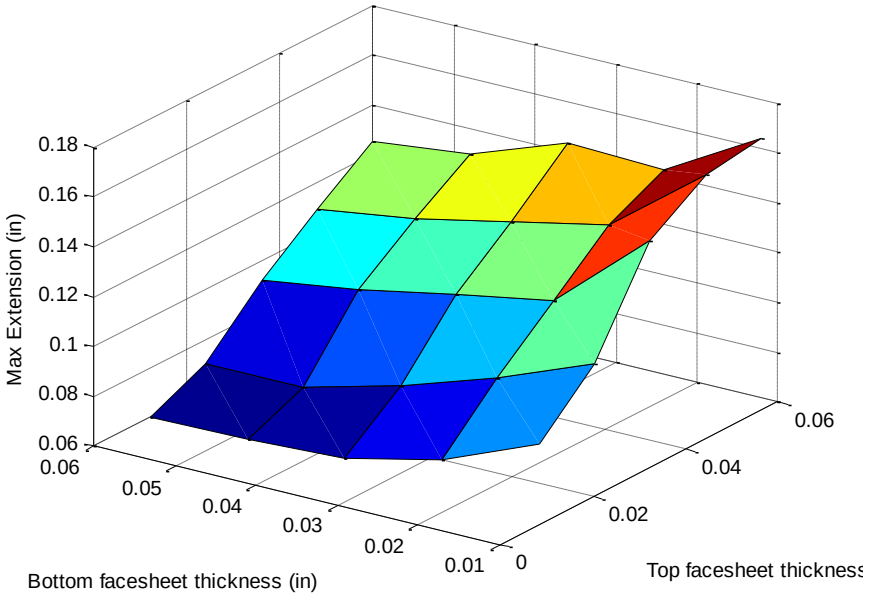

Figure 4.9. Three Dimensional Perspective of Failure Extensions for varying Face Sheet Thickness's

Figure 4.11 depicts the normalized bending strength with respect to minimum weight. The highest bending strength to minimum weight was encountered in the 3/1 (4 total plies) and 4/1 (5 total plies) configurations which agrees well with the theoretically determined optimal total ply count of 4.741 plies. It can be seen that increasing bottom face sheet ply count only hinders bending strength with respect to minimum weight. it can be seen that by moving one layer from the bottom face sheet to the top face sheet, a failure load increase of approximately 60% can be observed for specimens with a total face sheet to core thickness ratio of less than 0.2, Adding layers after that threshold does little to increase maximum failure load.

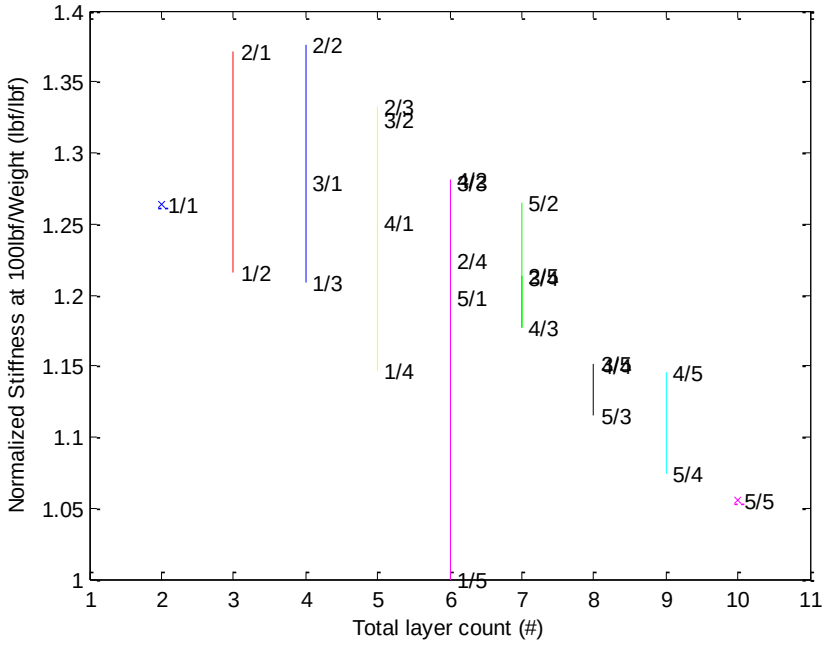

Figure 4.10. Normalized Stiffness by Weight for Varying Face Sheet Thickness
#/# indicates Top face layers/Bottom face layers

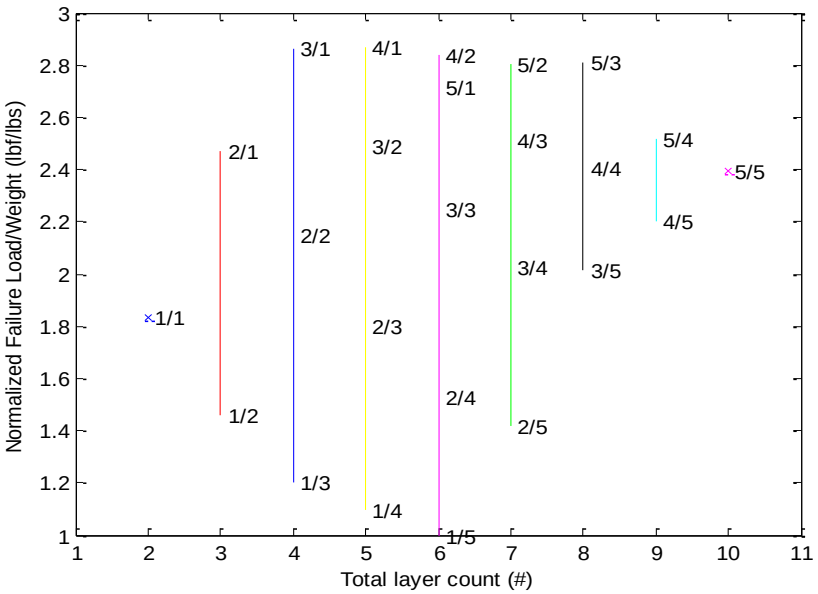

Figure 4.11. Normalized Bending Strength with respect to minimum weight.
#/# indicates Top face layers/Bottom face layers

5.0 FEA Analysis and Results

This section discusses the process to modelling and analyzing the experimentally tested specimens utilizing numerical methods. Finite element analysis has become the prevalent method for analysis of the behaviors of solids, structures and fluid mechanics. Composite materials and structures can be modelled and successfully analyzed in finite element programs.

Finite element analysis (FEA) was performed on the test composite sandwich beam configurations consisting of composite face sheets and honeycomb core to observe the mechanical behaviors of a simply supported composite sandwich plate under static bending tests. In each case the core orientation was adjusted in 15^o increments from 0^o to 90^o to see the effects of core ribbon orientation on the mechanical properties of the composite sandwich as a whole. Implicit finite element analysis was conducted to numerically analyze the bend tests of the test specimens. Equation 5.1 is the governing equation for implicit analysis.

$$F = \delta K \tag{5.1}$$

The finite element code assumes a displacement function which then the stiffness of the structure (K) is solved and resulting forces are then found. The forces are then used in Equation 5.1 to calculate displacements and then are repeated. Implicit methods have the process re-iterated a number of times until a specified tolerance is met between iterations. Each beam was subjected to three point bending with a 100lb force acting on across the 1.5 in width of the upper face of the composite structure. The face sheets were modeled as shell structures whilst the core was modeled as a solid element. A convergence study was performed and a seed size of 0.1 was used for analysis. It was found that the deflection of the structure at 100lb increased from core orientation of 0^o to 90^o in a sinusoidal manner with good agreement with theoretical results.

5.1 Development of FEA Model

The program used in this paper is ABAQUS, which is a program by Dassault Systems. All models were modeled in ABAQUS under three point bending. Each case consists of two structure parts modeled in ABAQUS

- Honeycomb Core
- Composite Face sheets

Each part was defined with an elastic definition, density, and dimension as shown in Table 5.1. All dimensions and numbers were defined in English units. The Mechanical properties shown were found through experimental works conducted under relevant ASTM standards shown in the previous section.

Table 5.1. Mechanical and Part properties of 6367 A280-5H used in ABAQUS Model

Mechanical Property	Value	Mechanical Property	Value
ρ	1.436e-4 lbf-s^2/in^4	G_{12}	6.23e5 psi
E_{11}	12.936e6 psi	$X_C = Y_C$	127.7 psi
E_{22}	12.936e6 psi	$X_T = Y_T$	168.4 psi
v_{12}	0.027	Length	6 in
Part Type	3-D Shell	Width	1.5 - 3 in
Section Type	3-D Shell	Depth	0.012 – 0.06 in

Table 5.2. Mechanical and Part properties of HRH-10-1/8-5 Honeycomb used in ABAQUS Model

Mechanical Property	Value	Mechanical Property	Value
ρ	7.5e-6 lbf-s^2/in^4	G_{12}	10200 psi
E_{11}	3.6793e4 psi	G_{21}	5400 psi
E_{22}	1.5242e4 psi	G_{13}	14151.15 psi
E_{33}	3.7e4 psi	G_{23}	8536.73
v_{12}	0.8036	Z_C	700 psi
V_{21}	0.4114	τ_{12} yield	325 psi
$V_{23} = V_{13}$	0.3	τ_{21} yield	175 psi
Length	6 in	Part Type	3-D Solid
Width	1.5 - 3 in	Section Type	3-D Solid
Height	0.375 in	---	---

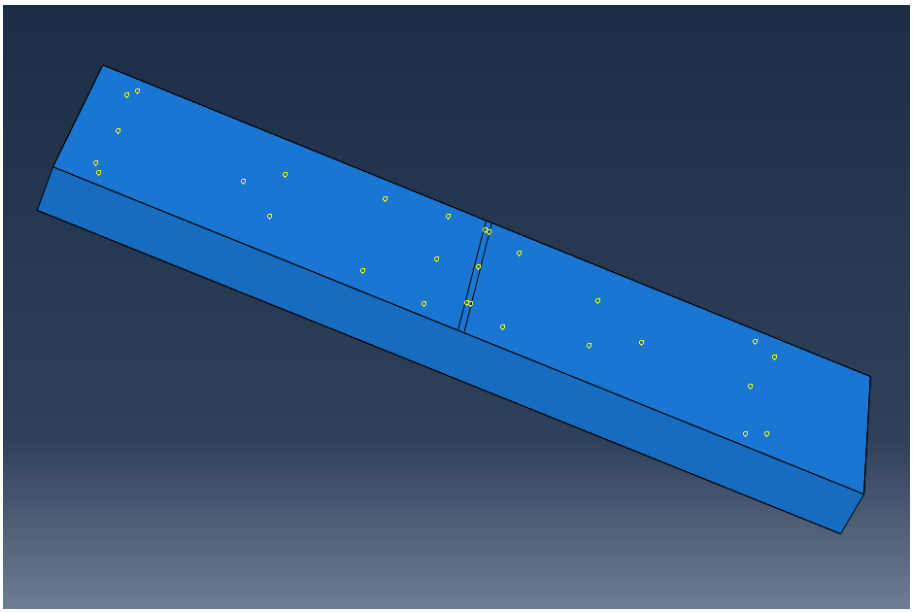

Figure 5.1. FEA Tie constraints on top and bottom shell elements.

The standard units were also English, but the pressures were measured in pounds per square inch (psi). The composite beam was modeled as two separate parts, the core as a 3-D deformable solid and the face sheets as a 3-D shell. A shell section was created with the carbon fiber face sheets with the required shell thickness defined as the face sheet thickness and a solid section was created with the honeycomb core from the mechanical properties shown in Table 5.2 above. The face sheets were constructed as two individual parts and in order to simulate the layers through the specified thickness of the face sheet, 9 integration points were stacked vertically from the mid-plane of the element and define the thickness of each layer within the laminate. Laminated shell theory was applied for the assumption that a uniform constant shear strain through the thickness of the shell occurs. If this correction is not applied, the stiffness of the shell can be highly inaccurate if drastic differences in elastic constants between ply are present, especially in sandwich type shells.

In the assembly the instances were translated to their respective coordinates before face and edge constraints were applied. As the bonding strength of the carbon fiber resin between the carbon

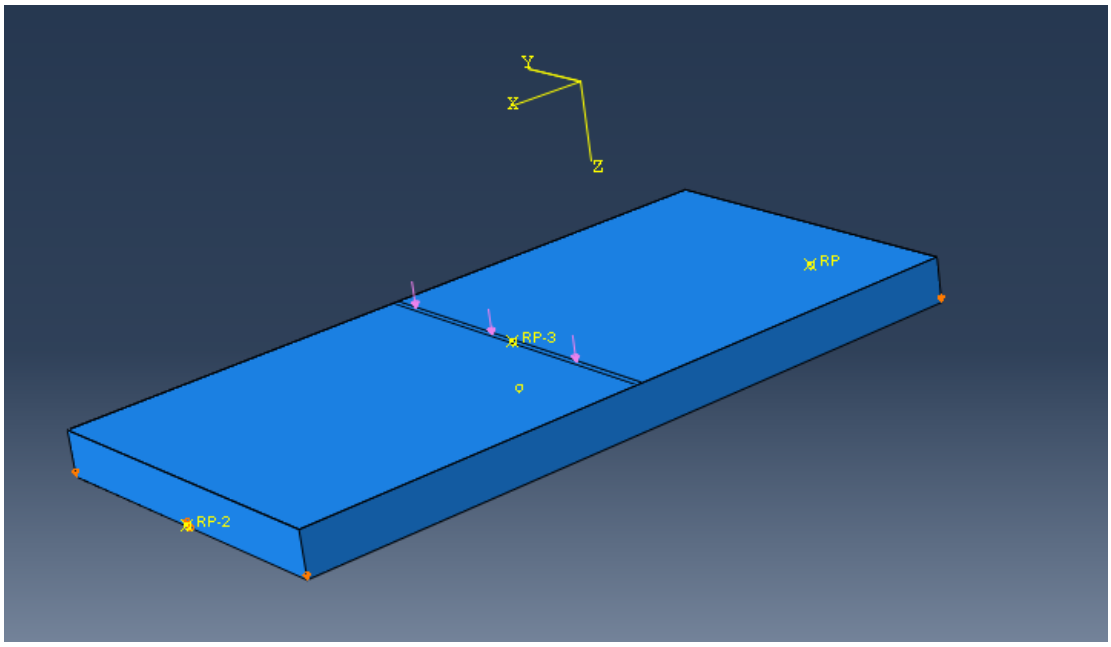

Figure 5.2. FEA Boundary Conditions and Loads.

fiber and the core is unknown, tie constraints shown Figure 5.1 were created in order to allow for shared nodes between face sheets and core. The first tie had the top surface of the core as the master and the bottom surface of the top face sheet as the slave. The second tie had the bottom surface of the core as the slave and the top surface of the bottom face sheet as the master. Boundary conditions were applied to both bottom edges parallel to the applied load. Both sides constrained displacement in U3 or the z orientation and displacement in the U2 or y direction was constrained at the center of the edges only, to allow deflections along the perpendicular edges to the applied load due to the anticlastic behavior of the core seen figure 5.2.

Once an FEA model was confirmed using materials with a known theoretical deflection was confirmed, the model could then be adapted for the experimental materials. Four node plate elements with orthotropic material properties (See Tables 5.1-2) were used to model the face and core laminates. It must be noted that this is a simplified model of the real structure, particularly with the vary face sheet thickness as the extension-bending coupling is ignored. This simplification can be justified because the face laminates are located far enough from the neutral axis relative to its thickness, that the deformation of the cross-section from flexure results in a near uniform strain distribution over the thickness of the faces. Thus we can consider the faces as being close to only extensional loading.

A study into element types was conducted in order to obtain deflection and stress results as close to theoretical values as possible seen table 5.3.

Table 5.3. Element Study

	Theoretical		Option 1		Option 2		Option 3	
	Core	**Face**	**Core**	**Face**	**Core**	**Face**	**Core**	**Face**
Element Type	-	-	Quad: Struct Hex	S4 Quad: Free	Quad: Struct Hex	S4 Quad: Free	Quad: Struct Hex	S4 Quad: Free
Standard or Explicit	-	-	S	S	S	S	E	S
Reduced Integration on	-	-						x
Linear or Quadratic	-	-	L	L	L	L	Q	L
Hourglass Control	-	-	x		x			
Incompressible Modes on	-	-			x			
Midspan Deflection (in)	0.017499		0.0168028		0.0167711		0.0184261	
Error (%)	-		3.979 %		4.16 %		5.29 %	

	Option 4		Option 5		Option 6		Option 7	
	Core	**Face**	**Core**	**Face**	**Core**	**Face**	**Core**	**Face**
Element Type	Quad: Struct Hex	S4 Quad: Free	Tetrhl: Struct	S4 Quad: Free	Quad: Struct Hex	S4 Quad: Struct	Quad: Struct Hex	S4 Quad: Free
Standard or Explicit	S	S	E	S	S	S	S	S
Reduced Integration on	x	x	x	x	X	x	X	x
Linear or quad	Q	L	Q	L	L	Q	L	L
Hourglass Control	x		x		X		X	
Incompressible Modes on								
Midspan Deflection (in)	0.0192311		0.02663		0.016166		0.016869	
Error	9.89 %		52.18 %		7.6176 %		3.6 %	

	Option 8		Option 9	
	Core	**Face**	**Core**	**Face**
Element Type	Quad: Struct Hex	S4 Quad: Free	Quad: Struct Hex	S4 Quad: Free
Standard or Explicit	S	S	S	S
Reduced Integration on	X		X	
Linear or quad	L	L	L	L
Hourglass Control	X		X	
Incompressible Modes on			x	
Midspan Deflection (in)	0.0168906		0.016769	
Error (%)	3.477 %		4.172 %	

The chosen element types was option 8 with the core being a C3D8R 8 node, standard, linear model, structured quadratic element type with reduced integration and hourglass control. The face element was S4: 4 node doubly curved generally purpose shell, free structured element type with finite member strains and produced an error of 3.477 % with the theoretical model.

5.2 Static Loading Analysis

The finite element models of the composite sandwich were modeled identically to the experimental models with the same static loading boundary conditions. Using this method, the FE maximum/mid-span deflection results could be compared with theoretical hand calculations by analysis

a closed form system. The model was layered with two steel face sheets between an aluminum core with mechanical properties shown in Table 5.4.

Table 5.4. Mechanical and part properties used for FEA model validation

Part	Material	E (Msi)	Poisson's Ratio	Length (in)	Width (in)	Depth (in)	Part Type	Section Type
Core	Aluminum 2024	10	0.3	6	1.5	0.375	3-D Solid	3-D Solid
Face Sheets	Steel 1018	29	0.297	6	1.5	0.024	3-D Shell	3-D Shell

The structure was then loaded with a 100lb mid-span force. The total load was chosen to be 100lb to lie in the linear elastic region of the load – deflection curve for all configurations as determined by experimental results, this load also is kept in the range of the simulation assumption of small angle deflections.

5.3 Validation of FEA Model

The static load case above was used to compare FEA results with theoretical hand calculations. The method of equivalent stiffness's was used for theoretical deflections and MATLAB code can be seen in the apendix.[33] The elastic modulus of steel is three times as much as aluminum, an equivalent cross section of aluminum can be made by replacing the steel with aluminum that is three times as large. The equation for the mid-span or maximum deflection for a simply supported beam under three point bending can be seen Equation 3.3 in section 3.2. The FEA results came reasonably close to theoretical results seen in Table 5.5.

Table 5.5. Comparison of Theoretical and Experimental deflection for model validation with Aluminium face sheets and Steel core.

Model	Results
Theoretical Deflection at 100 lbf (in)	0.02
FEA Maximum Deflection at 100lbf (in) correlating to a seed size of 0.1	0.019997
Error (%)	0.01499%

From the acceptable results produced by the validation model, we can assume the model is sufficiently modelled in regards to boundary conditions, area of applied load and interactions between layers. Square linear elements were used to fit the rectangular geometry of the specimens.

5.4 Mesh Convergence

To check mesh convergence, to simulate a simply supported beam like that conducted experimentally. The 100 lb. load was modeled, as a pressure load with a total pressure of 100 psi. This area was chosen to emulate the three point bending loading fixture of 0.075in^2. Two convergence

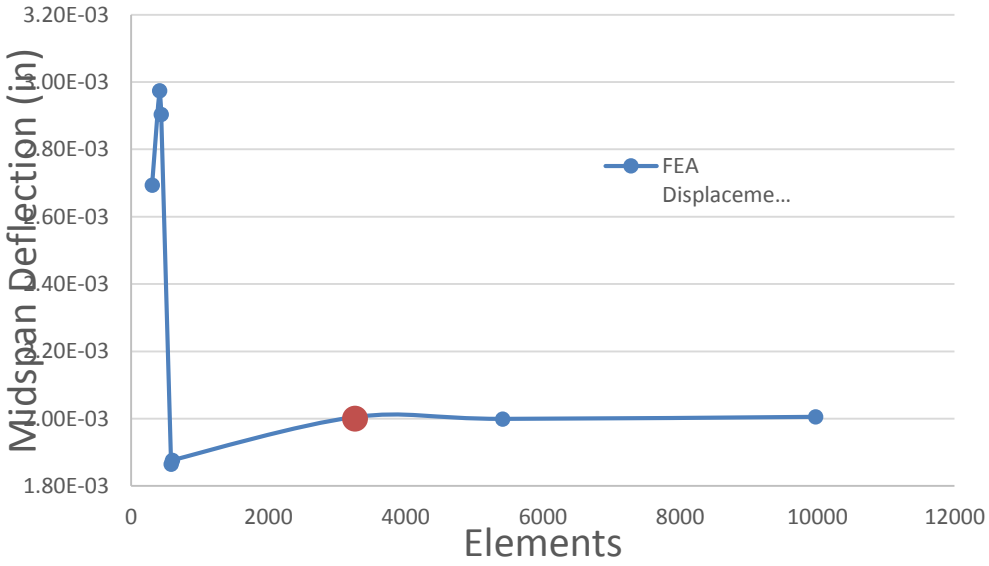

Figure 5.3. Convergence Plot for Midspan Beam deflection modelled in Abaqus

studies were analyzed for mesh convergence, maximum deflection and stress of upper face of the top face sheet. Figure 5.3 shows the convergence plot for maximum deflection taken at the mid-span top surface of the top face sheet. The degrees of freedom was changed by altering the seed size between 0.06 and 0.3 in. The graph converges at 3263 elements indicated by the orange dot, corresponding to a seed size of 0.1. Further FEA analysis was then conducted with a part mesh of 0.1 in in the model. Linear elements were used in the 3-D solid element parts with reduced integration turned off so each element was analyzed as an 8 node element, which resulted in 3263 8 node elements in the entire model, with a seed size of 0.1 in.

6.0 Comparison of Experimental, Theoretical, and FEA Results

This section covers the comparison of Experimental, Theoretical and Finite Element analysis.

6.1 Composite Sandwich Panels with Varying Core Ribbon Orientation

The three-point loading was applied to all configurations of the model shown in Fig.5.1. The stress and displacements at 100lbf for all configurations under three point bending can be seen in Table 6.1 below.

Table 6.1. Comparison of FEA, Experimental and Theoretical data for Core Ribbon Orientation variations

Core Ribbon Direction (degrees)	Maximum Deflection FEA (in)	Maximum Deflection Theoretical (in)	Maximum Deflection Experimental (in)	Difference Theoretical - FEA (%)	Difference Theoretical - Experimental (%)	Difference FEA - Experimental (%)	Maximum Stress (ksi)
0°	0.03275	0.03517	0.0337 ±0.00078	6.88	4.18	2.99	10980
15°	0.03431	0.03592	0.0363 ±0.0011	4.48	1.06	5.79	11140
30°	0.03875	0.03826	0.038 ±0.0012	1.28	0.68	1.93	11100
45°	0.04505	0.0423	0.0453 ±0.0013	6.5	7.09	0.55	10970
60°	0.05157	0.04781	0.0486 ±9.13e-4	7.86	1.65	5.76	12650
75°	0.05646	0.05329	0.0555 ±0.0022	5.95	3.77	1.71	14060
90°	0.05827	0.05575	0.0558 ±0.0019	4.52	0.09	4.25	14590

The finite element results were observed to have minimal error when compared to the theoretical data, which confirmed that the model was acceptable. The maximum stress in the specimen increases with an increase in core orientation. This is due to two factors, the core's Young's moduli in the bending orientation decreases, taking less shear stress and there is a greater anticlastic curvature in the core at 90° than 0°. This means that as Load is applied the rate at which the perpendicular edges to applied load inflect away from the applied load is greater at 90° and so as the anticlastic curvature increases, the area of which load is applying decreases at a greater rate, causing stress concentrations at the perpendicular

edges seen figure 2. The 45° core orientation has the anticlastic curvature at a 45° degree angle to the applied load and thus applied load area reduction rate is at its minimum.

Finite element deflection results varied by no more than 5.76% from experimental results and as expected the maximum normal stress is located at the supports of the beam. A typical Beam deflection can be seen in Figure 6.2 below. Figure 6.1 shows the visual comparison between Experimental, analytical and numerical deflections at 100lbf. It can be seen that beam and plate theory deflections are

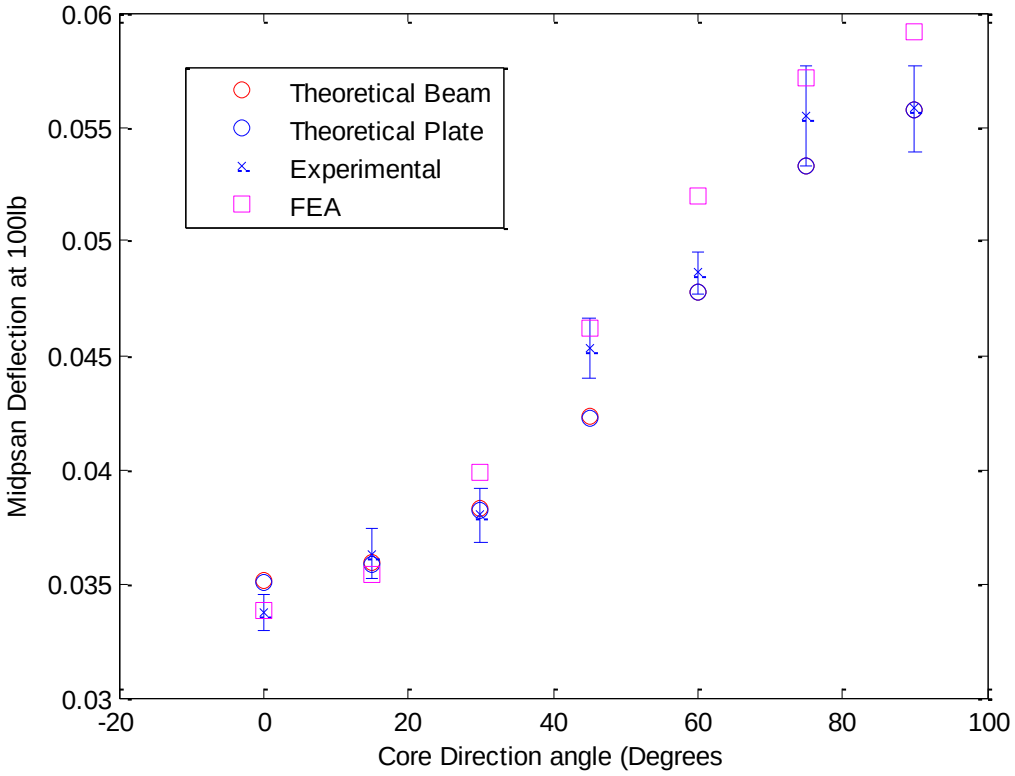

Figure 6.1. Comparison of Experimental, FEA, and Theoretical deflection for Varying Core Angle

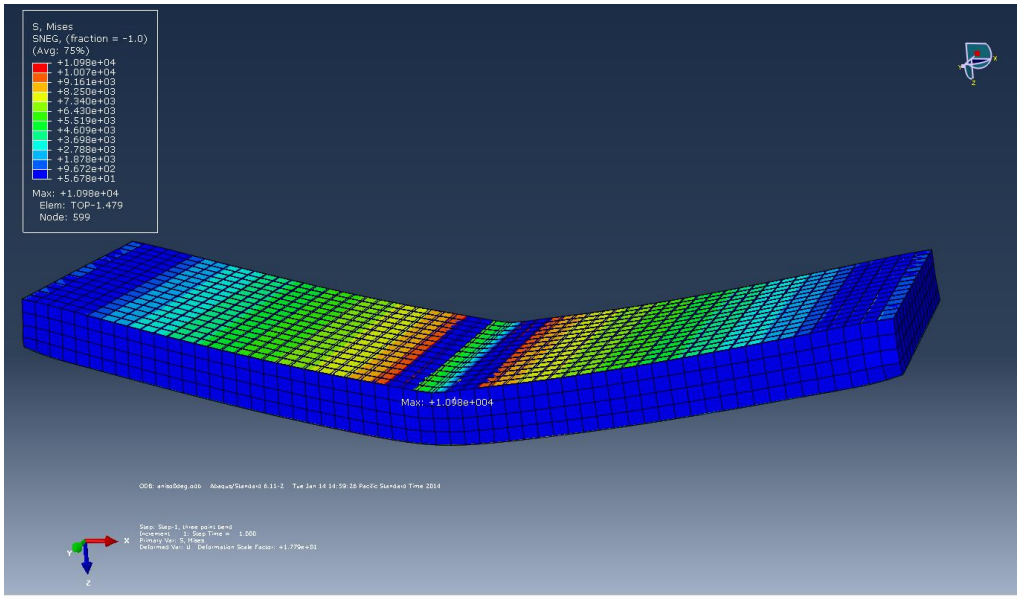

Figure 6.2. Stress distribution for Beam for Core orientation of 0 degrees at 100lbf applied load

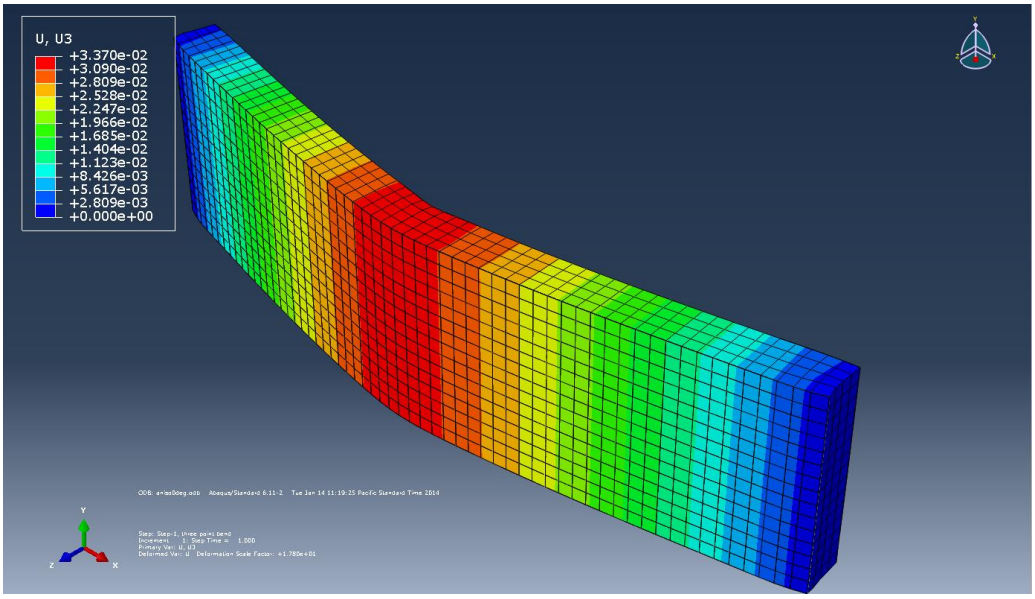

Figure 6.3. Deflection for Beam with Core orientation of 0 degrees at 100lbf applied load

almost identical. Finite element analysis had reasonable agreement with analytical results with an average percentage error of 5.837% and maximum percent error of 9.095% with Classical beam theory. The finite element model did marginally better with plate theory with an average percent error of

5.783% and a maximum error of 9.1761%. Both maximum errors occurred at the 45° core ribbon orientation. This is due to the mechanical properties of the honeycomb being estimated by using the transformation matrix to rotate the mechanical properties of the core to model the mechanical properties of the Nomex honeycomb core at 45°.

6.2 Composite Sandwich Panels with Varying Face Sheet Thickness's

The stress and displacements for all configurations under three point bending can be seen in Table 6.2 below.

Table 6.2. Comparison of FEA, Theoretical and Experimental Mid Span Deflections at 100 lbf

			Top Face Sheet Thickness (in)				
			0.012 (1 Layer)	**0.024 (2 Layers)**	**0.036 (3 Layers)**	**0.048 (4 Layers)**	**0.06 (5 Layers)**
Bottom Face Sheet Thickness (in)	**0.012 (1 Layer)**	**Experimental**	0.0265 ±0.002	0.0201 ±0.0003	0.0185 ±0.0003	0.0164 ±0.0002	0.0149 ±0.0002
		Theoretical	0.0247	0.0201	0.0177	0.0161	0.0149
		FEA	0.0242	0.0205	0.0192	0.0182	0.0176
	0.024 (2 Layers)	**Experimental**	0.0231 ±0.0006	0.0169 ±0.0005	0.0155 ±0.0004	0.0139 ±0.0005	0.0127 ±0.0011
		Theoretical	0.0201	0.0175	0.0159	0.0147	0.0138
		FEA	0.0204	0.0168	0.0155	0.0147	0.0141
	0.036 (3 Layers)	**Experimental**	0.0193 ±0.0008	0.0152 ±0.0004	0.0141 ±0.0002	0.0137 ±0.0005	0.0131 ±0.0003
		Theoretical	0.0177	0.0159	0.0146	00137	0.0130
		FEA	0.0189	0.0155	0.0142	00134	0.0128
	0.048 (4 Layers)	**Experimental**	0.0176 ±0.0003	0.0147 ±0.0004	0.0134 ±0.0006	0.0127 ±0.0004	0.0124 ±0.0004
		Theoretical	0.0161	0.0147	0.0137	0.0129	0.0123
		FEA	0.0182	0.0147	0.0133	0.0126	0.0121
	0.06 (5 Layers)	**Experimental**	0.0178 ±0.0007	0.0132 ±0.0007	0.0126 ±0.0003	0.0116 ±0.0006	0.0117 ±0.0007
		Theoretical	0.0149	0.0138	0.0130	0.0123	0.0117
		FEA	0.0175	0.0141	0.0129	0.0121	0.0116

Finite element analysis showed reasonable agreement with theoretical and experimental midspan deflections. Specimens with a top to bottom face sheet ratio outside of $0.4 \leq t_t/t_b \leq 3$ produce greater error due to assumption that the bending-extension coupling matrix being zero is no longer valid due to the sandwich structure no longer being close to symmetric. Specimens outside the specified face sheet ratio range have been highlighted pink. Figure 6.4 shows a three dimensional curve fitting to finite element analysis performed on unequal face sheet configurations.

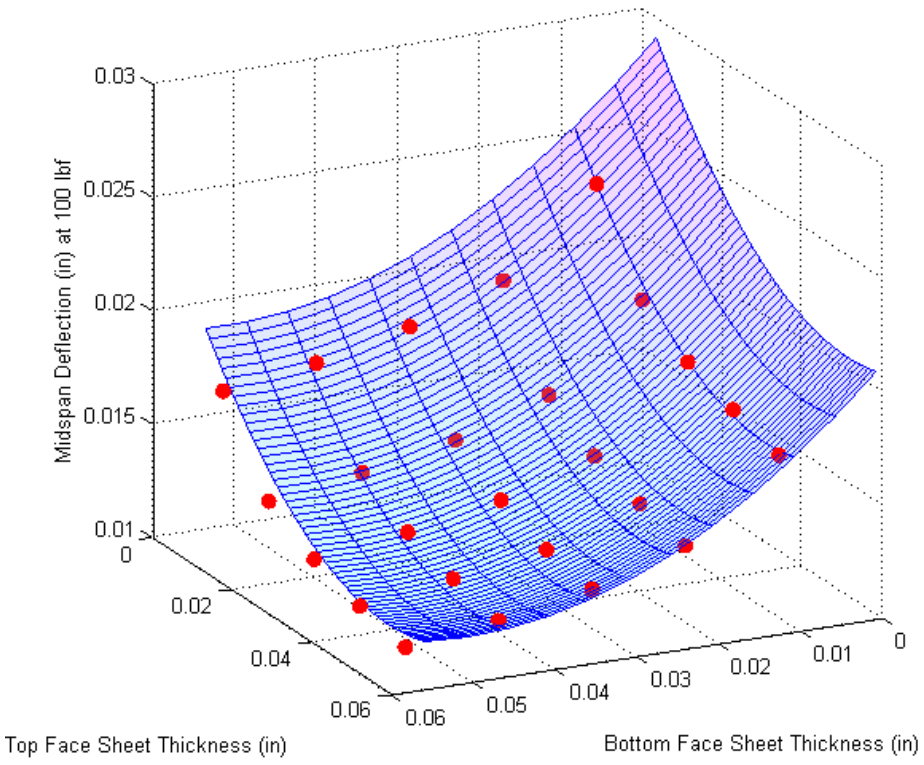

Figure 6.4. 3D Curve Fitting for FEA Deflections at 100 lbf.

Table 6.3. Difference Between Finite Element and Theoretical Midspan Deflection for Varying Face Sheet Thickness at 100 lbf

		Top Face Sheet Thickness (in)				
		0.012	**0.024**	**0.036**	**0.048**	**0.06**
Bottom Face Sheet Thickness (in)	**0.012**	2.06 %	2.175 %	8.44 %	13.14 %	17.97 %
	0.024	1.28 %	3.87 %	2.38 %	0.12 %	1.94 %
	0.036	7.23 %	2.62 %	3.34 %	2.43 %	1.11 %
	0.048	12.95 %	0.34 %	3.27 %	2.33 %	1.74 %
	0.06	17.11 %	2.29 %	0.9 %	2.45 %	1.25 %

Finite element deflections had better agreement with experimental deflections than theoretical deflections indicating an agreeable model. As expected specimens above the face sheet thickness ratio of 3 produced larger errors. Interestingly the finite element model had agreement with experimental specimens with face sheet thickness ratio under 0.4

Table 6.4. Difference Between Finite Element and Experimental Midspan Deflection for Varying Face Sheet Thickness at 100 lbf

		Top Face Sheet Thickness (in)				
		0.012	**0.024**	**0.036**	**0.048**	**0.06**
Bottom Face Sheet Thickness (in)	**0.012**	9.79 %	1.95 %	3.40 %	10.00 %	15.63 %
	0.024	13.27 %	0.32 %	0.26 %	5.64 %	10.05 %
	0.036	1.87 %	1.35 %	0.39 %	2.50 %	2.21 %
	0.048	3.27 %	0.16 %	0.64 %	0.58 %	2.71 %
	0.06	1.69 %	6.83 %	2.38 %	4.22 %	0.84 %

Figures 6.5-9 visually show the differences between specimens keeping the bottom layer constant.

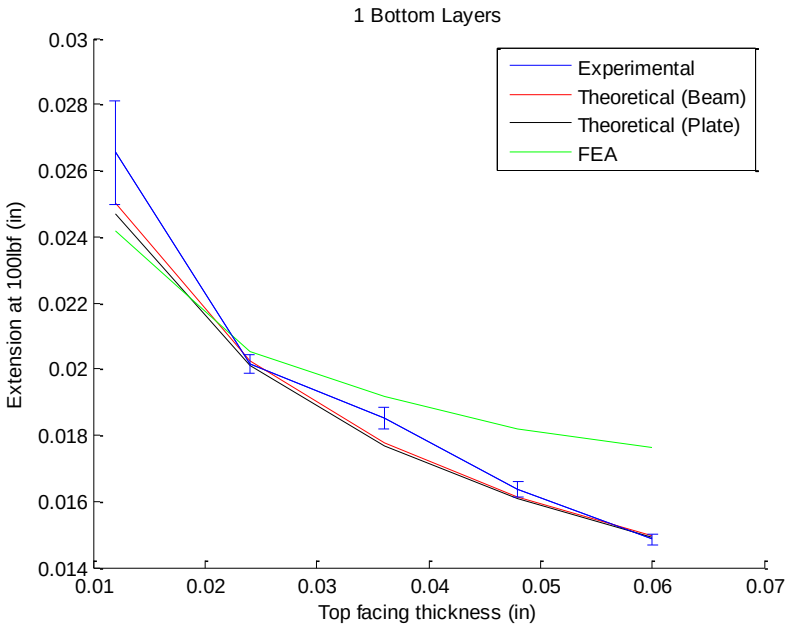

Figure 6.5. FEA, Experimental and Analytical Comparison for all configurations with 0.012in bottom layer at 100lbf load

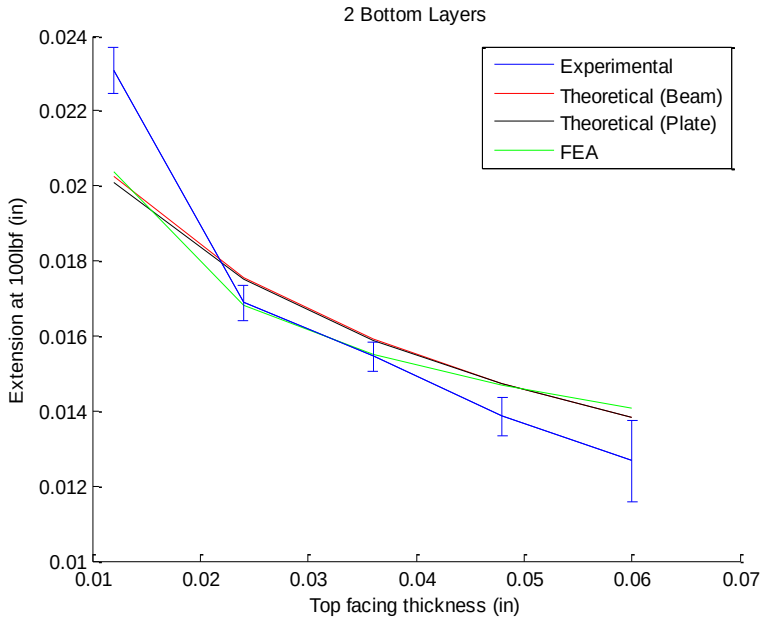

Figure 6.6. FEA, Experimental and Analytical Comparison for all configurations with 0.012in bottom layer at 100lbf load

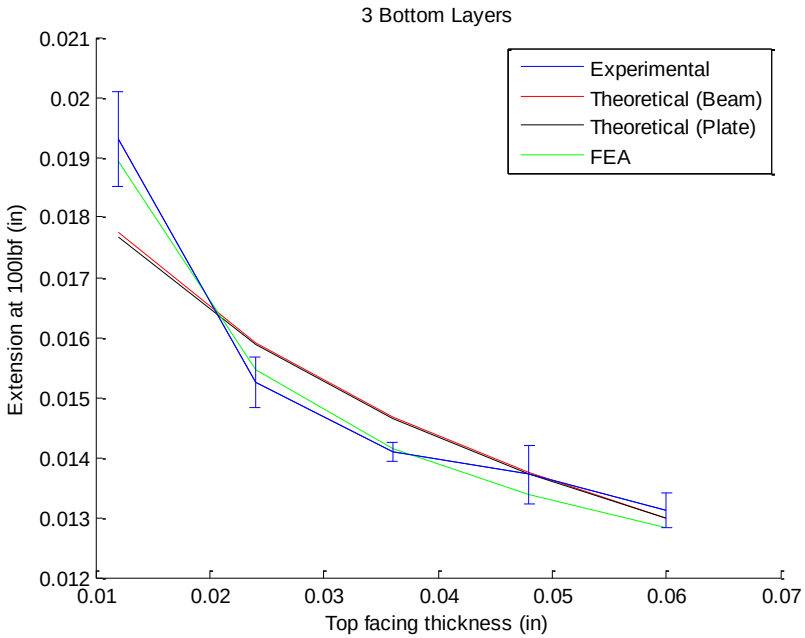

Figure 6.7. FEA, Experimental and Analytical Comparison for all configurations with 0.024in bottom layer at 100lbf load

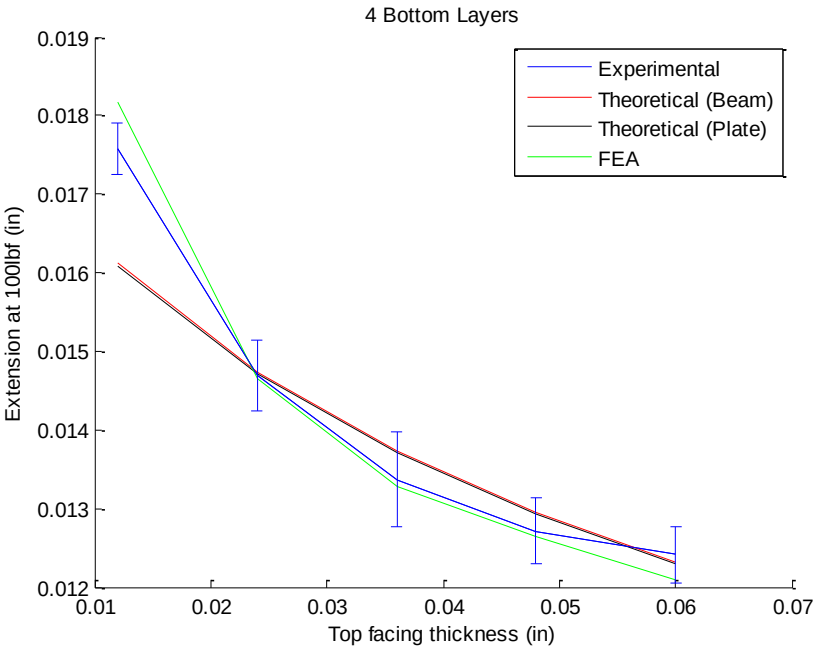

Figure 6.8. FEA, Experimental and Analytical Comparison for all configurations with 0.048in bottom layer

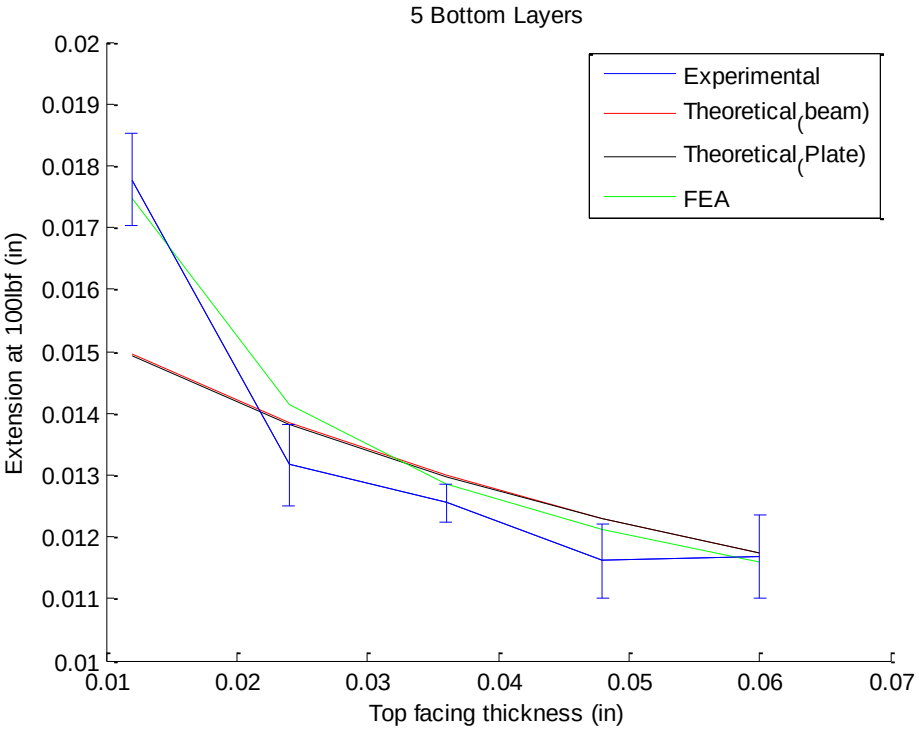

Figure 6.9. FEA, Experimental and Analytical Comparison for all configurations with 0.06in bottom layer at 100lbf load

7.0 Conclusion

The objective of this study was to determine the effects on the mechanical behavior of sandwich structures with varying the core ribbon orientation of the honeycomb in composite honeycomb structures as well as varying face sheet thickness's with constant core subjected to three-point bend loadings. Nine core orientations from 0^o to 90^o degrees were tested, with test data available in the appendix. Twenty five specimen configurations with unique face sheet thickness varying from 0.012 to 0.06 in were also tested, with data available in the appendix. In addition to testing of sandwich structures ASTM standard tests were conducted to obtain the mechanical properties of the constituent materials. From the analytical and experimental work presented in this thesis the following conclusions were found:

- A simplified procedure for stiffness calculations, based on material properties found by testing under ASTM standards, was found to predict deflections within approximately 17% accuracy.
- The initiation of failure modes in composite sandwich structures is dependent on the constituent material properties, geometric dimensional and type of loading. Failure of Nomex honeycomb carbon fiber sandwich structures occurs by failure of the facing in compression of the core in shear and never due to face wrinkling.
- For relatively small beam spans and high face sheet to core thickness ratio, the predominant failure mode is core shear, and is then dominated by core compression as the face sheet to core thickness ratio is reduced. As the beam span is increased face failure in compression becomes the dominant mode of failure.
- Core indentation from cross head movement only takes affect when face to core thickness is less than 0.032 which is equivalent to one ply for materials used in this thesis. Failure near load point due to core indentation was not modelled well. An adequate model of the contact area

and core failure criteria coupled with higher order beam theory is necessary to improve indentation analysis for honeycomb core sandwich structures.

- Improving the consistency of the analytical determination of failure loads is still in need of work, particularly with predicting failure loads in specimens with unequal face sheet thicknesses.
- Ensuring better quality control in the manufacturing and testing procedures will greatly improve ultimate load capabilities and reduce the scatter of data.
- Adding a layer of sheet adhesive between honeycomb core and pre-impregnated carbon fiber face sheets had little effect on the mechanical properties of the structure. Adding the adhesive layer also increased the structures weight, thus having a negative effect on structure optimization.

- The ultimate shear strength of the core decreased in a sinusoidal behavior when the core ribbon orientation is increased from 0^o (longitudinal orientation) to 90^o (transverse orientation).
- Increasing the core ribbon orientation from 0^o (longitudinal orientation) to 90^o (transverse orientation) increased ultimate deflection at failure and decreased ultimate failure load.
- Maximum stress on facing sheet increases with increasing core ribbon orientation angle. This is due to the anticlastic curvature induced in the transverse orientation of the core under bending which is a function of poissons. The rate of transverse curvature increases with core orientation, due to the transformation of the poissons. Thus a greater increase in anticlastic curvature causes an increase in area reduction at the applied load, which results in a greater stress (higher stress concentration on the smaller area) on the beam than that of the stress at 0 degree core orientation for equivalent applied loads.

- Deflection due to shear rigidity must be included in theoretical deflections of sandwich structures when the core's Young's modulus is much less than the facing Young's modulus in the bending orientation.
- Increasing bottom face sheet thickness along constant top face sheet thickness lines increases flexural rigidity, but does not increase stiffness with respect to minimum weight.
- Optimal face sheet thickness for a given core thickness is a function of core and face sheet densities and for materials used in this thesis optimal bending stiffness occurs when the core weight accounts for 2/3 of the total sandwich weight.
- Specimens with a top to bottom face sheet ratio outside of $0.4 \leq t_t/t_b \leq 3$ produce greater error due to assumption that the bending-extension coupling matrix being zero is no longer valid due to the sandwich structure no longer being close to symmetric about its middle axis.
- Deflections due to Indentation at the cross head contact point are not accounted for in classical beam or plate theory, which results in smaller calculated midpsan deflections for face sheet thicknesses of 0.012 (1ply) or less.

These results show that it is recommended that in the design of honeycomb sandwich structures subjected to three point bending, core ribbon orientation must be considered when optimizing strength and stiffness.

Finite element analysis models were created to compare test results to numerical data to validate the experimental results. All beams were validated within an error of 17% for midspan deflections between experimental and numerical data. A potential source of error between experimental and numerical data could be due to inaccuracies in mechanical properties found experimentally and the experimental processes.

As composite sandwich structures become more widely used in engineering fields in the near future, the need for slight advantages in sandwich structure design will be crucial. Depending on design

specifications, core orientation of honeycomb core sandwiches could be that slight advantage. As this report has shown, considering the core orientation within composite sandwiches, and for structures experiencing only static loading in one direction, increasing ply count on the face of applied force results in optimized designs of a structure and a better overall performance, which, in any industry, leads to an increase in money saved.

8.0 Future Considerations

There have few studies into the behaviors of honeycomb core composite sandwich structures resulting in an increased safety factor in industries, which is against the ideal of optimization of weight reduction in design. This study delves into the behavior of honeycomb cores at different orientations but more can be learned about this material. The main idea behind design optimization, particularly in the aerospace industry, is to minimize weight while still obtaining the same, or improved, structural capabilities as typical materials found in industry, such as aluminum and steel. Further studies could include but are not limited to:

- Testing of the effects on the mechanical behavior of sandwich composites with different core materials, thickness's, densities, cell sizes and cell shapes coupled with the varying core ribbon orientations.
- Repeating this study under four point bends to verify face sheet to core thickness ratios for optimal bending stiffness and strength with respect to minimum weight
- Modelling specimens with the inclusion of plastic deformation of the indenter at the applied load, coupled with higher order beam theory.

References

1. "Composite Materials." *Composite Materials*. The Aviation History On-Line Museum, 28 Mar. 2010. Web. 23 Jan. 2014.
2. Gay D., Hoa S,V., Tsai S,W. Composites Materials Design and Application. CRC Press
3. Analysis and Performance of Fiber Composites, 2nd Ed., B.D. Agarwal and L.J. Broutman, Wiley, 1990, pp. 1-4.
4. Dr. Ray Franco, PhD., PE. "Bimetal Strips." *Bimetal Strips*. N.p., 2006. Web. 23 Jan. 2014.
5. "Arborite - High Pressure Laminates." *Arborite*. N.p., 2010. Web. 23 Jan. 2014.
6. Jones, R. Mechanics of Composite Materials 2nd Edition.
7. Ferreira S., Lopez P., Monteiro S., Nascimento D., Natural-Fiber Polymer-Matrix Composites: Cheaper, Tougher, and Environmentally Friendly. JOM, a publication of the minerals, metals and materials society. January 2009.
8. Soutis C, Curtis PT. Fiber Reinforced Composites in Aircraft Construction. Aerospace Engineering, The University of Sheffield, Mappin Street, Sheffield S1 3JD, UK.
9. "Carbon Fiber Processing Part 1 – Wet / Hand Lay-up." *Carbon Fiber Guru*. N.p., 18 Jan. 2010. Web. 23 Jan. 2014.
10. Lee, S. Handbook of Composite Reinforcements. John Wiley & Sons, Nov 30, 1992.
11. "What Is Vacuum Infusion Processing (VIP)." *Structural Composite Designs*. N.p., n.d. Web. 23 Jan. 2014.
12. "How Are Filament Winding Working?" Hebei Maple Fiberglass Industry Co., 2013. Web. 23 Jan. 2014.
13. Soutis C, Curtis PT. Prediction of the post-impact compressive strength of CFRP laminated composites. Comp Sci Technol 1996;56(6):677–84.
14. "Aluminum Honeycomb Panels." *Honeycomb Panel, Aluminum Honeycomb Panel, Aluminum Honeycomb Core Manufacturers*. Universal Metaltek, 2014. Web. 23 Jan. 2014.
15. Cross D, N. The Use of Honeycomb Sandwich Panels in the Engineering Field. Ciba-Geigy.
16. Nomex Honeycomb Data Sheet. Hexcel
17. Foo. C., Chai. G., Seah. L., Mechanical Properties of Nomex Material and Nomex Honeycomb Structure.
18. Walker C, H. Honeycomb Fastening. Fort Worth Div. General Dynamics Corp. Oct 5-9, 1970.
19. Petras, A. Design of Sandwich Structures. Robinson College, Cambridge (1998)
20. Chesser, Paul. "Technical Glitches and Payments for Down Time Still Nag Boeing's Dreamliner." *Somewhat Reasonable*. N.p., 10 Aug. 2013. Web. 23 Jan. 2014.
21. Norris, Guy (January 9, 2009). "Boeing Rules Out 787 Window Change". *Aviation Week*. Retrieved June 14, 2013.
22. Baruch. M , Frostig. Y., Sheinman. I., Vilnay., O. Bending of Nonsymmetric Sandwich Beams with Transversely Flexible Core. Journal of Engineering Mechanics. September 1991.
23. Lim, T.S., Lee, C.S. and Lee. D.G. Failure Modes of Foam Core Sandwich Beams under Static and Impact Loads. Mechanical Design Laboratory with Advanced Materials, Department of Mechanical Engineering, ME3261, Korea Advanced Institute of Science and Technology, 373-1, Guseong-dong, Yuseong-gu, Daejeon-shi, 305-701, Korea

24. Khan, Subhotosh. Bonding of Sandwich Structures – The Facesheet/Honeycomb Interface. E.I. DuPont Nemours Co., Inc. Advanced Fibers System, Richmondm VA 23234. Jan 25, 2007.
25. Allen, H. G., Analysis and Design of Structural Sandwich Panels. Oxford New York, Pergamon, (1969).
26. Triantafillou, T.C. and Gibson, L.J. (1987). Failure Mode Maps for Foam Core Sandwich Beams, Materials Science and Engineering, 95: 37–53.
27. Plantema, F. J. Sandwich Construction, John Wiley and Sons, New York (1966)
28. Ashby M. F., Gibson, L.J., Cellular Solids: structure and Properties. Pergamon Press, Oxford, 1988.
29. Gibson, L. J., Triantafillou, T. C. Minimum Weight Design of Foam Core Sandwich Panels for a Given Strength. Materials Science and Engineering, 95, 1987, pp.55-62.
30. ASTM D3039; Standard Test Method for Tensile Properties of Polymer Matrix Composite Materials.
31. ASTM E132; Standard Test Method for Poisson's Ratio at Room Temperature.
32. ASTM D6641; Standard Test Method for Compressive Properties of Polymer Matrix Composite Materials Using a Combined Loading Compression (CLC) Test Fixture.
33. ASTM D3518; Standard Test Method for In-Plane Shear Response of Polymer Matrix Composite Materials by Tensile Test of a +/-45° Laminate
34. ASTM D2584; Standard Test Method for Ignition Loss of Cured Reinforced Resins
35. 3M Scotch-Weld Structural Adhesive Film AF 163-2 Technical Datasheet.
36. ASTM D638; Standard Test Method for Tensile Properties of Plastics
37. ASTM C273; Standard Test Method for Shear Properties of Sandwich Core Materials
38. ASTM D6790; Standard Test Method for Determining Poisson's Ratio of Honeycomb Cores
39. ASTM C 393; Standard Test Method for Flexural Properties of Sandwich Constructions.
40. ASTM D7249; Standard Test Method for Facing Properties of Sandwich Constructions by Long Beam Flexure
41. ASTM D7250; Standard Practice for Determining Sandwich Beam Flexural and Shear Stiffness
42. American Society for Testing and Materials Annual Book of ASTM Standards, (2000).
43. Tae Seong Lim, Chang Sup Lee, Dai Gil Lee. "Failure Modes of Foam Core Sandwich Beams under Static and Impact Loads". Journal of Composite Materials. Sage Publications. August 27, 2004.
44. Whitney, J. A Local Model for Bending of Weak Core Sandwich Plates. Journal of sandwich structures and Materials 2001 3: 269. Oct 1, 2001.
45. T.R.A.Pearce, The stability of Simply-Supported Sandwich Panels with Fiber Reinforced Face Plates, Ph.D. thesis, University of Bristol, U.K., 1973.
46. Selvadurai, A. Elastic Analysis of soil – foundation interaction, Developments in Geotechincal Engineering, 17, 1979.
47. Froud, G. R. (1980). Your Sandwich Order, Sir, Composites, 11(3): 133–138.
48. Johnson, A. F. and Sims, G. D. (1986). Mechanical Properties and Design of Sandwich Materials, Composites,17(4): 321–328.

Appendices

A1. Mechanical Properties

A.1.1 Tensile tests of Hexply 6376 AGP-250H

	Specimen label	Maximum Load (lbf)	Maximum Tensile stress (ksi)	Extension at Maximum Load (in)
1	1	5391.79915	78.37032	0.05786
2	2	5721.65313	83.15148	0.05901
3	3	6248.14169	92.97830	0.06458
4	4	5475.95435	86.82894	0.06404
5	5	6017.21470	89.77702	0.06353
6	6	5688.56670	82.85487	0.05999
7	7	5433.49352	80.30228	0.05736
Mean		5710.97475	84.89474	0.06091
Standard Deviation		320.68958	5.22463	0.00307
Coefficient of Variation		5.61532	6.15424	5.03561
Mean + 1 SD		6031.66433	90.11937	0.06398
Mean - 1 SD		5390.28517	79.67012	0.05784

	Modulus (Automatic Young's) (ksi)	Length (in)	Thickness (in)	Width (in)
1	12510.26100	8.00000	0.07100	0.96900
2	12853.71141	8.00000	0.07000	0.98300
3	13135.08604	8.00000	0.07000	0.96000
4	13281.96035	8.00000	0.06900	0.91400
5	12062.47697	8.00000	0.07100	0.94400
6	12734.32547	8.00000	0.07100	0.96700
7	12801.96279	8.00000	0.07100	0.95300
Mean	12911.39772	8.00000	0.07043	0.95571
Standard Deviation	263.86456	0.00000	0.00079	0.02218
Coefficient of Variation	2.21523	0.00000	1.11715	2.32066
Mean + 1 SD	12175.26228	8.00000	0.07122	0.97789
Mean - 1 SD	11647.53316	8.00000	0.06964	0.93354

	Area (in^2)	Tensile stress at Maximum Load (ksi)	Tensile strain at Maximum Load (in/in)
1	0.06880	165.37032	0.00723
2	0.06881	162.15148	0.00738
3	0.06720	167.97830	0.00807

	Area (in^2)	Tensile stress at Maximum Load (ksi)	Tensile strain at Maximum Load (in/in)
4	0.06307	159.82894	0.00800
5	0.06702	154.77702	0.00793
6	0.06866	165.85487	0.00750
7	0.06766	163.30228	0.00716
Mean	0.06732	163.89474	0.00761
Standard Deviation	0.00202	5.22463	0.00038
Coefficient of Variation	3.00249	6.15424	5.01825
Mean + 1 SD	0.06934	90.11937	0.00799
Mean - 1 SD	0.06530	79.67012	0.00723

A.1.2 Compressive Tests of Hexply 6367

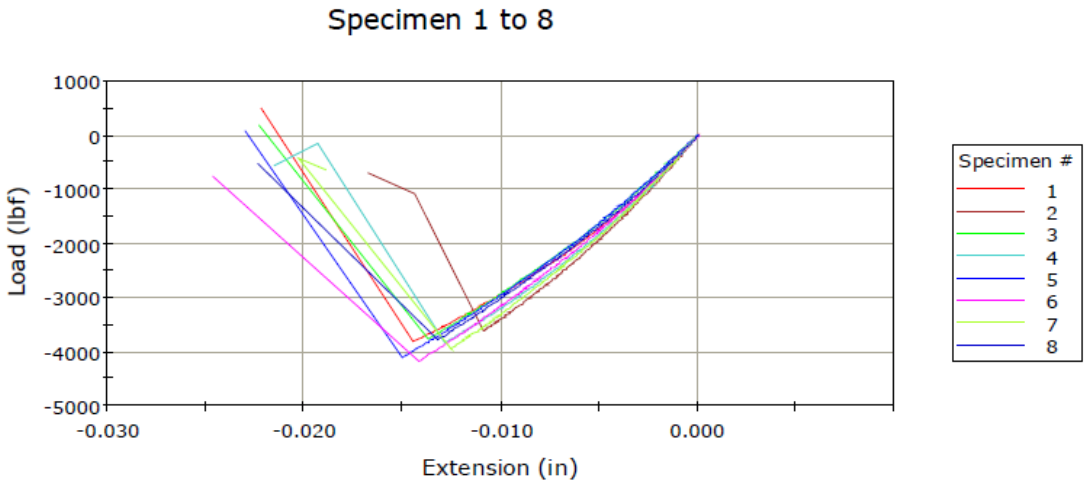

	Tensile Strength		**Modulus**
	(psi)		(psi)
	128640.1		4125682
	124878.5		4956487
	125167.9		3932457
	129528.1		5282718
	125776.4		3912480
	125703.2		4715906
	134373.2		4484488
Mean	127723.9		4487174
std	3435.438		489041.3

A.2 Core Orientation Load and stress plots

Figure 2.1.A. & 2.2.A. 0 Degree Core Load and Facing Stress Curves – Longitudinal Core Direction

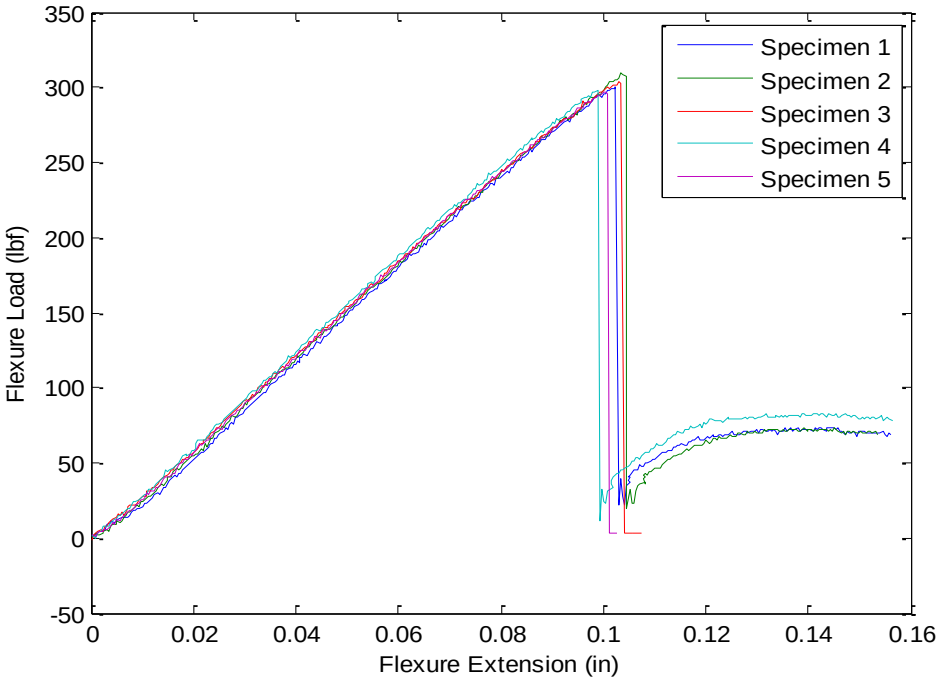

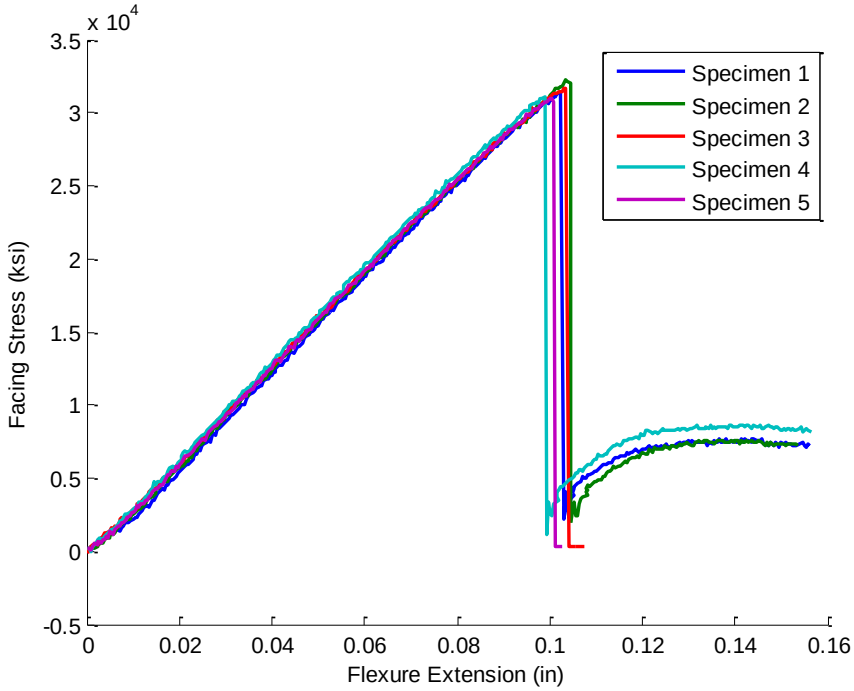

Figures 2.3.A & 2.4.A. 15 Degree – Longitudinal Core Direction

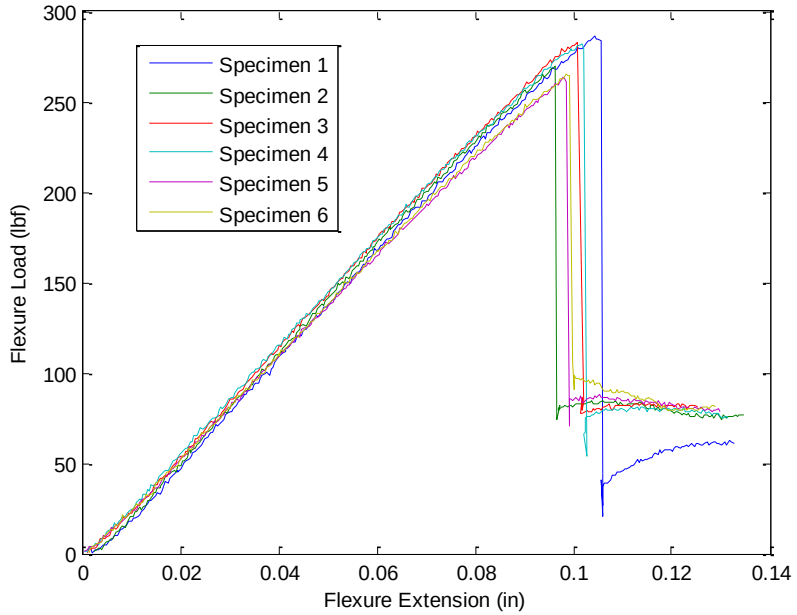

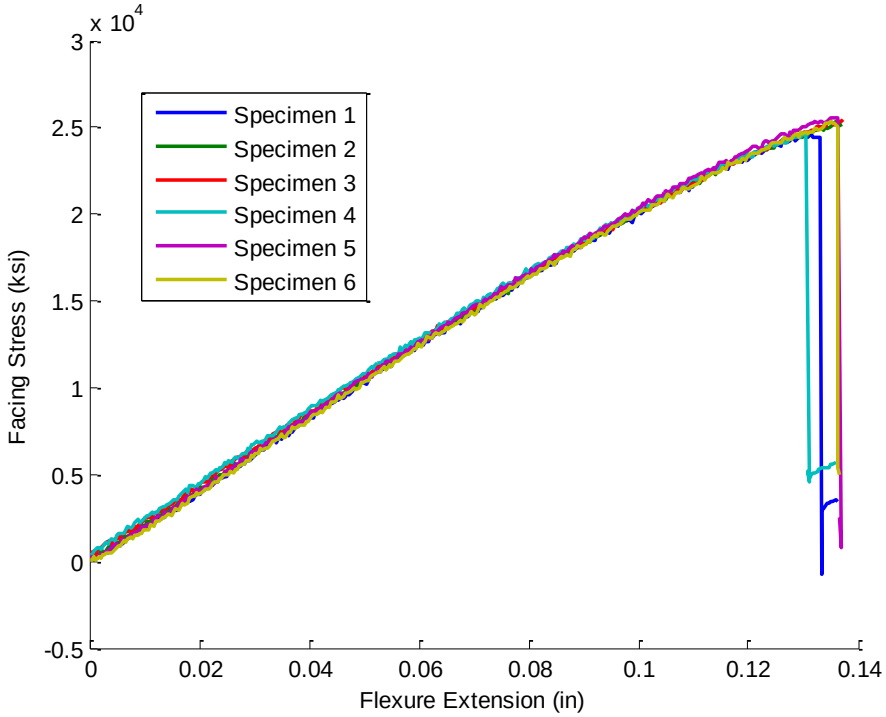

Figure 2.5.A. & 2.6.A. 30-Degree Core Direction

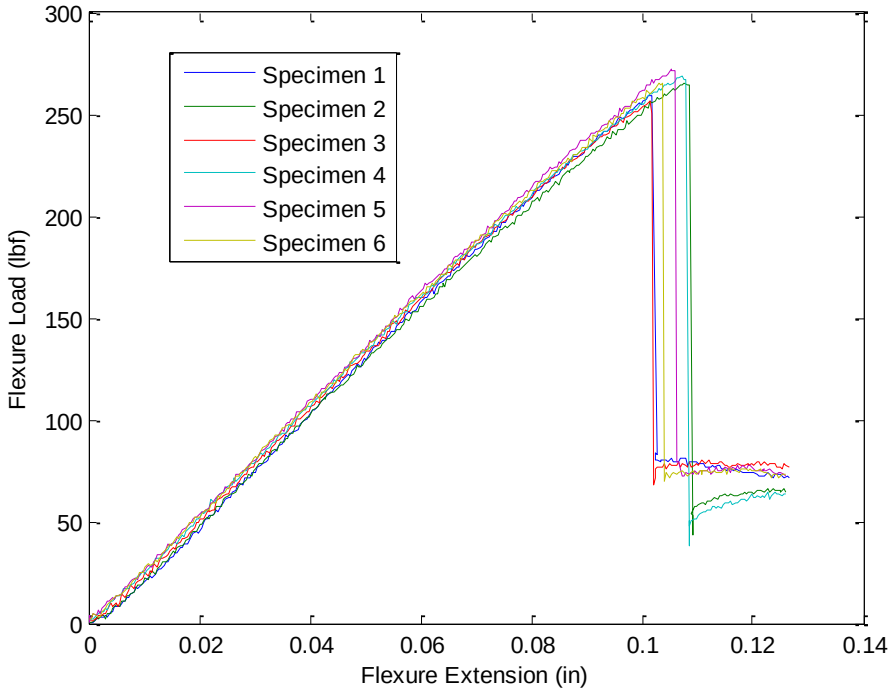

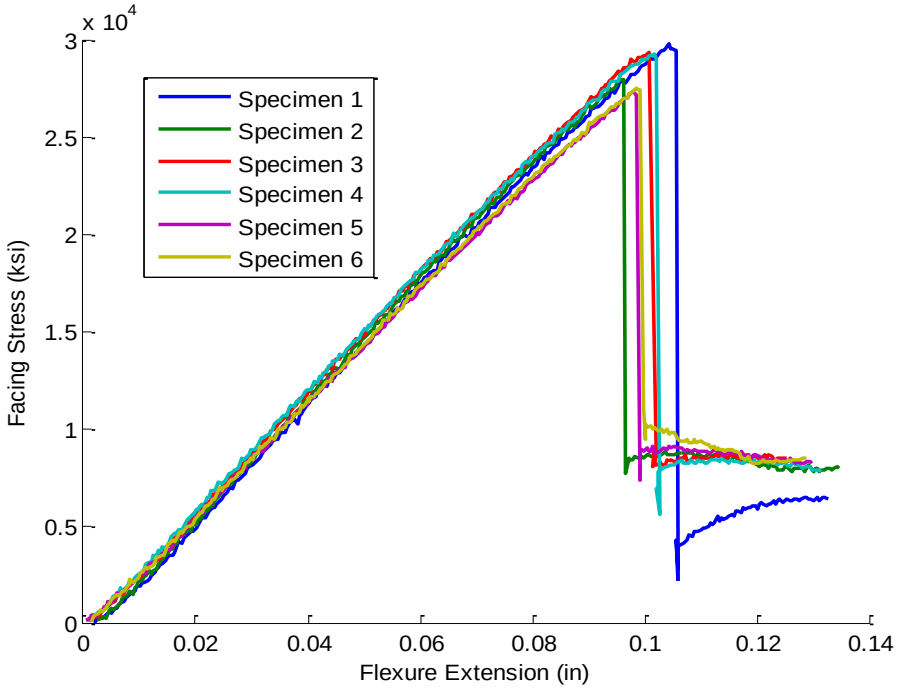

Figures 2.7.A. & 2.8.A. 45-Degree Core Direction

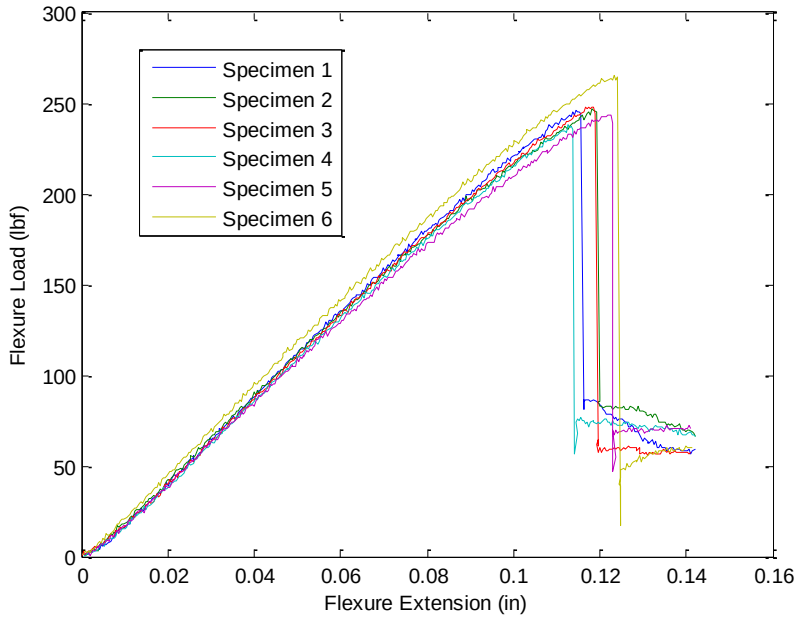

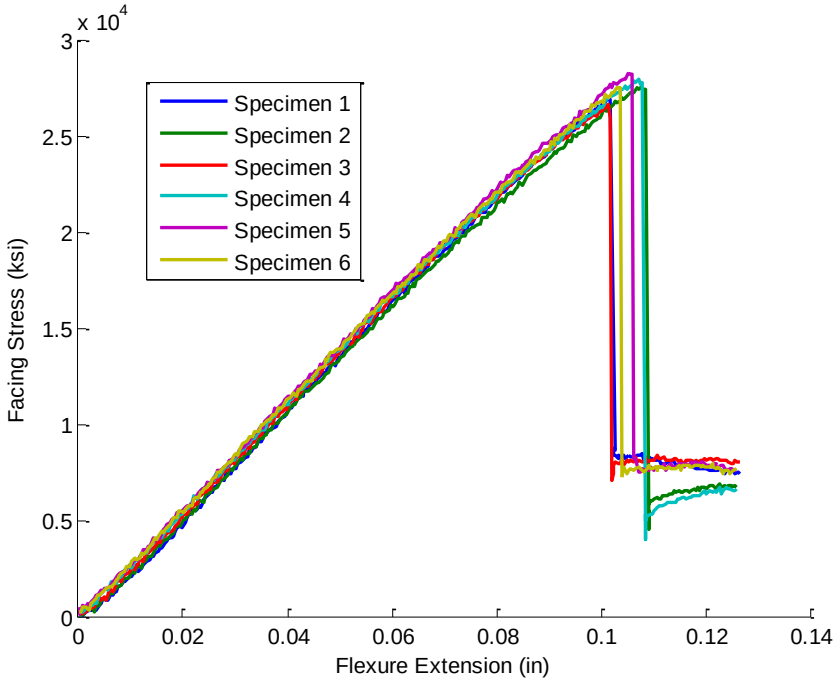

Figures 2.9.A. & 2.10.A. 60-Degree Core Direction

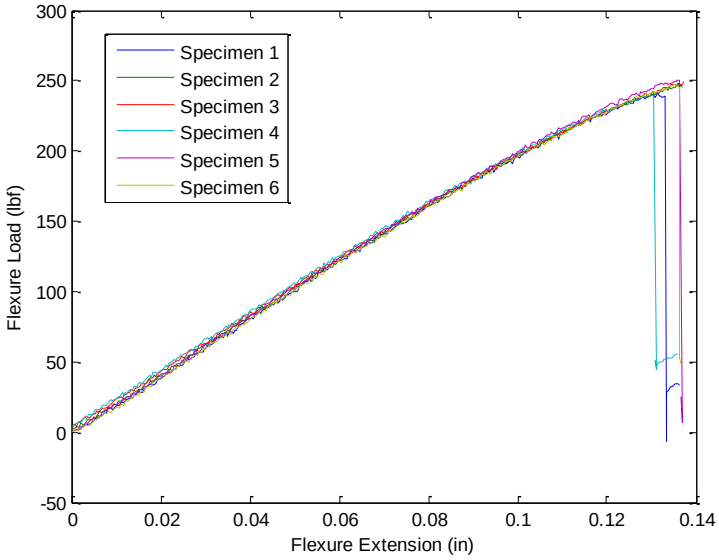

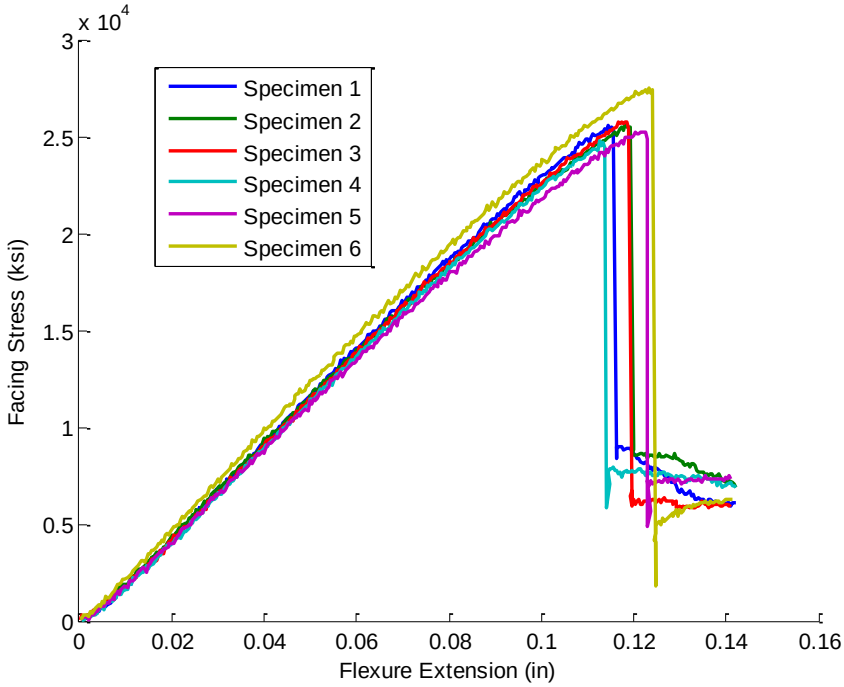

Figures 2.11.A. & 2.12.A. 75-Degree Core Direction

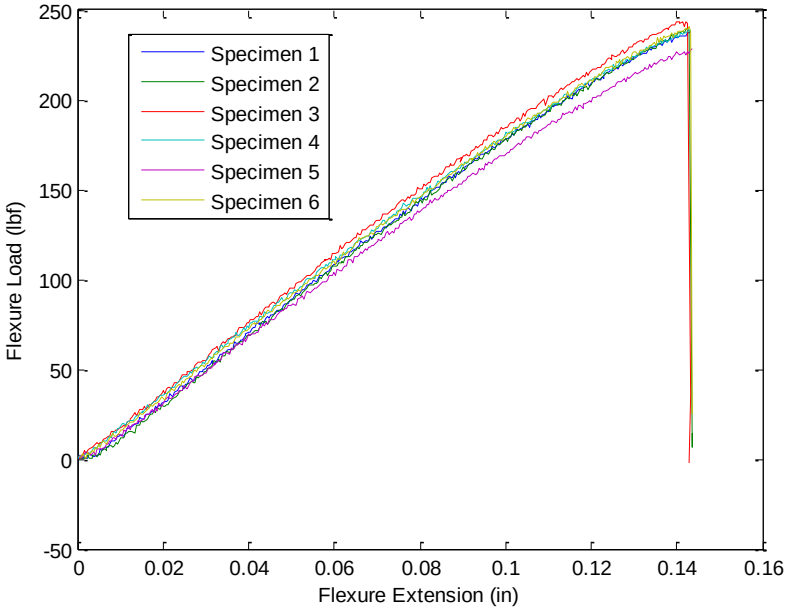

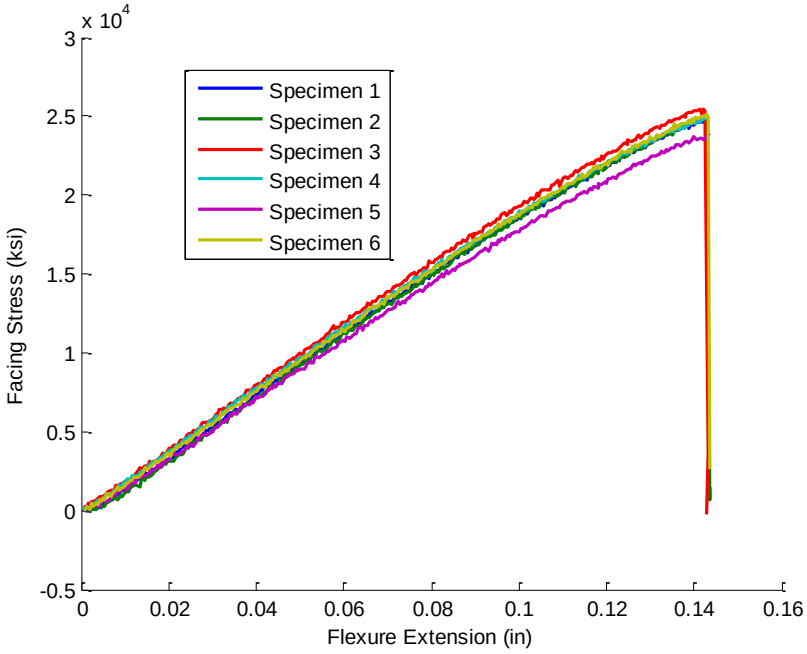

Figures 2.13.A. & 2.14.A. 90-Degree Core Direction

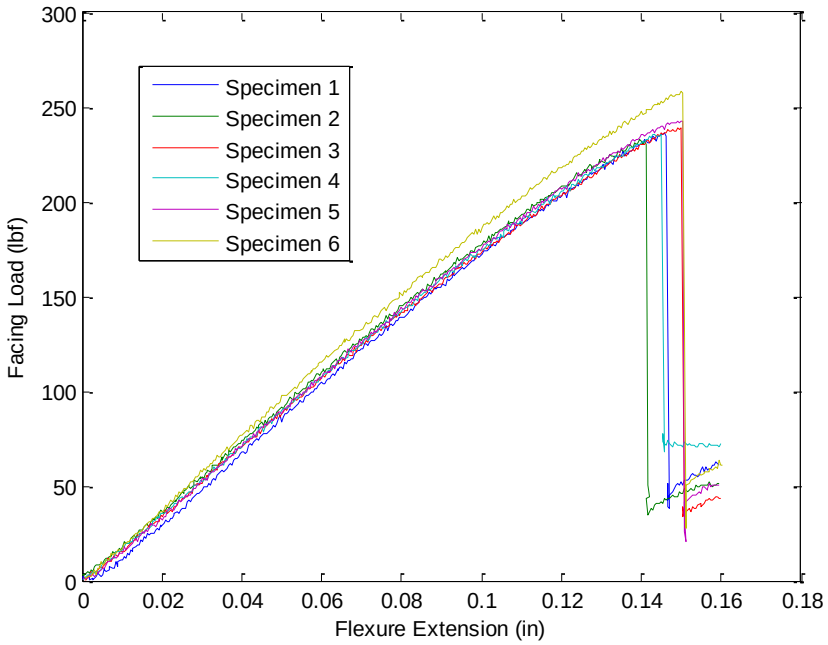

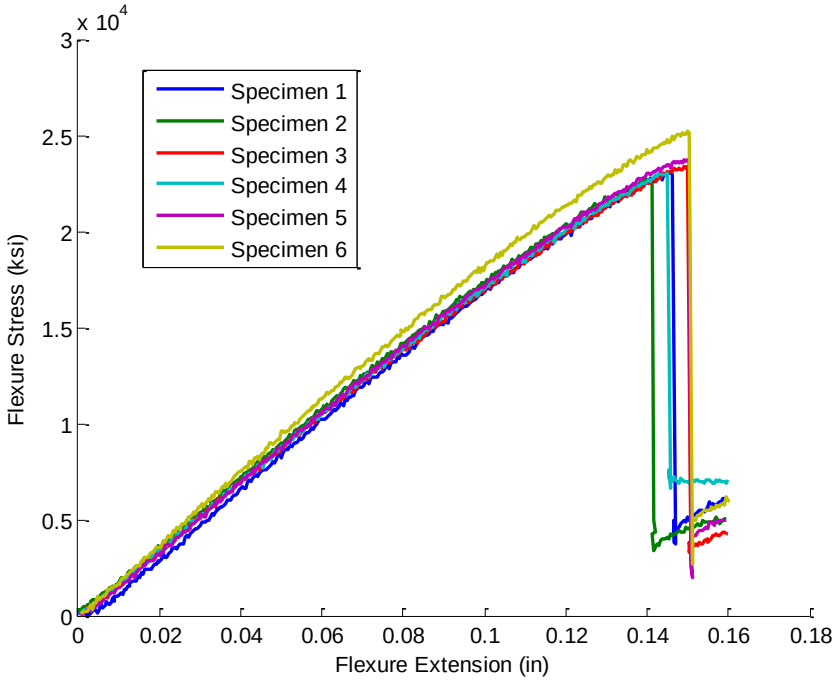

A.3 Varying Face Sheet Thickness Load and Stress Plots

* Bold Lines in stress plots Indicate bottom face sheet stress.

Figures 3.1.A. & 3.2.A. 1/1 Configuration Load and Facing stress vs Extension Plots

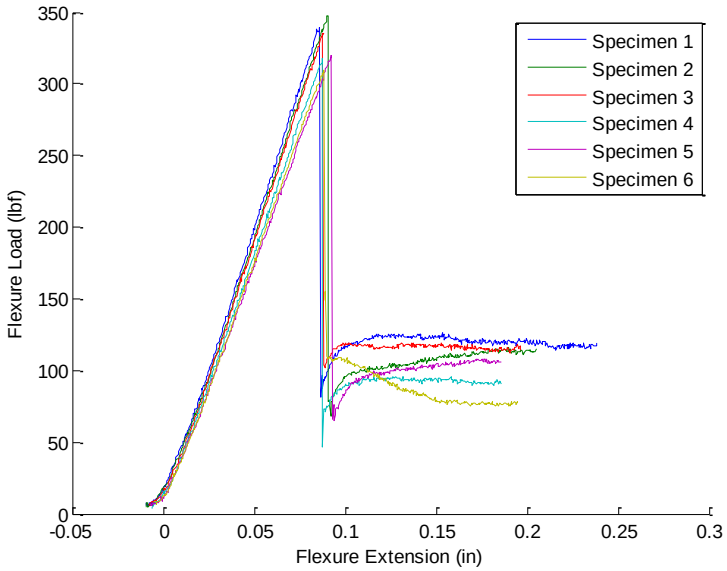

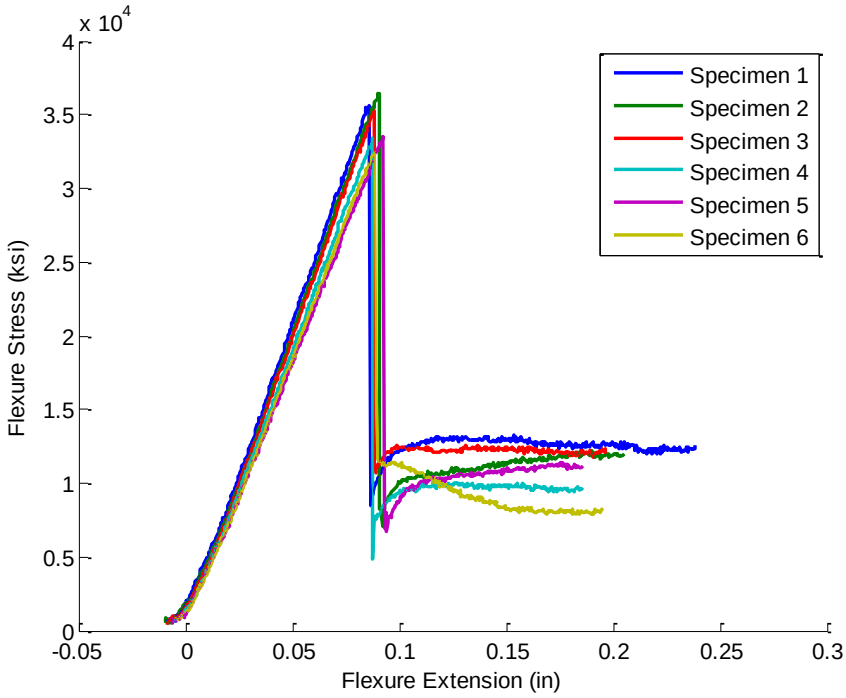

Figures 3.3.A. & 3.4.A. 2/1 Configuration Load and Facing stress vs Extension Plots

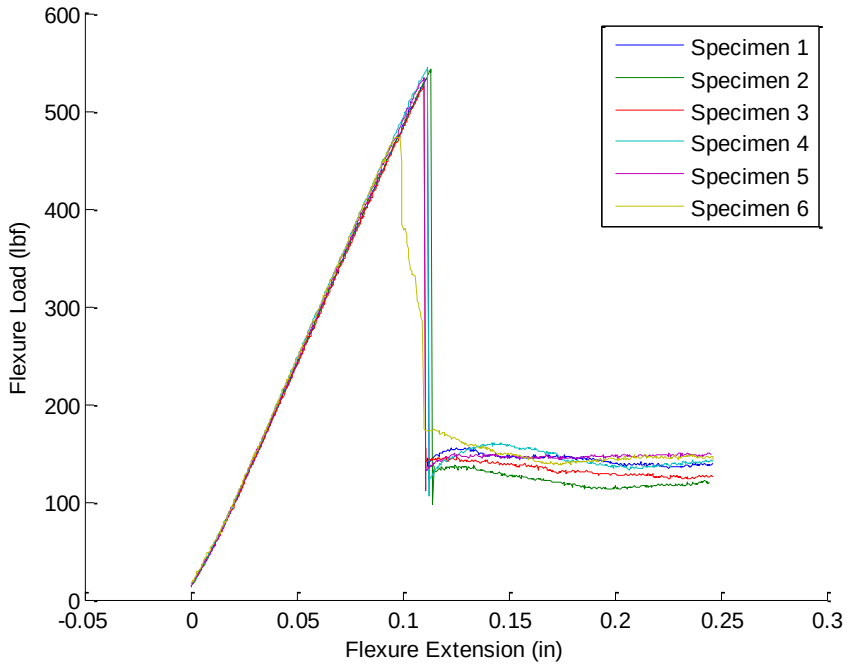

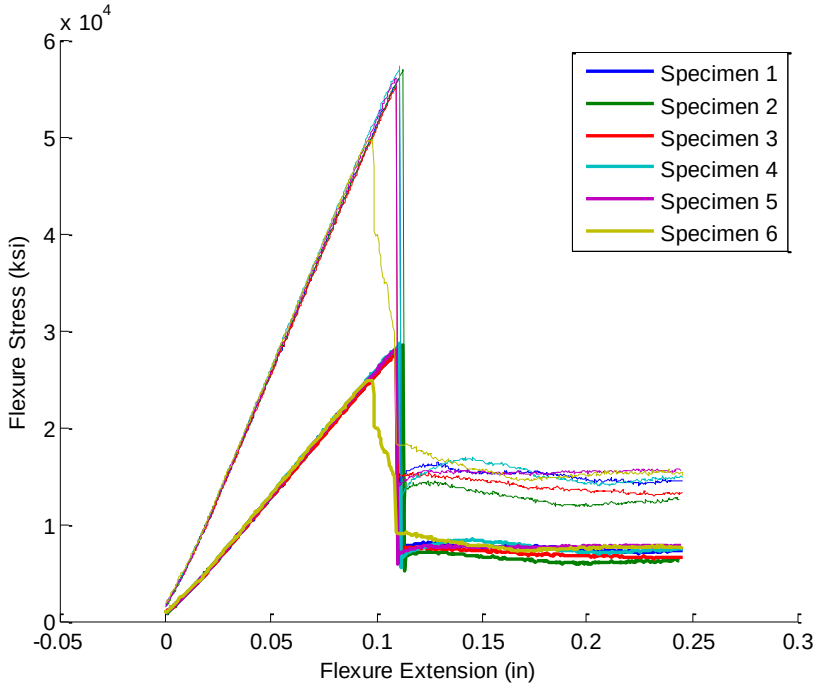

Figures 3.5.A. & 3.6.A. 3/1 Configuration Load and Facing stress vs Extension Plots

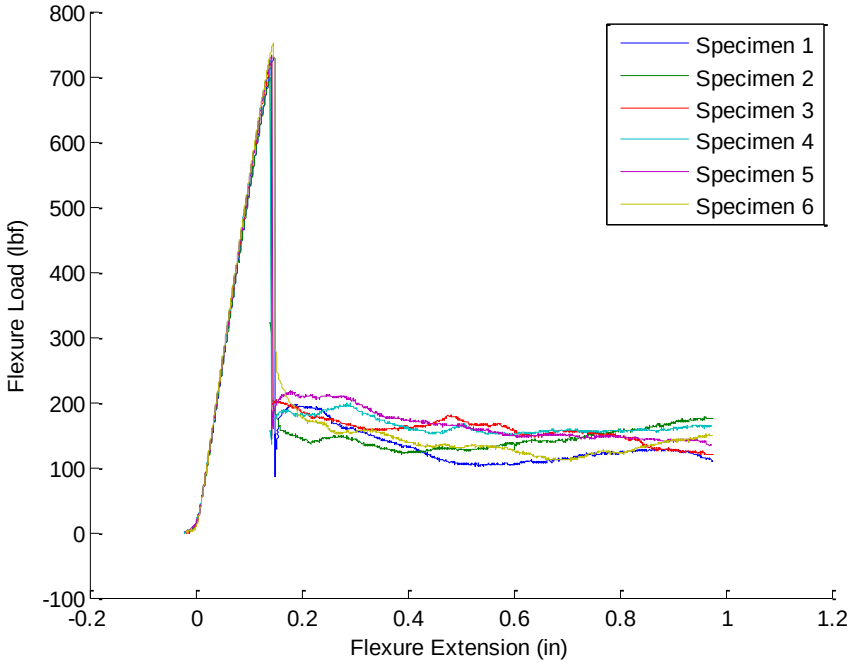

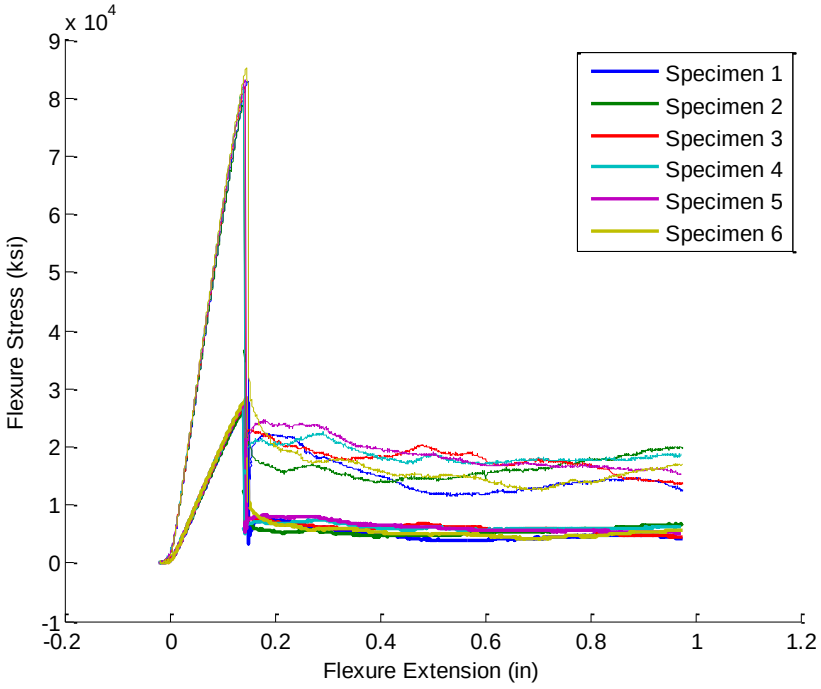

Figures 3.7.A. & 3.8.A. 4/1 Configuration Load and Facing stress vs Extension Plots

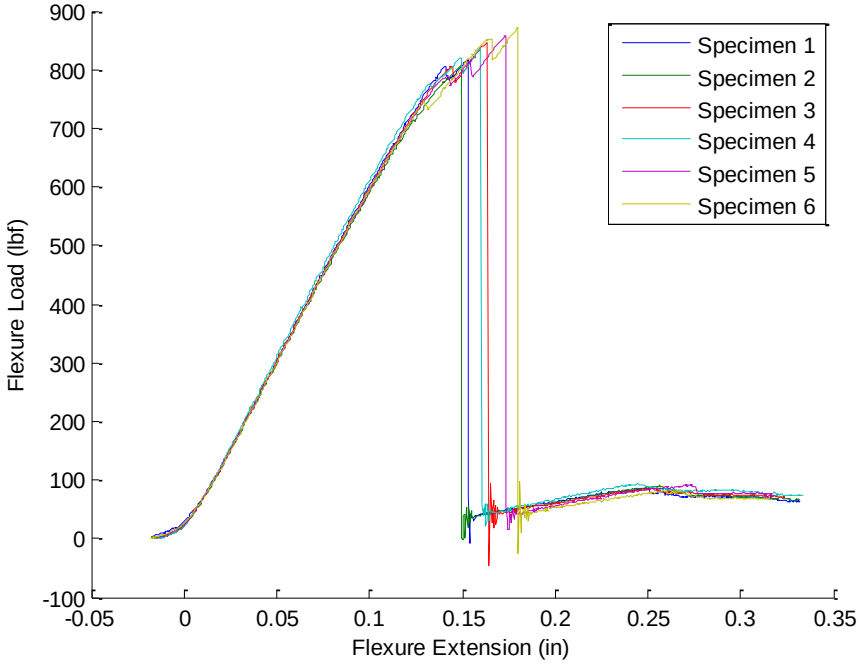

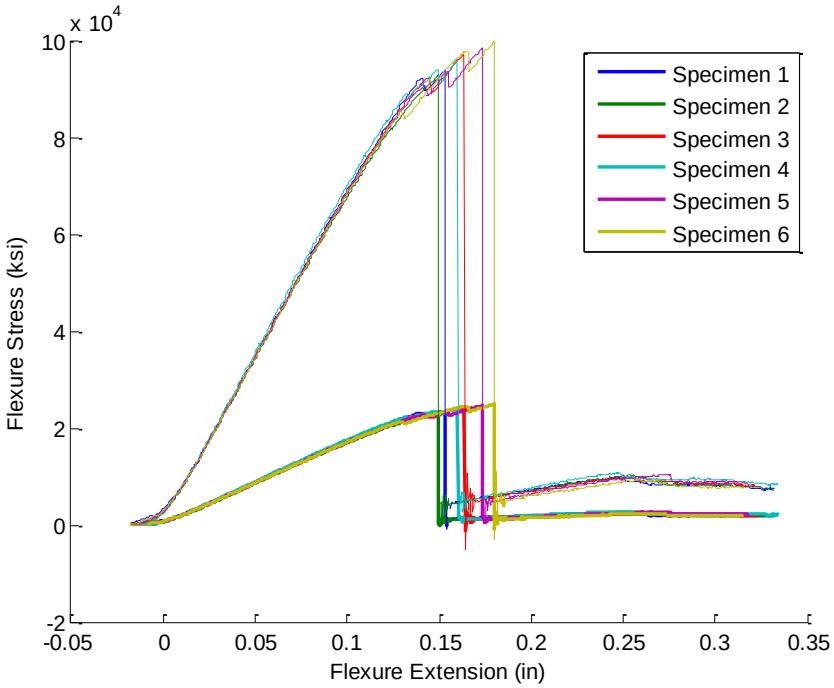

Figures 3.9.A. & 3.10.A. 5/1 Configuration Load and Facing stress vs Extension Plots

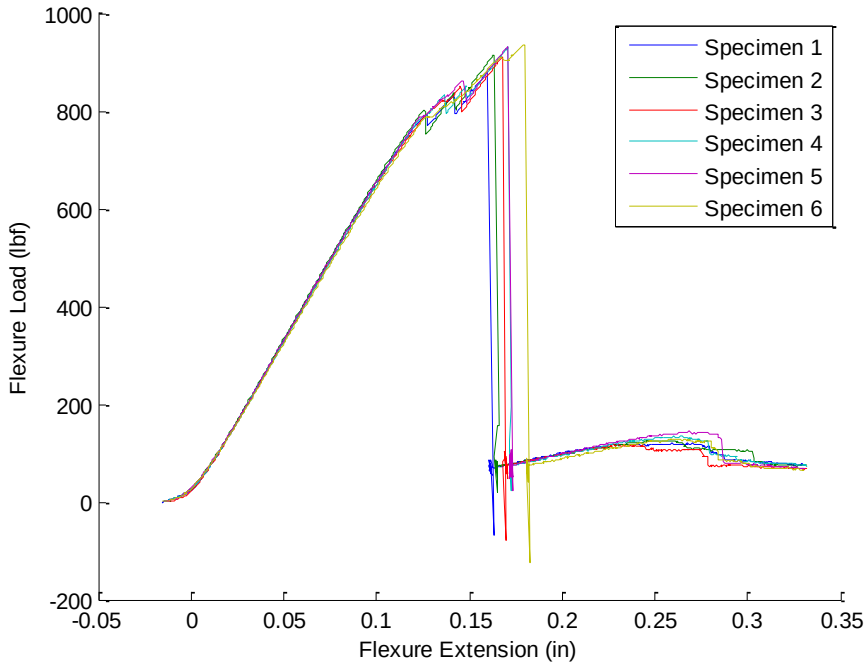

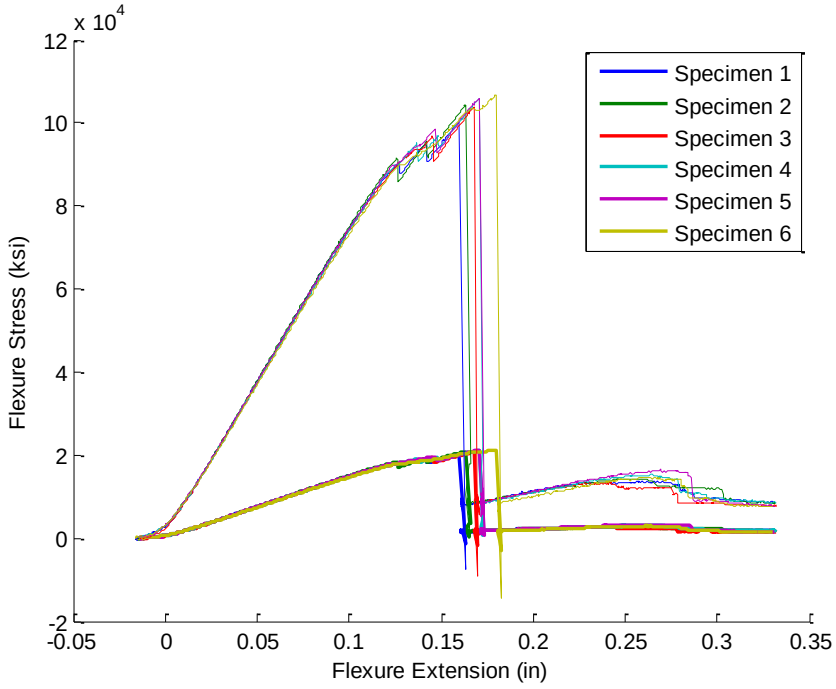

Figures 3.11.A. & 3.12.A. 1/2 Configuration Load and Facing stress vs Extension Plots

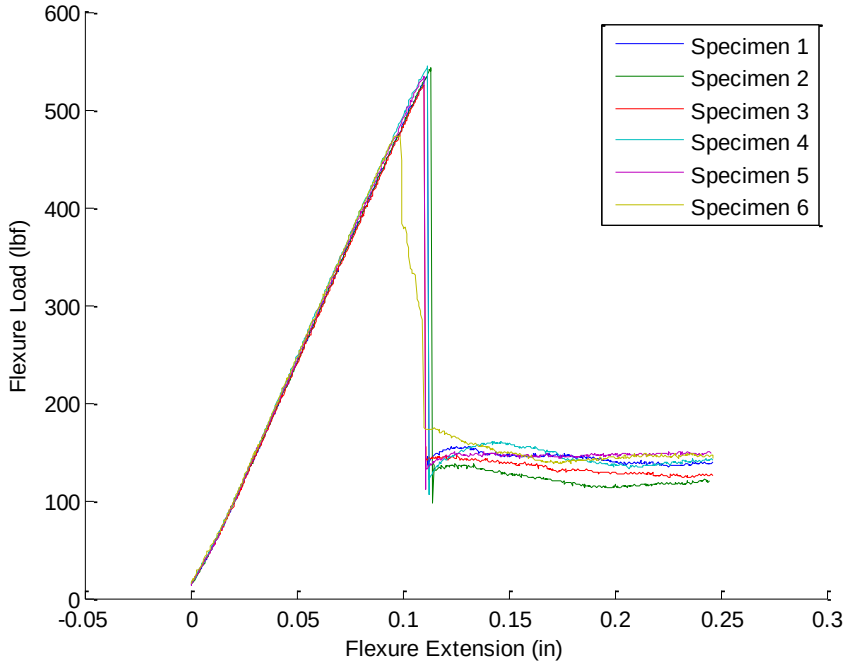

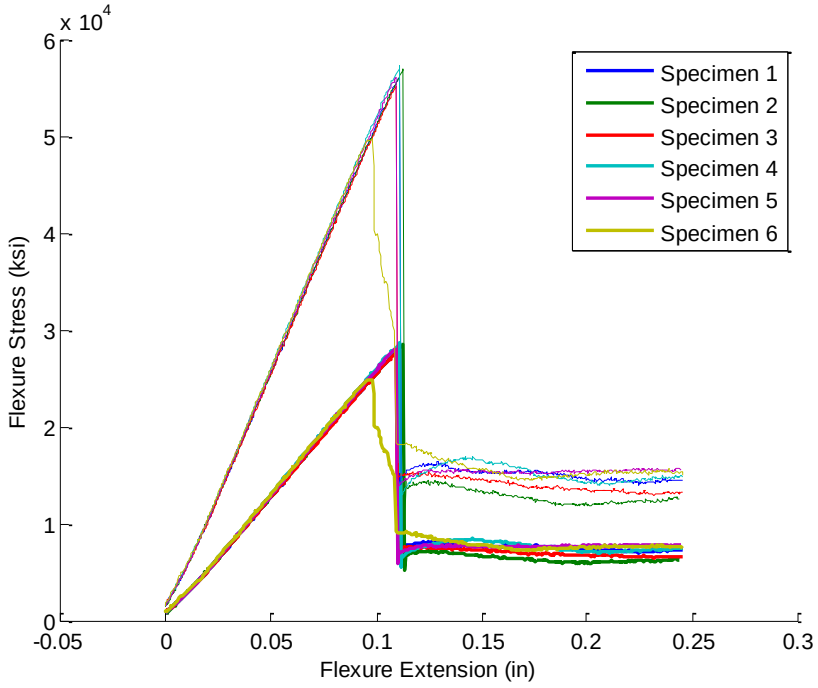

Figures 3.13.A. & 3.14.A. 2/2 Configuration Load and Facing stress vs Extension Plots

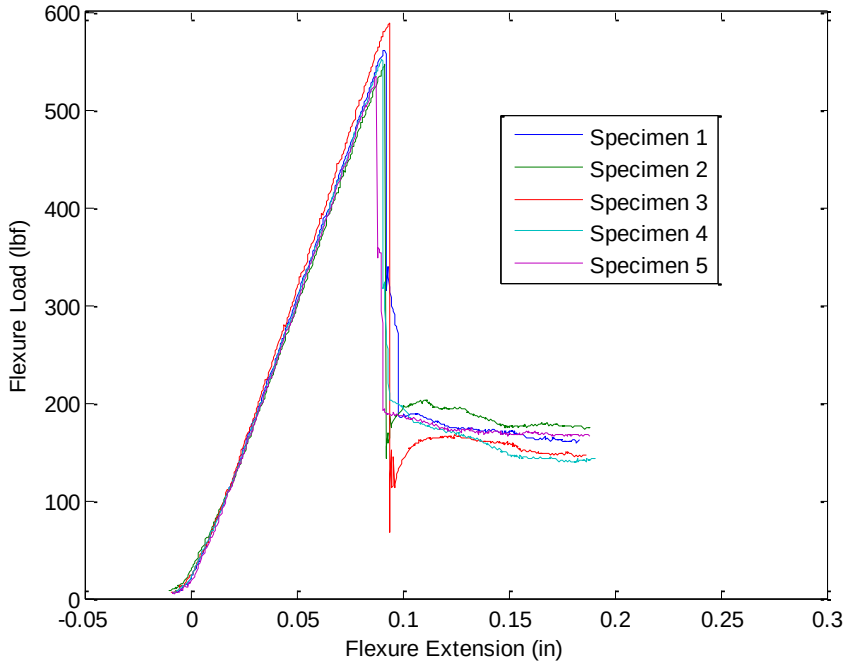

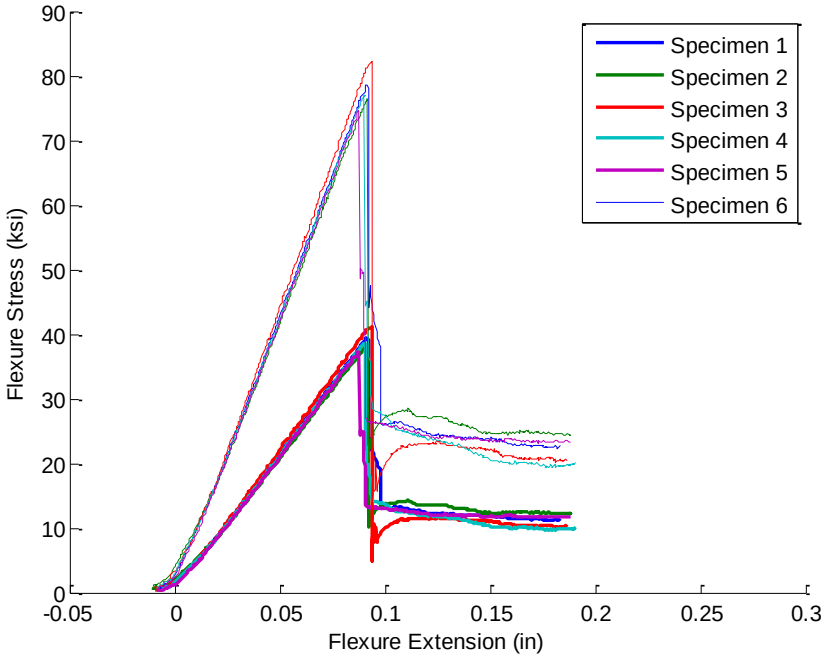

Figures 3.5.A. & 3.16.A. 3/2 Configuration Load and Facing stress vs Extension Plots

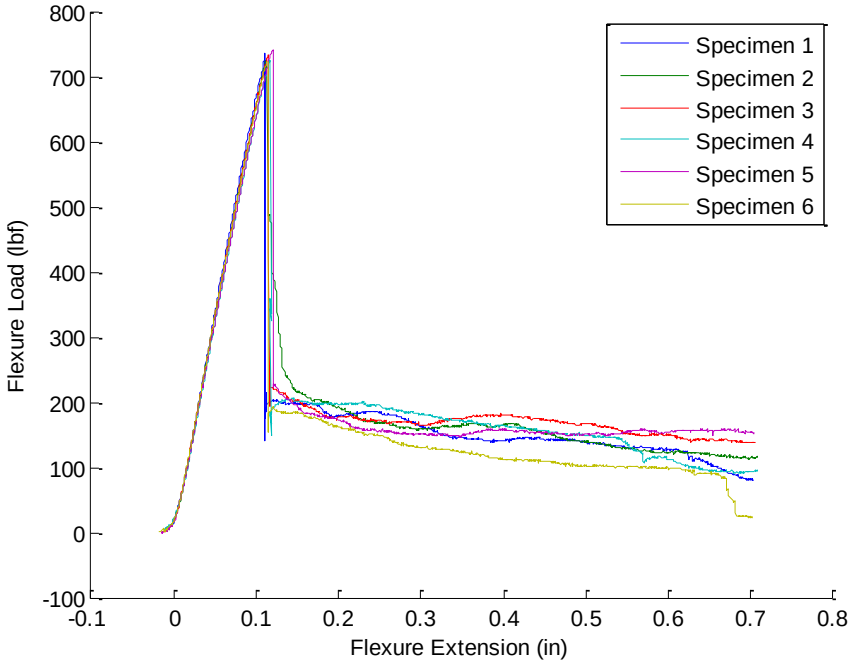

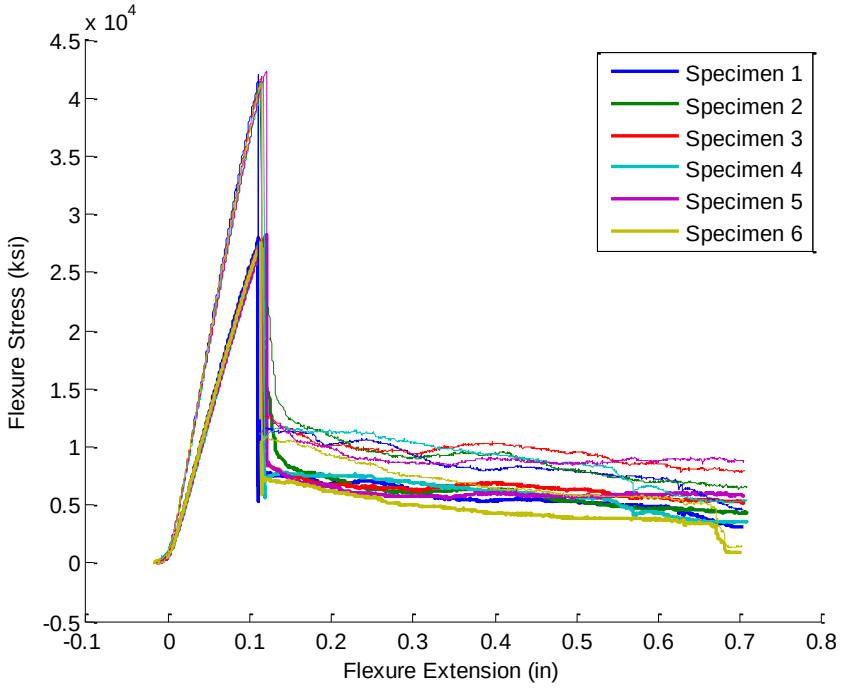

Figures 3.17.A. & 3.18.A. 4/2 Configuration Load and Facing stress vs Extension Plots

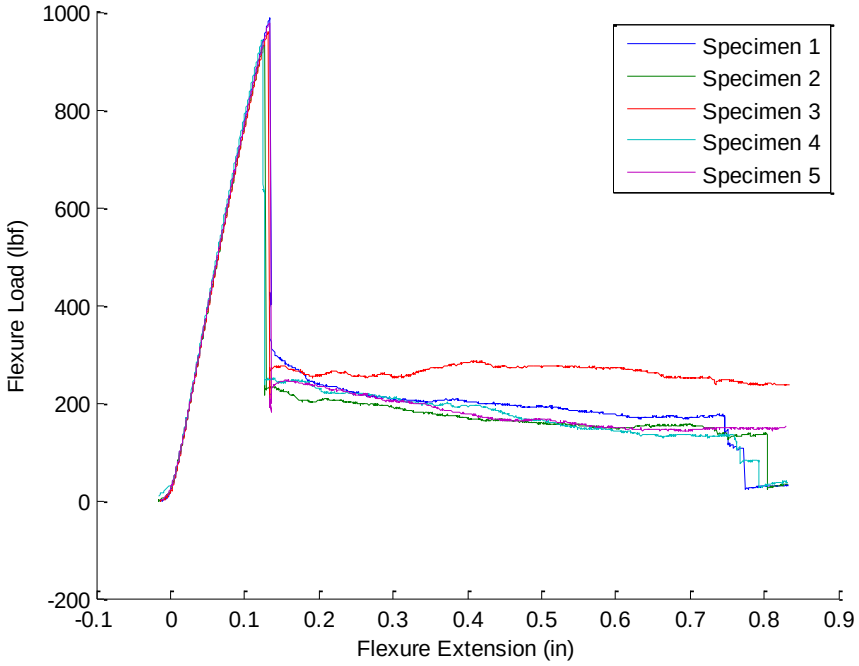

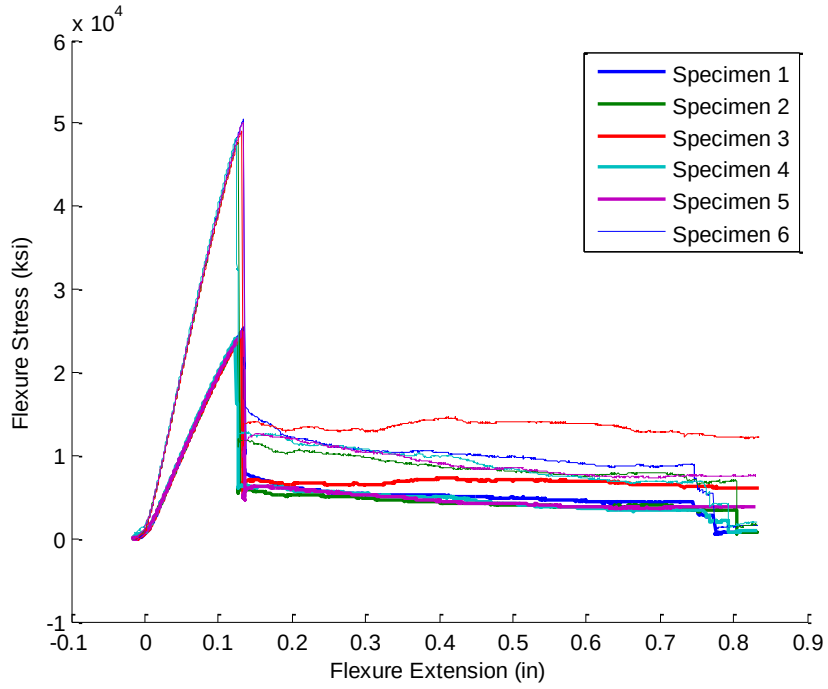

Figures 3.19.A. & 3.20.A. 5/2 Configuration Load and Facing stress vs Extension Plots

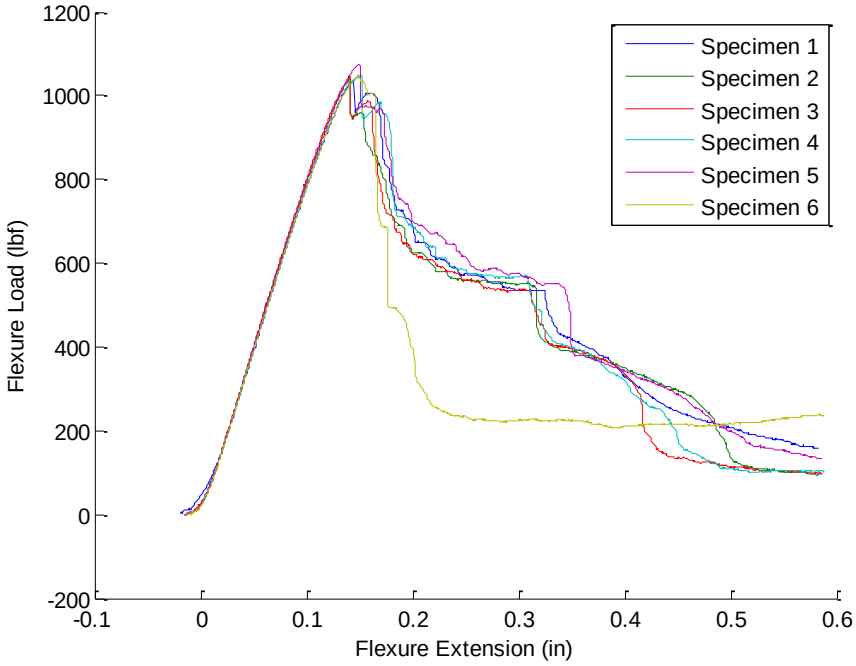

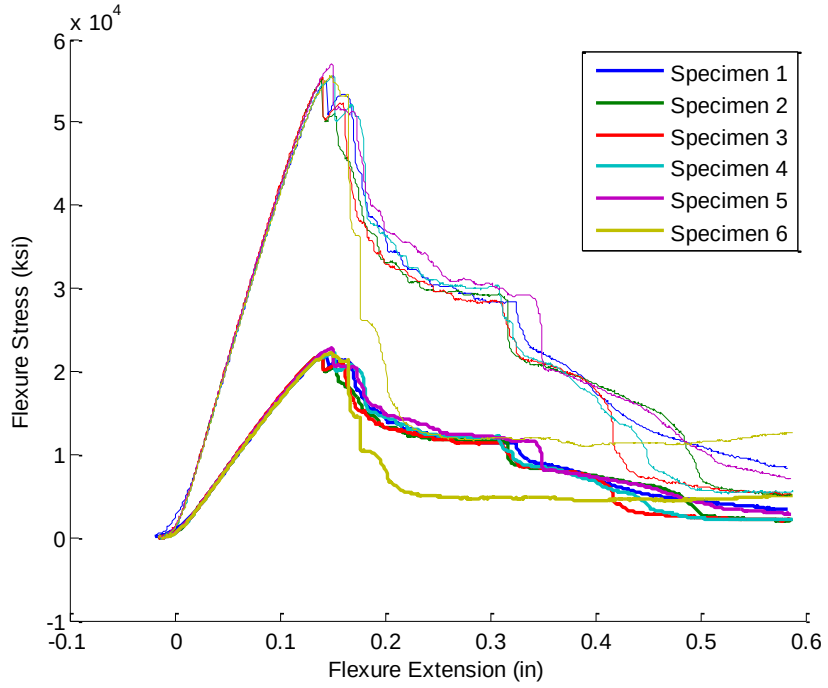

Figures 3.21.A. & 3.22.A. 1/3 Configuration Load and Facing stress vs Extension Plots

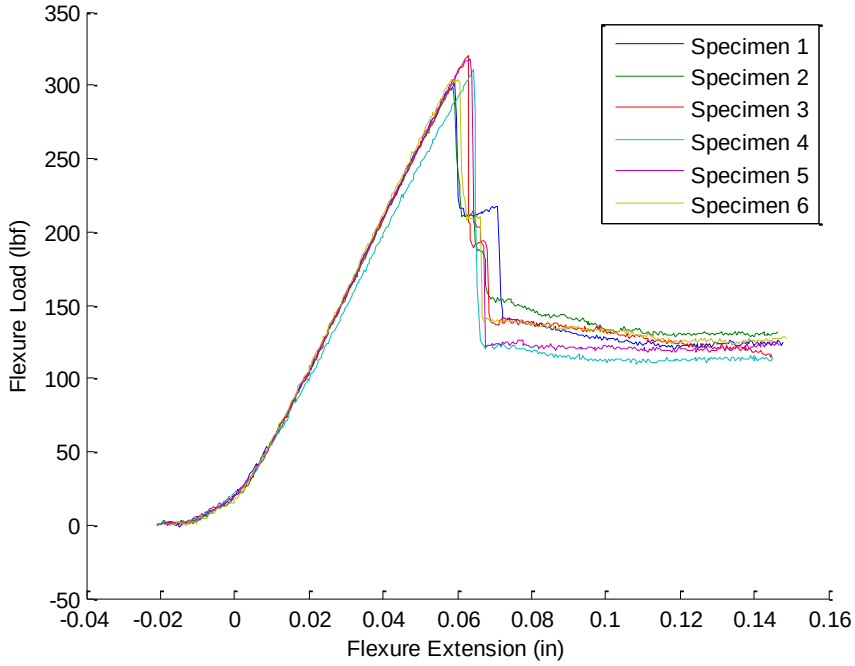

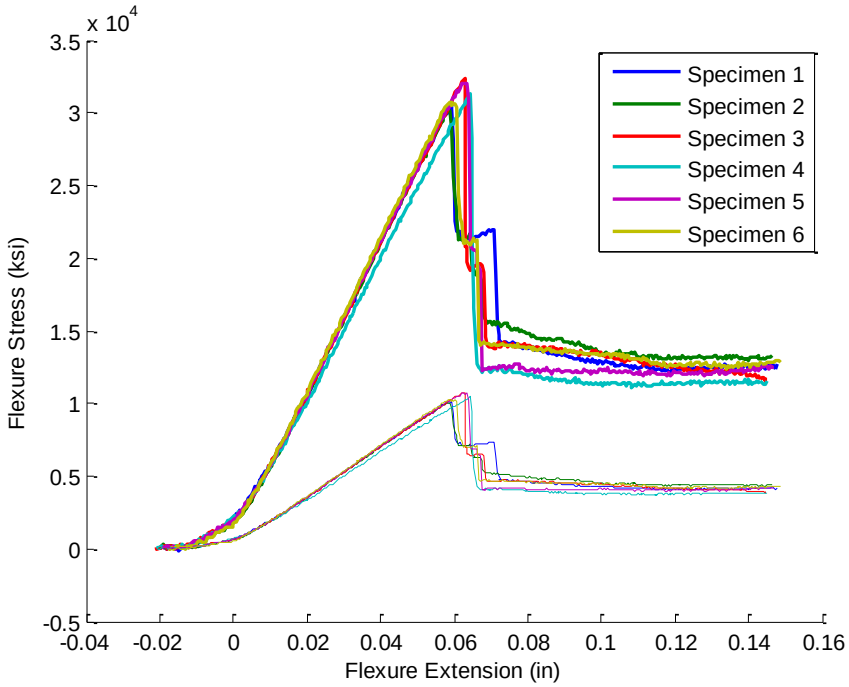

Figures 3.23.A. & 3.24.A. 2/3 Configuration Load and Facing stress vs Extension Plots

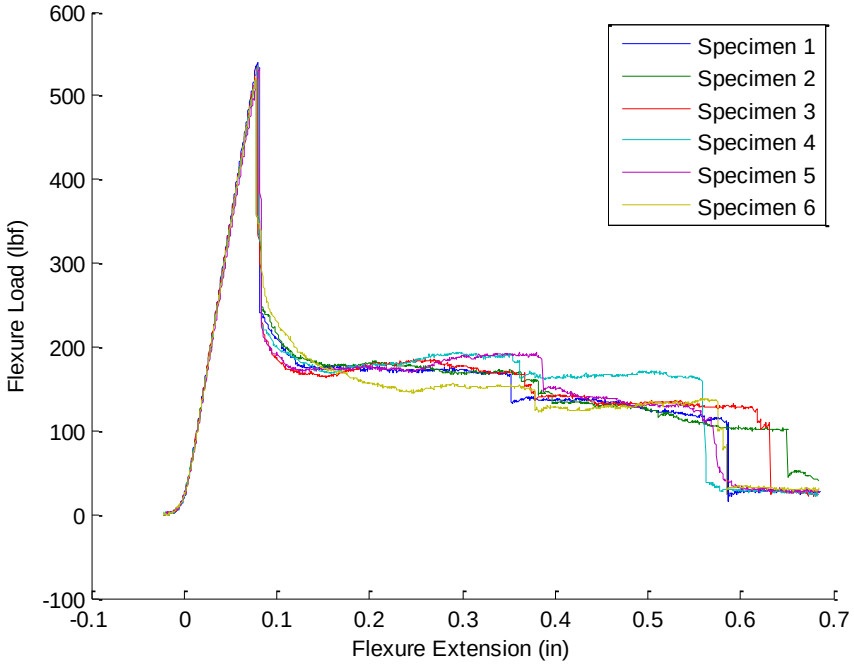

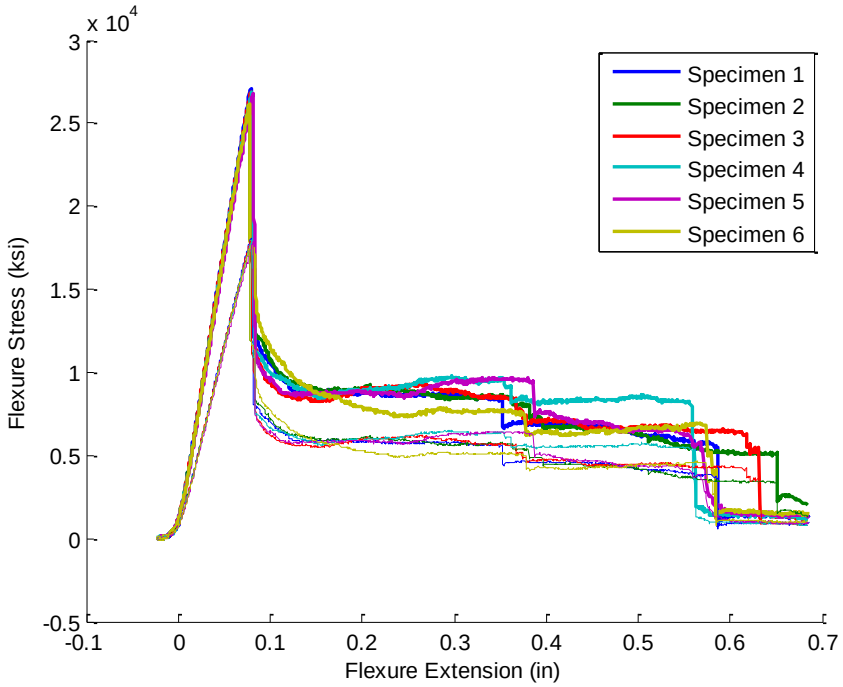

Figures 3.25.A. & 3.26.A. 3/3 Configuration Load and Facing stress vs Extension Plots

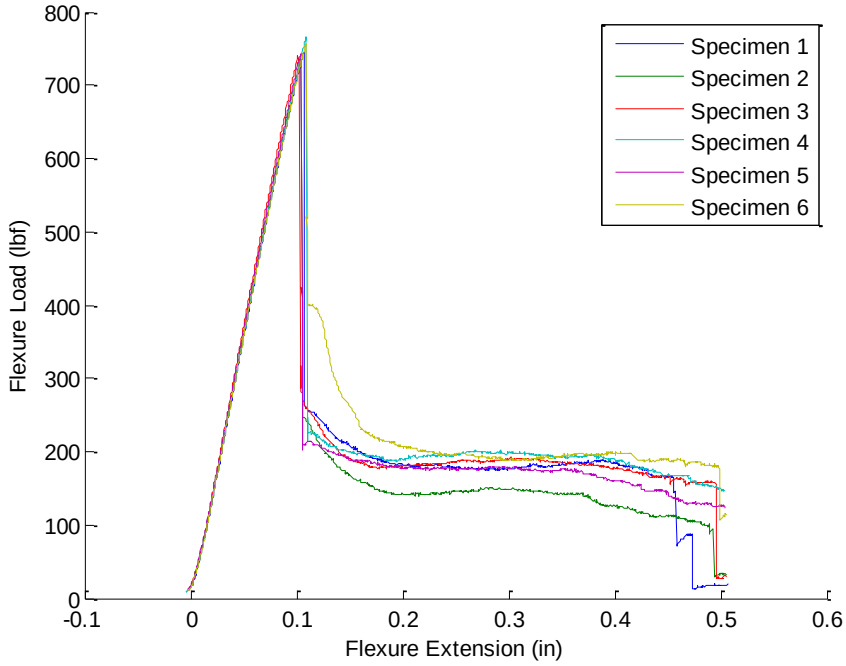

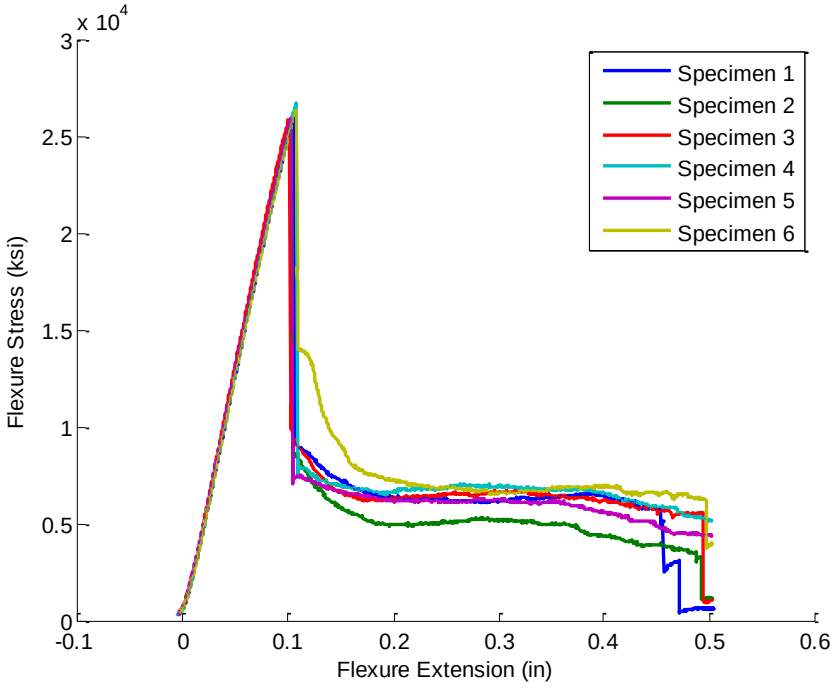

Figures 3.27.A. & 3.28.A. 4/3 Configuration Load and Facing stress vs Extension Plots

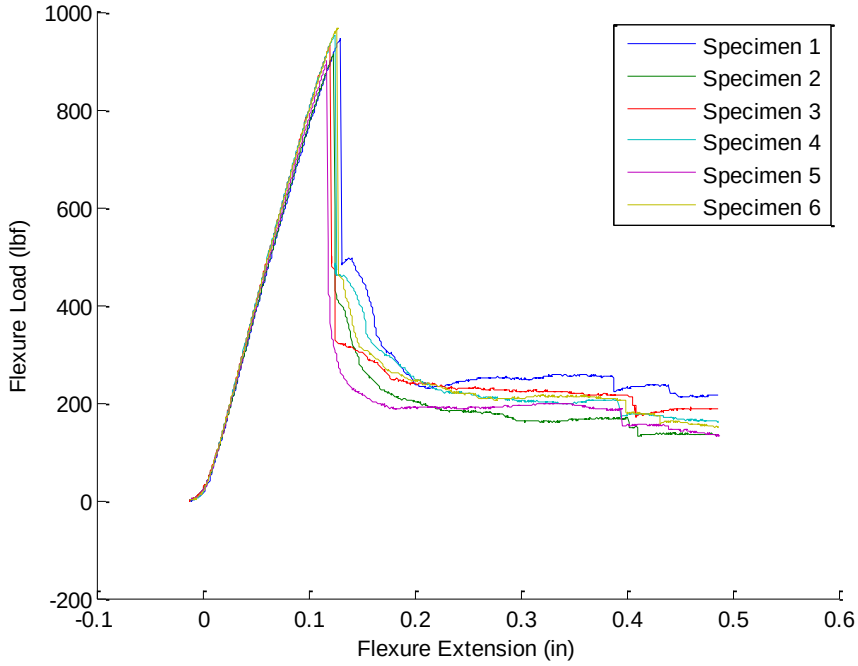

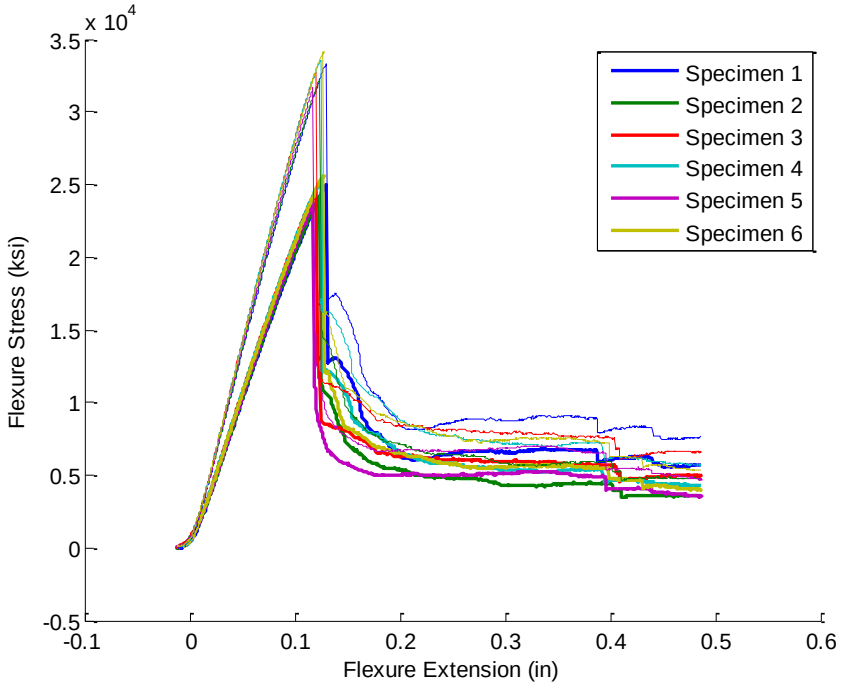

Figures 3.29.A. & 3.30.A. 5/3 Configuration Load and Facing stress vs Extension Plots

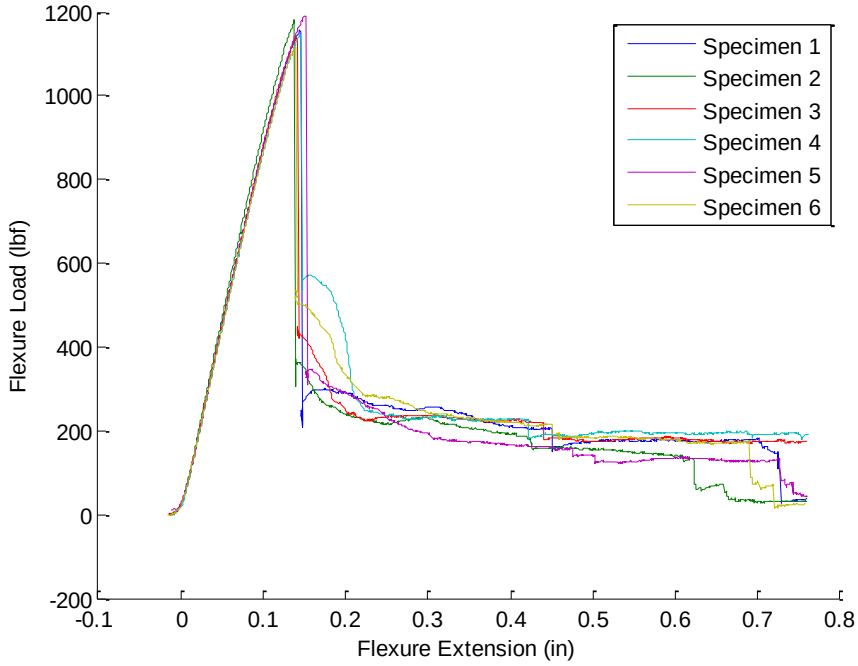

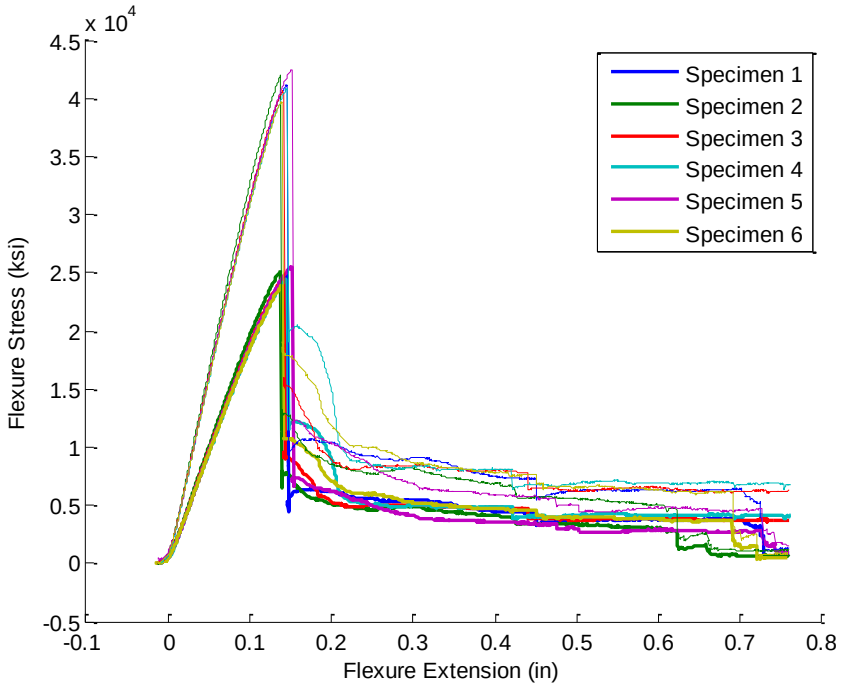

Figures 3.31.A. & 3.32.A 1/4 Configuration Load and Facing stress vs Extension Plots

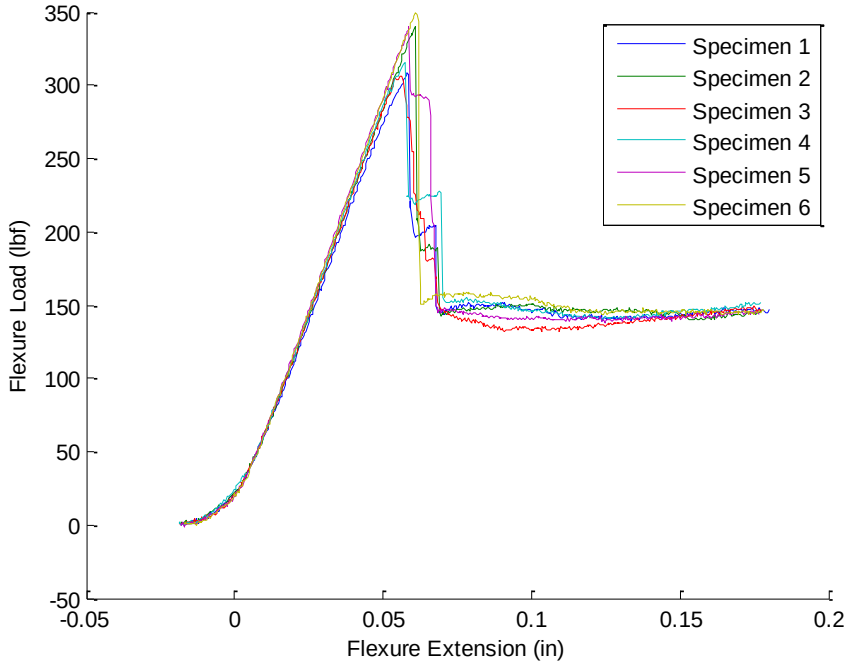

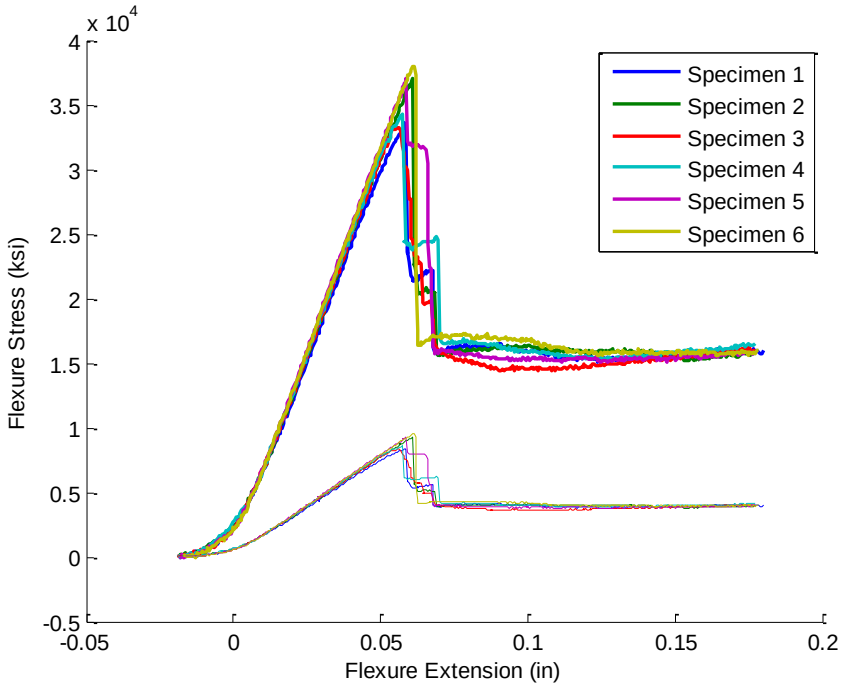

Figures 3.33.A. & 3.34.A. 2/4 Configuration Load and Facing stress vs Extension Plots

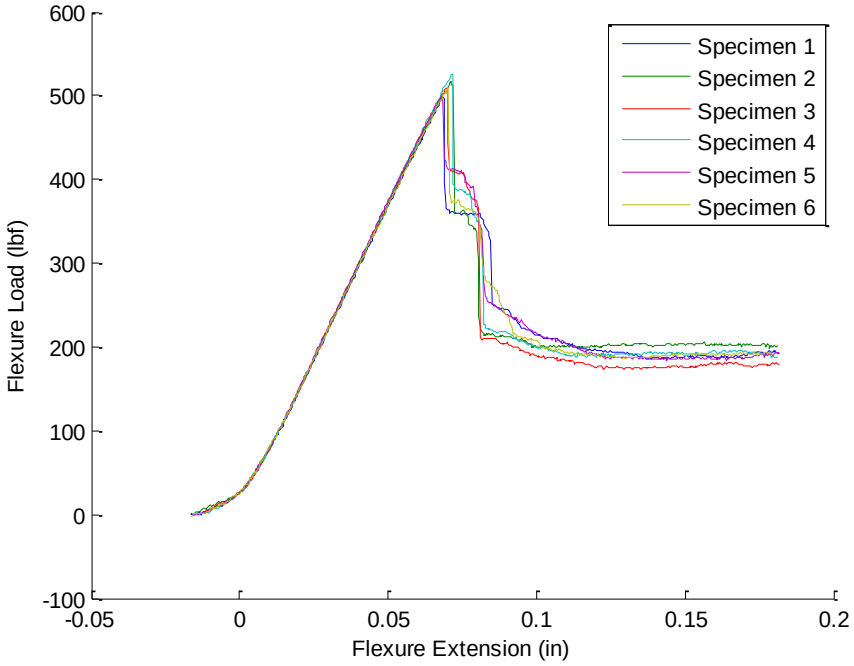

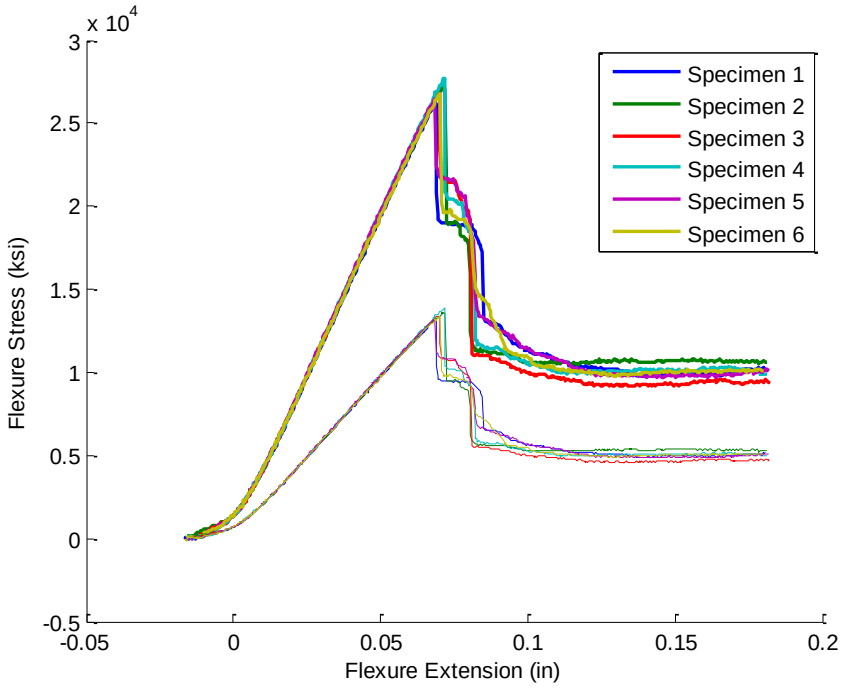

Figures 3.35.A. & 3.36.A. 3/4 Configuration Load and Facing stress vs Extension Plots

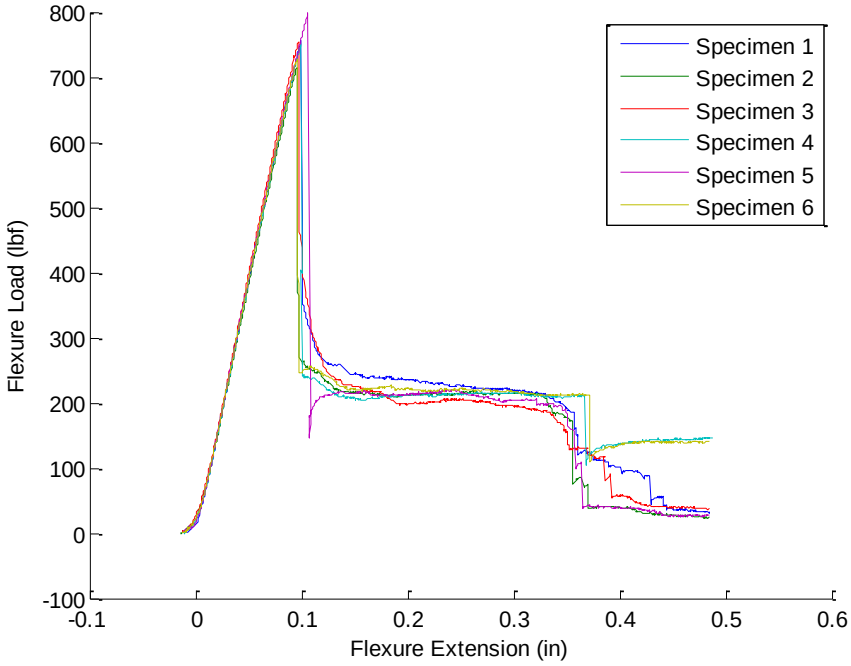

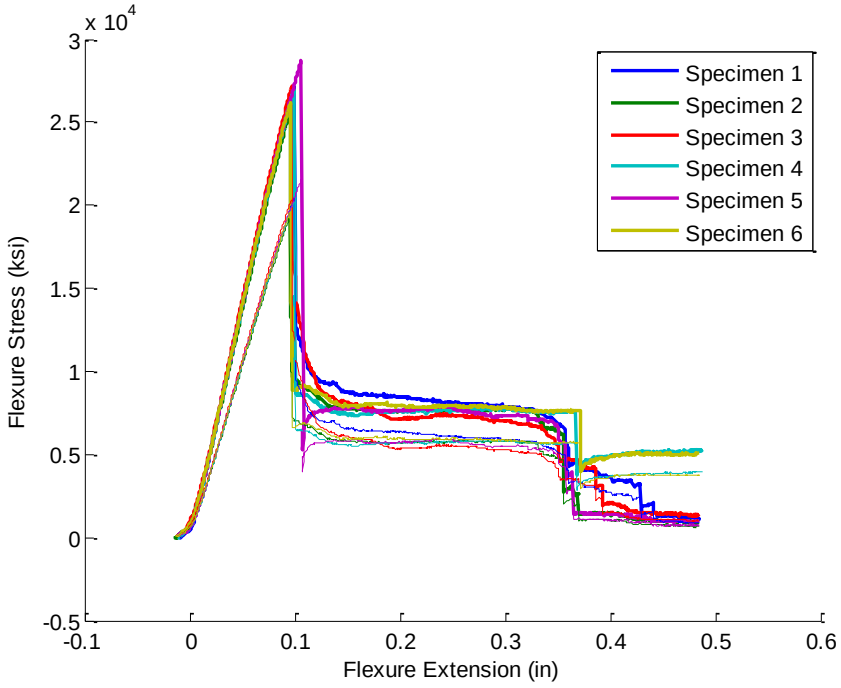

Figures 3.37.A. & 3.38.A. 4/4 Configuration Load and Facing stress vs Extension Plots

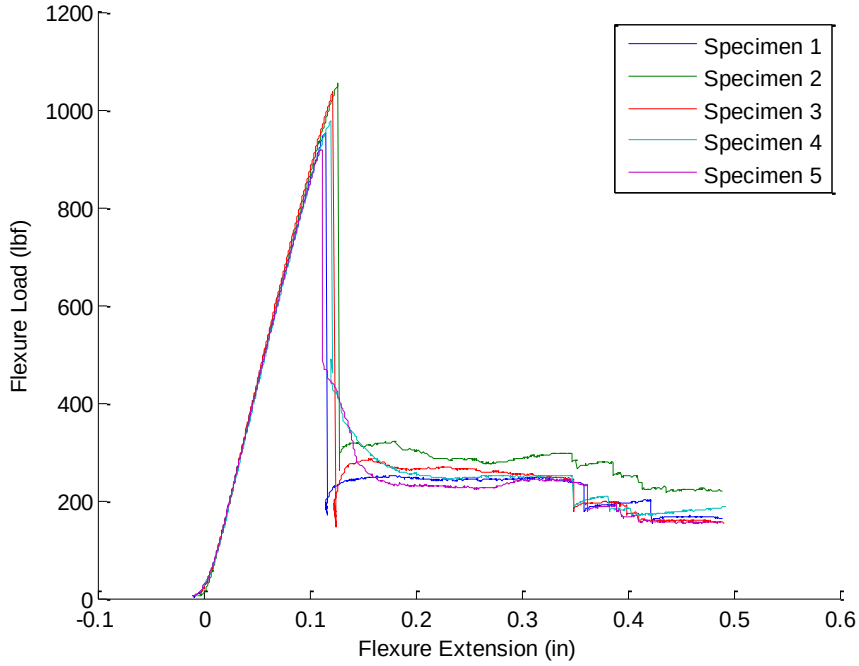

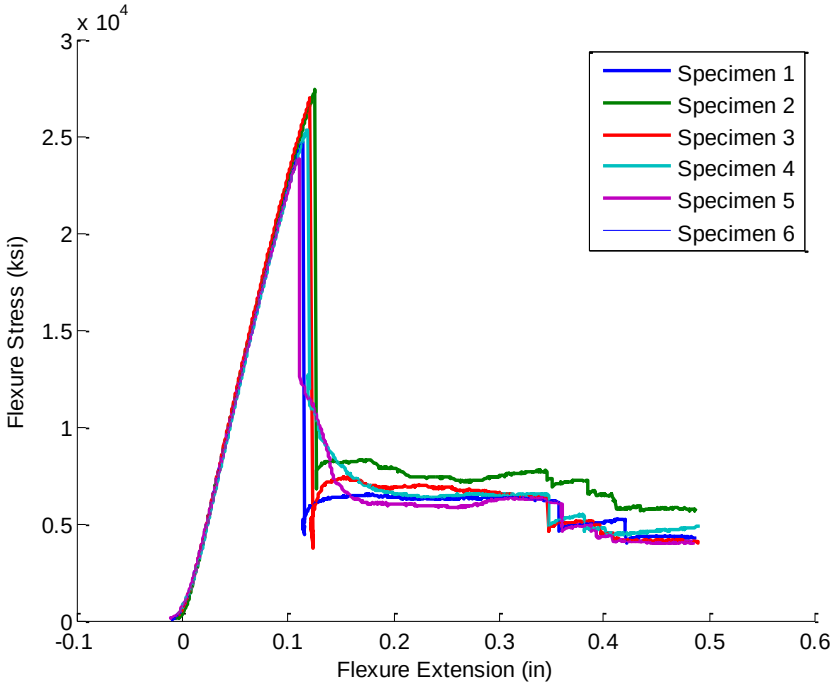

Figures 3.39.A. & 3.40.A. 5/4 Configuration Load and Facing stress vs Extension Plots

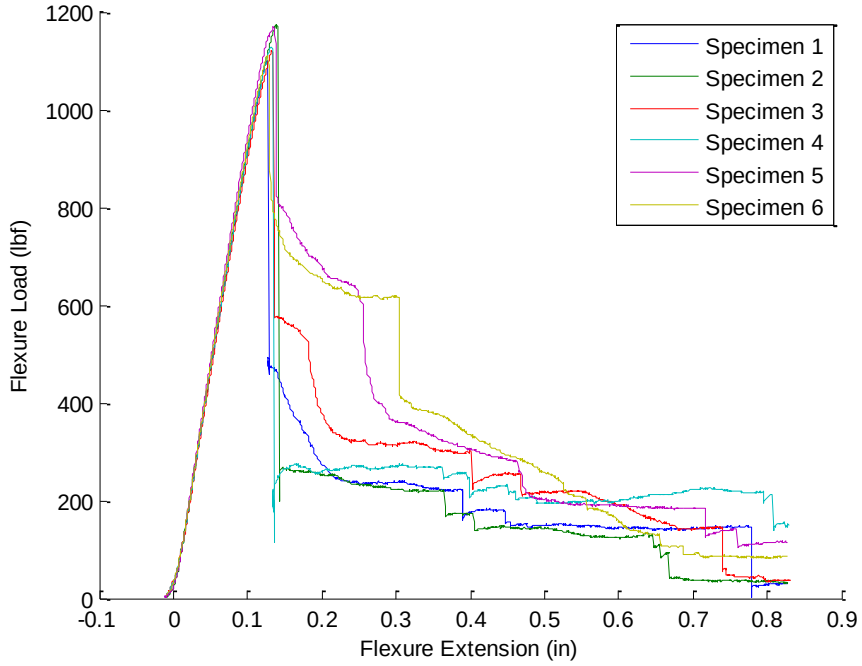

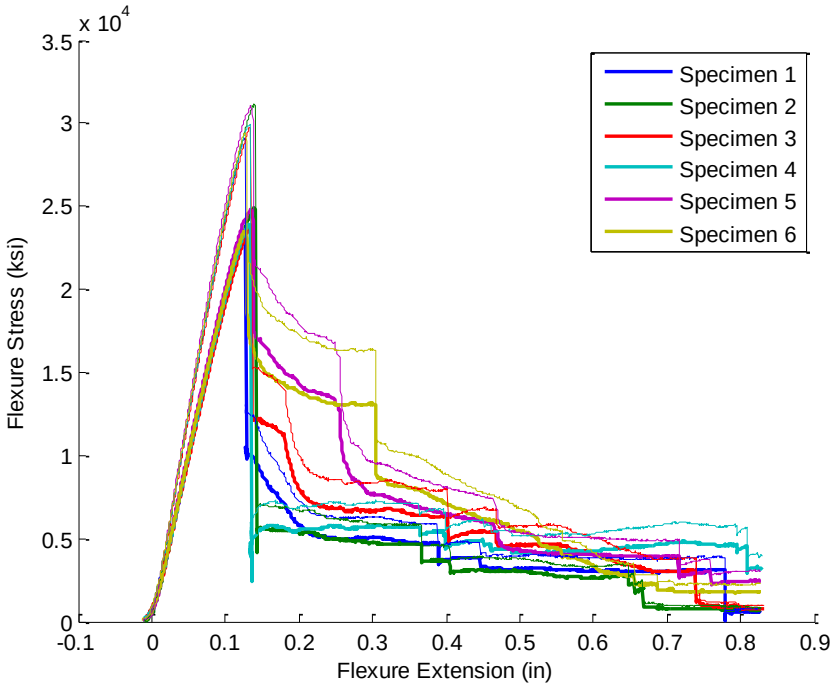

Figures 3.41.A. & 3.42.A. 1/5 Configuration Load and Facing stress vs Extension Plots

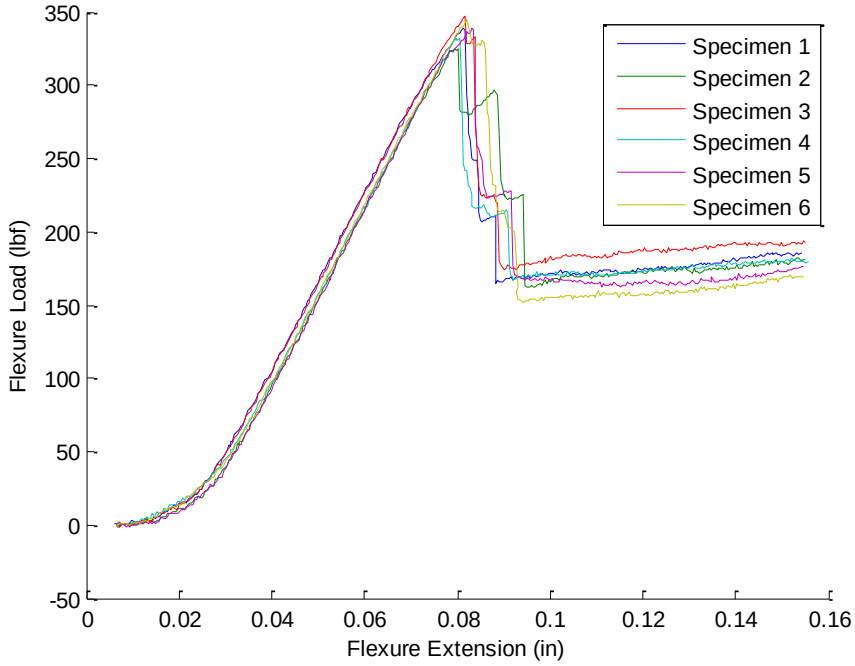

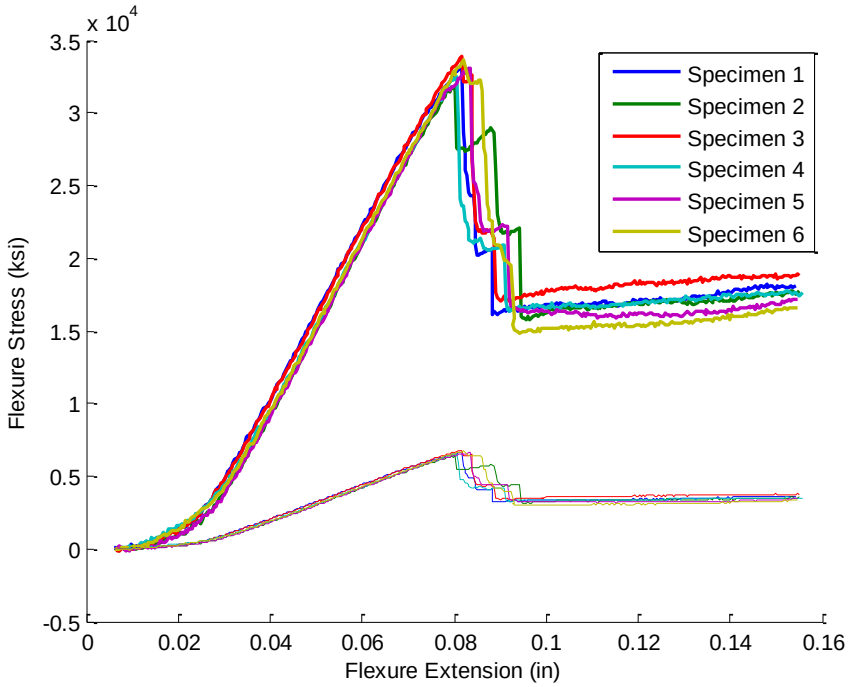

Figures 3.43.A. & 3.44.A. 2/5 Configuration Load and Facing stress vs Extension Plots

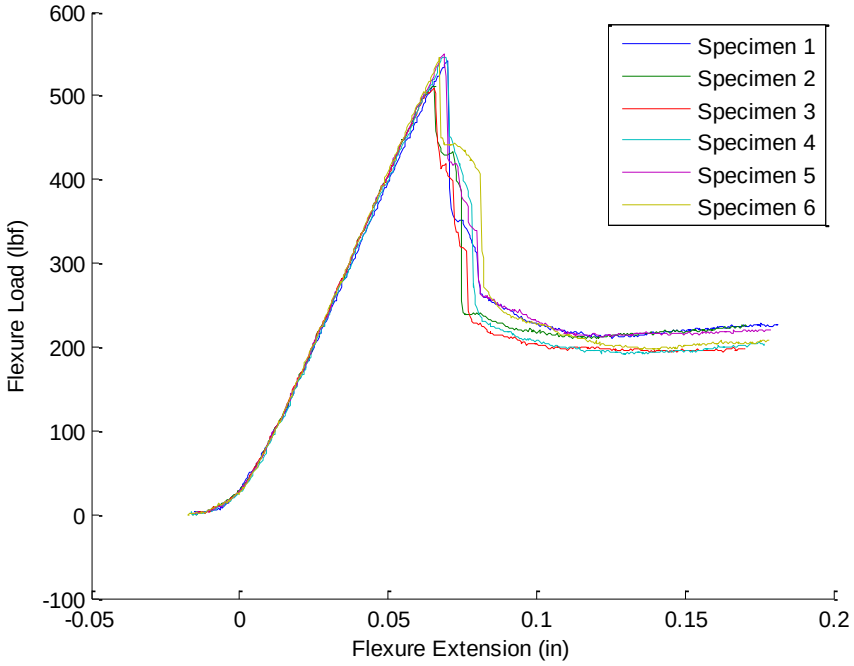

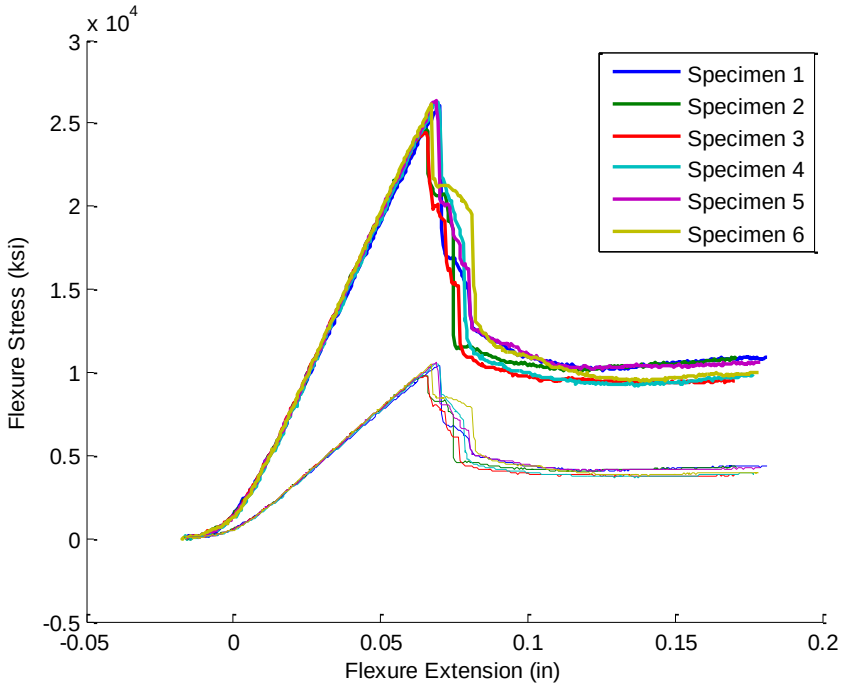

Figures 3.45.A. & 3.46.A. 3/5 Configuration Load and Facing stress vs Extension Plots

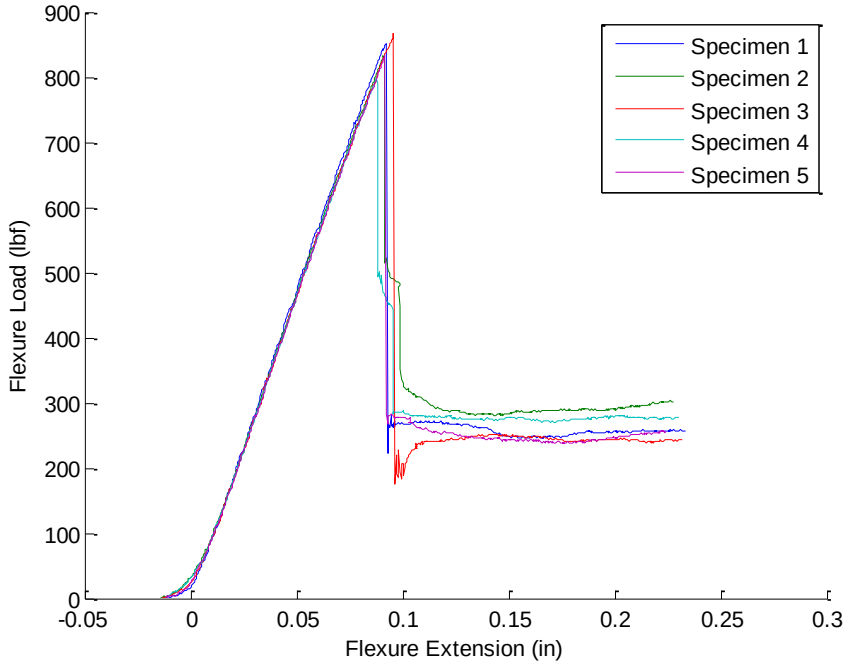

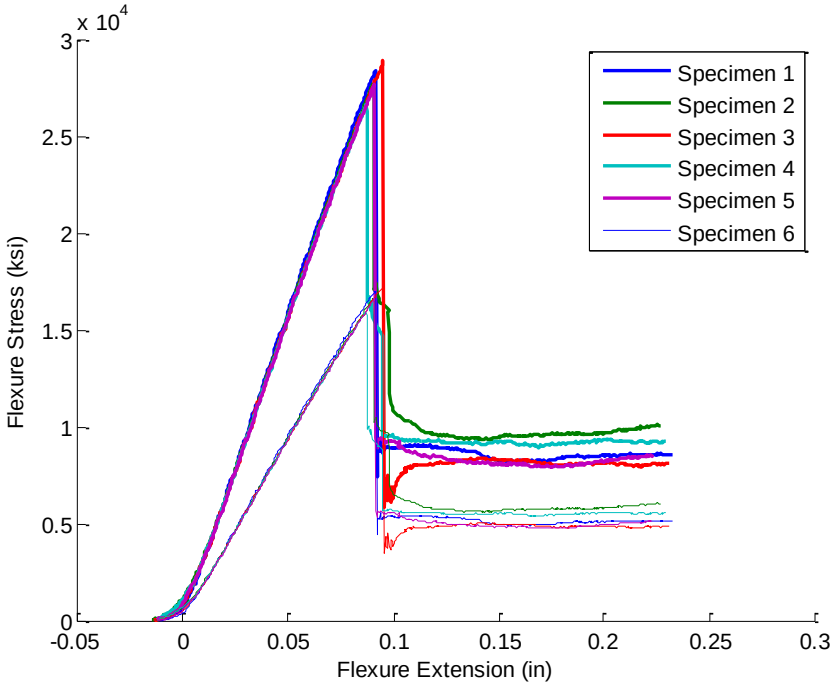

Figures 3.47.A. & 3.48.A. 4/5 Configuration Load and Facing stress vs Extension Plots

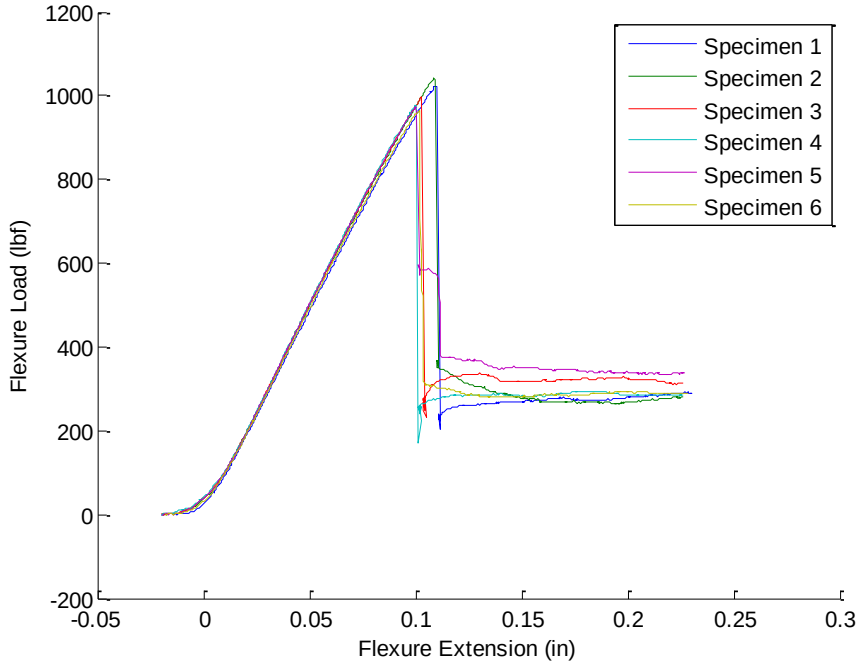

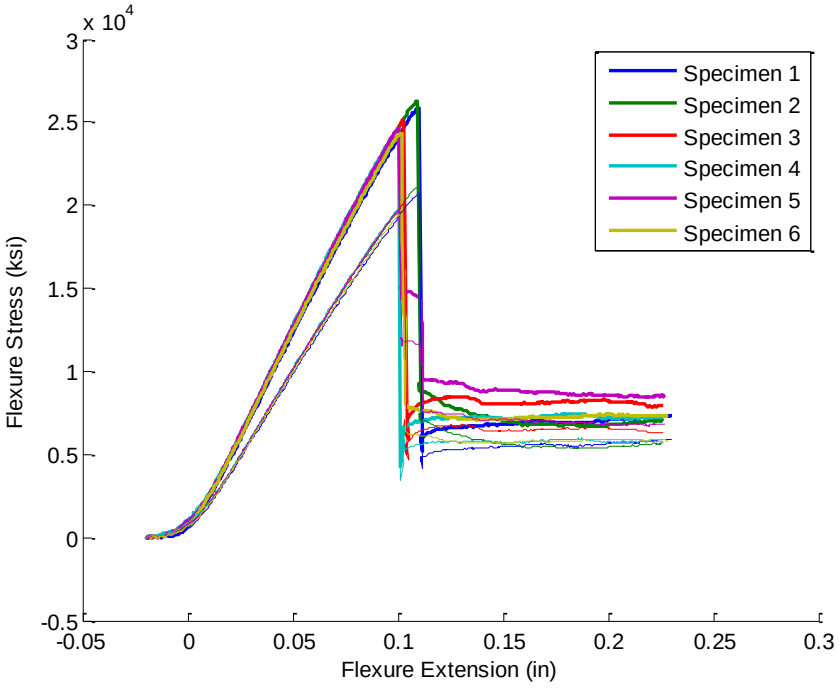

Figures 3.49.A. & 3.50.A. 5/5 Configuration Load and Facing stress vs Extension Plots

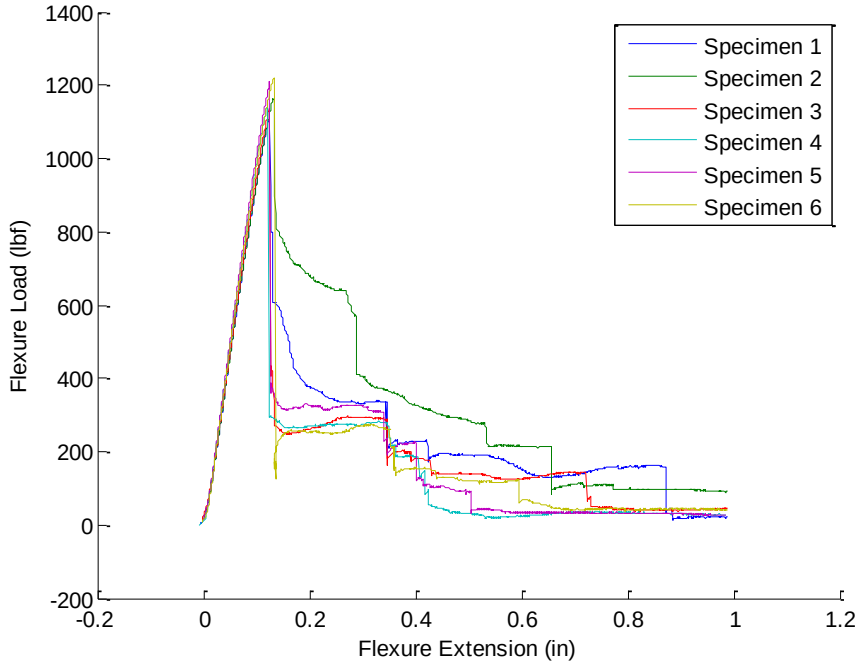

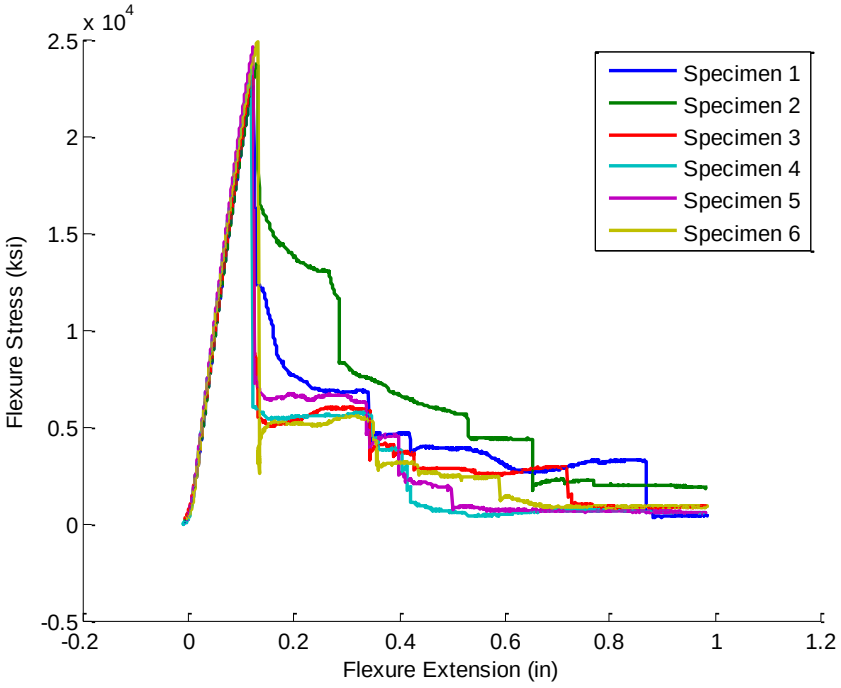

A.4 Finite Element Analysis – Core Ribbon Direction

Figures 4.1.A. & 4.2.A 15 Degree Core FEA Stress and Deflection Plots

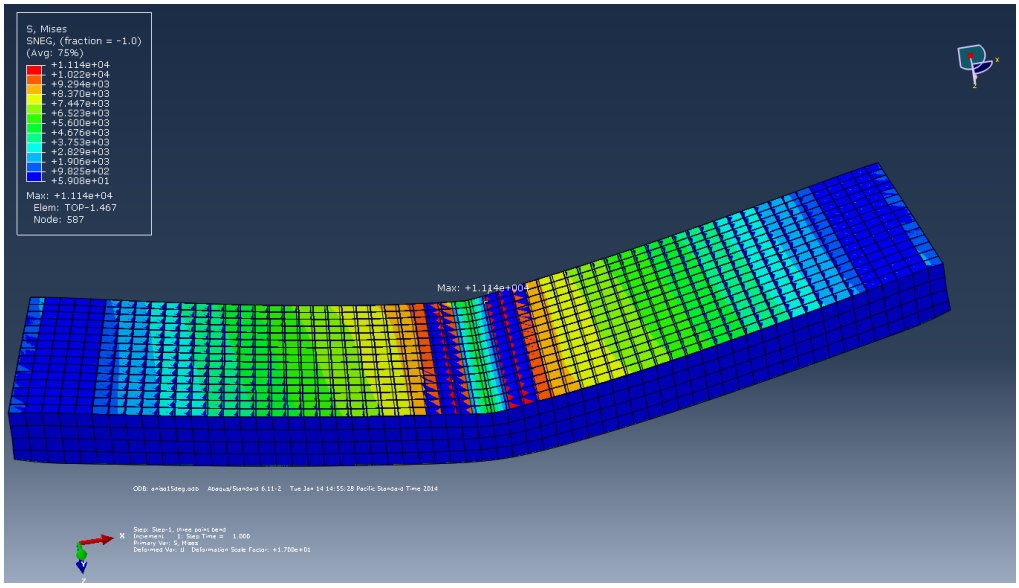

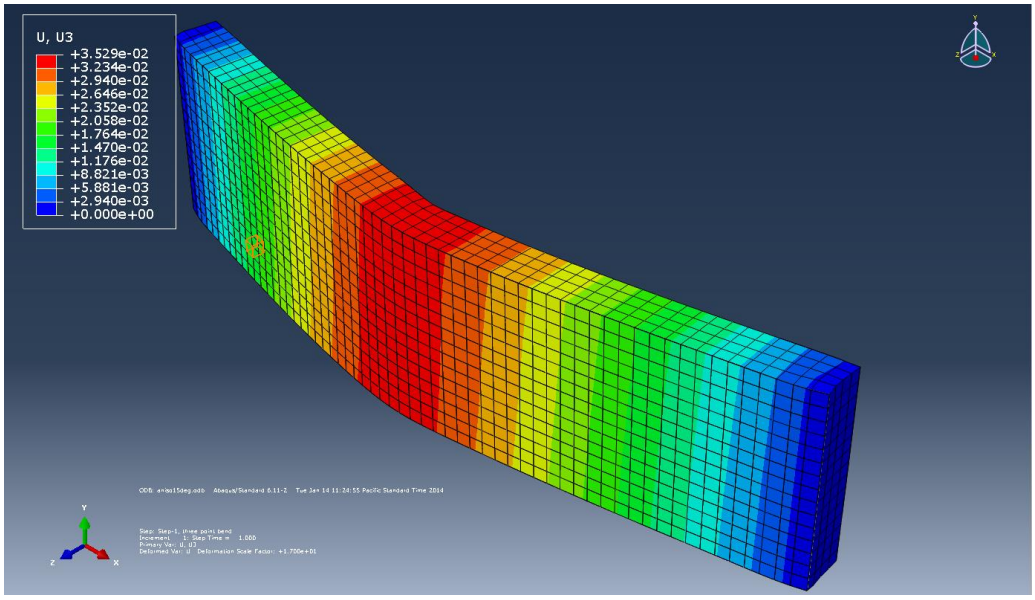

Figures 4.3.A. & 4.4.A 30 Degree Core FEA Stress and Displacement plots

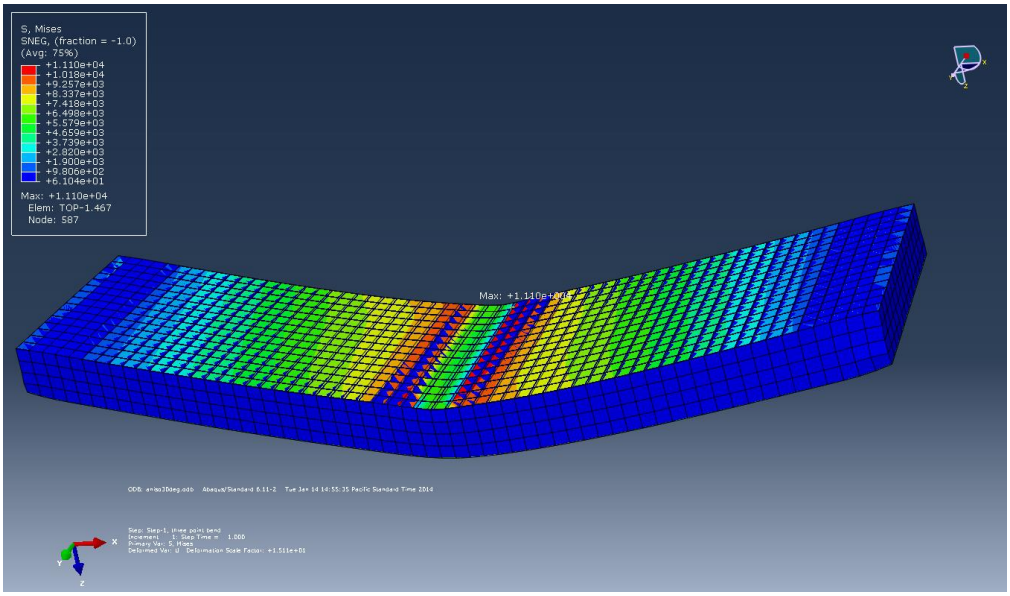

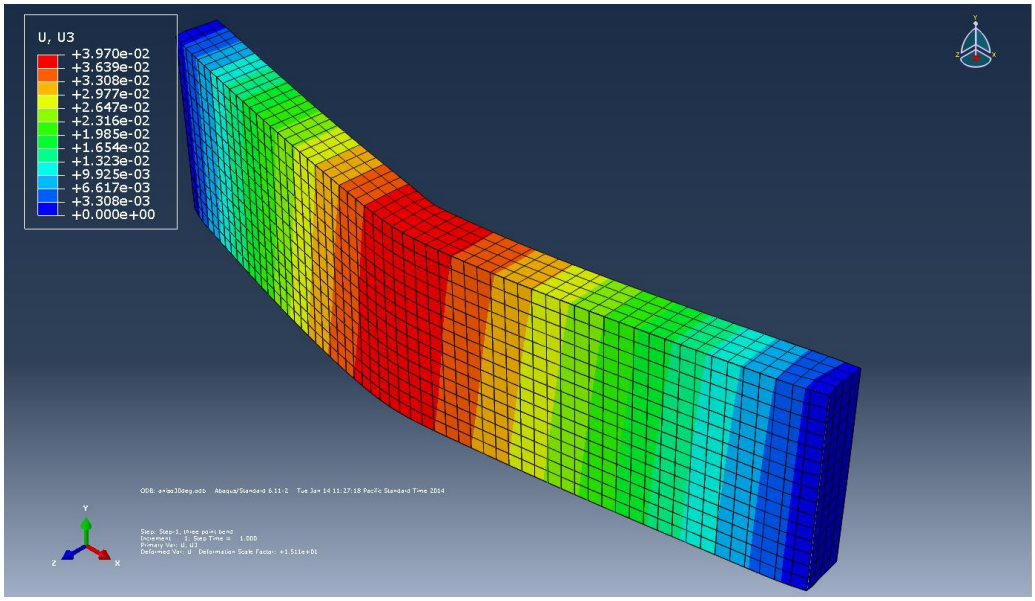

Figures 4.5.A. & 4.6.A 45 Degree Core FEA Stress and Displacement Plots

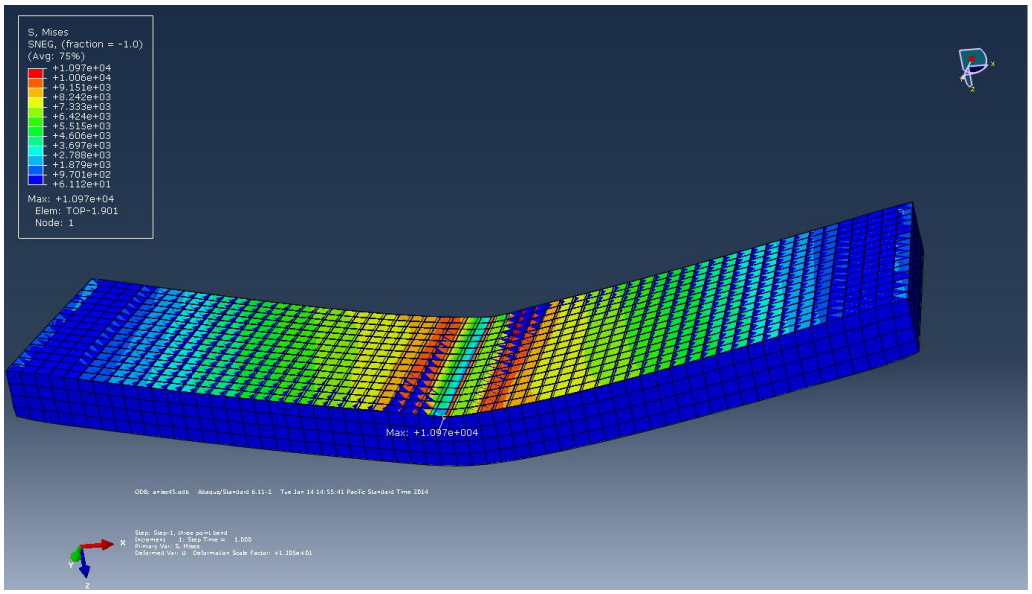

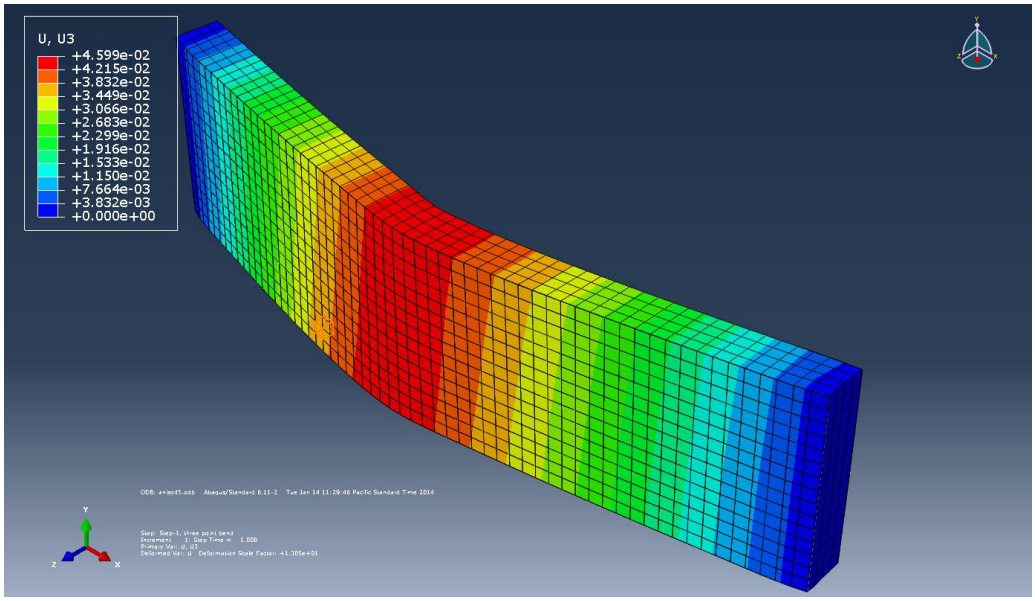

Figures 4.7.A. & 4.8.A 60 Degree Core FEA Stress and Displacement Plots

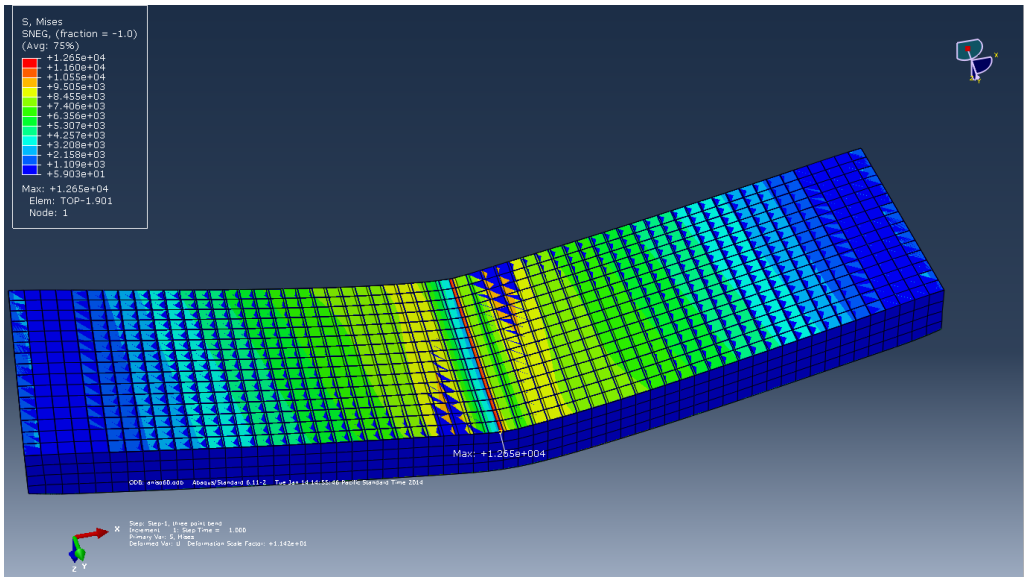

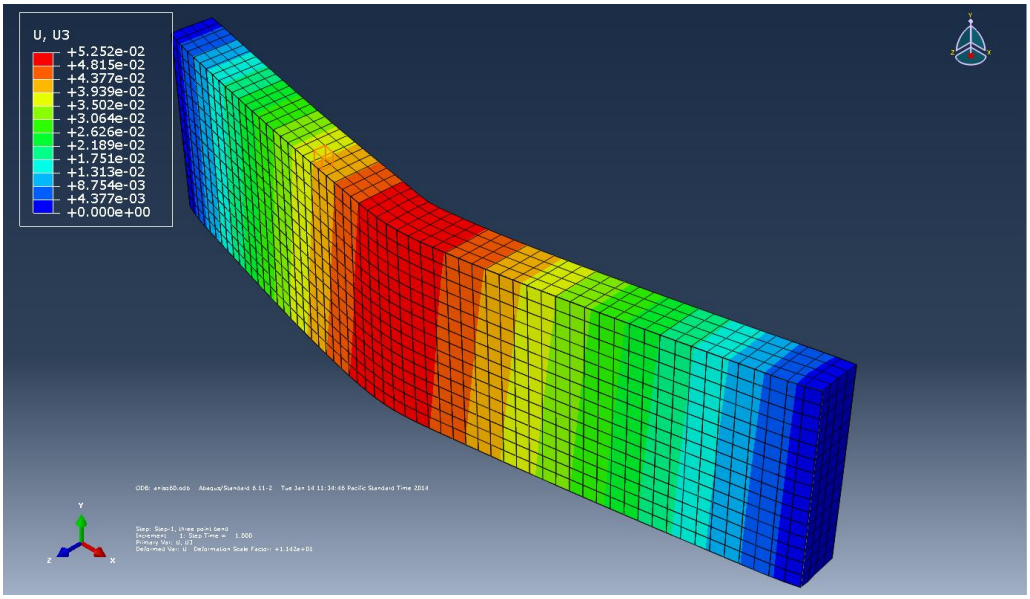

Figures 4.9.A. & 4.10.A 75 Degree Core FEA Stress and Displacement Plots

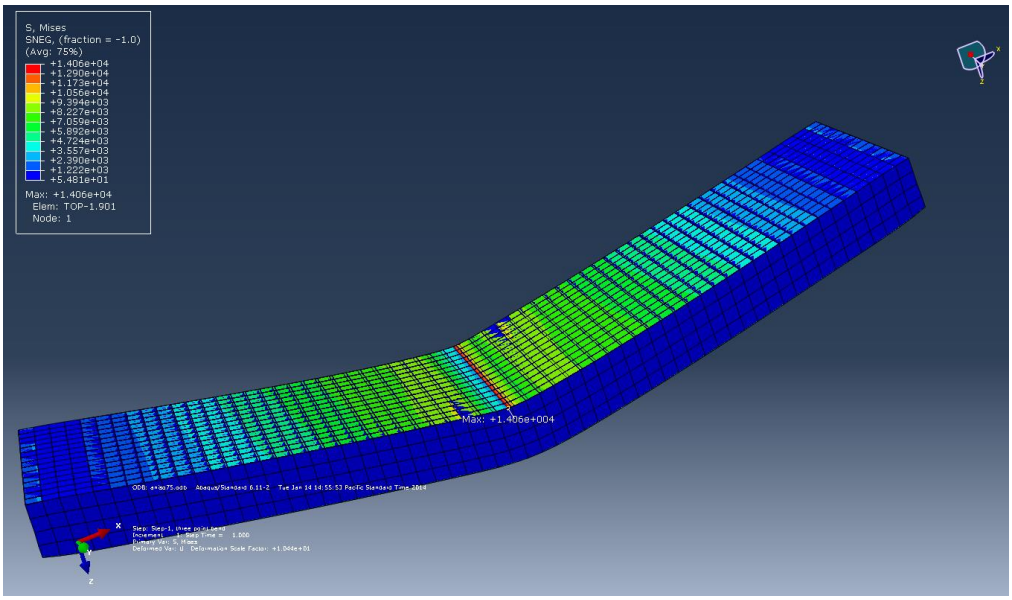

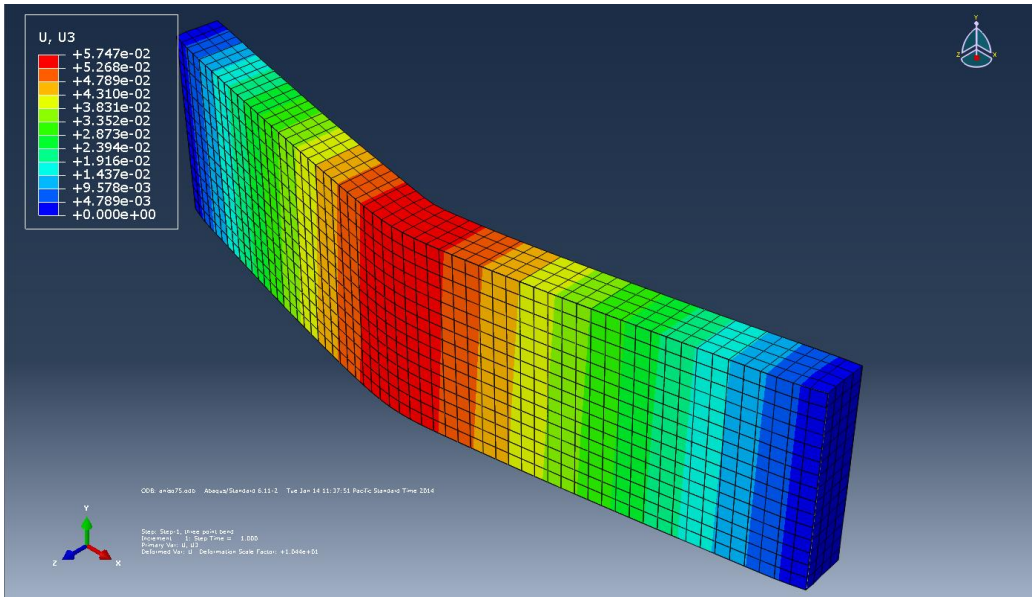

Figures 4.11.A. & 4.12.A 90 Degree Core FEA Stress and Displacement Plots

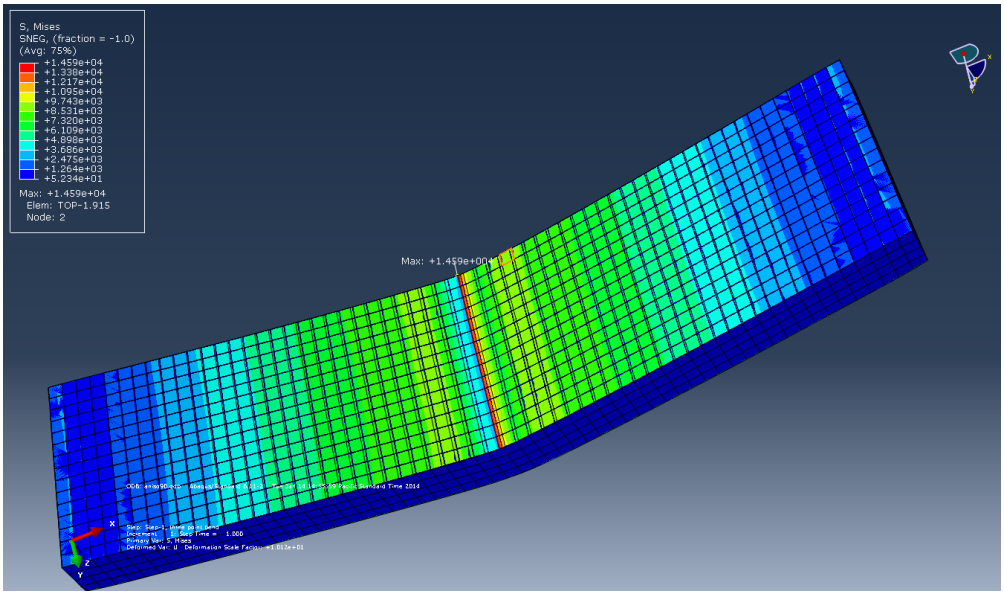

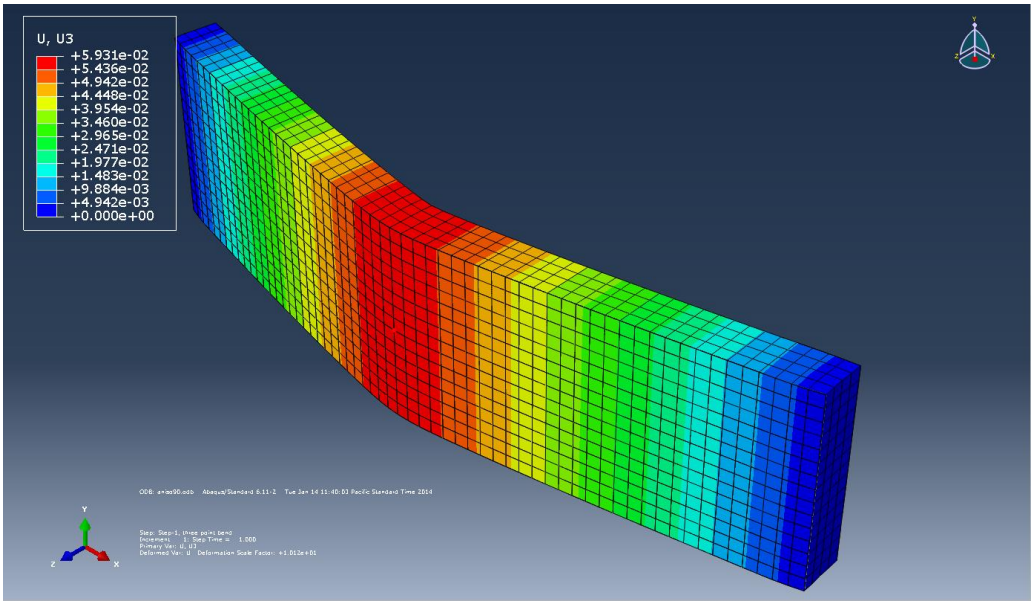

A.5 Core Ribbon Direction Failure Mode Maps

Figure 5.1.A 15 Degree Core Failure Mode Map

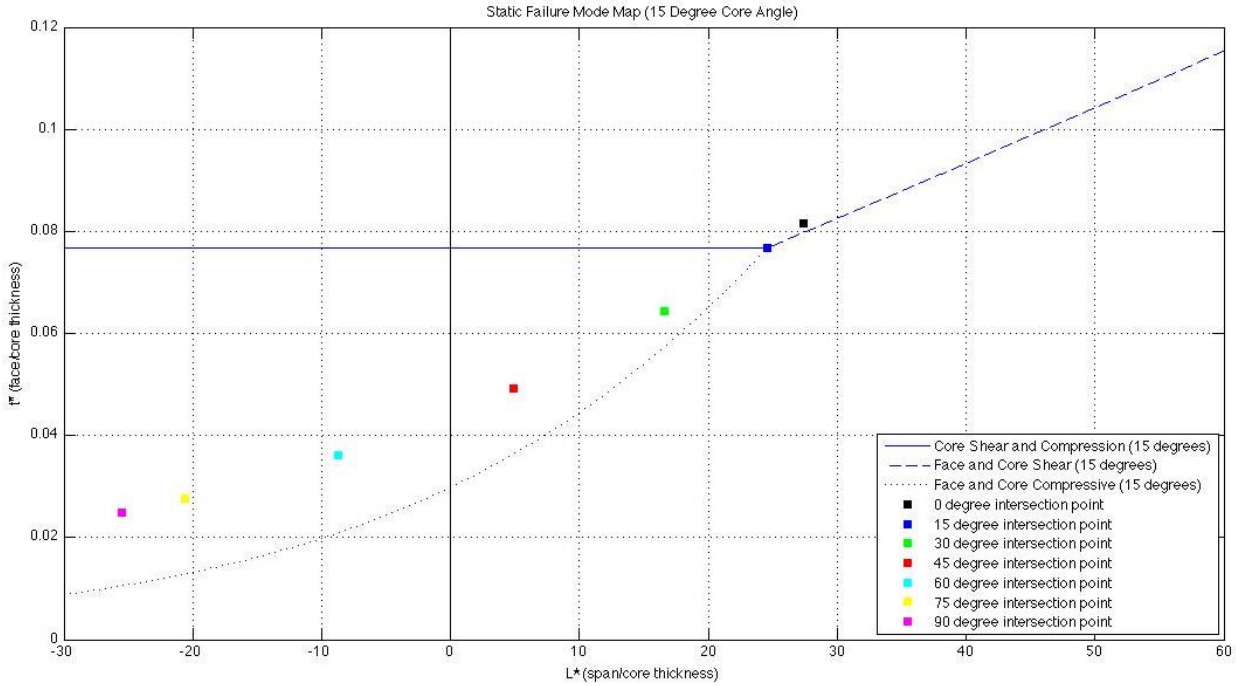

Figure 5.2.A 30 Degree Core Failure Mode Map

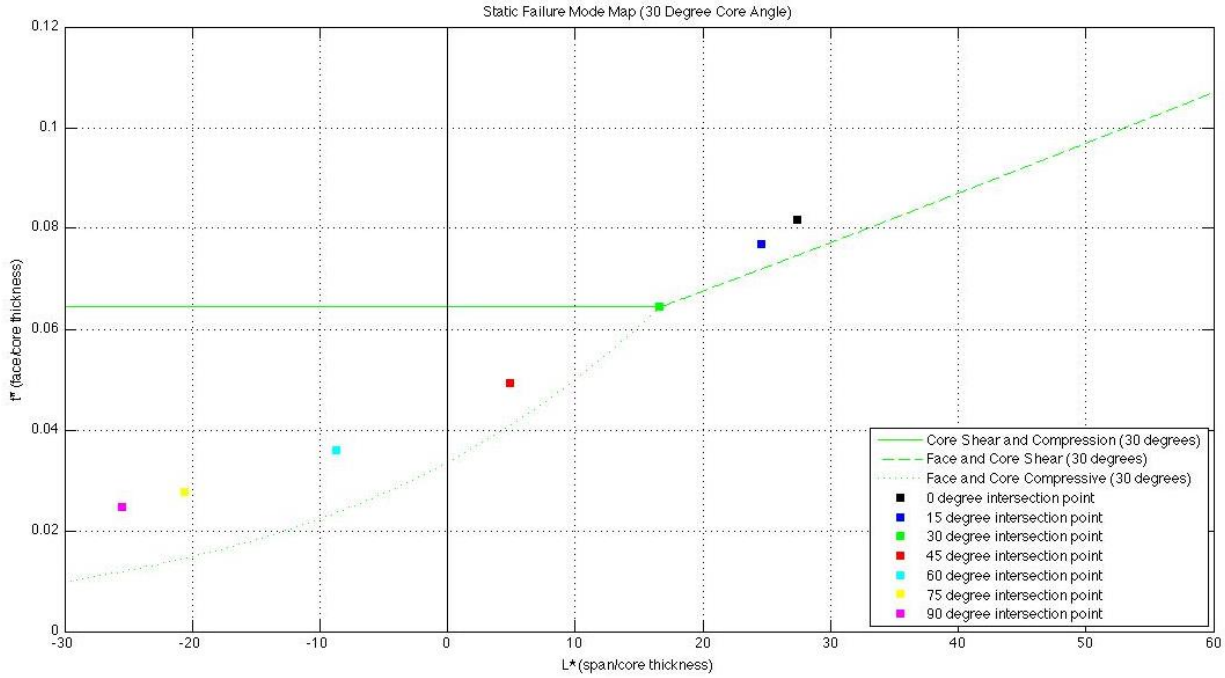

Figure 5.3.A 45 Degree Core Failure Mode Map

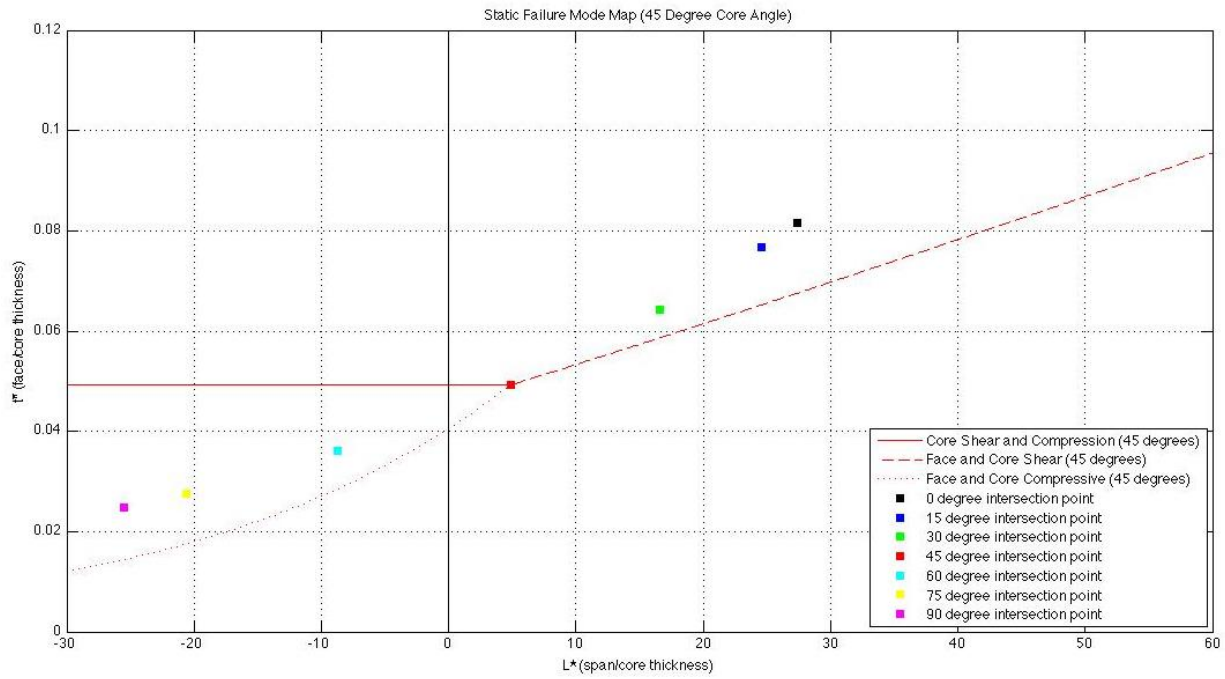

Figure 5.4.A 60 Degree Core Failure Mode Map

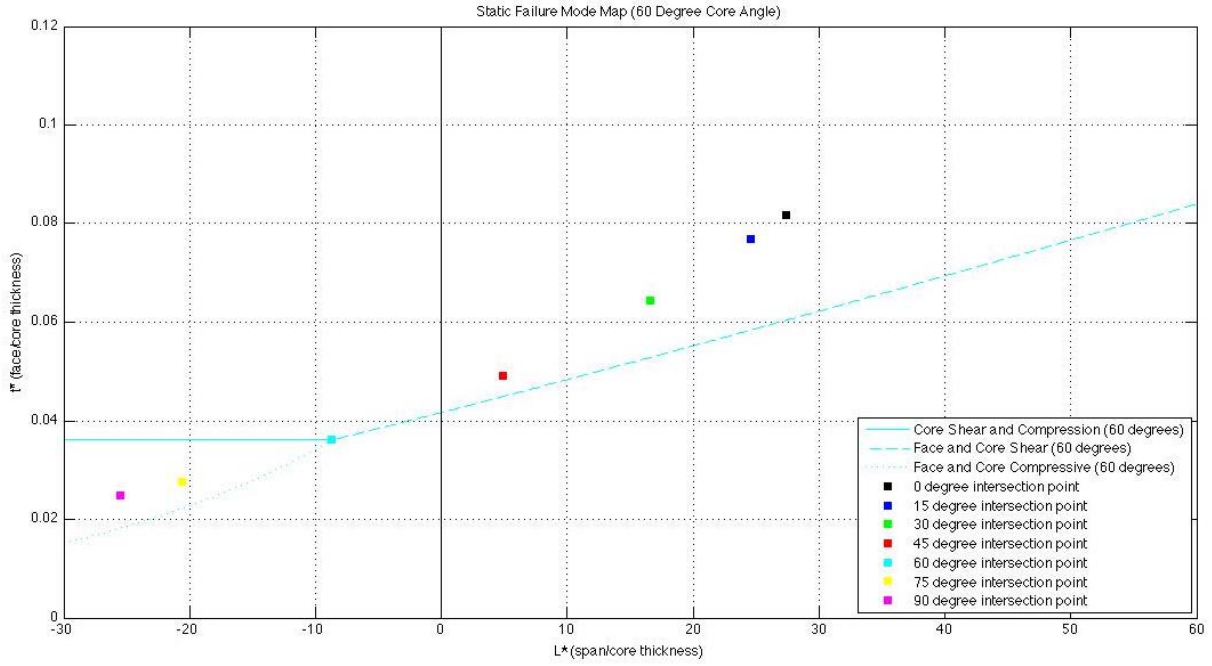

Figure 5.5.A 75 Degree Core Failure Mode Map

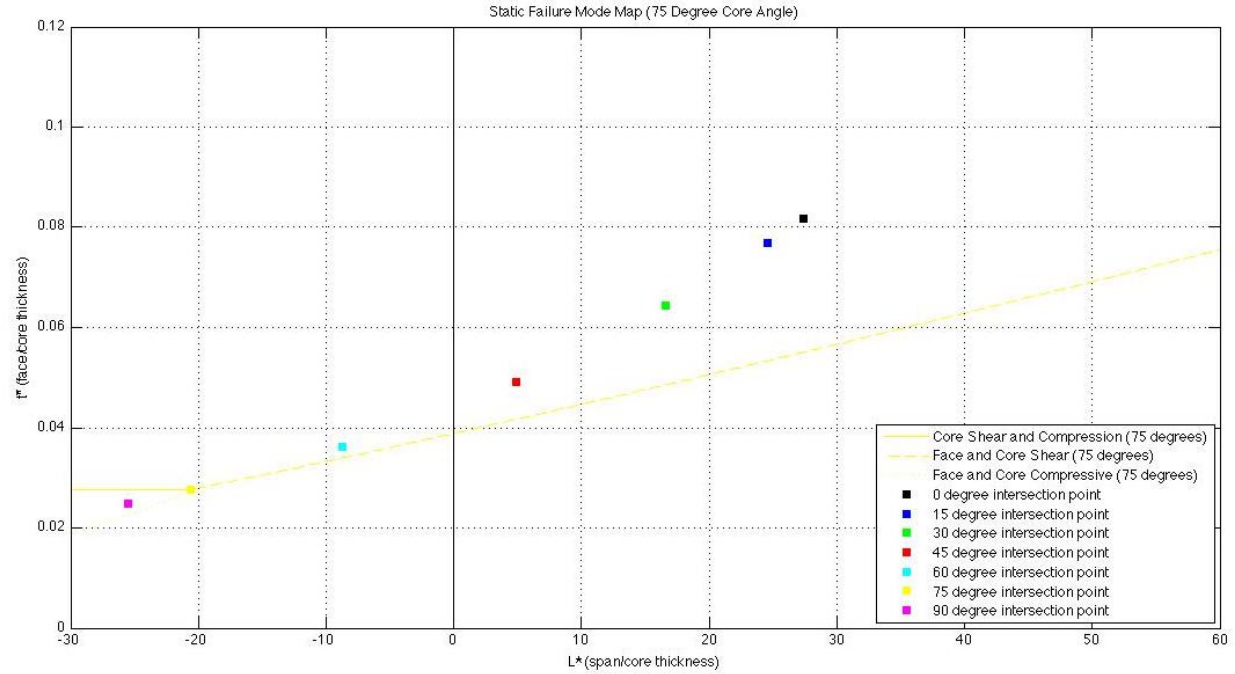

Figure 5.6.A 90 Degree Core Failure Mode Map

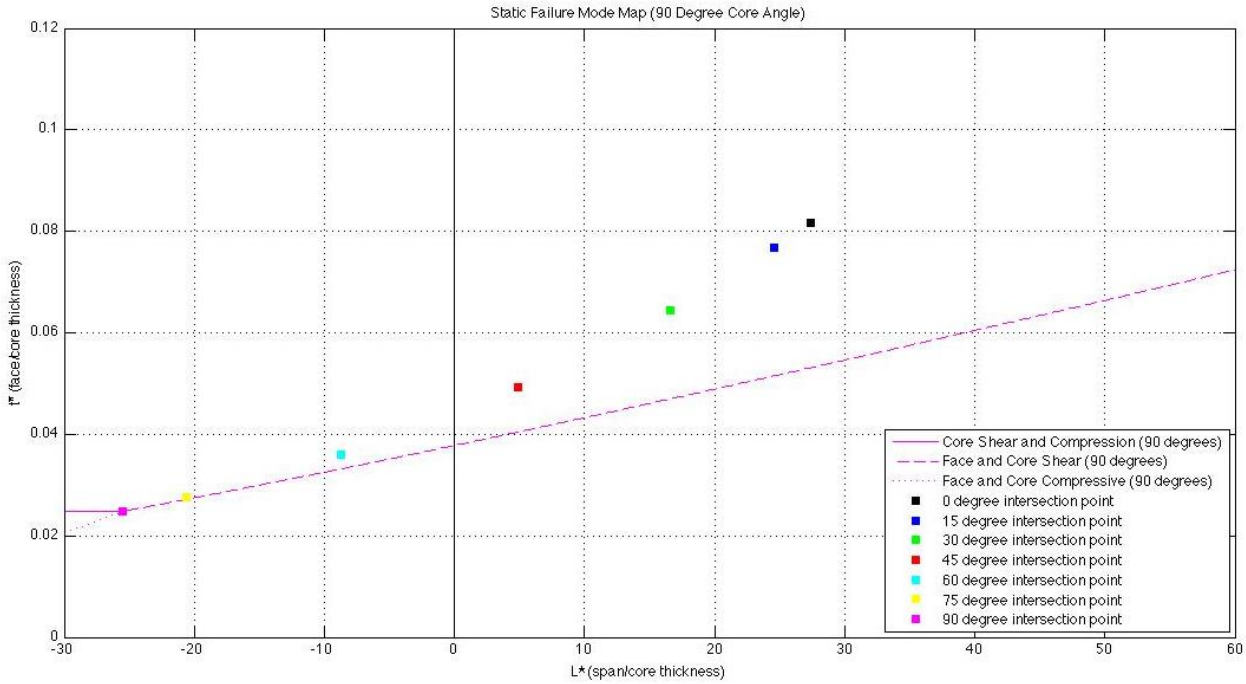

A.6 Varying Face Sheet thicknesses Failure Loads

Figure 6.1.A Varying Top Face Sheet thicknesses Failure Loads for 2 Bottom Layers

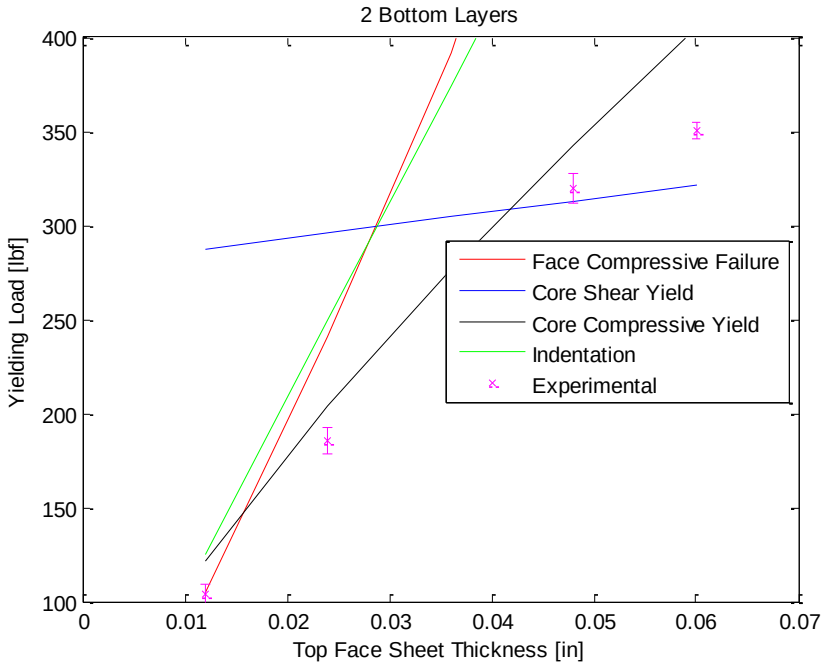

Figure 6.2.A Varying Top Face Sheet thicknesses Failure Loads for 3 Bottom Layers

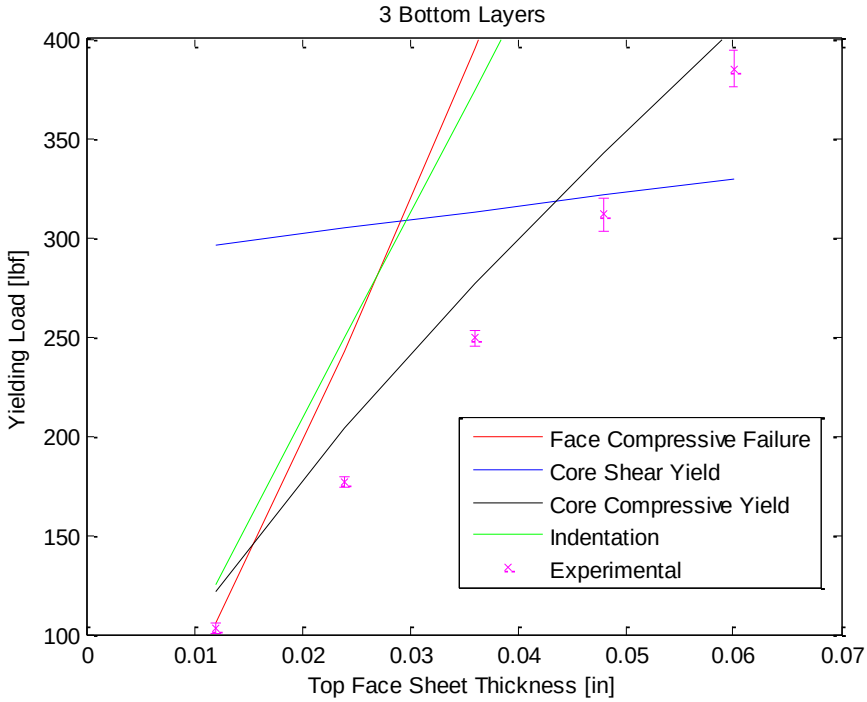

Figure 6.3.A Varying Top Face Sheet thicknesses Failure Loads for 4 Bottom Layers

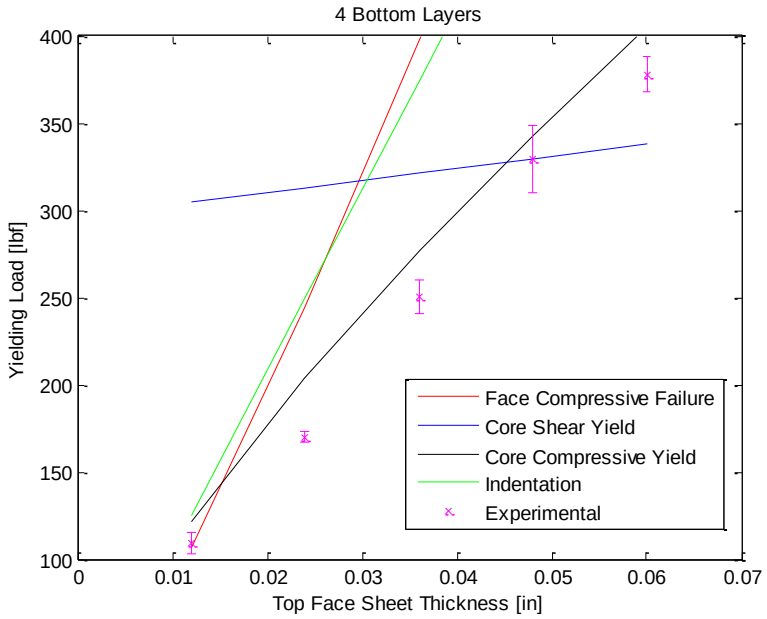

Figure 6.4.A Varying Top Face Sheet thicknesses Failure Loads for 5 Bottom Layers

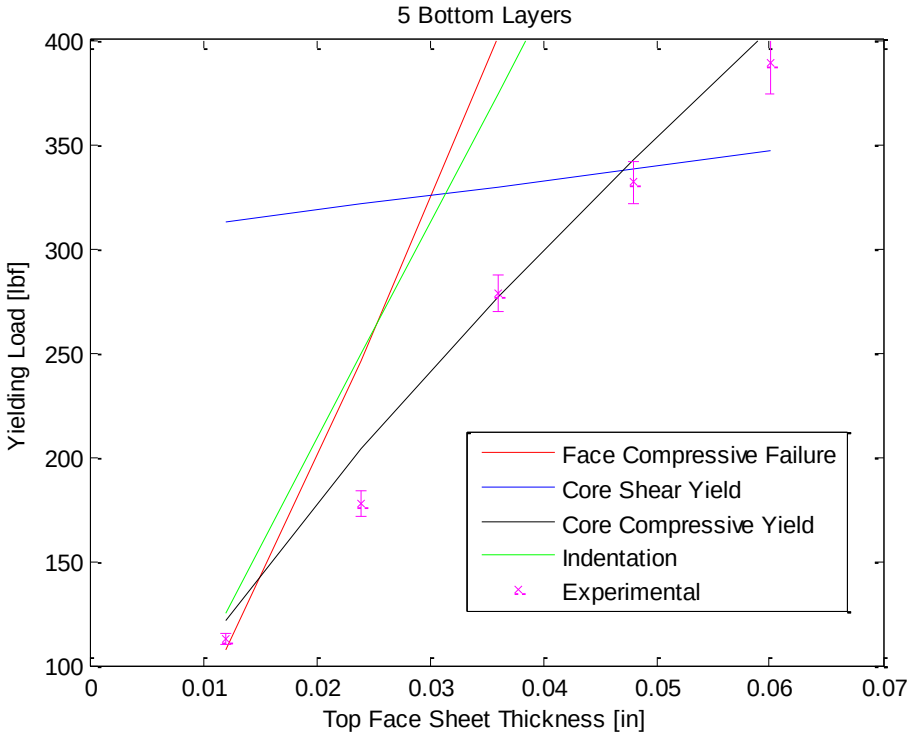

A.7 Varying Face sheet Thickness FEA Plots

Figures 7.1.A. & 7.2.A. 4/5 Configuration FEA Stress and Displacements Graphs

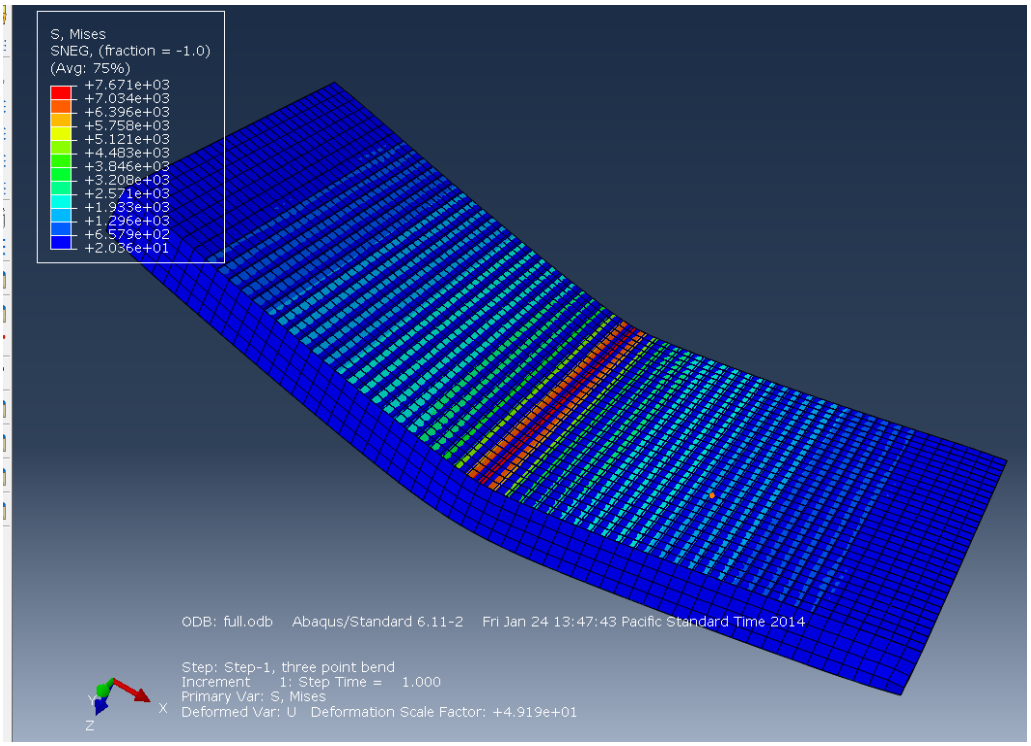

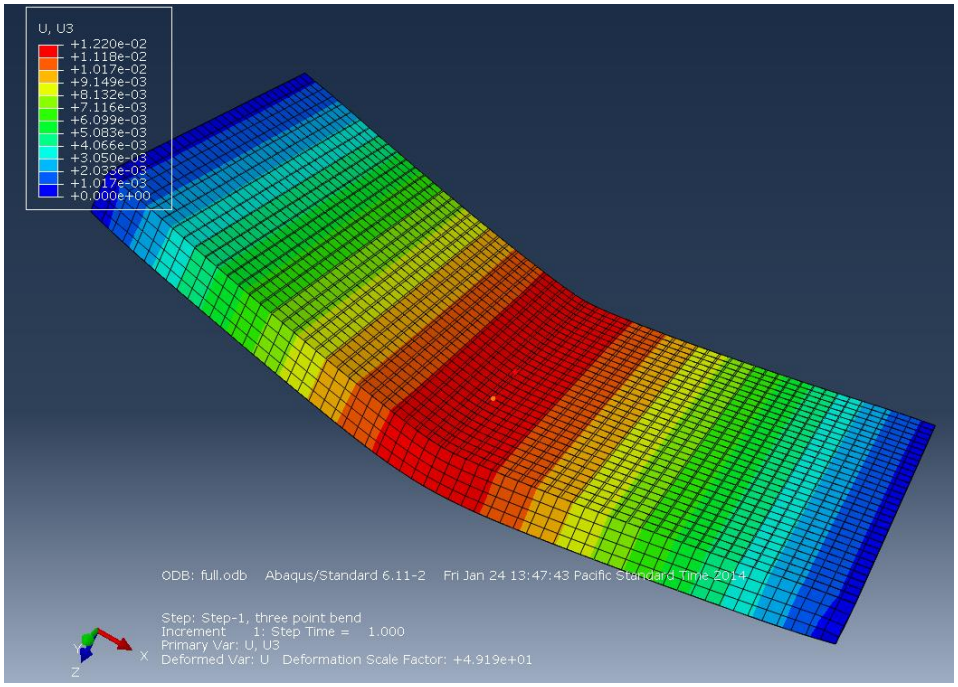

Figures 7.3.A. & 7.4.A. 3/5 Configuration FEA Stress and Displacements Graphs

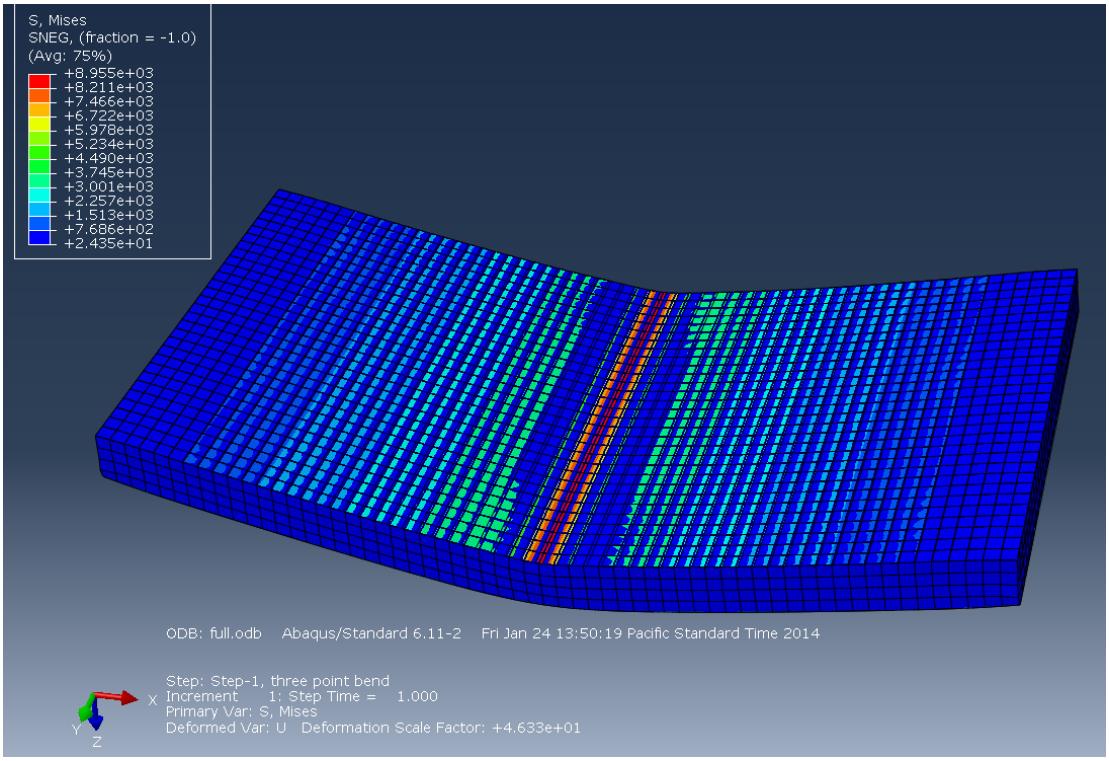

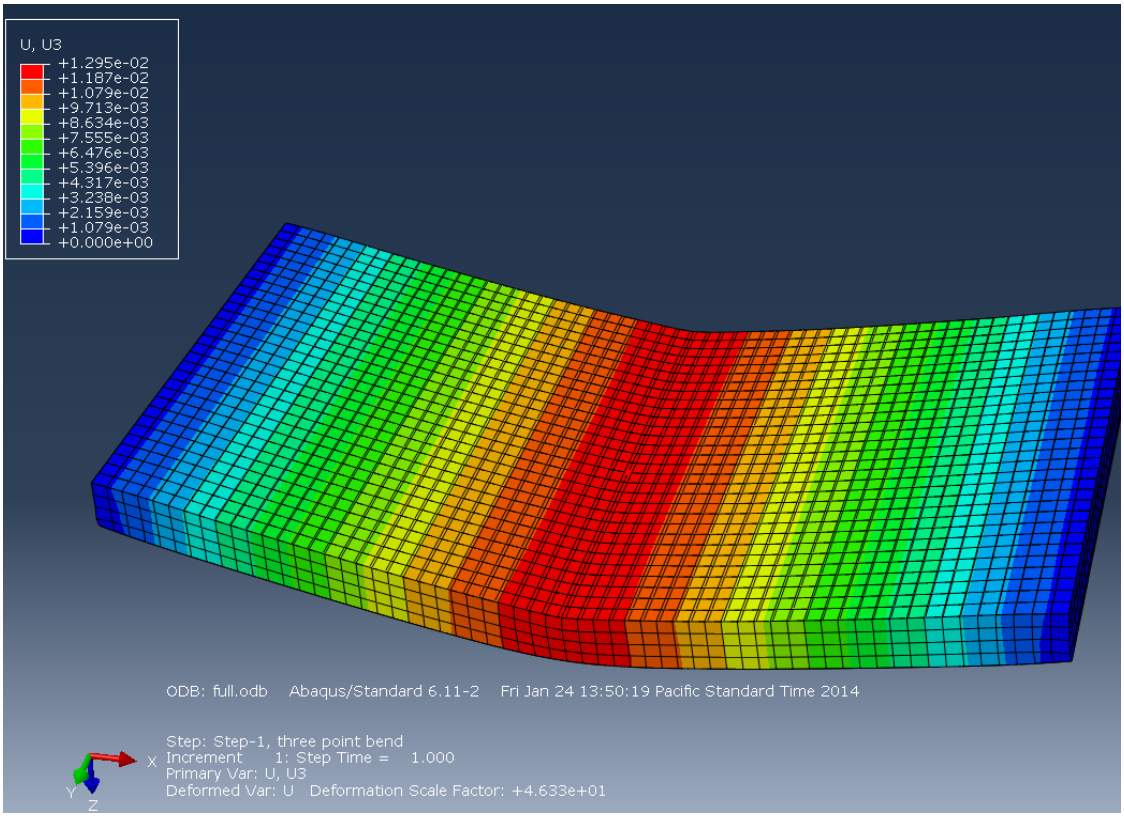

Figures 7.5.A. & 7.6.A. 2/5 Configuration FEA Stress and Displacements Graphs

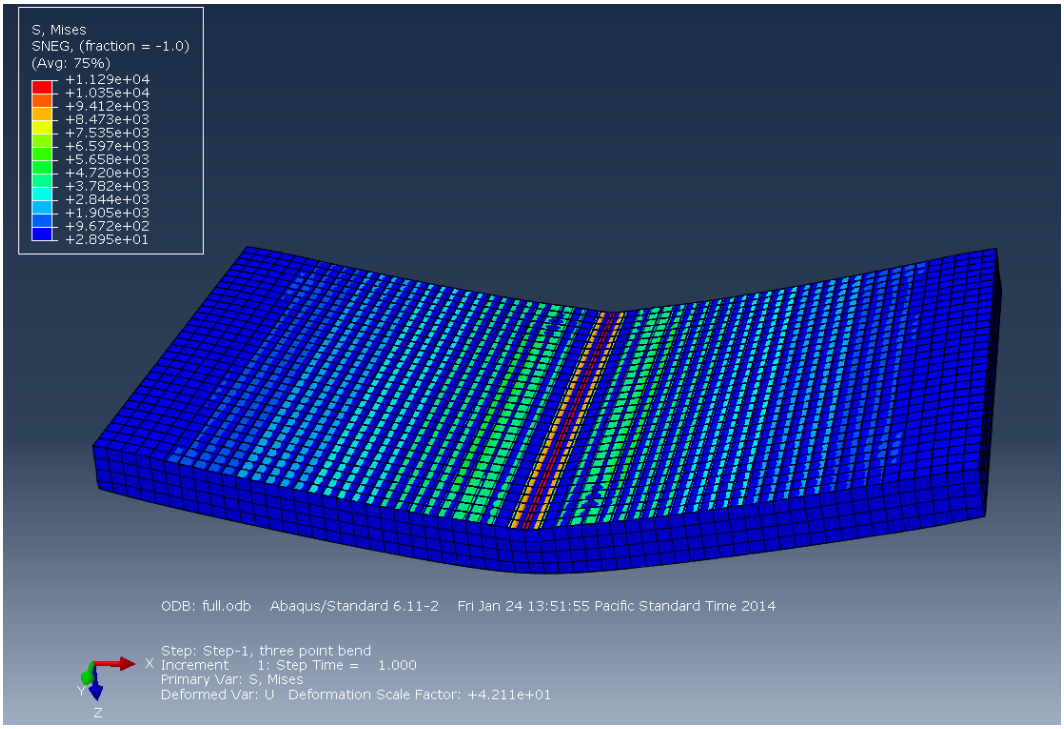

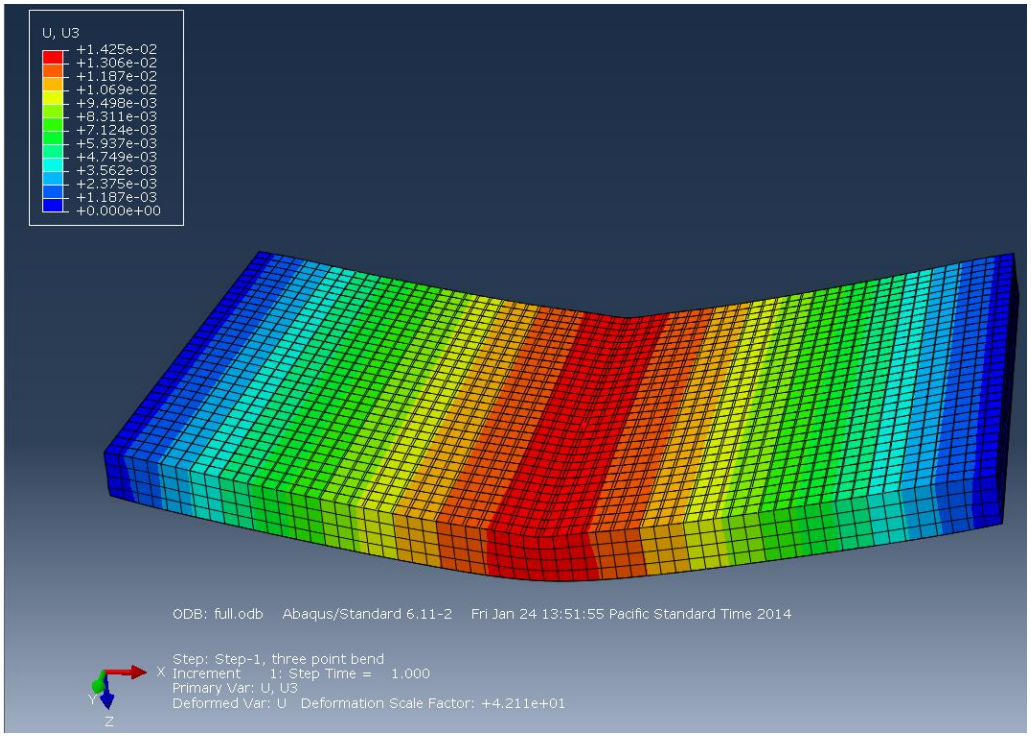

Figures 7.7.A. & 7.8.A. 1/5 Configuration FEA Stress and Displacements Graphs

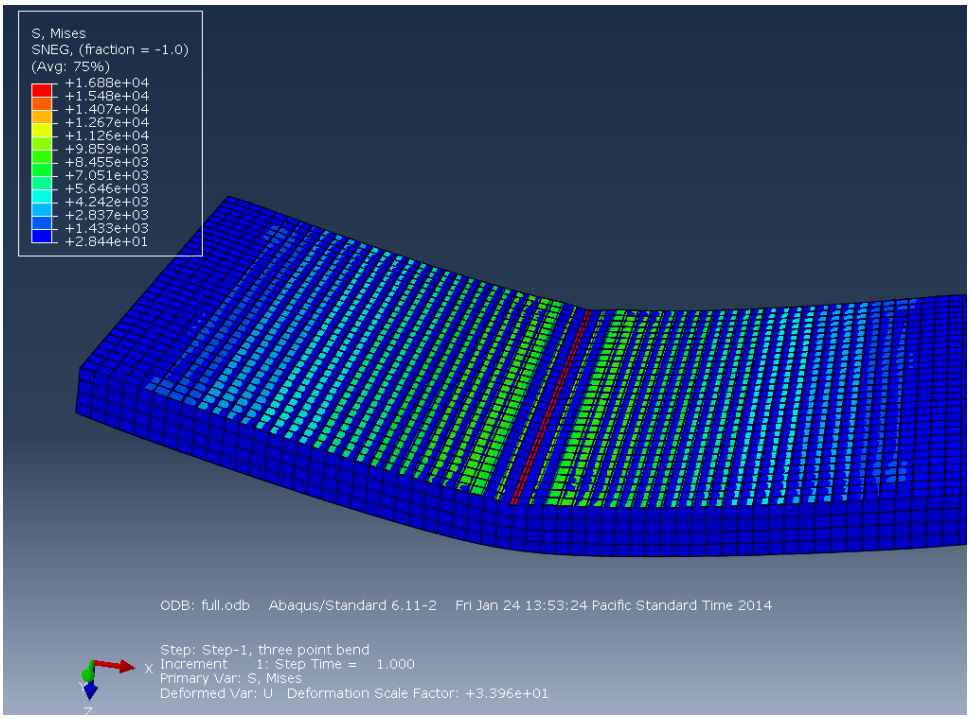

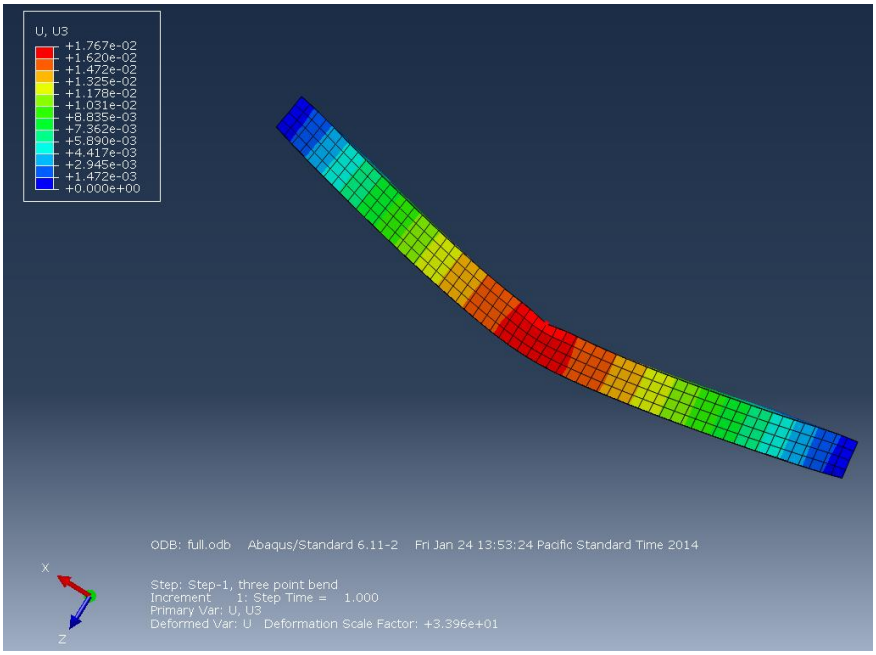

Figures 7.9.A. & 7.10.A. 1/4 Configuration FEA Stress and Displacements Graphs

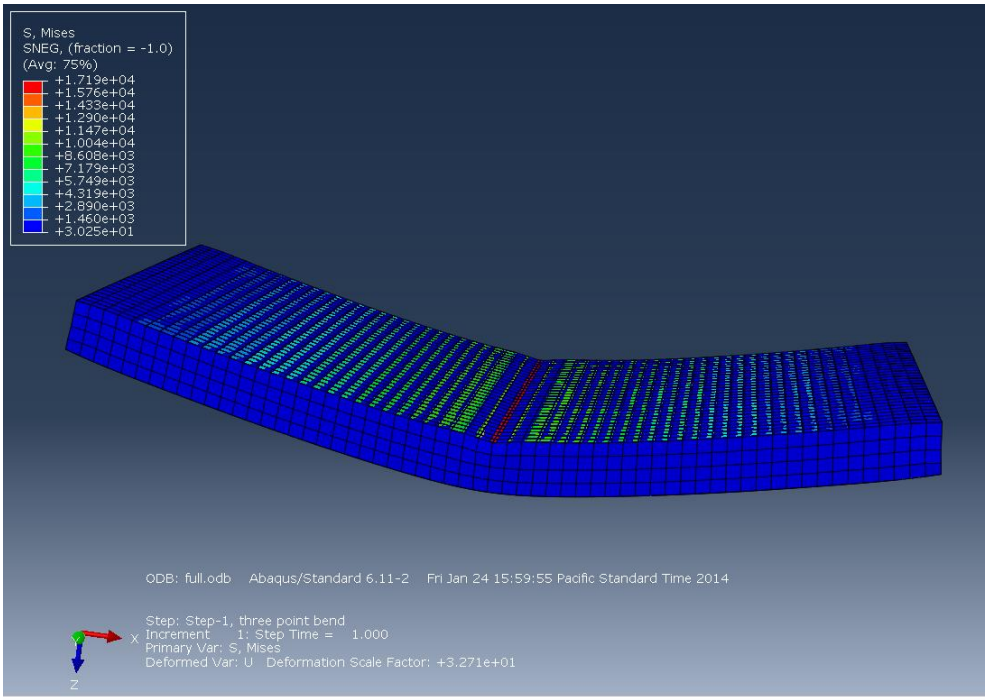

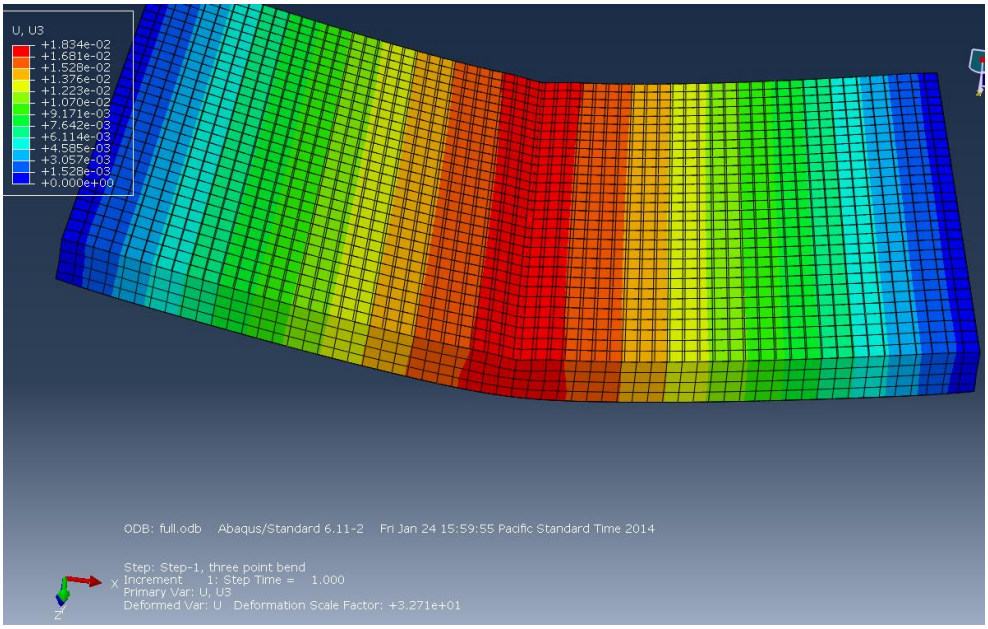

Figures 7.11.A. & 7.12.A. 2/4 Configuration FEA Stress and Displacements Graphs

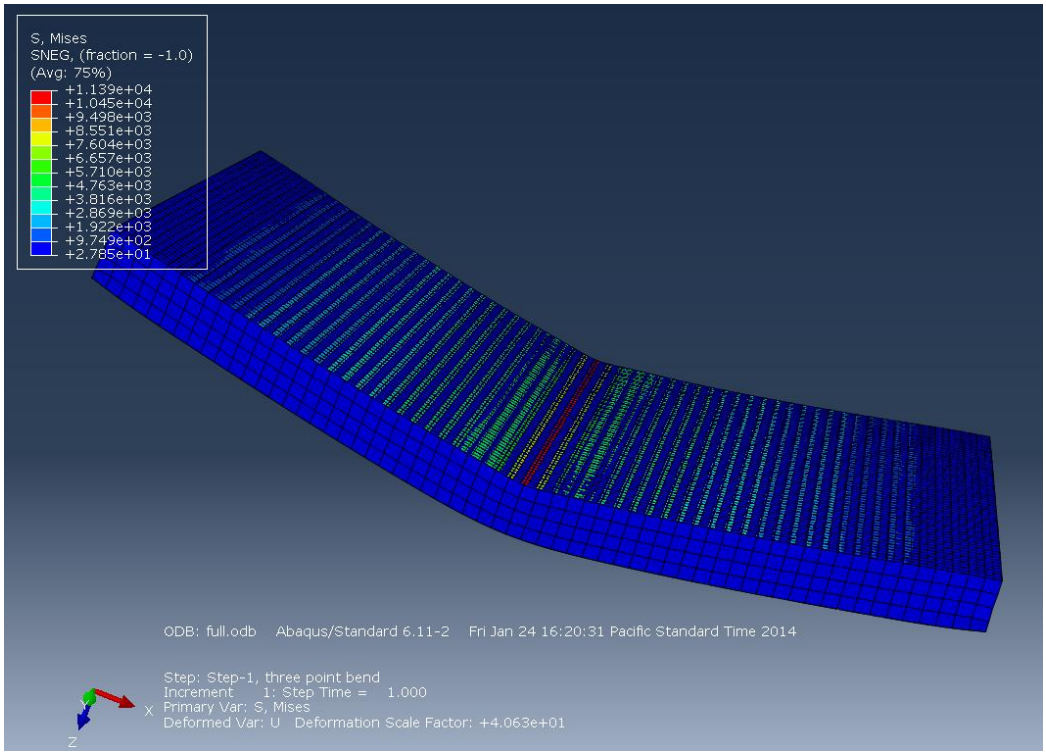

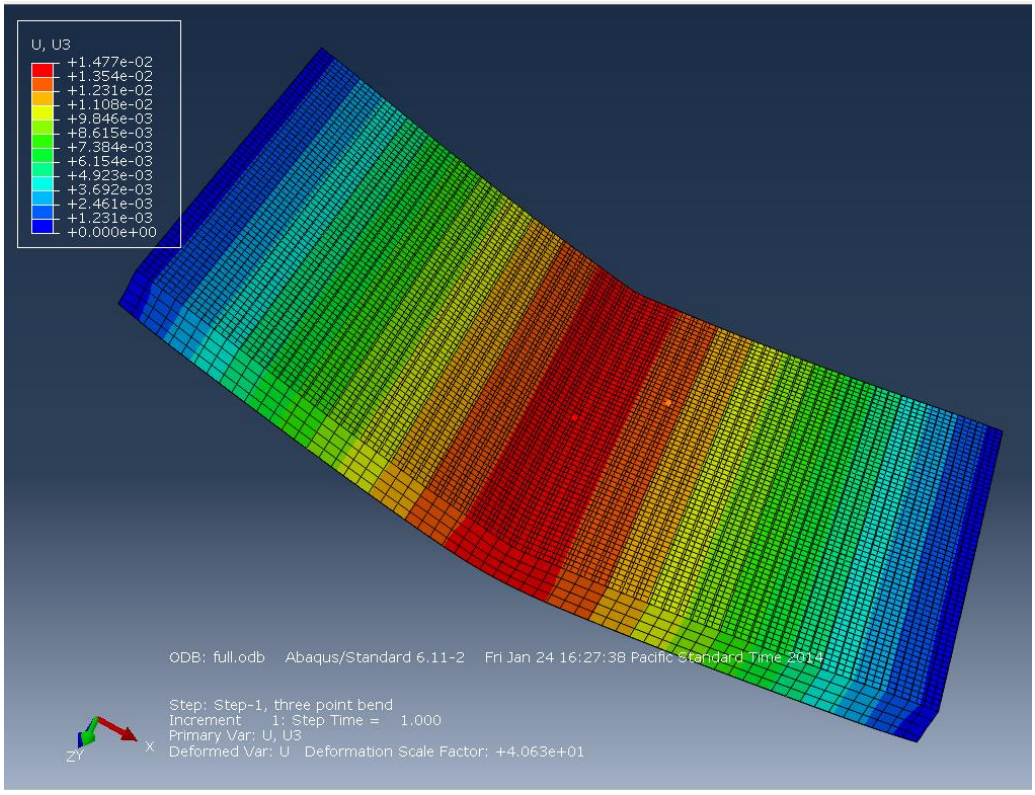

Figures 7.13.A. & 7.14.A. 3/4 Configuration FEA Stress and Displacements Graphs

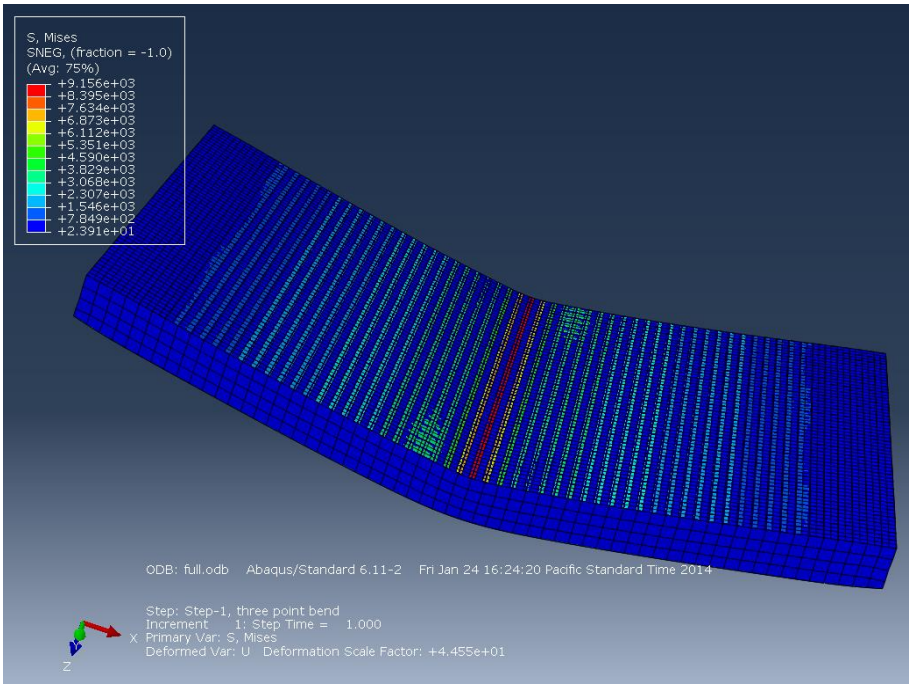

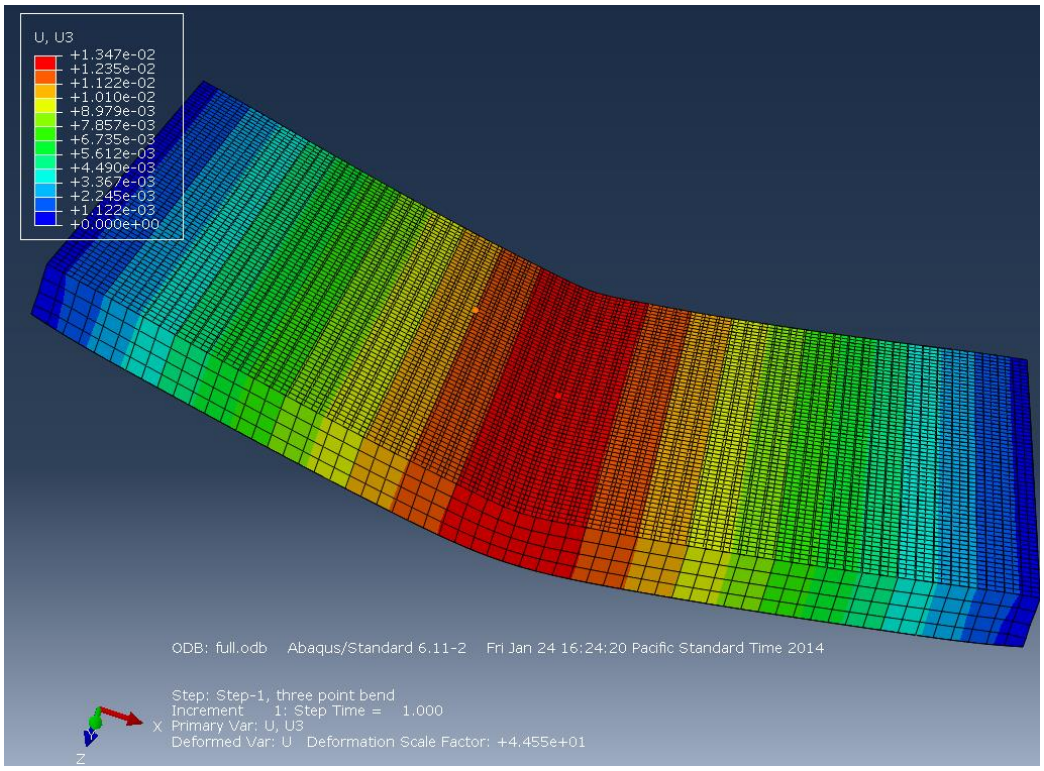

Figures 7.15.A. & 7.16.A. 4/4 Configuration FEA Stress and Displacements Graphs

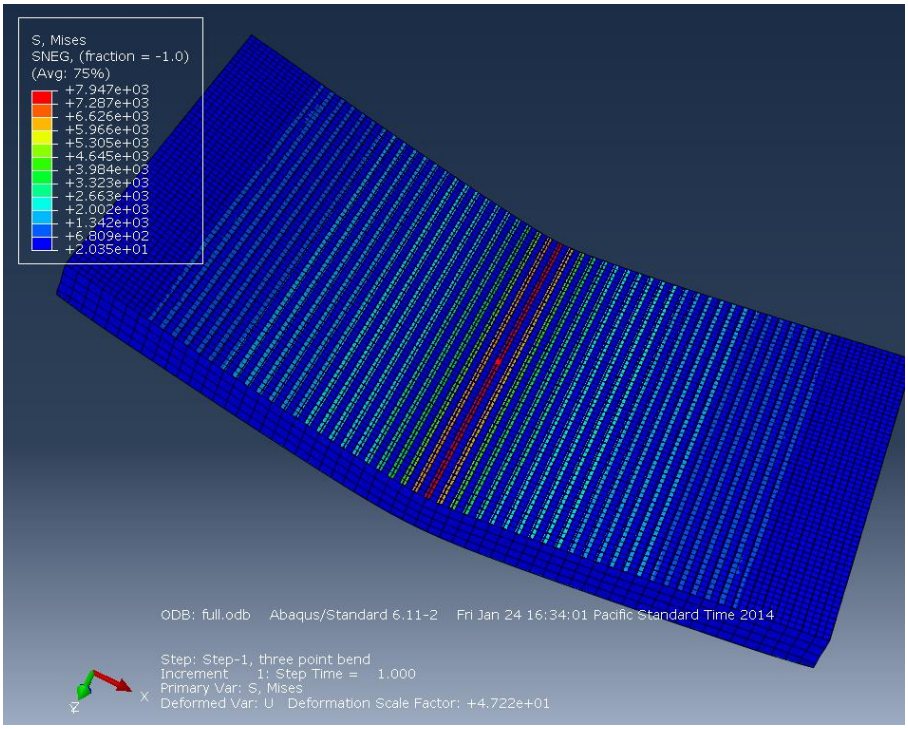

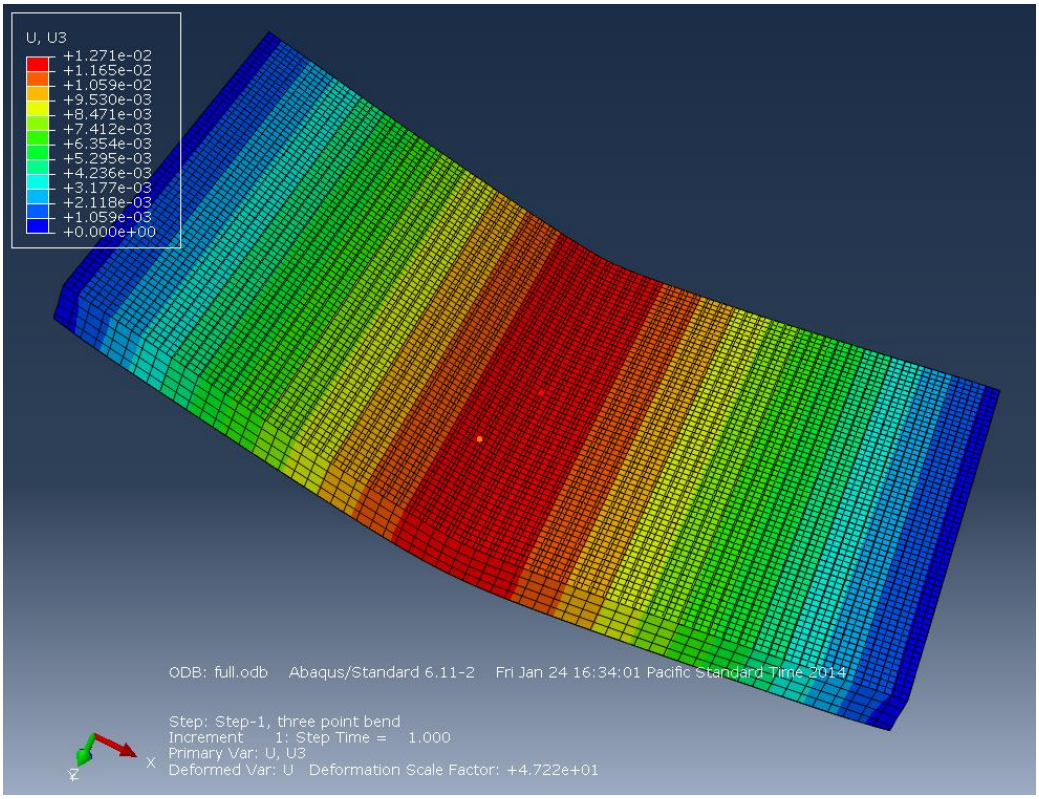

Figures 7.17.A. & 7.18.A. 5/4 Configuration FEA Stress and Displacements Graphs

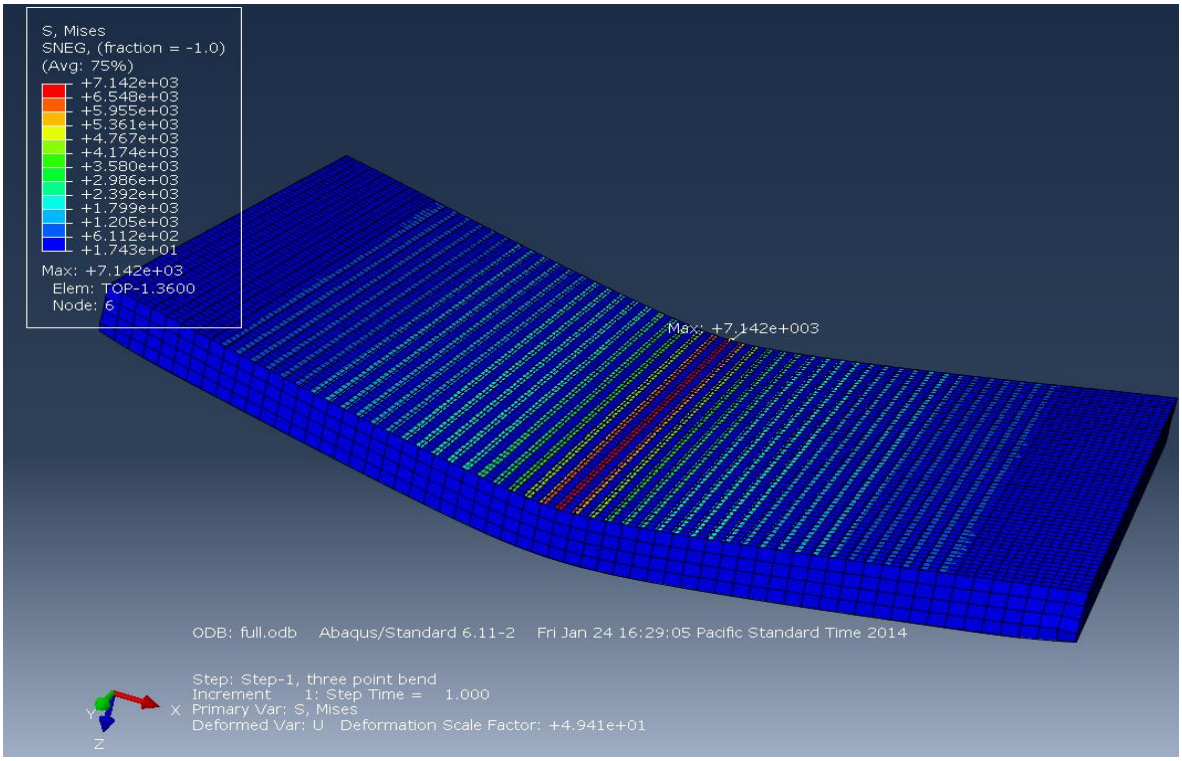

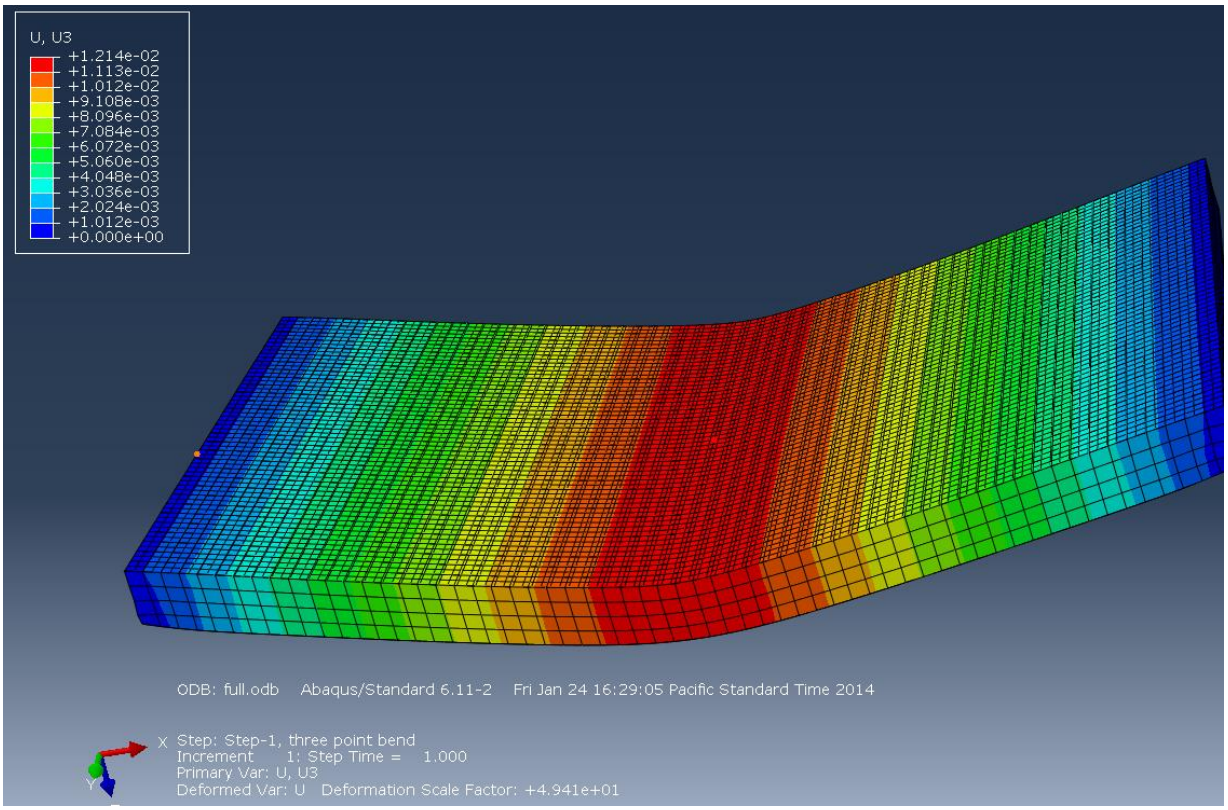

Figures7.19.A. & 7.20.A. 5/3 Configuration FEA Stress and Displacements Graphs

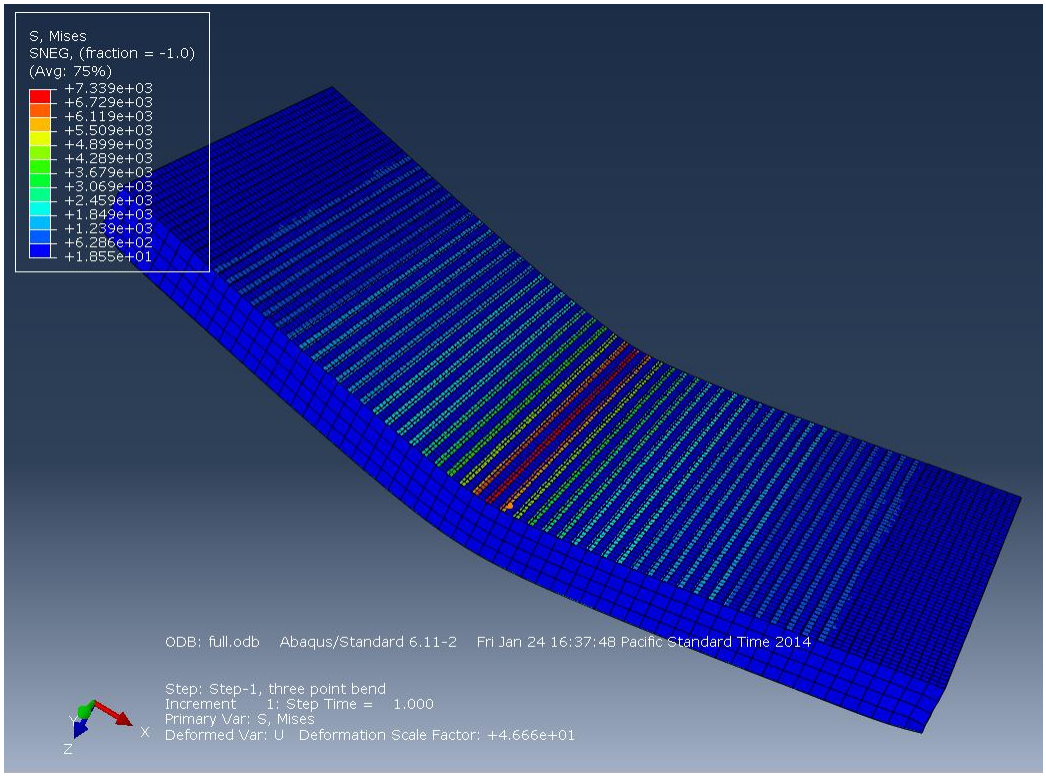

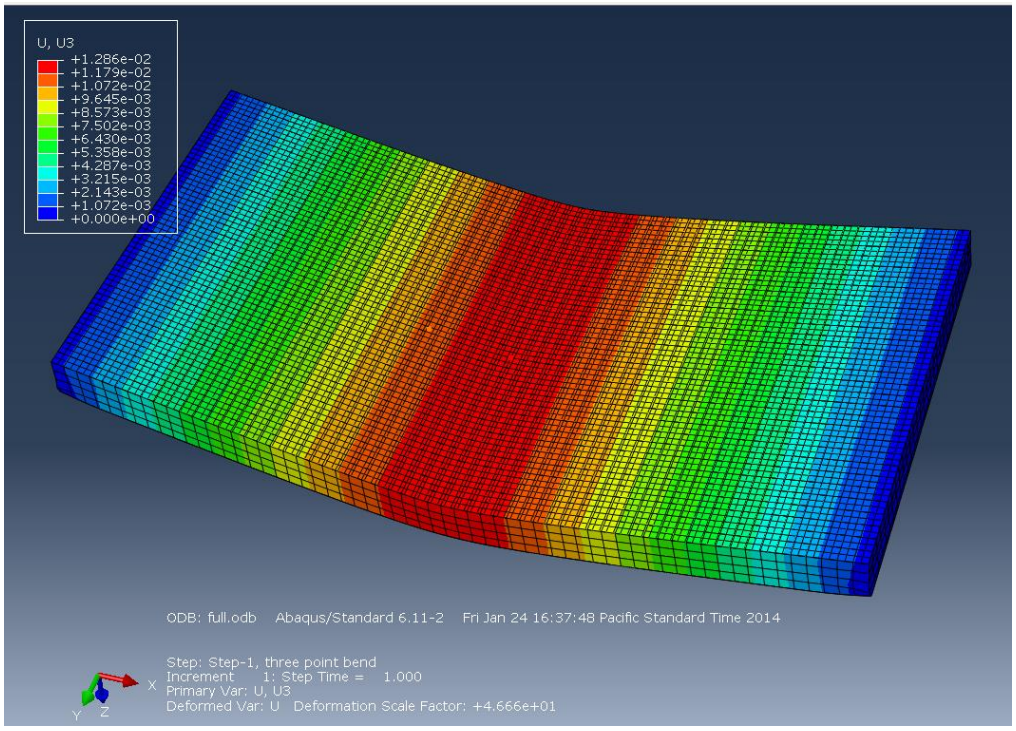

Figures 7.21.A. & 7.22.A 4/3 Configuration FEA Stress and Displacements Graphs

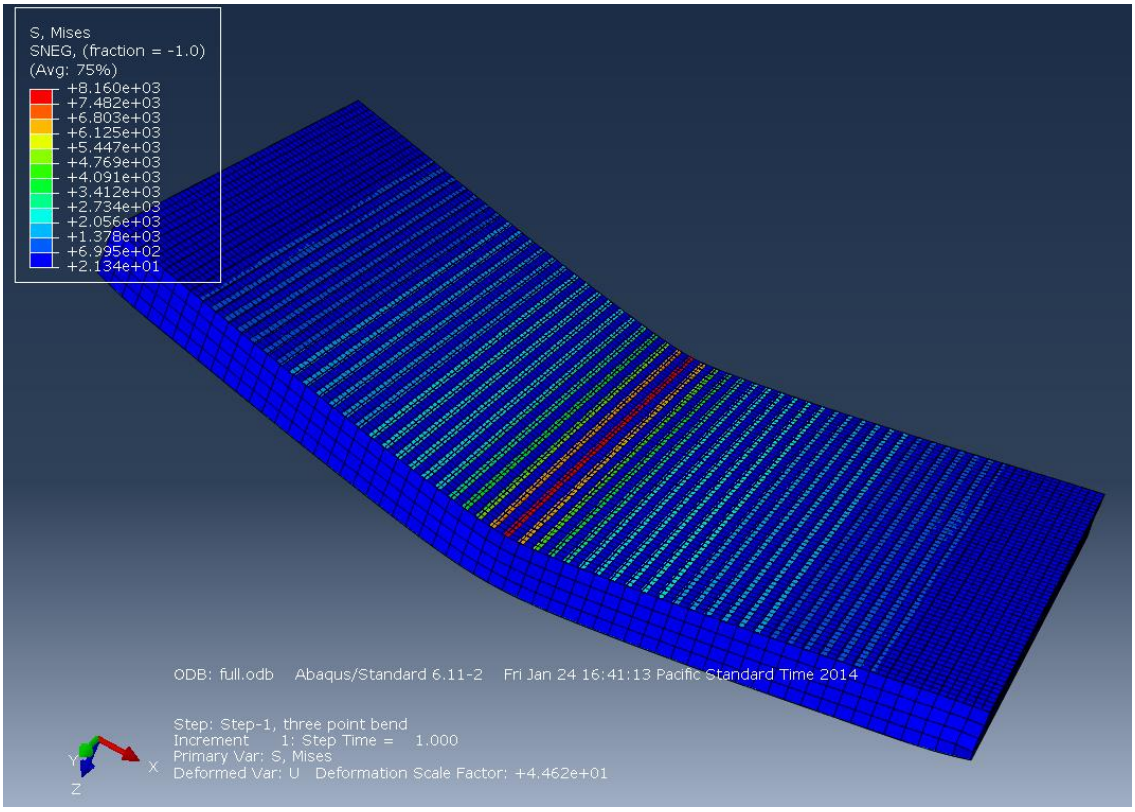

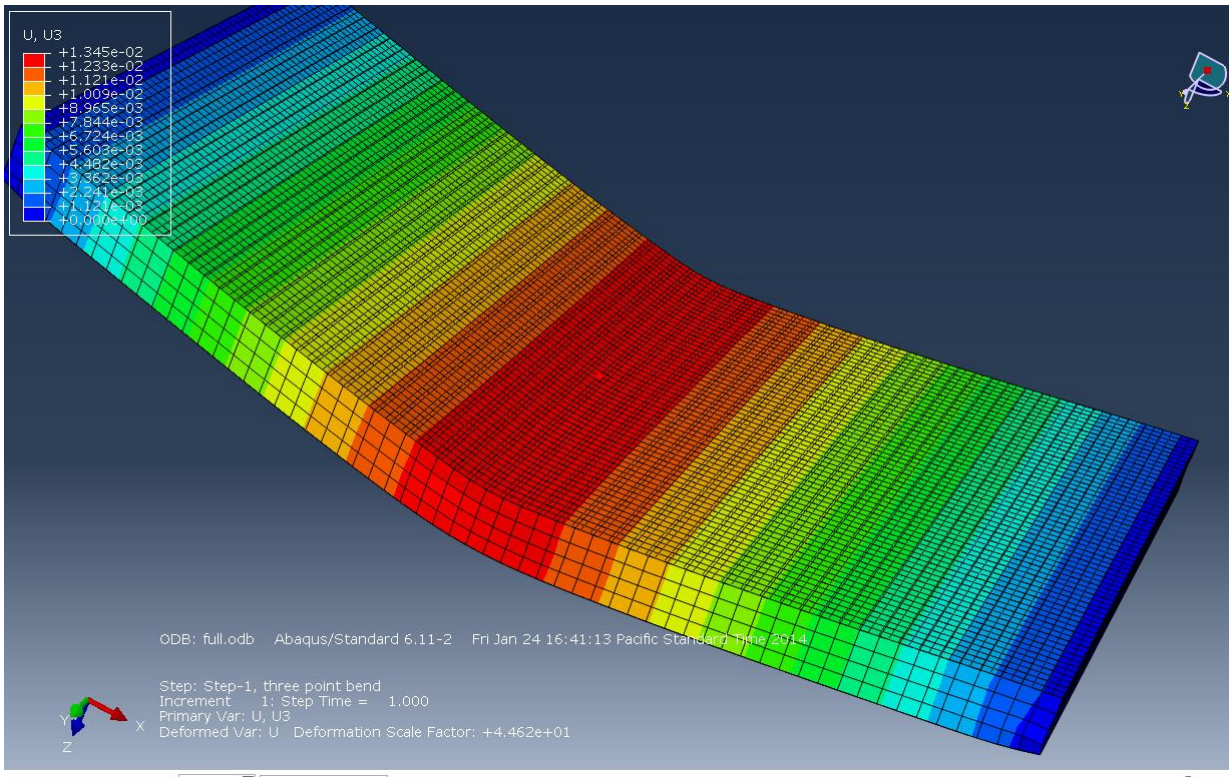

Figures 7.23.A. & 7.24.A. 3/3 Configuration FEA Stress and Displacements Graphs

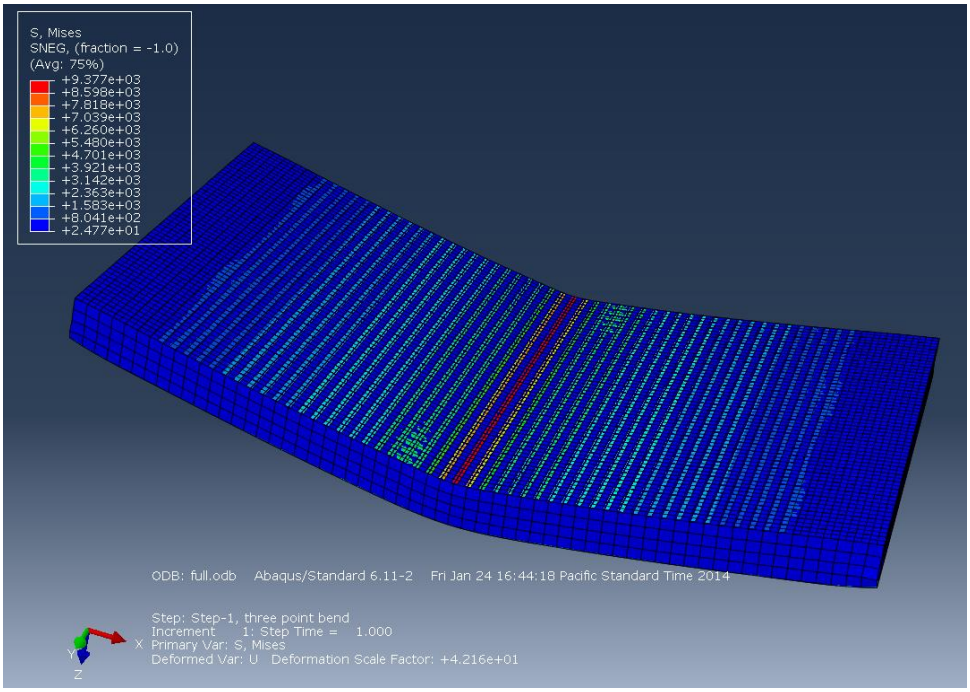

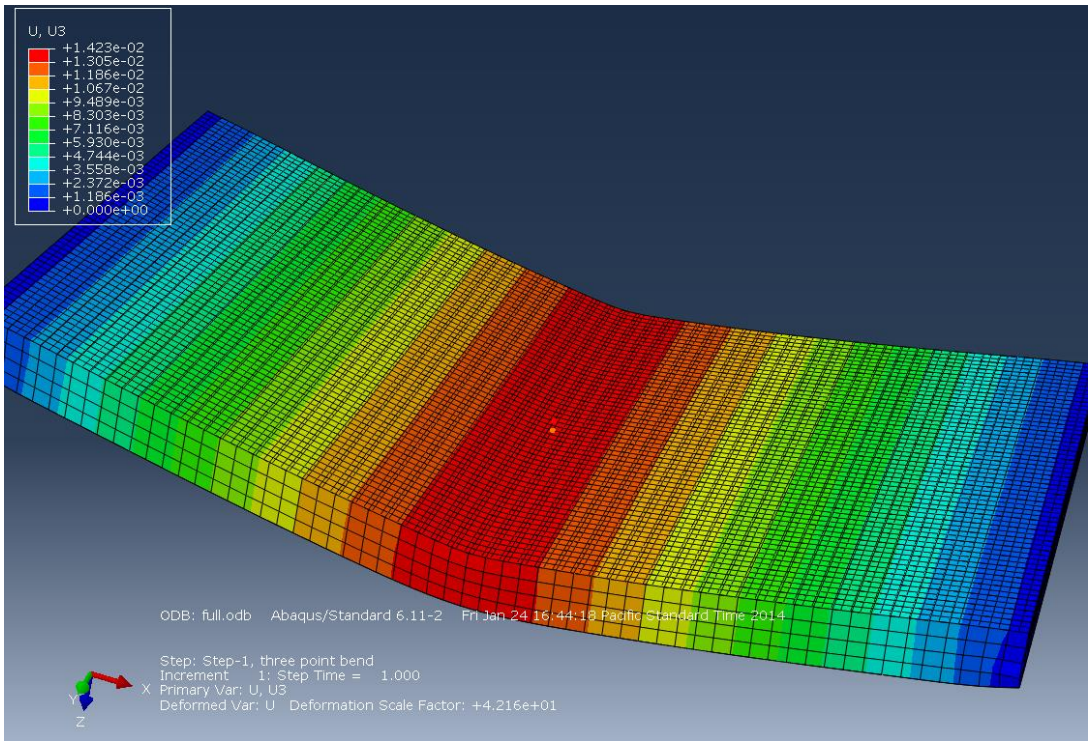

Figures 7.25.A. & 7.26.A. 2/3 Configuration FEA Stress and Displacements Graphs

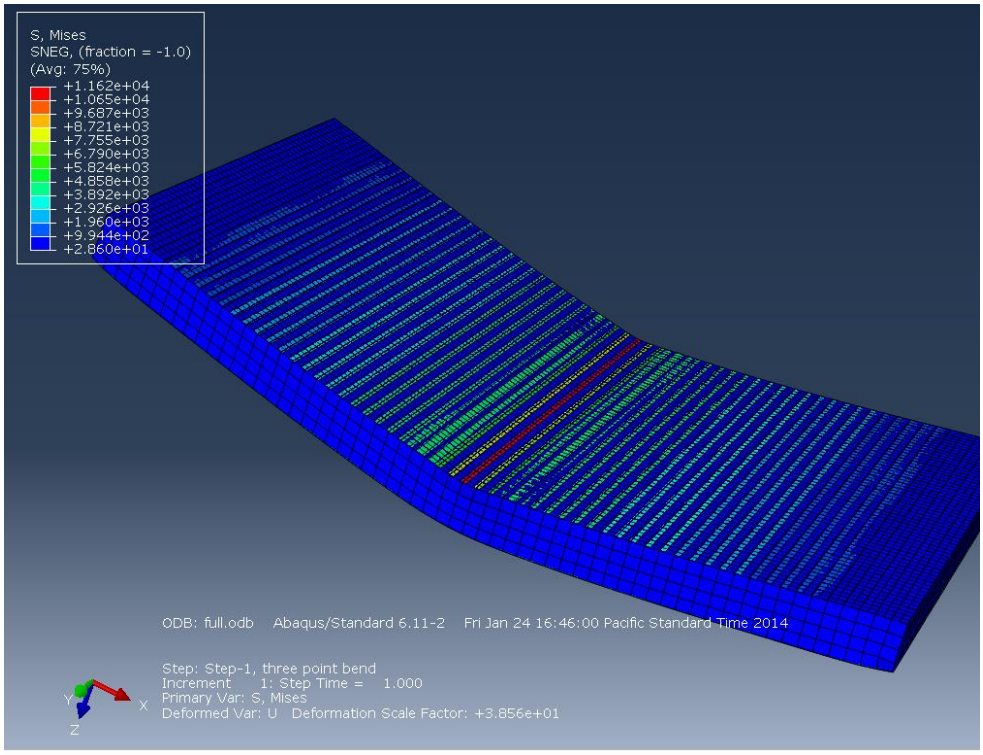

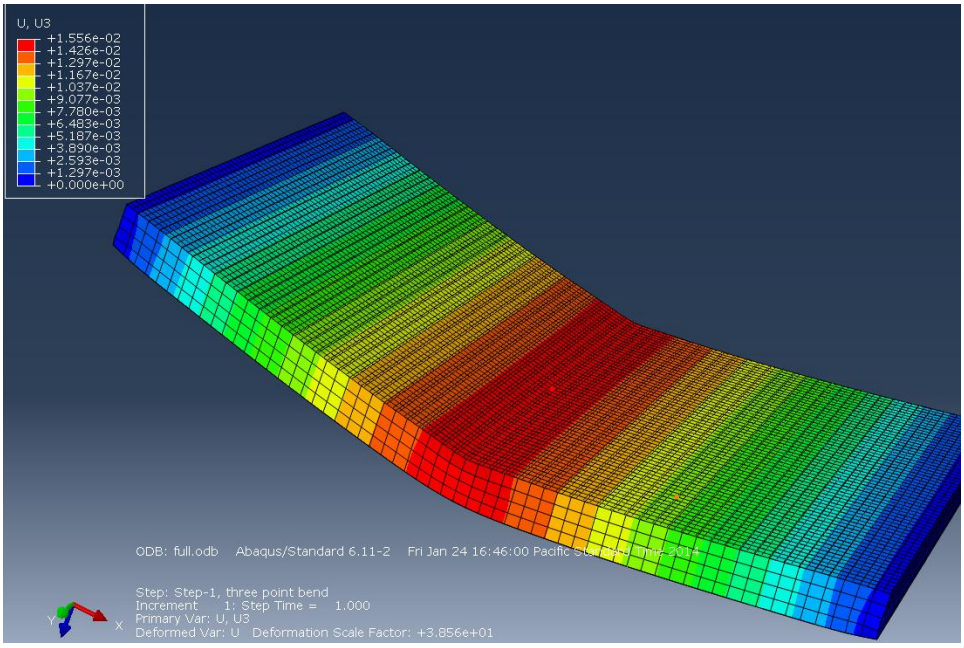

Figures 7.27.A. & 7.28.A. 1/3 Configuration FEA Stress and Displacements Graphs

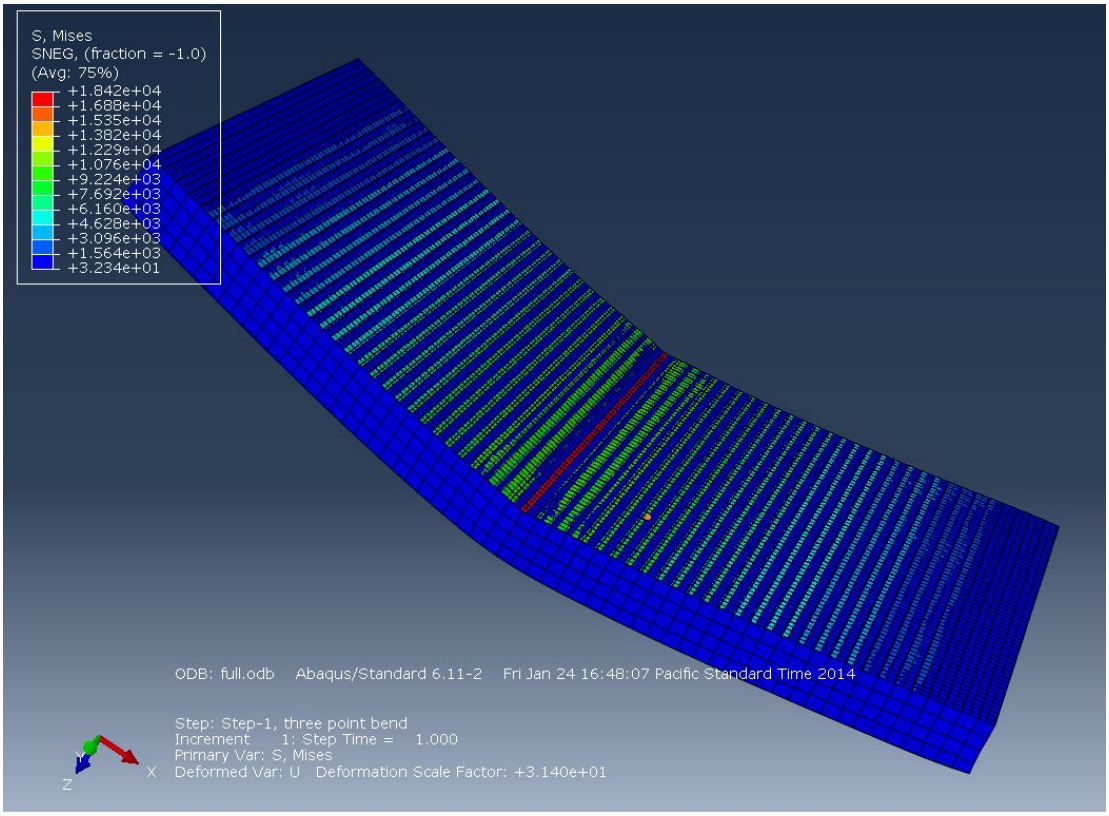

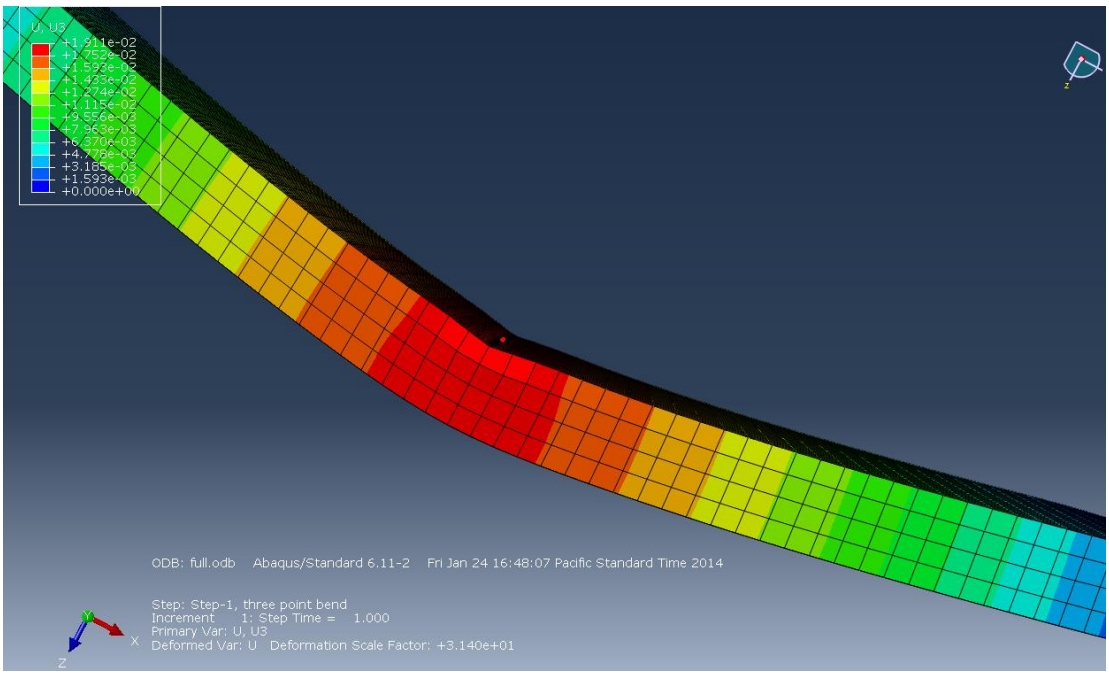

Figures 7.29.A. & 7.30.A. 5/2 Configuration FEA Stress and Displacements Graphs

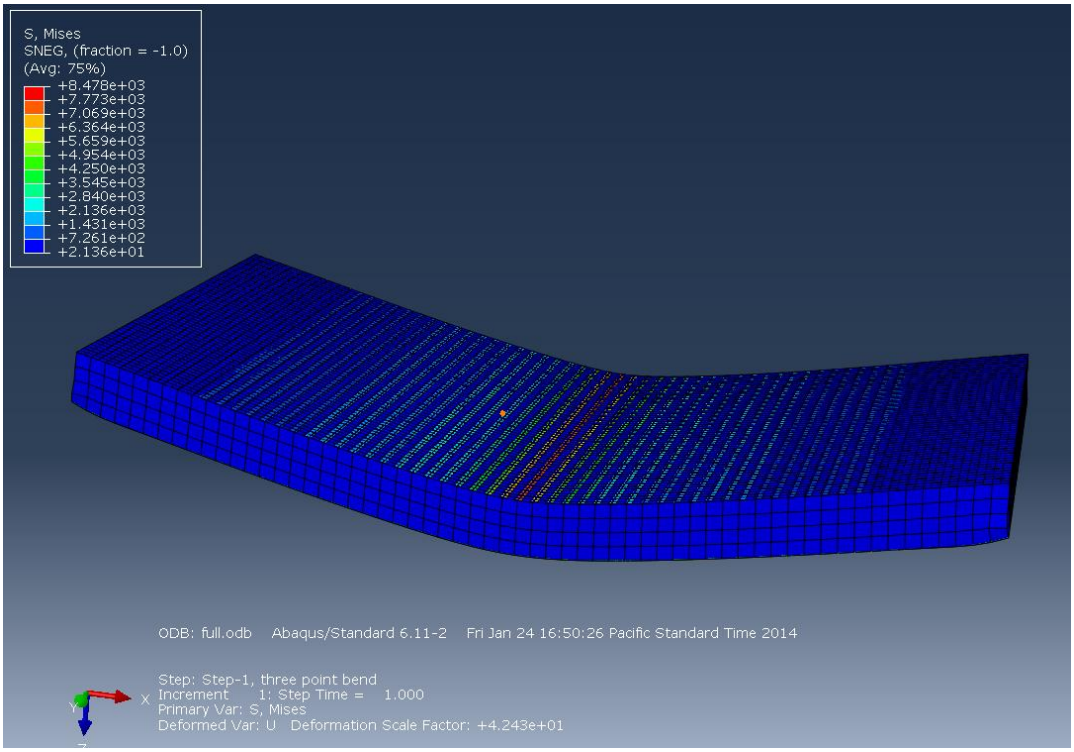

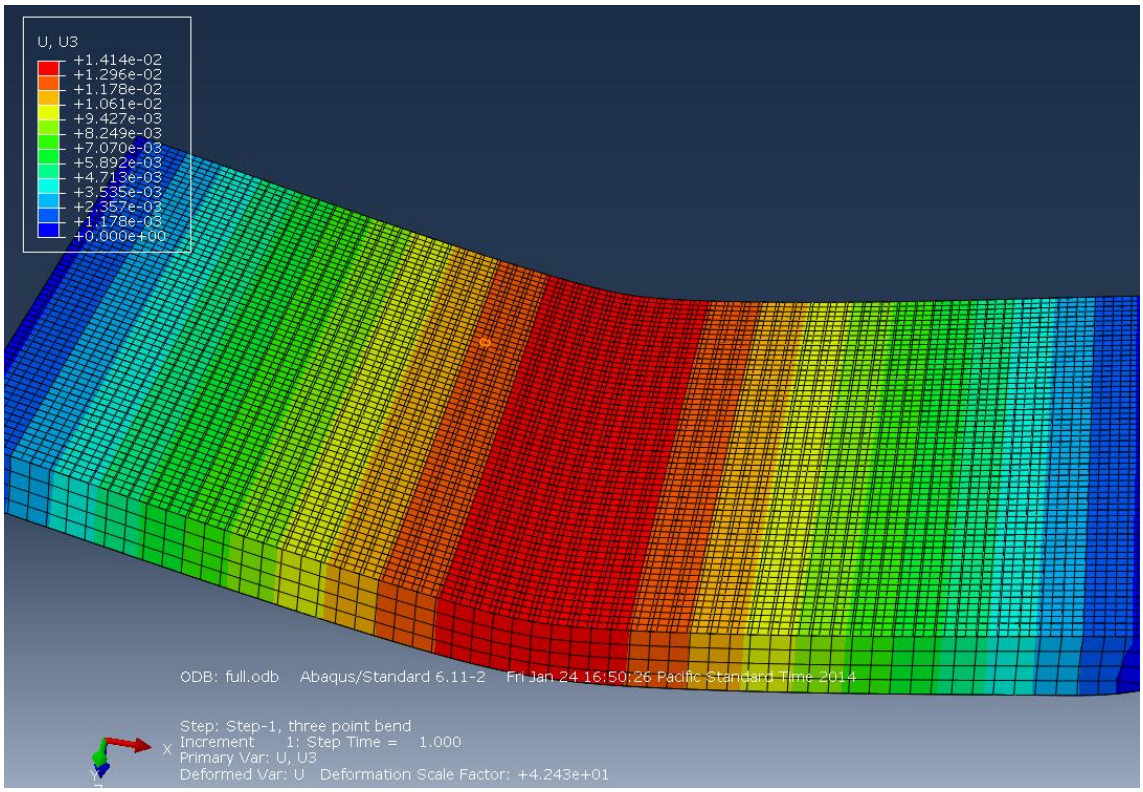

Figures 7.31.A. & 7.32.A. 4/2 Configuration FEA Stress and Displacements Graphs

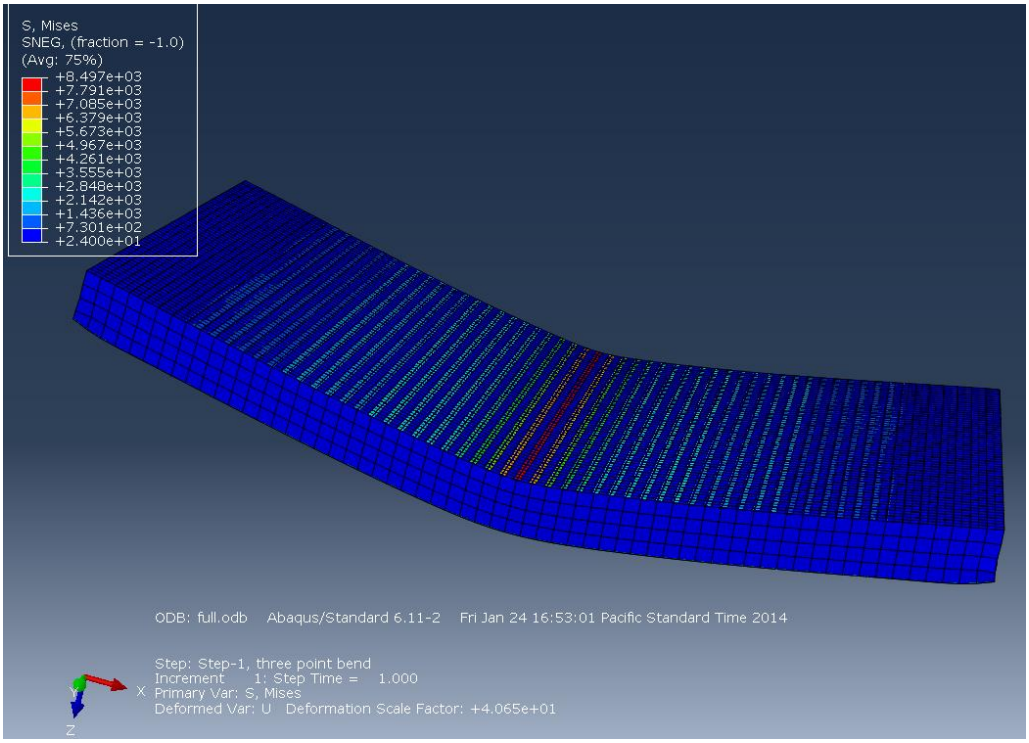

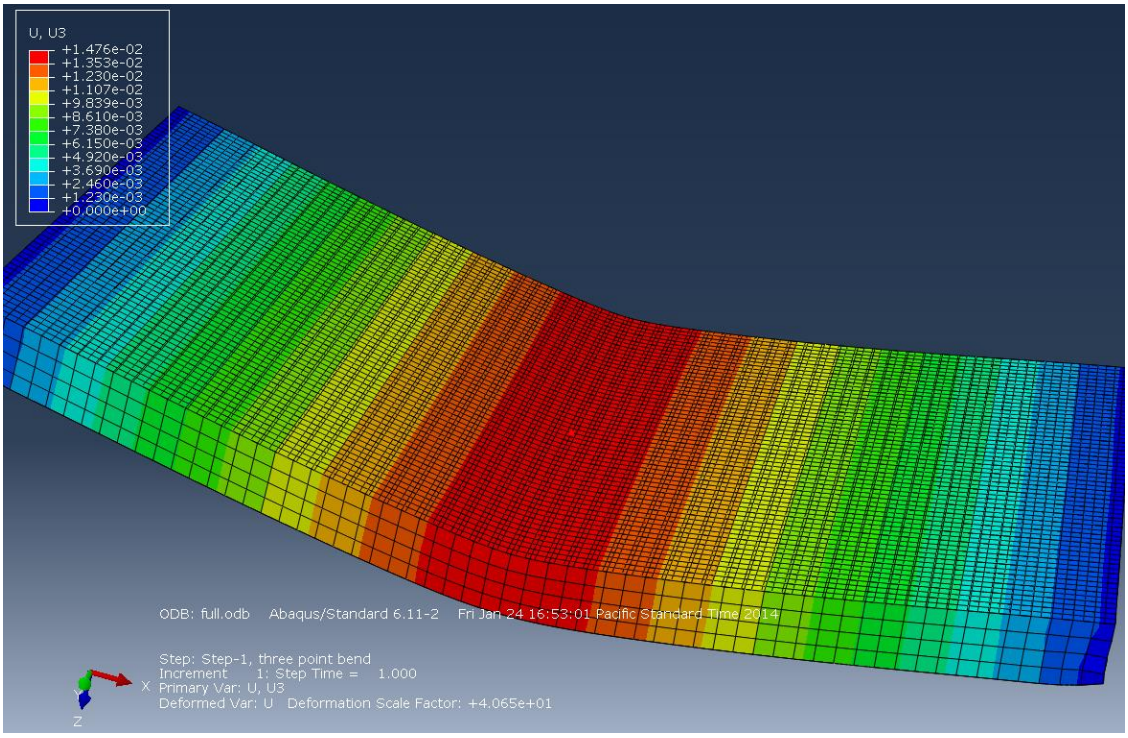

Figures 7.33.A. & 7.34.A. 3/2 Configuration FEA Stress and Displacements Graphs

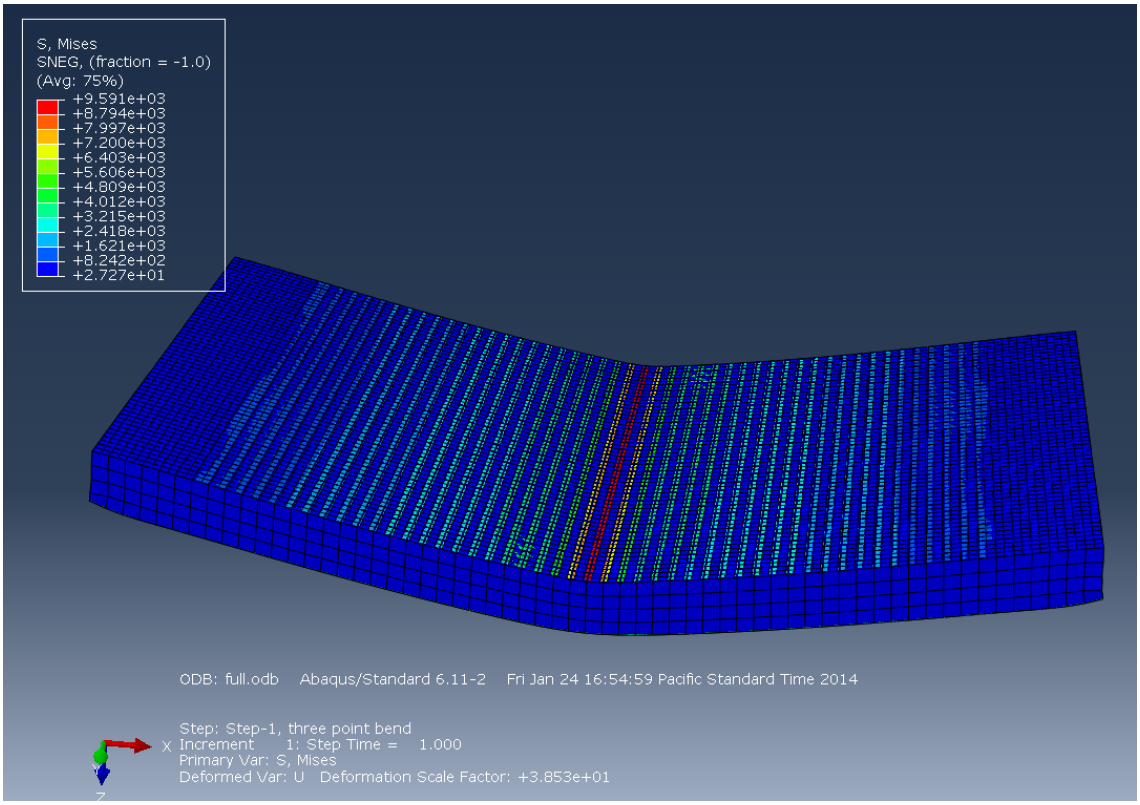

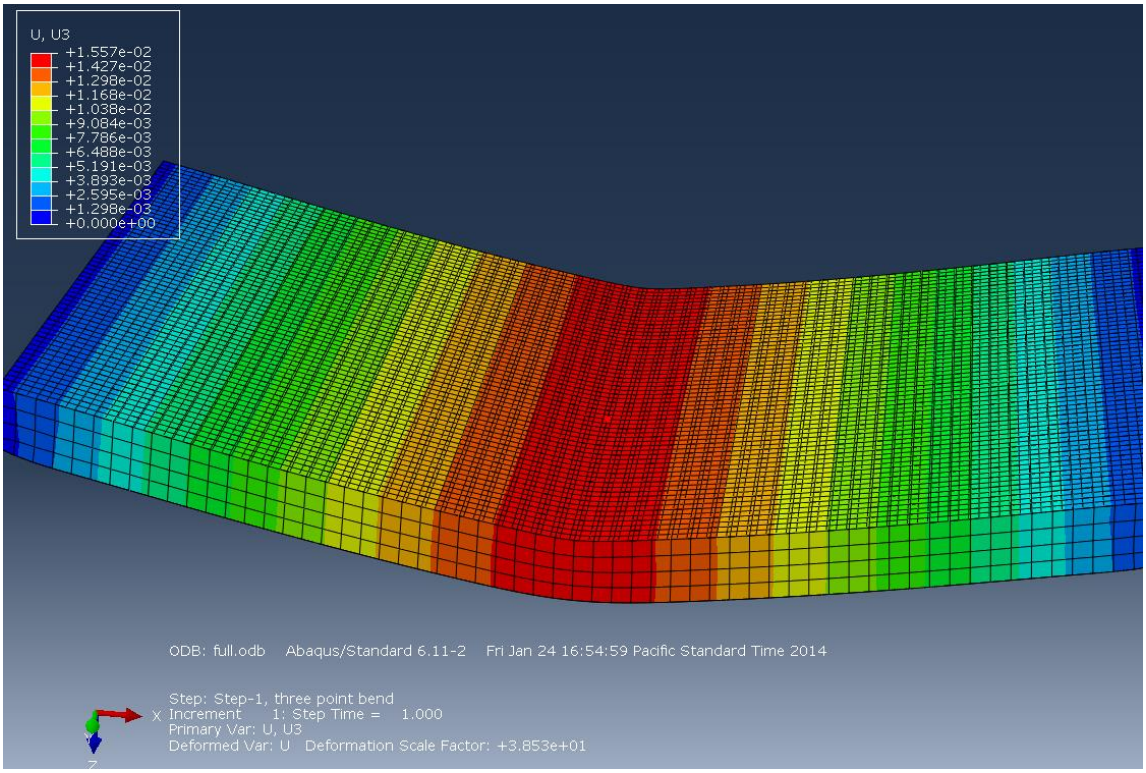

Figures 7.35.A. & 7.36.A. 2/2 Configuration FEA Stress and Displacements Graphs

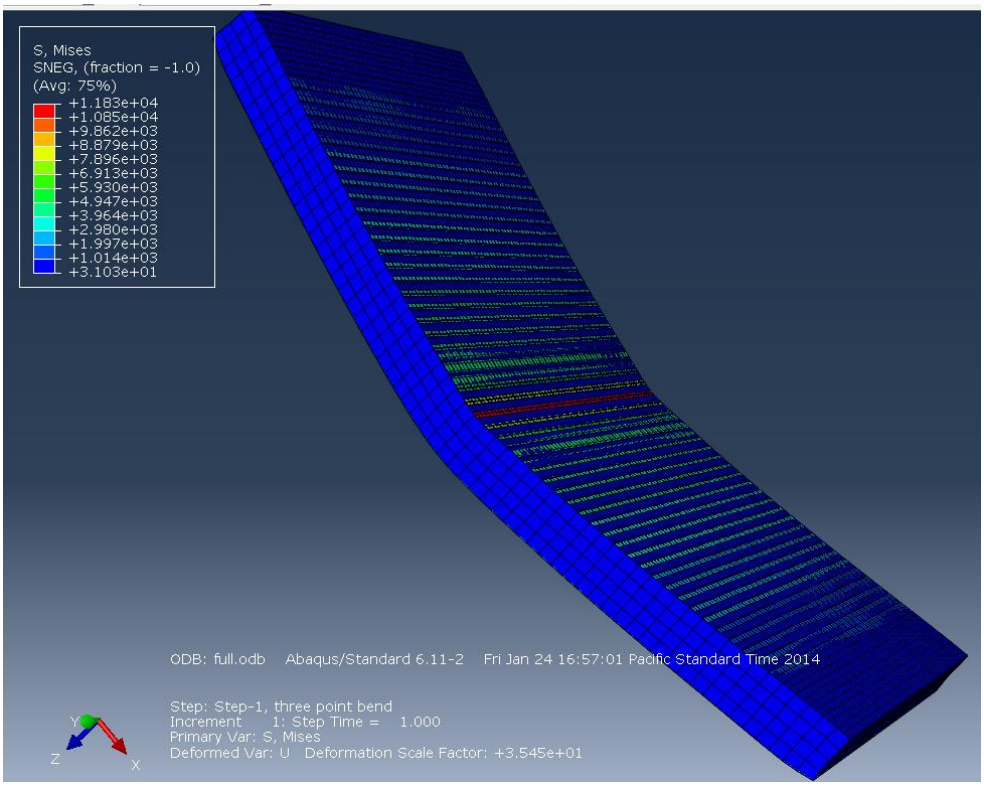

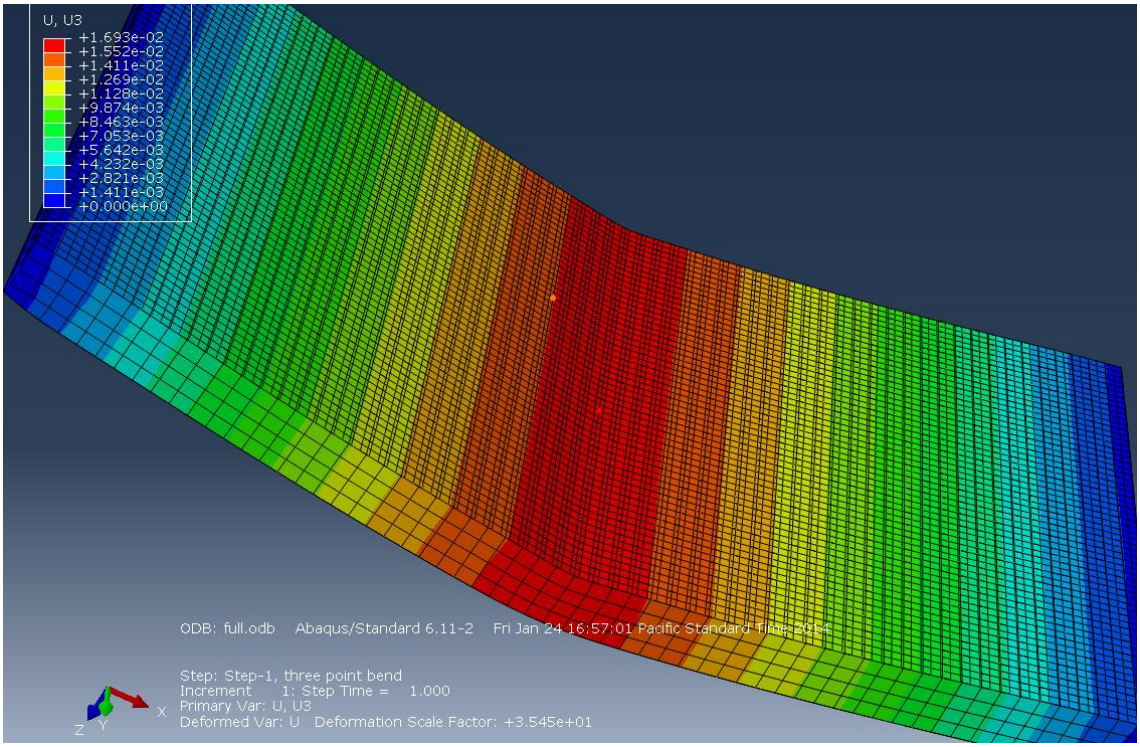

Figures 7.37.A. & 7.38.A. 1/2 Configuration FEA Stress and Displacements Graphs

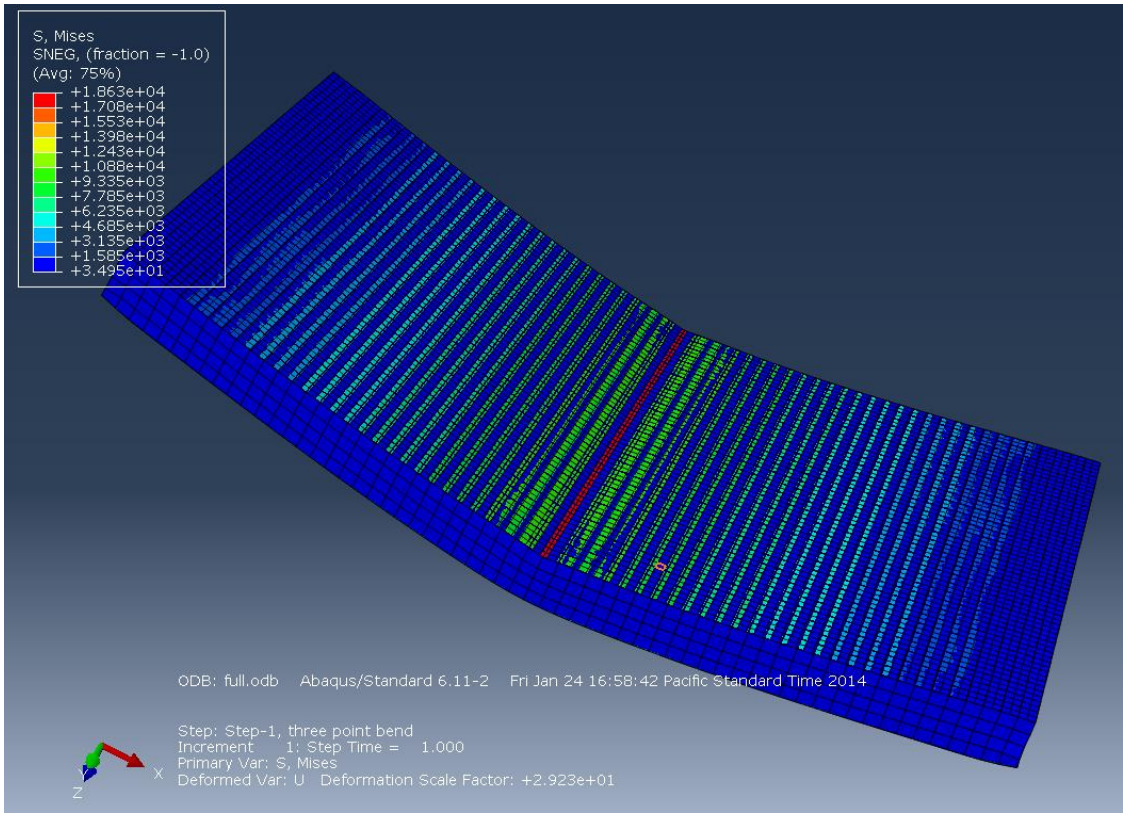

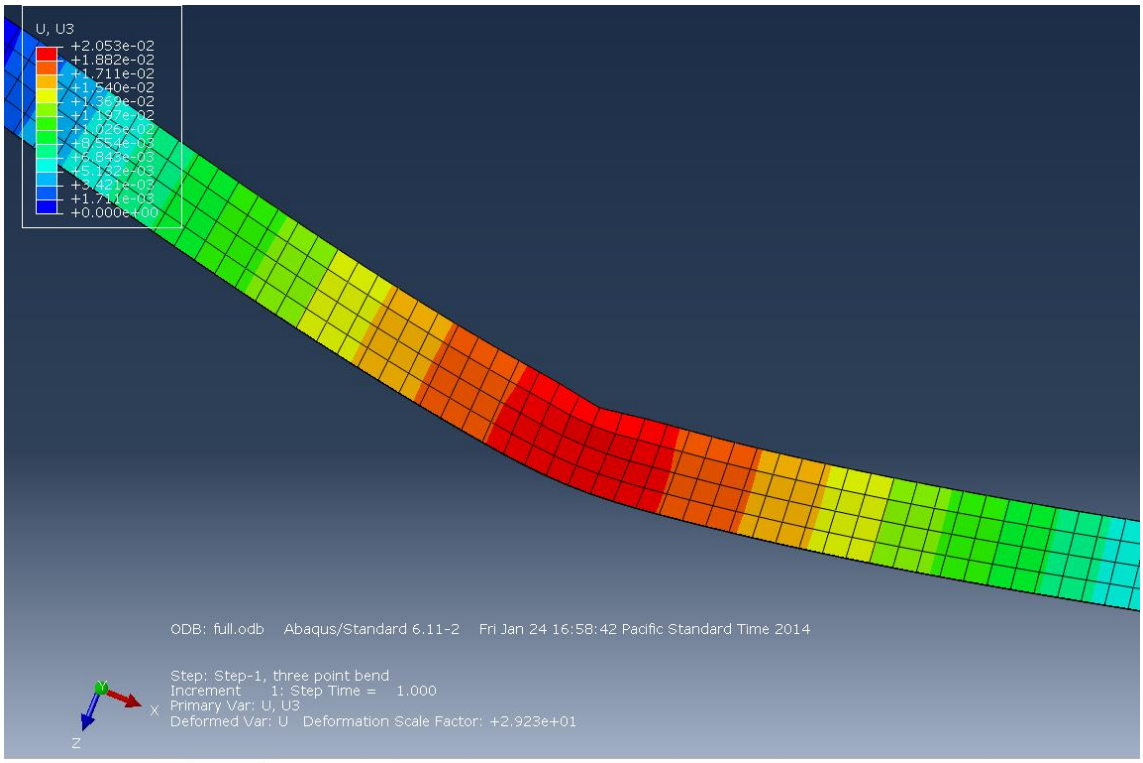

Figures 7.39.A. & 7.40.A. 5/1 Configuration FEA Stress and Displacements Graphs

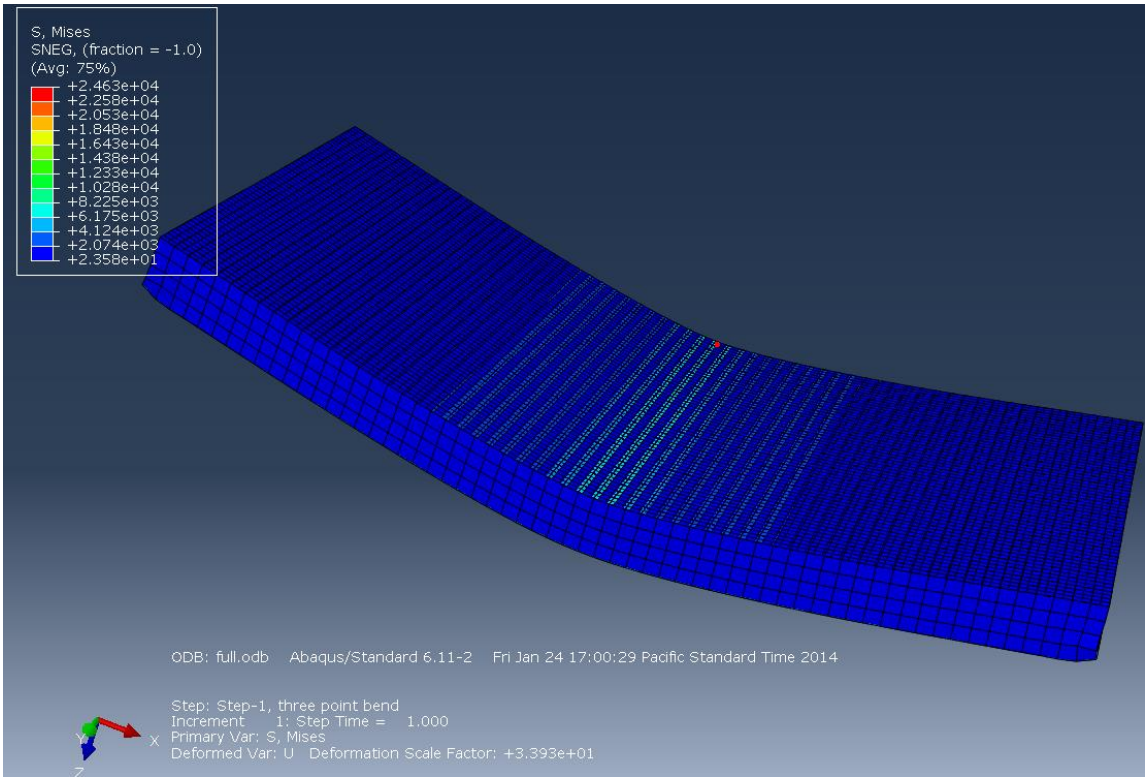

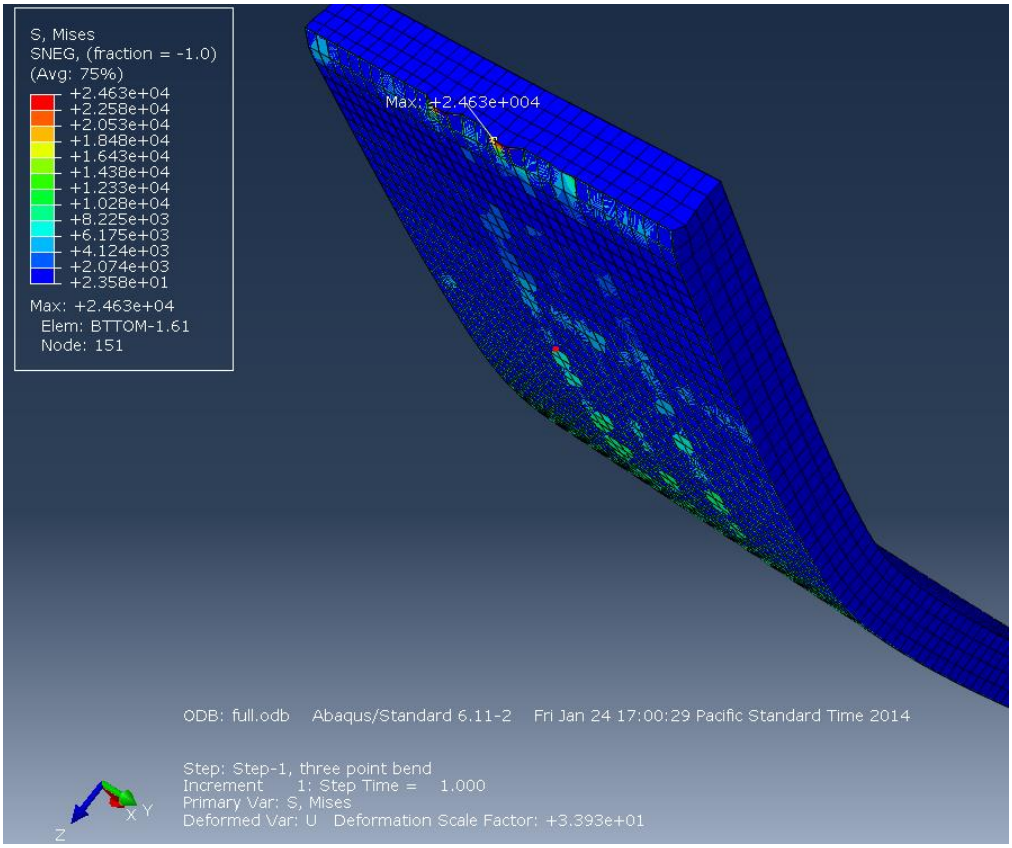

Figures 7.41.A. & 7.42.A. 4/1 Configuration FEA Stress and Displacements Graphs

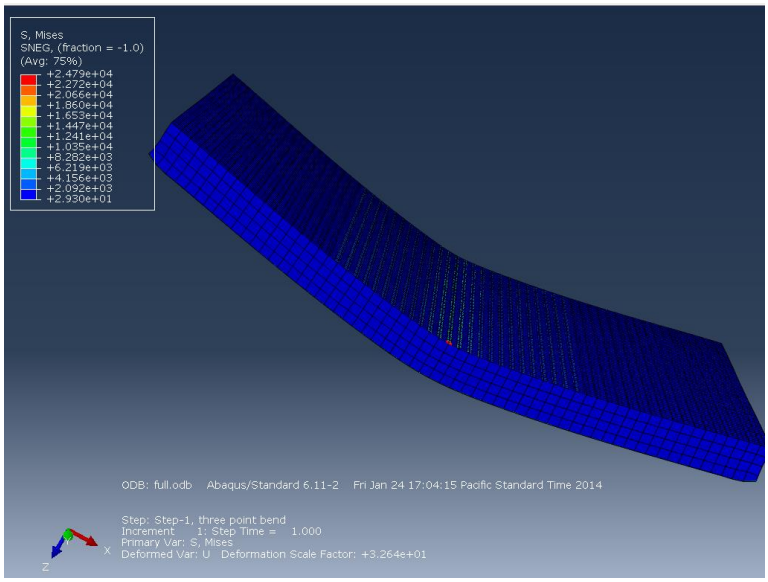

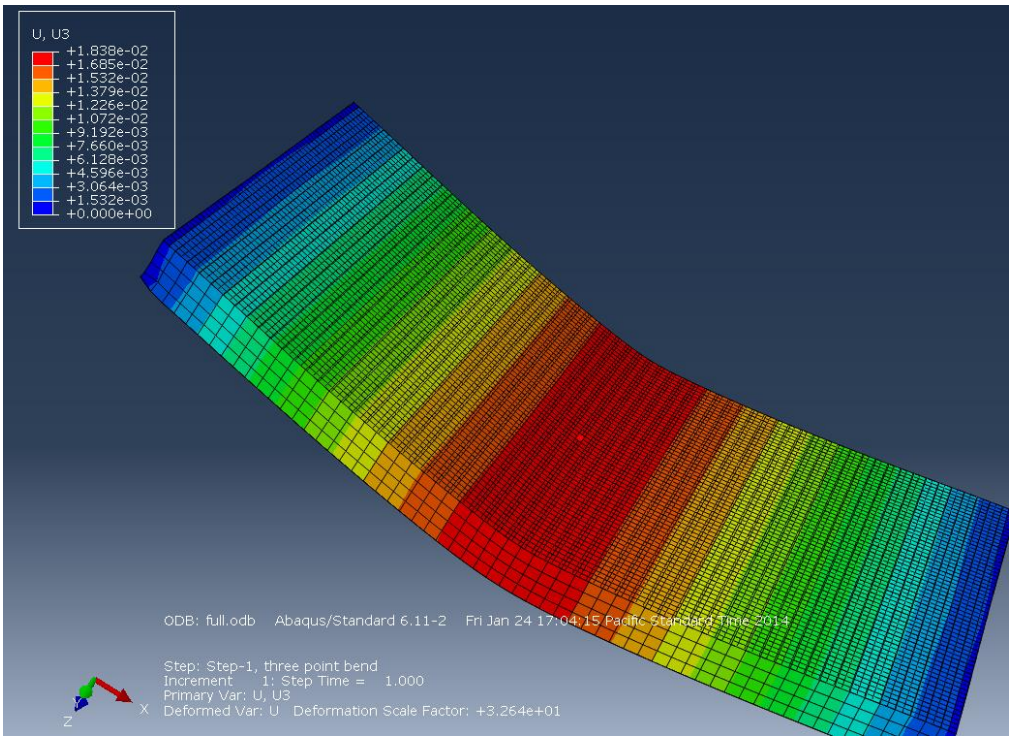

Figures 7.43.A. & 7.44.A. 3/1 Configuration FEA Stress and Displacements Graphs

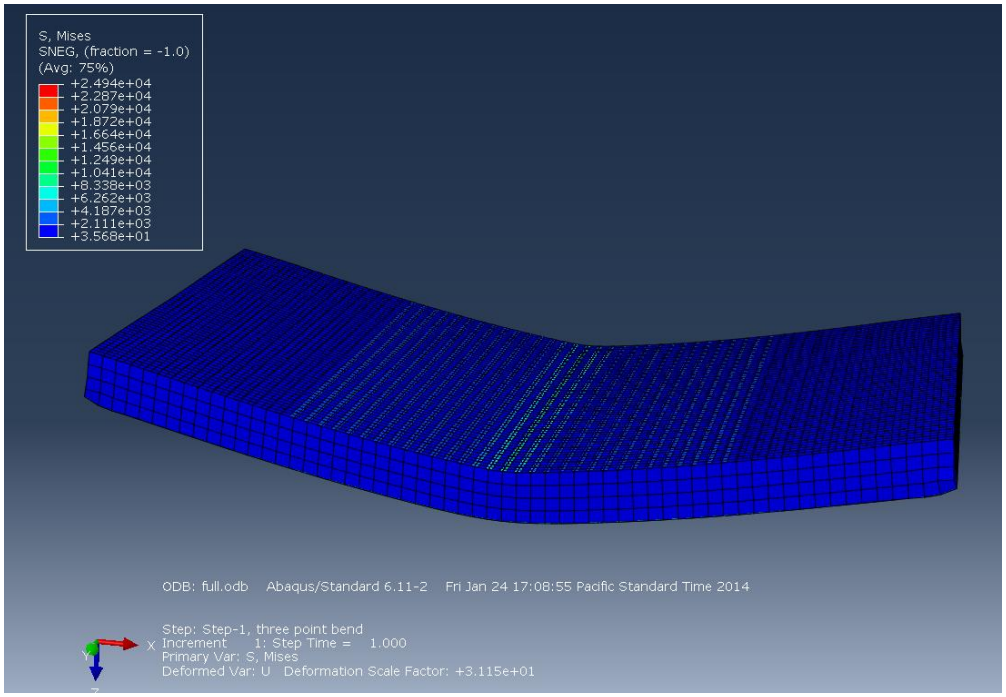

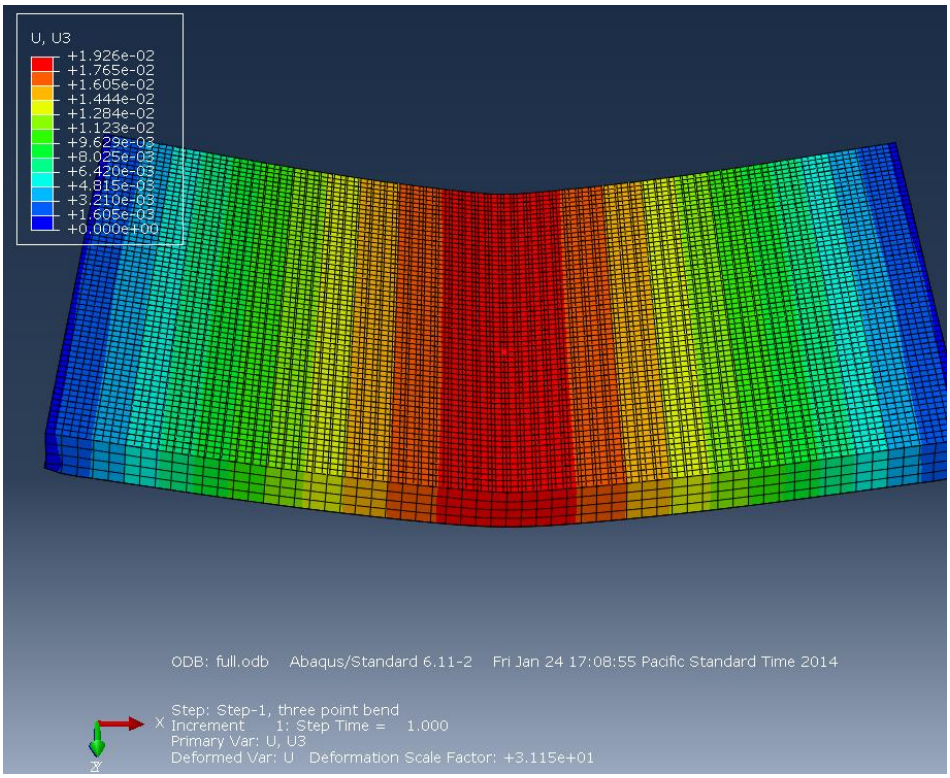

Figures 7.45.A. & 7.46.A. 2/1 Configuration FEA Stress and Displacements Graphs

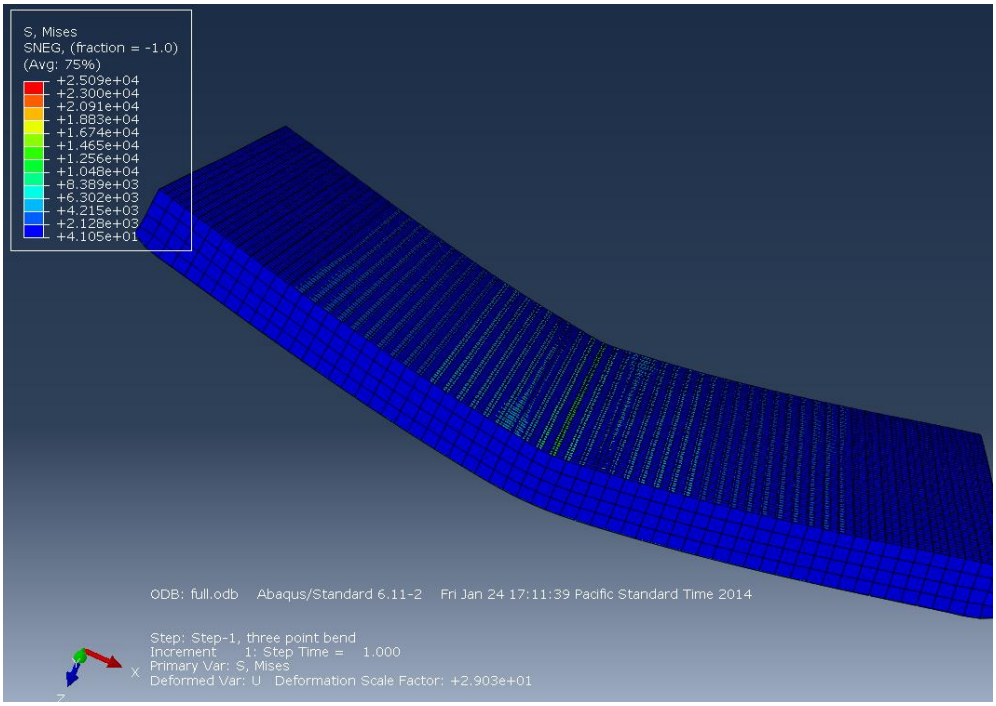

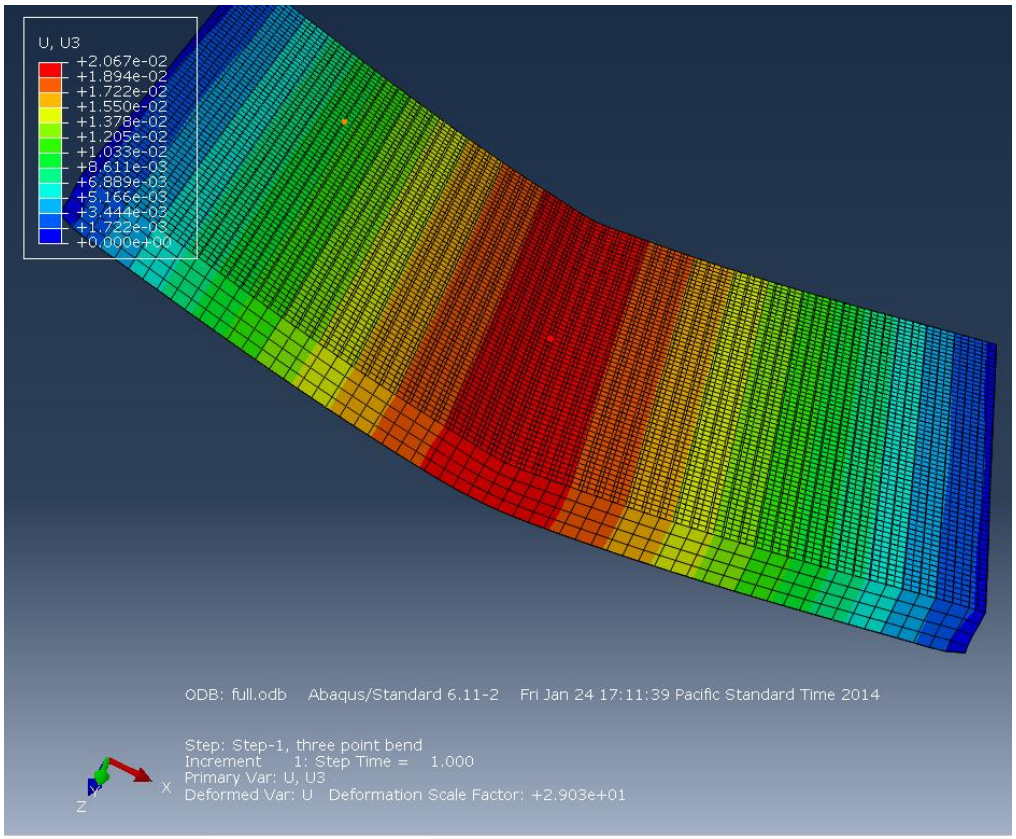

Figures 7.47.A. & 7.48.A. 1/1 Configuration FEA Stress and Displacements Graphs

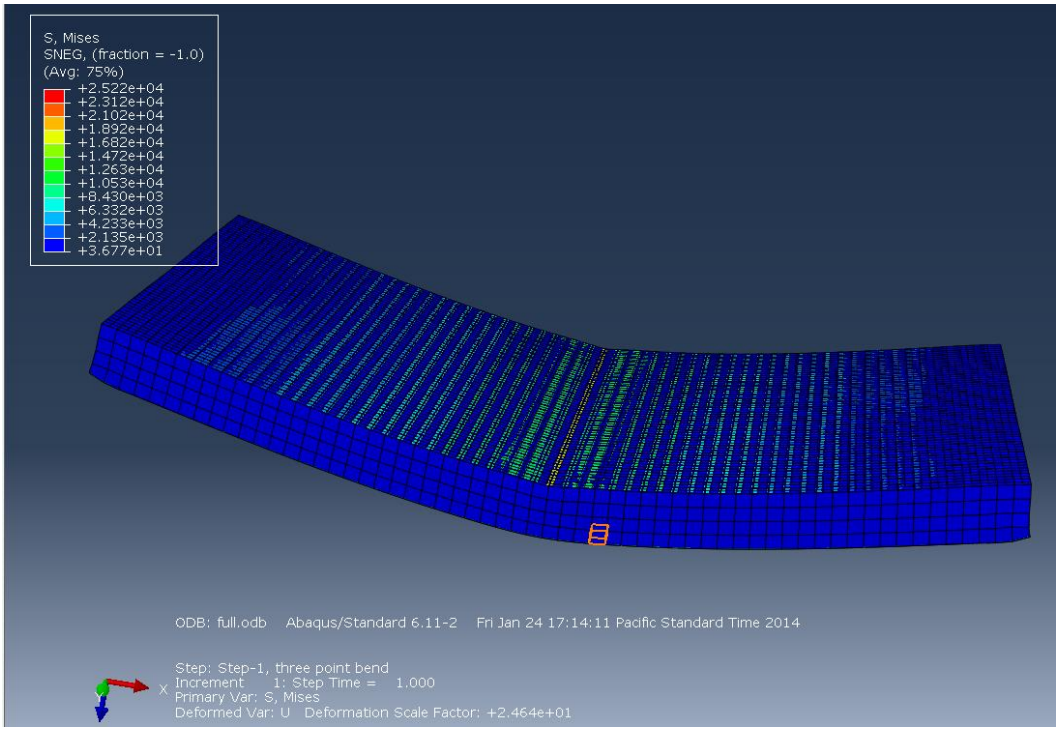

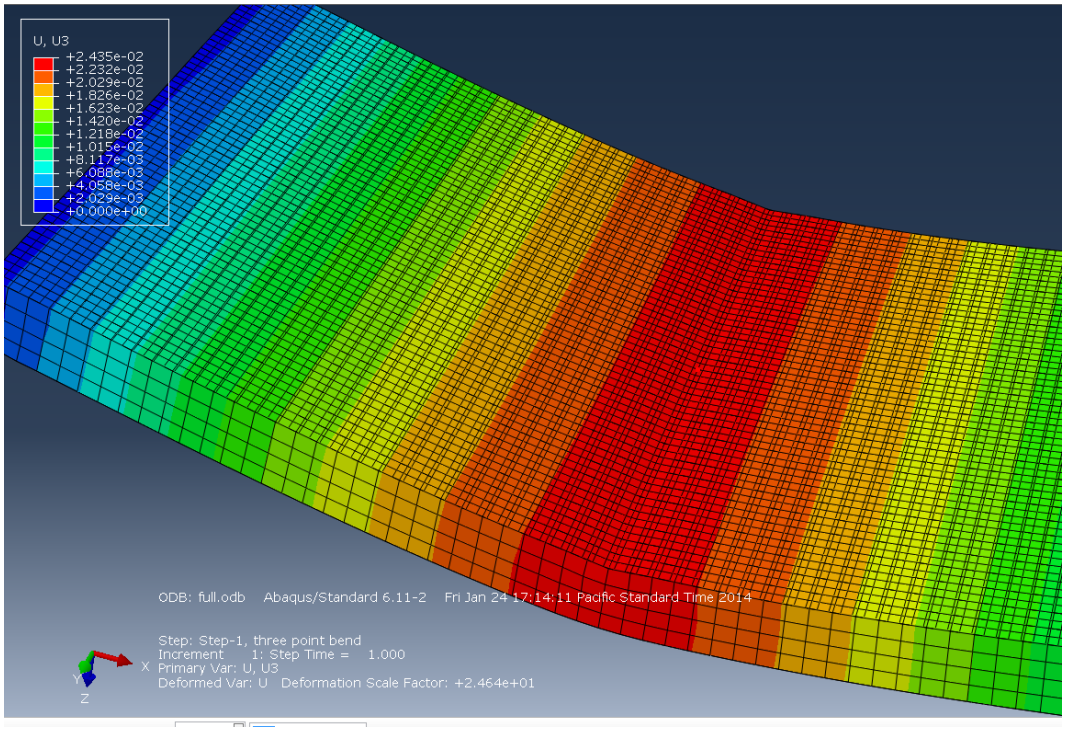

A.8 MATLAB code

This section includes all MATLAB code used during this thesis.

A.8.1. Classical Beam and Plate Theory for Midspan Deflections of Specimens with Varying Core Ribbon Direction

```
% Josh Lister
% Thesis
% Theoretical Deflections for Beams
clear all
close all
clc



% Equations
% I = I +Ay^2
% I = (1/12)*b*h^3
% deflection = PL^3/48EI +PL/4U
% U = G((d+c)^2)b/4c
% where d = total sandwich height
% c = core height and b = sandwich width
% centroid = sum(An*Cn)/sum(An)
% where A is area of section, Cn is distance from y=0 to centroid of
area

%Constants
P = 100;            % Load (lbf)
Es = 30e6;          % Youngs moduli of Steel 6064
vs = 0.297;         % Poissons of steel 6064
Gs = Es/(2*(1+vs)); % Core Shear of steel 6064
Eal = 10e6;         % youngs moduli of aluminium 1018
val = 0.3;          % Poissons of Aluminium 1018
Gal = Eal/(2*(1+val)); % Core Shear of Aluminium 1018
Ec = 12.9e6;        % Youngs moduli of 6376 A280h carbon fibre
vc = 0.03;          % Youngs moduli of 6376 A280h carbon fibre
Gc = Ec/(2*(1+vc)); % Core Shear of Aluminium 1018

% Beam Dimension
c = 0.375;          % Core Height
d = 0.375+0.048;    % Sandwich height
tf = 0.024;         % Facesheet height
b = 1.5;            % sandwich width
L = 6;              % Sandwich Length

%% Theoretical Complete Steel Beam
Af = b*tf;      % area of facing
Ac = b*c;       % area of core
Cf1 = tf/2;     % centroid of bottom facing
Cf2 = tf+c+tf/2;% centroid of top facing
```

```
Cc = tf+c/2;    % centroid of core

% Centroid of Complete Steel Bar
Csteel = (Af*Cf1+Af*Cf2+Ac*Cc)/(2*Af+Ac);

% Moment of Inertia
I1 = (1/12)*b*tf^3;     % moment of inertia of bottom facing
I2 = (1/12)*b*c^3;      % moment of inertia of core
I3 = I1;                % moment of inertia of top facing

If1 = (I1+ Af*(tf/2-Csteel)^2);          % Inertia of bottom facing
Ic =(I2+ Ac*((tf+c/2)-Csteel)^2) ;       % Inertia of core
If2 = (I3+ Af*(((tf/2)+c+tf)-Csteel)^2);   % Inertia of top facing

EI_totalsteel = Es*If1+Es*Ic+Es*If2;

% Shear Rigidity
Us = Gs*(d+c)^2*b/(4*c);

% Midspan Deflection
ds1 = P*L^3/(48*EI_totalsteel); % Deflection due to facings
ds2 = P*L/(4*Us);               % Deflection due to shear
Steel_def = ds1+ds2;


%% Aluminium Facings with Steel Core
% All Dimensional parameters same as Complete Steel Beam



EI_totalalst = Eal*If1+Es*Ic+Eal*If2;

% Shear Rigidity
Us = Gs*(d+c)^2*b/(4*c);

% Midspan Deflection
ds1 = P*L^3/(48*EI_totalalst);   % Deflection due to facings
ds2 = P*L/(4*Us);                % Deflection due to shear
AlSteel_def = ds1+ds2;


%% Carbon Fibre Face Sheets with Honeycomb Core version 1

% poisson ov 0.8031 coupled with G = 10.2e3

vh1 = [0.8036 0.7773 0.7055 0.6074 0.5094 0.4376 0.4113] ;
theta = [ 0 15 30 45 60 75 90];
```

```
for i = 1:length(theta)
Gh1(1,i) = 10.2e3*(cosd(theta(i)))^2 + 5.4e3*(sind(theta(i)))^2;

end
Eh1 = Gh1.*(2.*(1+vh1));

% Dimesnoinal Propeties the same as above
EI_totalCH1 = Ec*If1+Eh1.*Ic+Ec*If2;

% Shear Rigidity
Uh1 = Gh1.*(d+c)^2*b/(4*c);

% Midspan Deflection 1
dch1 = P*L^3./(48.*EI_totalCH1); % Deflection due to facings
dch2 = P*L./(4.*Uh1);                % Deflection due to shear
CH_def1 = dch1+dch2;            % Total Deflection

figure
plot(theta,CH_def1,'x')
xlabel('Core Direction (degrees)')
ylabel('Deflection (in)')



% Comparison

Experimentald = [ 0.0337 0.0363 0.0380 0.0453 0.0486 0.0555 0.0558];
expstd = [7.7968e-4 0.0011 0.0012 0.0013 9.1335e-4 0.0022 0.0019];
Theoreticald = CH_def1;
%FEA = [3.48038e-002 3.58072e-002 3.89588e-002 4.45480e-002 5.23770e-
002 6.03650e-002 6.18512e-002];
FEAortho = [3.2756e-2 3.43119e-2 3.87508e-2 4.50503e-2 5.1571e-2
5.64642e-2 5.82776e-2];

figure
plot(theta,Theoreticald,'ro')
hold on
errorbar(theta,Experimentald,expstd,'bx')
%plot(theta,FEA,'gs')
plot(theta,FEAortho,'ms')
xlabel('Core Direction angle (Degrees')
ylabel('Midpsan Deflection at 100lb')
legend('Theoretical','Experimental','FEA')



%% Mesh Convergence With Aluminium Face and Steel Core
```

```
Mesh = [0.06 0.08 0.1 0.12 0.14 0.17 0.18 0.2 0.22 0.24 .245 .247 0.25
0.255 0.26 0.27 0.3];
Mesh1 = fliplr(Mesh) ;
disp = [2.014e-3 2.00522e-3 1.99917e-3 2.00474e-3 1.99434e-3 1.97683e-
3 2.01402e-3 1.9653e-3 1.91571e-3 1.8763e-3 1.86528e-3 1.86528e-3
1.86253e-3 2.90438e-3 2.974e-3 2.85389e-3 2.69396e-3];
disp1 = fliplr(disp);
figure
plot(Mesh1,disp1,'x')
hold on
xlabel('Seed')
ylabel('Displacement (in)')

figure
meshels = [ 0.28 0.24 0.26 0.245 0.255];
els = [402 600 414 582 438];
plot(els,meshels,'x')

%% Maximum Stress at 100lb

stress = P*6/(2*(0.375*2+0.048)*1.5*0.024);
FEA = [ 1.098e4 1.114e4 1.11e4 1.097e4 1.265e4  1.406e4 1.459e4];
Theoretical = [  10442.7 10442.7 10442.7 10442.7 10442.7 10442.7
10442.7];

figure
plot(theta,FEA,'ro')
hold on
plot(theta,Theoretical,'b')
xlabel('Core Direction angle (Degrees')
ylabel('Maximum Von Mises Stress at 100lbf (psi)')
legend('FEA','Theoretical')
```

A.8.2. Honeycomb Poisson's Ratio

```
% Honeycomb Core Constants
%
% Determines experimentally the transvers and longitudinal poissons ratio
% For honeycomb in accordance with ASTM D6790-2
clear all
close all
clc

% Data
% s# = [ cT cL ; dT dL]; inches

s1 = [11.6 11.625  1.08 0.6];
```

```
s2 = [11.625 11.75  1.2 0.6];
s3 = [11.375 11.75  1.175 0.6];
s4 = [11.375 11.75  1.1 0.585];
s5 = [11.625 11.75  1.2 0.6];
s6 = [11.375 11.75  1.175 0.6];
s7 = [11.375 11.75  1.1 0.585];

s = [s1;s2;s3;s4;s5;s6;s7];
% Equations
Ri = 12;                          % Radius of Cylinder
Rat = (4*s(:,3).^2+s(:,1).^2)./(8*s(:,3));    % Radius of core curve
Ral = (4*s(:,4).^2+s(:,2).^2)./(8*s(:,4));
utall = Ri./Rat;                   % Transverse mu
ulall = Ri./Ral;                  % Longitudinal mu

ut = mean(utall);                  % Mean transverse E
utstd = std(utall);                % stddev transverse E

ul = mean(ulall);                  % Mean longitudinal E
ulstd = std(ulall);                % stddev longitudinal E
```

A.8.3. Experimental Density Measurements for Composite Laminates

```
% Density Tests
% Josh Lister
clear all
close all
clc

%% Density Calculations Experimentally

% 8 Layers
% [t w l weight] inches lbs
lay8 =[ 0.088 0.522 4.47 0.0115;
    0.088 0.496 4.474 0.011;
    0.088 0.476 4.473 0.0105;
    0.088 0.959 8.938 0.0430;
    0.089 1.018 4.954 0.0255;
    0.09 0.978 4.96 0.0235];


% 6 Layers

lay6 = [0.067 1.01 8.938 0.0335;
    0.068 0.91 8.938 0.03;
    0.069 0.94 8.938 0.0315;
    0.071 0.985 8.938 0.033];

% 4 Layers

lay4 = [0.045 0.954 4.054 0.0095;
```

```
    0.046 0.963 4.056 0.01;
    0.045 0.953 4.047 0.01;
    0.045 0.968 4.037 0.01];

rhoC4 = lay4(:,4)./((lay4(:,1).*lay4(:,2).*lay4(:,3)));
rhoC6 = lay6(:,4)./((lay6(:,1).*lay6(:,2).*lay6(:,3)));
rhoC8 = lay8(:,4)./((lay8(:,1).*lay8(:,2).*lay8(:,3)));

rhoC4mean = mean(rhoC4);
rhoC4std = std(rhoC4);
rhoC6mean = mean(rhoC6);
rhoC6std = std(rhoC6);
rhoC8mean = mean(rhoC8);
rhoC8std = std(rhoC8);
rhoCexpmean = mean([rhoC4;rhoC6;rhoC8]);
rhoCexpstd = std([rhoC4;rhoC6;rhoC8]);

% Data Sheet Densities
rhoE = 0.0473267525;
rhoC = 0.057;
rhoF = (0.057-rhoE*(1-0.5529))/0.5529;

%% Volume Fraction

% 4 Layers
 V4 = [45.2-36.4  42.4-36.4  ; % 11:10am - 11:50
       45.6-36.7  42.4-36.7];        %11:55 -
massf4 = V4(:,2);
 massc4 = V4(:,1);
 masse4 = V4(:,1)-V4(:,2);
 rhof4 = massf4./(massc4./rhoC4mean-masse4./rhoE);
rhofexp4mean = mean(rhof4);
Vf4 =(massc4./rhoC4mean - masse4./rhoE)./(massc4./rhoC4mean);


 % 8 layers facesheet by itself
 V8 = [48.2-36.8    43.4-36.8;
     47.6-37.0      43.4-37.0 ];
massf8 = V8(:,2);
 massc8 = V8(:,1);
 masse8 = V8(:,1)-V8(:,2);
 rhof8 = massf8./(massc8./rhoC8mean-masse8./rhoE);
rhofexp8mean = mean(rhof8);
Vf8 =(massc8./rhoC8mean - masse8./rhoE)./(massc8./rhoC8mean);

VfTotal = [Vf4;Vf8];
Vftotal_mean = mean(VfTotal);
Vftotal_std = std(VfTotal);
```

A.8.4. Volume Fraction Calculations

```
% Volume Fraction Tests
```

```
% Josh Lister
clear all
close all
clc

% V = [ initial weight  Final Weight ];  in grams
% weight of plate1 107.8 g
% weight of plate2 to 54,6 g,
% plate 2 =53.4g from 6 test onwards

% Weight/Volume/Density of 6 lay Composite Laminate
% Experimental
cw1 = 0.00396832;   % lbs
cv1 = 0.07*1.007*0.977 % in^3
crho1 = cw1/cv1;     % lb/in^3

cw2 = 0.0035274;
cv2 = 0.07*(.952+0.965)/2*0.957;
crho2 = cw2/cv2;

rhoc = (crho1+crho2)/2;

% Density of Resin

% Fibre
rhof = 0.065;
Vfnom =55.29;



% Resin
rhoe = 0.0470;   % lb/in3
Rtensilestr = 17.5;  % ksi
REt = 0.677;         % msi
Venom = 1-Vfnom;

% 6 layers

V6 = [
       60.6-54.2 57.6-54.2  ;
       114-107.8   111.8-107.8   ;
       112.6-107.8  110.8-107.8;
       59.4-53.4  57.4-53.4;

       % can use from here on.
       6.6  60.8-56.4;  6.2  114-111.6;
       113.8-107.8  110.4-107.8   ;
       59.6-53.4    57.2-53.4  ;
        114.2-107.8   112-107.8 ;
        113.4-107.8   111.2-107.8;
        58.8-54.6 56.8-54.6;
        58.2-54.6   56.4-54.6 ];

V2 = [ 59-54.6 56.6-54.6;
     112.8-108   109.6-108;
```

```
     58.6-53.4  55.6-53.4;
     57.8-52.8   0];


 % 4 layers facesheet by itself
 p1 = 36.4;
 V4 = [45.2-36.4  42.4-36.4  ; % 11:10am - 11:50
       45.6-36.7  42.4-36.7];        %11:55 -

 % 8 layers facesheet by itself
 V8 = [48.2-36.8    43.4-36.8;
     47.6-37.0      43.4-37.0           ];        %2:05
% Equations for 6 layers

mfrace6 = (V6(:,1)-V6(:,2))./V6(:,1);
mfracf6 = V6(:,2)./V6(:,1);
mfracc6 = 1;
me_mean6 = mean(mfrace6);
mf_mean6 = mean(mfracf6);
massf6 = V6(:,2);
masse6 = V6(:,1)-V6(:,2);
massc6 = V6(:,1);
% Fibmean = mean(weightFiber);
% Epoxmean =mean(weightEpoxy);


rhoc = 0.057;
rhoe = 0.0473;
% Volume Fraction for 6layers

rhof = massf6./(massc6/rhoc-masse6./rhoe);
rhofmean = mean(rhof);
Vf6 =(massc6/rhoc - masse6./rhoe)./(massc6./rhoc)

% Volume Fraction for 2 layer sandwich

% Equation for 2 layers in sandwich

mfrace2 = (V2(:,1)-V2(:,2))./V2(:,1);
mfracf2 = V2(:,2)./V2(:,1);
mfracc2 = 1;
me_mean2 = mean(mfrace2);
mf_mean2 = mean(mfracf2);
massf2 = V2(:,2);
masse2 = V2(:,1)-V2(:,2);
massc2 = V2(:,1);

rhof = massf2./(massc2/rhoc-masse2./rhoe);
rhofmean = mean(rhof);
Vf2 =(massc2/rhoc - masse2./rhoe)./(massc2./rhoc)

% Fiber Volume Fraction from densities
rhof = 0.065;
rhoc = 0.057;
```

```
rhoe = 0.0473;
FVFtheo = (rhoc-rhoe)./(rhof-rhoe);

% Fibre volume fraction from Fibre Weight Fraction
rhof = 0.065;
FWF2 = V2(:,2)./V2(:,1);
FWF6 = V6(:,2)./V6(:,1);

FVF2exp = 1./(1+rhof/rhoe*(1./FWF2-1));
FVF6exp = 1./(1+rhof/rhoe*(1./FWF6-1));
```

A.8.5. Theoretical Midspan Deflections for FEA Validity

```
% Josh Lister
% Thesis
% Theoretical Deflections for Beams
clear all
close all
clc



% Equations
% I = I +Ay^2
% I = (1/12)*b*h^3
% deflection = PL^3/48EI +PL/4U
% U = G((d+c)^2)b/4c
% where d = total sandwich height
% c = core height and b = sandwich width
% centroid = sum(An*Cn)/sum(An)
% where A is area of section, Cn is distance from y=0 to centroid of area

%Constants
P = 100;            % Load (lbf)
Es = 30e6;          % Youngs moduli of Steel 6064
vs = 0.297;         % Poissons of steel 6064
Gs = Es/(2*(1+vs)); % Core Shear of steel 6064
Eal = 10e6;         % youngs moduli of aluminium 1018
val = 0.3;          % Poissons of Aluminium 1018
Gal = Eal/(2*(1+val)); % Core Shear of Aluminium 1018
Ec = 12.9e6;        % Youngs moduli of 6376 A280h carbon fibre
vc = 0.03;          % Youngs moduli of 6376 A280h carbon fibre
Gc = Ec/(2*(1+vc)); % Core Shear of Aluminium 1018

% Beam Dimension
c = 0.375;          % Core Height
d = 0.375+0.048;    % Sandwich height
tf = 0.024;         % Facesheet height
b = 1.5;            % sandwich width
L = 6;              % Sandwich Length

%% Theoretical Complete Steel Beam
Af = b*tf;      % area of facing
Ac = b*c;       % area of core
Cf1 = tf/2;     % centroid of bottom facing
```

```
Cf2 = tf+c+tf/2;% centroid of top facing
Cc = tf+c/2;    % centroid of core

% Centroid of Complete Steel Bar
Csteel = (Af*Cf1+Af*Cf2+Ac*Cc)/(2*Af+Ac);

% Moment of Inertia Beam
I1 = (1/12)*b*tf^3;     % moment of inertia of bottom facing
I2 = (1/12)*b*c^3;      % moment of inertia of core
I3 = I1;                % moment of inertia of top facing

% Beam
If1 = (I1+ Af*(tf/2-Csteel)^2);          % Inertia of bottom facing
Ic =(I2+ Ac*((tf+c/2)-Csteel)^2) ;       % Inertia of core
If2 = (I3+ Af*(((tf/2)+c+tf)-Csteel)^2);   % Inertia of top facing

EI_totalsteel = Es*If1+Es*Ic+Es*If2;

% Shear Rigidity
Us = Gs*(d+c)^2*b/(4*c);

% Midspan Deflection
ds1 = P*L^3/(48*EI_totalsteel); % Deflection due to facings
ds2 = P*L/(4*Us);               % Deflection due to shear
Steel_def = ds1+ds2;


%% Aluminium Facings with Steel Core
% All Dimensional parameters same as Complete Steel Beam

EI_totalalst = Eal*If1+Es*Ic+Eal*If2;

% Shear Rigidity
Us = Gs*(d+c)^2*b/(4*c);

% Midspan Deflection
ds1 = P*L^3/(48*EI_totalalst);   % Deflection due to facings
ds2 = P*L/(4*Us);                % Deflection due to shear
AlSteel_def = ds1+ds2;


%% Carbon Fibre Face Sheets with Honeycomb Core version 1

% poisson ov 0.8031 coupled with G = 10.2e3

vh1 = [0.8036 0.7773 0.7055 0.6074 0.5094 0.4376 0.4113] ;
theta = [ 0 15 30 45 60 75 90];
for i = 1:length(theta)
Gh1(1,i) = 10.2e3*(cosd(theta(i)))^2 + 5.4e3*(sind(theta(i)))^2;

end
Eh1 = Gh1.*(2.*(1+vh1));
```

```
% Moment of Inertia Plate
I1p = (1/(12*(1-vc^2)))*b*tf^3;     % moment of inertia of bottom facing
I2p = (1./(12*(1-vh1.^2))).*b*c.^3;      % moment of inertia of core
I3p = I1;                % moment of inertia of top facing

% Plate
If1p = (I1p+ Af*(tf/2-Csteel)^2);          % Inertia of bottom facing
Icp =(I2p+ Ac*((tf+c/2)-Csteel)^2) ;       % Inertia of core
If2p = (I3p+ Af*(((tf/2)+c+tf)-Csteel)^2);   % Inertia of top facing

% Dimesnoinal Propeties the same as above
EI_totalCH1beam = Ec*If1+Eh1.*Ic+Ec*If2;
EI_totalCH1plate = Ec*If1p+Eh1.*Icp+Ec*If2p;

% Shear Rigidity
Uh1 = Gh1.*(d+c)^2*b/(4*c);

% Midspan Deflection beam
dch1 = P*L^3./(48.*EI_totalCH1beam); % Deflection due to facings
dch2 = P*L./(4.*Uh1);                % Deflection due to shear
CH_def1 = dch1+dch2;            % Total Deflection

% Midspan Deflection plate
dch1p = P*L^3./(48.*EI_totalCH1plate); % Deflection due to facings
dch2p = P*L./(4.*Uh1);                % Deflection due to shear
CH_defplate1 = dch1p+dch2p;            % Total Deflection



figure
plot(theta,CH_def1,'x')
xlabel('Core Direction (degrees)')
ylabel('Deflection (in)')



% Comparison

Experimentald = [ 0.0337 0.0363 0.0380 0.0453 0.0486 0.0555 0.0558];
expstd = [7.7968e-4 0.0011 0.0012 0.0013 9.1335e-4 0.0022 0.0019];
Theoretical_beam = CH_def1;
Theoretical_plate = CH_defplate1;
%FEA = [3.48038e-002 3.58072e-002 3.89588e-002 4.45480e-002 5.23770e-002
6.03650e-002 6.18512e-002];
%FEAortho1 = [3.2756e-2 3.43119e-2 3.87508e-2 4.50503e-2 5.1571e-2 5.64642e-2
5.82776e-2];
FEAortho2 = [3.37852e-2 3.5369e-2 3.98261e-2 4.61509e-2 5.20063e-2 5.71674e-2
5.91619e-2];

figure
plot(theta,Theoretical_beam,'ro')
hold on
plot(theta,Theoretical_plate,'bo')

errorbar(theta,Experimentald,expstd,'x')
```

```
%plot(theta,FEA,'gs')
%plot(theta,FEAortho1,'ms')
plot(theta,FEAortho2, 'magentas')
xlabel('Core Direction angle (Degrees')
ylabel('Midpsan Deflection at 100lb')
legend('Theoretical Beam','Theoretical Plate','Experimental','FEA')

Error_plate_FEA = (Theoretical_plate-FEAortho2)./Theoretical_plate*100;
Error_beam_FEA = (Theoretical_beam-FEAortho2)./Theoretical_beam*100;
Error_FEA_Exp = (FEAortho2-Experimentald)./FEAortho2*100;
%% Mesh Convergence With Aluminium Face and Steel Core

Mesh = [0.06 0.08 0.1 0.12 0.14 0.17 0.18 0.2 0.22 0.24 .245 .247 0.25 0.255
0.26 0.27 0.3];
Mesh1 = fliplr(Mesh) ;
disp = [2.014e-3 2.00522e-3 1.99917e-3 2.00474e-3 1.99434e-3 1.97683e-3
2.01402e-3 1.9653e-3 1.91571e-3 1.8763e-3 1.86528e-3 1.86528e-3 1.86253e-3
2.90438e-3 2.974e-3 2.85389e-3 2.69396e-3];
disp1 = fliplr(disp);
figure
plot(Mesh1,disp1,'x')
hold on
xlabel('Seed')
ylabel('Displacement (in)')

figure
meshels = [ 0.24 0.26 0.245 0.255 0.1 0.06];
els = [ 600 414 582 438 5415 20025 9975 3263 305];
displace = [ 1.8763e-3  2.974e-3  1.86528e-3 2.90438e-3 1.99917e-3 2.014e-3
2.00522e-3 2.00474e-3 2.69396e-3];
plot(els,displace,'x')
```

A.8.6. Failure Mode Analysis

```
% Static Failure Modes (AERO 500)

clear all; close all; clc

theta=linspace(0,90);
% theta=[0 15 30 45 60 75 90];
% theta=0;

%%% Flexural Rigidity

for i=1:length(theta)

Ef=12.936e6; % face Young's modulus (Longitudinal) [psi]
Ec_L=3.679e4; % core Young's modulus (Longitudinal) [psi]
% Ef_W=12.7e6; % face Young's modulus (Transverse) [psi]
Ec_W=1.5242e4; % core Young's modulus (Transverse) [psi]
```

```
tf=0.024; % face thickness [in]
tc=0.375; % core thicknessm [in]
P=301/1.5; % Central load per unit width [lbf/in]
L=6; % span [in]
Xf=127e3; % Face Compressive Strength
Sc_L=325; % Core Longitudinal Shear Yield Strength (175 for transverse)
Sc_W= 175; % "  "
Xc=700; % Core Compressive Streng100
b = 1.5;
% Ef=Ef_L.*(cosd(theta(i))).^2+Ef_W.*(sind(theta(i))).^2;
Ec=Ec_L.*(cosd(theta(i))).^2+Ec_W.*(sind(theta(i))).^2;
Sc=Sc_L.*(cosd(theta(i))).^2+Sc_W.*(sind(theta(i))).^2;

d=tf+tc; % distance between the centroids of the faces
Df=Ef.*tf.^3./12; % Bending stiffness of faces about their individual neutral
axis
Dc=Ec.*tc.^3./12; % Bending Stiffness of core
Do=Ef.*tf.*d.^2./2; % Bending stiffness of faces about the middle axis
D=Df.*2+Dc+Do; % Flexural Rigidity

%%% Deflection and Moment
k=Ec./tc;
beta=(k./(4.*Df)).^(1/4);
Defl_local(i)=P.*beta./(2.*k); % Deflection at center of beam
M_local=P./(4.*beta); % Moment per unit width at center of beam

%%% Stress

sigmaf_overall=P.*L./(4.*tf.*d);
sigmaf_local(i)=6.*P./(4.*(tf.^2).*beta);
sigmaf_total=sigmaf_overall+sigmaf_local; % Compressive stress at the face of
sandwich beams under bending load [psi]
tau_c=P./(2.*d); % Shear stress in the core material [psi]
sigma_c(i)=Defl_local(i).*Ec./tc; % Compressive stress of the core

%%% Maximum Loads per unit width for each failur modes

Pmax_f_compressive_failure(i)=Xf./((L./(4.*tf.*d))+(6./(4.*(tf.^2).*beta)));
% Face compressive failure load
Pmax_c_shear_yield(i)=2.*Sc.*d; % core shear yield load
Pmax_c_compressive_yield(i)=2.*Xc./beta; % core compressive yield load
Pmax_f_Microbuckling = 4*tf*tc*(80e3)/L;  % Microbuckling face yield
Pmax_Indentation = tf*((pi^2*Ef*tc*Xc^2)/(3*L))^(1/3); % indentation with
face buckling (plastic)

end


Loads=[301.61 274.9 264.71 248.16 246.02 238.13 240.73]/1.5;
Loads_std=[5.051 10 5.77 9.09 4.29 5.1 9.23]/1.5;
theta_loads=[0 15 30 45 60 75 90];

%%% Failure Load Plots

figure
```

```
plot(theta,sigmaf_total)
% hold on
% plot(theta,sigma_c,'r')
legend('Compressive Stress at Facesheet')

figure
plot(theta,Pmax_f_compressive_failure,'r')
hold on
plot(theta,Pmax_c_shear_yield,'b')
plot(theta,Pmax_c_compressive_yield,'k')
plot(linspace(0,90,1000),Pmax_Indentation,'green')

 errorbar(theta_loads,Loads,Loads_std,'gx')
title('Core Angle vs. Yielding Load')
xlabel('Core Angle [degrees]')
ylabel('Yielding Load [lbf]')
legend('Face Compressive Failure','Core Shear Yield','Core Compressive
Yield','Indentation','Location','SouthWest')
axis([-5 95 140 300])

% The plot shows where the sandwich will yield due to the core and where it
% will failure due to the face, however, it does not show where the
% sandwich would fail due to core shear and compression because we can't
% do the test on honeycomb to find those values.


%% Failure Mode Plots
theta_ALL=[0 15 30 45 60 75 90];

Ec_L=3.679e4; % core Young's modulus (Longitudinal) [psi]
Ec_W=1.5242e4; % core Young's modulus (Transverse) [psi]
Sc_L=325; % Core Longitudinal Shear Yield Strength (175 for transverse)
Sc_W=175; % "  "

Ec_ALL=Ec_L.*(cosd(theta_ALL)).^2+Ec_W.*(sind(theta_ALL)).^2;
Sc_ALL=Sc_L.*(cosd(theta_ALL)).^2+Sc_W.*(sind(theta_ALL)).^2;

Ef=12.936e6; % face Young's modulus (Longitudinal) [psi]
Xc=700; % Core Compressive Strength

E_star_ALL=[Ef./Ec_ALL(1) Ef./Ec_ALL(2) Ef./Ec_ALL(3) Ef./Ec_ALL(4)
Ef./Ec_ALL(5) Ef./Ec_ALL(6) Ef./Ec_ALL(7)];
s_star_ALL=[Xc./Sc_ALL(1) Xc./Sc_ALL(2) Xc./Sc_ALL(3) Xc./Sc_ALL(4)
Xc./Sc_ALL(5) Xc./Sc_ALL(6) Xc./Sc_ALL(7)];

t_star_ALL_Angles=[0.0816443033 0.0767928356 0.06436835891 0.04922730924
0.0360752422 0.02764804693 0.02481052489];
t_star_ALL_Angles_Round=[0.08 0.075 0.065 0.05 0.035 0.03 0.025];

theta=theta_ALL(1);


Ef=12.936e6; % face Young's modulus (Longitudinal) [psi]
Ec_L=3.679e4; % core Young's modulus (Longitudinal) [psi]
```

```
Ec_W=1.5242e4; % core Young's modulus (Transverse) [psi]
tf=0.024; % face thickness [in]
tc=0.375; % core thicknessm [in]
L=6; % span [in]
Xf=136e3; % Face Compressive Strength
Sc_L=325; % Core Longitudinal Shear Yield Strength (175 for transverse)
Sc_W=175; % "  "
Xc=700; % Core Compressive Strength

Ec=Ec_L.*(cosd(theta)).^2+Ec_W.*(sind(theta)).^2;
Sc=Sc_L.*(cosd(theta)).^2+Sc_W.*(sind(theta)).^2;

t_star=tf./tc;
L_star=L./tc;
E_star=Ef./Ec;
sigma_star=Xf./Xc;
s_star=Xc./Sc;
Pmax_Indentation = tf*((pi^2*Ef*tc*Xc^2)/(3*L))^(1/3);

t_star=linspace(0,1,10000);
L_star_1=2.*sigma_star.*s_star.*t_star-
2.*(3.^(3/4)).*(E_star./t_star).^(1/4).*(t_star+1);
L_star_2=(-2.*3.^(3/4).*(3.*sqrt(E_star./t_star)-
sigma_star.*sqrt(3)).*(t_star+1))./(3.*(E_star./t_star).^(1/4));

% Non dimensional Load

[C,IA,IB]=intersect(L_star_1,L_star_2,'rows');

%%% Plots
% 0 Degree Core
figure
% plot([0 C],[L_star_1(I) L_star_2(I)],'r')
plot([-30 27.4],[t_star_ALL_Angles(1)
t_star_ALL_Angles(1)],'k','LineWidth',1.1)
hold on
% plot(L_star_1(IA:end),t_star(IB:end),'r') %817:end
% plot(L_star_2(1:IA),t_star(1:IB),'r')
plot(L_star_1(817:end),t_star(817:end),'k--','LineWidth',1.1) %817:end
plot(L_star_2(1:817),t_star(1:817),'k:','LineWidth',1.1)
plot(27.4,t_star_ALL_Angles(1),'ks','MarkerFaceColor','k')
plot(24.59,t_star_ALL_Angles(2),'bs','MarkerFaceColor','b')
plot(16.63,t_star_ALL_Angles(3),'gs','MarkerFaceColor','g')
plot(4.851,t_star_ALL_Angles(4),'rs','MarkerFaceColor','r')
plot(-8.7,t_star_ALL_Angles(5),'cs','MarkerFaceColor','c')
plot(-20.65,t_star_ALL_Angles(6),'ys','MarkerFaceColor','y')
plot(-25.5,t_star_ALL_Angles(7),'ms','MarkerFaceColor','m')
plot([0 0],[0 0.12],'k')
grid on
title('Static Failure Mode Map (0 Degree Core Angle)')
xlabel('L* (span/core thickness)')
ylabel('t* (face/core thickness)')
axis([-30 60 0 0.12])
legend('Core Shear and Compression (0 degrees)','Face and Core Shear (0
degrees)','Face and Core Compressive (0 degrees)','0 degree intersection
point','15 degree intersection point','30 degree intersection point','45
```

```
degree intersection point','60 degree intersection point','75 degree
intersection point','90 degree intersection point','Location','SouthEast')
text(10, .1, {' Core Shear', 'Failure
Mode'},'LineWidth',3,'FontSize',14,'FontWeight','Bold')
text(-20, .063, {'Core Compressive', ' Failure
Mode'},'LineWidth',3,'FontSize',14,'FontWeight','Bold')
text(35, 0.065, {'Face Fracture', 'Failure
Mode'},'LineWidth',3,'FontSize',14,'FontWeight','Bold')
hold off

%%%%%%%%%%%%%%%%%%%%%%%%%%%%%%%%%%%%%%%
% 15 Degree Core

theta=theta_ALL(2);

Ec=Ec_L.*(cosd(theta)).^2+Ec_W.*(sind(theta)).^2;
Sc=Sc_L.*(cosd(theta)).^2+Sc_W.*(sind(theta)).^2;

t_star=tf./tc;
L_star=L./tc;
E_star=Ef./Ec;
sigma_star=Xf./Xc;
s_star=Xc./Sc;

t_star=linspace(0,1,10000);
L_star_1=2.*sigma_star.*s_star.*t_star-
2.*(3.^(3/4)).*(E_star./t_star).^(1/4).*(t_star+1);
L_star_2=(-2.*3.^(3/4).*(3.*sqrt(E_star./t_star)-
sigma_star.*sqrt(3)).*(t_star+1))./(3.*(E_star./t_star).^(1/4));

% [C]=intersect(L_star_1,L_star_2);

figure
plot([-30 24.59],[t_star_ALL_Angles(2)
t_star_ALL_Angles(2)],'b','LineWidth',1.1)
hold on
plot(L_star_1(769:end),t_star(769:end),'b--','LineWidth',1.1) %817:end
plot(L_star_2(1:769),t_star(1:769),'b:','LineWidth',1.1)
plot(27.4,t_star_ALL_Angles(1),'ks','MarkerFaceColor','k')
plot(24.59,t_star_ALL_Angles(2),'bs','MarkerFaceColor','b')
plot(16.63,t_star_ALL_Angles(3),'gs','MarkerFaceColor','g')
plot(4.851,t_star_ALL_Angles(4),'rs','MarkerFaceColor','r')
plot(-8.7,t_star_ALL_Angles(5),'cs','MarkerFaceColor','c')
plot(-20.65,t_star_ALL_Angles(6),'ys','MarkerFaceColor','y')
plot(-25.5,t_star_ALL_Angles(7),'ms','MarkerFaceColor','m')
plot([0 0],[0 0.12],'k')
grid on
title('Static Failure Mode Map (15 Degree Core Angle)')
xlabel('L* (span/core thickness)')
ylabel('t* (face/core thickness)')
axis([-30 60 0 0.12])
legend('Core Shear and Compression (15 degrees)','Face and Core Shear (15
degrees)','Face and Core Compressive (15 degrees)','0 degree intersection
point','15 degree intersection point','30 degree intersection point','45
```

```
degree intersection point','60 degree intersection point','75 degree
intersection point','90 degree intersection point','Location','SouthEast')

%%%%%%%%%%%%%%%%%%%%%%%%%%%%%%%%%%%%%%%%
%30 Degree Core

theta=theta_ALL(3);

Ec=Ec_L.*(cosd(theta)).^2+Ec_W.*(sind(theta)).^2;
Sc=Sc_L.*(cosd(theta)).^2+Sc_W.*(sind(theta)).^2;

t_star=tf./tc;
L_star=L./tc;
E_star=Ef./Ec;
sigma_star=Xf./Xc;
s_star=Xc./Sc;

t_star=linspace(0,1,10000);
L_star_1=2.*sigma_star.*s_star.*t_star-
2.*(3.^(3/4)).*(E_star./t_star).^(1/4).*(t_star+1);
L_star_2=(-2.*3.^(3/4).*(3.*sqrt(E_star./t_star)-
sigma_star.*sqrt(3)).*(t_star+1))./(3.*(E_star./t_star).^(1/4));

% [C]=intersect(L_star_1,L_star_2);

figure
plot([-30 16.63],[t_star_ALL_Angles(3)
t_star_ALL_Angles(3)],'g','LineWidth',1.1)
hold on
plot(L_star_1(644:end),t_star(644:end),'g--','LineWidth',1.1) %817:end
plot(L_star_2(1:644),t_star(1:644),'g:','LineWidth',1.1)
plot(27.4,t_star_ALL_Angles(1),'ks','MarkerFaceColor','k')
plot(24.59,t_star_ALL_Angles(2),'bs','MarkerFaceColor','b')
plot(16.63,t_star_ALL_Angles(3),'gs','MarkerFaceColor','g')
plot(4.851,t_star_ALL_Angles(4),'rs','MarkerFaceColor','r')
plot(-8.7,t_star_ALL_Angles(5),'cs','MarkerFaceColor','c')
plot(-20.65,t_star_ALL_Angles(6),'ys','MarkerFaceColor','y')
plot(-25.5,t_star_ALL_Angles(7),'ms','MarkerFaceColor','m')
plot([0 0],[0 0.12],'k')
grid on
title('Static Failure Mode Map (30 Degree Core Angle)')
xlabel('L* (span/core thickness)')
ylabel('t* (face/core thickness)')
axis([-30 60 0 0.12])
legend('Core Shear and Compression (30 degrees)','Face and Core Shear (30
degrees)','Face and Core Compressive (30 degrees)','0 degree intersection
point','15 degree intersection point','30 degree intersection point','45
degree intersection point','60 degree intersection point','75 degree
intersection point','90 degree intersection point','Location','SouthEast')

%%%%%%%%%%%%%%%%%%%%%%%%%%%%%%%%%%%%%%%%
%45 Degree Core

theta=theta_ALL(4);
```

```
Ec=Ec_L.*(cosd(theta)).^2+Ec_W.*(sind(theta)).^2;
Sc=Sc_L.*(cosd(theta)).^2+Sc_W.*(sind(theta)).^2;

t_star=tf./tc;
L_star=L./tc;
E_star=Ef./Ec;
sigma_star=Xf./Xc;
s_star=Xc./Sc;

t_star=linspace(0,1,10000);
L_star_1=2.*sigma_star.*s_star.*t_star-
2.*(3.^(3/4)).*(E_star./t_star).^(1/4).*(t_star+1);
L_star_2=(-2.*3.^(3/4).*(3.*sqrt(E_star./t_star)-
sigma_star.*sqrt(3)).*(t_star+1))./(3.*(E_star./t_star).^(1/4));

% [C]=intersect(L_star_1,L_star_2);

figure
plot([-60 4.851],[t_star_ALL_Angles(4)
t_star_ALL_Angles(4)],'r','LineWidth',1.1)
hold on
plot(L_star_1(493:end),t_star(493:end),'r--','LineWidth',1.1) %817:end
plot(L_star_2(1:493),t_star(1:493),'r:','LineWidth',1.1)
plot(27.4,t_star_ALL_Angles(1),'ks','MarkerFaceColor','k')
plot(24.59,t_star_ALL_Angles(2),'bs','MarkerFaceColor','b')
plot(16.63,t_star_ALL_Angles(3),'gs','MarkerFaceColor','g')
plot(4.851,t_star_ALL_Angles(4),'rs','MarkerFaceColor','r')
plot(-8.7,t_star_ALL_Angles(5),'cs','MarkerFaceColor','c')
plot(-20.65,t_star_ALL_Angles(6),'ys','MarkerFaceColor','y')
plot(-25.5,t_star_ALL_Angles(7),'ms','MarkerFaceColor','m')
plot([0 0],[0 0.12],'k')
grid on
title('Static Failure Mode Map (45 Degree Core Angle)')
xlabel('L* (span/core thickness)')
ylabel('t* (face/core thickness)')
axis([-30 60 0 0.12])
legend('Core Shear and Compression (45 degrees)','Face and Core Shear (45
degrees)','Face and Core Compressive (45 degrees)','0 degree intersection
point','15 degree intersection point','30 degree intersection point','45
degree intersection point','60 degree intersection point','75 degree
intersection point','90 degree intersection point','Location','SouthEast')

%%%%%%%%%%%%%%%%%%%%%%%%%%%%%%%%%%%%%%%%
% 60Degree Core

theta=theta_ALL(5);

Ec=Ec_L.*(cosd(theta)).^2+Ec_W.*(sind(theta)).^2;
Sc=Sc_L.*(cosd(theta)).^2+Sc_W.*(sind(theta)).^2;

t_star=tf./tc;
L_star=L./tc;
E_star=Ef./Ec;
sigma_star=Xf./Xc;
s_star=Xc./Sc;
```

```
t_star=linspace(0,1,10000);
L_star_1=2.*sigma_star.*s_star.*t_star-
2.*(3.^(3/4)).*(E_star./t_star).^(1/4).*(t_star+1);
L_star_2=(-2.*3.^(3/4).*(3.*sqrt(E_star./t_star)-
sigma_star.*sqrt(3)).*(t_star+1))./(3.*(E_star./t_star).^(1/4));

% [C]=intersect(L_star_1,L_star_2);

figure
plot([-60 -8.7],[t_star_ALL_Angles(5)
t_star_ALL_Angles(5)],'c','LineWidth',1.1)
hold on
plot(L_star_1(362:end),t_star(362:end),'c--','LineWidth',1.1) %817:end
plot(L_star_2(1:362),t_star(1:362),'c:','LineWidth',1.1)
plot(27.4,t_star_ALL_Angles(1),'ks','MarkerFaceColor','k')
plot(24.59,t_star_ALL_Angles(2),'bs','MarkerFaceColor','b')
plot(16.63,t_star_ALL_Angles(3),'gs','MarkerFaceColor','g')
plot(4.851,t_star_ALL_Angles(4),'rs','MarkerFaceColor','r')
plot(-8.7,t_star_ALL_Angles(5),'cs','MarkerFaceColor','c')
plot(-20.65,t_star_ALL_Angles(6),'ys','MarkerFaceColor','y')
plot(-25.5,t_star_ALL_Angles(7),'ms','MarkerFaceColor','m')
plot([0 0],[0 0.12],'k')
grid on
title('Static Failure Mode Map (60 Degree Core Angle)')
xlabel('L* (span/core thickness)')
ylabel('t* (face/core thickness)')
axis([-30 60 0 0.12])
legend('Core Shear and Compression (60 degrees)','Face and Core Shear (60
degrees)','Face and Core Compressive (60 degrees)','0 degree intersection
point','15 degree intersection point','30 degree intersection point','45
degree intersection point','60 degree intersection point','75 degree
intersection point','90 degree intersection point','Location','SouthEast')

%%%%%%%%%%%%%%%%%%%%%%%%%%%%%%%%%%%%%%%%
% 75 Degree Core

theta=theta_ALL(6);

Ec=Ec_L.*(cosd(theta)).^2+Ec_W.*(sind(theta)).^2;
Sc=Sc_L.*(cosd(theta)).^2+Sc_W.*(sind(theta)).^2;

t_star=tf./tc;
L_star=L./tc;
E_star=Ef./Ec;
sigma_star=Xf./Xc;
s_star=Xc./Sc;

t_star=linspace(0,1,10000);
L_star_1=2.*sigma_star.*s_star.*t_star-
2.*(3.^(3/4)).*(E_star./t_star).^(1/4).*(t_star+1);
L_star_2=(-2.*3.^(3/4).*(3.*sqrt(E_star./t_star)-
sigma_star.*sqrt(3)).*(t_star+1))./(3.*(E_star./t_star).^(1/4));

% [C]=intersect(L_star_1,L_star_2);
```

```
figure
plot([-60 -20.65],[t_star_ALL_Angles(6)
t_star_ALL_Angles(6)],'y','LineWidth',1.1)
hold on
plot(L_star_1(277:end),t_star(277:end),'y--','LineWidth',1.1) %817:end
plot(L_star_2(1:277),t_star(1:277),'y:','LineWidth',1.1)
plot(27.4,t_star_ALL_Angles(1),'ks','MarkerFaceColor','k')
plot(24.59,t_star_ALL_Angles(2),'bs','MarkerFaceColor','b')
plot(16.63,t_star_ALL_Angles(3),'gs','MarkerFaceColor','g')
plot(4.851,t_star_ALL_Angles(4),'rs','MarkerFaceColor','r')
plot(-8.7,t_star_ALL_Angles(5),'cs','MarkerFaceColor','c')
plot(-20.65,t_star_ALL_Angles(6),'ys','MarkerFaceColor','y')
plot(-25.5,t_star_ALL_Angles(7),'ms','MarkerFaceColor','m')
plot([0 0],[0 0.12],'k')
grid on
title('Static Failure Mode Map (75 Degree Core Angle)')
xlabel('L* (span/core thickness)')
ylabel('t* (face/core thickness)')
axis([-30 60 0 0.12])
legend('Core Shear and Compression (75 degrees)','Face and Core Shear (75
degrees)','Face and Core Compressive (75 degrees)','0 degree intersection
point','15 degree intersection point','30 degree intersection point','45
degree intersection point','60 degree intersection point','75 degree
intersection point','90 degree intersection point','Location','SouthEast')

%%%%%%%%%%%%%%%%%%%%%%%%%%%%%%%%%%%%%%%%
% 90 Degree Core

theta=theta_ALL(7);

Ec=Ec_L.*(cosd(theta)).^2+Ec_W.*(sind(theta)).^2;
Sc=Sc_L.*(cosd(theta)).^2+Sc_W.*(sind(theta)).^2;

t_star=tf./tc;
L_star=L./tc;
E_star=Ef./Ec;
sigma_star=Xf./Xc;
s_star=Xc./Sc;

t_star=linspace(0,1,10000);
L_star_1=2.*sigma_star.*s_star.*t_star-
2.*(3.^(3/4)).*(E_star./t_star).^(1/4).*(t_star+1);
L_star_2=(-2.*3.^(3/4).*(3.*sqrt(E_star./t_star)-
sigma_star.*sqrt(3)).*(t_star+1))./(3.*(E_star./t_star).^(1/4));

% [C]=intersect(L_star_1,L_star_2);

figure
plot([-60 -25.5],[t_star_ALL_Angles(7)
t_star_ALL_Angles(7)],'m','LineWidth',1.1)
hold on
plot(L_star_1(249:end),t_star(249:end),'m--','LineWidth',1.1) %817:end
plot(L_star_2(1:249),t_star(1:249),'m:','LineWidth',1.1)
plot(27.4,t_star_ALL_Angles(1),'ks','MarkerFaceColor','k')
```

```
plot(24.59,t_star_ALL_Angles(2),'bs','MarkerFaceColor','b')
plot(16.63,t_star_ALL_Angles(3),'gs','MarkerFaceColor','g')
plot(4.851,t_star_ALL_Angles(4),'rs','MarkerFaceColor','r')
plot(-8.7,t_star_ALL_Angles(5),'cs','MarkerFaceColor','c')
plot(-20.65,t_star_ALL_Angles(6),'ys','MarkerFaceColor','y')
plot(-25.5,t_star_ALL_Angles(7),'ms','MarkerFaceColor','m')
plot([0 0],[0 0.12],'k')
grid on
title('Static Failure Mode Map (90 Degree Core Angle)')
xlabel('L* (span/core thickness)')
ylabel('t* (face/core thickness)')
axis([-30 60 0 0.12])
legend('Core Shear and Compression (90 degrees)','Face and Core Shear (90
degrees)','Face and Core Compressive (90 degrees)','0 degree intersection
point','15 degree intersection point','30 degree intersection point','45
degree intersection point','60 degree intersection point','75 degree
intersection point','90 degree intersection point','Location','SouthEast')
```

A.8.7. Master Code for all varying face thickness matlab files.

```
% Josh Lister
% Thesis - Sandwich composites
% MASTER FILE
clear all
close all
clc


%% Loops through all data.

% Set Figures = 1 if wanted or = 0 if not wanted
Figures = 0;


% To Run single specimen, apply set as needed.
%        T O P
%      1   2   3   4   5
% B 1  1   6  11  16  21
% O 2  2   7  12  17  22
% T 3  3   8  13  18  23
% T 4  4   9  14  19  24
% O 5  5  10  15  20  25
% M
%

% 5 specimen sets
set = 7;
FileNames=dir('*.xls');

if set ==0;
%this gets all the file names in current director that have extension .xls,
as a structure
for i=1:length(FileNames)
```

```
    while i == 6 || 7 || 18 || 19

FileToLoad=FileNames(i).name;
%this is a xls file, load it, run code and loop
specimen1 = xlsread(FileToLoad,2);
specimen2 = xlsread(FileToLoad,3);
specimen3 = xlsread(FileToLoad,4);
specimen4 = xlsread(FileToLoad,5);
specimen5 = xlsread(FileToLoad,6);
string = FileToLoad;
[output] = Datacode5(specimen1, specimen2, specimen3, specimen4, specimen5,
string, Figures);
 i = i+1;
    end
FileToLoad=FileNames(i).name;
%this is a xls file, load it, run code and loop
specimen1 = xlsread(FileToLoad,2);
specimen2 = xlsread(FileToLoad,3);
specimen3 = xlsread(FileToLoad,4);
specimen4 = xlsread(FileToLoad,5);
specimen5 = xlsread(FileToLoad,6);
specimen6 = xlsread(FileToLoad,7);
string = FileToLoad;
[output] = Datacode(specimen1, specimen2, specimen3, specimen4, specimen5
,specimen6, string, Figures);
end

else

FileToLoad=FileNames(set).name;
%this is a xls file, load it, run code and loop

 if set == 2 || 7 || 14 || 19

FileToLoad=FileNames(set).name;
%this is a xls file, load it, run code and loop
specimen1 = xlsread(FileToLoad,2);
specimen2 = xlsread(FileToLoad,3);
specimen3 = xlsread(FileToLoad,4);
specimen4 = xlsread(FileToLoad,5);
specimen5 = xlsread(FileToLoad,6);
string = FileToLoad;
[output] = Datacode5(specimen1, specimen2, specimen3, specimen4, specimen5 ,
string, Figures);

 else

specimen1 = xlsread(FileToLoad,2);
specimen2 = xlsread(FileToLoad,3);
specimen3 = xlsread(FileToLoad,4);
specimen4 = xlsread(FileToLoad,5);
specimen5 = xlsread(FileToLoad,6);
specimen6 = xlsread(FileToLoad,7);
string = FileToLoad;
```

```
[output] = Datacode(specimen1, specimen2, specimen3, specimen4, specimen5
,specimen6, string, Figures, set)
% output = [P Ex D U G F sigma1ult sigma2ult Exten200avg Pstd Exstd Ex200std
Kstd]
 end
end
```

A.8.8. Data Manipulation Code for Varying Face Sheet Thickness Specimens

```
% Josh Lister
% Thesis - Sandwich composites
%
%
% NOTES - Reads in .mat files of Sandwich Composite Panel Data
% Make sure to CTRL (F)  find what: 11  11: filename
%
%
% INPUTS By Column
%
% 1  - Time              (sec)
% 2  - Extension         (inches)
% 3  - Load              (lbf)
% 4  - Flexure Stress    (ksi)
% 5  - Cycle Count       (-)
% 6  - Total cycles      (-)
% 7  - Repetitions Count (-)
% 8  - Channel  1        (-)
% 9  - Marked Data       (-)
% 10 - PIP Count         (-)
% 11 - Flexure extension (inches)
% 12 - Flexure strain    (%)
% 13 - Flexure load      (lbf)
% 14 - Displacement      (inches)
% 15 - Displacement      (Channel  1) (in)
% 16 - Position          (inches)
% 17 - Corrected Position(inches)
%
% OUTPUTS
% Displays Graphs90
% Mechanical Properties of Panels and consititutent materials


%% Read in Raw data files from RAW DATA folder
clear all
close all
clc

% Reads Data in from Sandwich Diaries xls file
datafilename = ['E:\Dropbox\Classes\Year 5\JJJ Theses\Data\Sandwich
beams\Second Sets\TheSandwichDiaries.xls'];
data = xlsread(datafilename); %Load the data file based on its number
```

```
% For numbering Purposes
string = '11';
toplayer = str2num(string(1));
botlayer = str2num(string(2));

specimen1 = xlsread('11.xls',2);
specimen2 = xlsread('11.xls',3);
specimen3 = xlsread('11.xls',4);
specimen4 = xlsread('11.xls',5);
specimen5 = xlsread('11.xls',6);
specimen6 = xlsread('11.xls',7);

blah1 = length(specimen1);
blah2 = length(specimen2);
blah3 = length(specimen3);
blah4 = length(specimen4);
blah5 = length(specimen5);
blah6 = length(specimen6);

blah = [blah1 blah2 blah3 blah4 blah5 blah6];
blah = min(blah);

l1 = specimen1(88:blah,:);
l2 = specimen2(88:blah,:);
l3 = specimen3(88:blah,:);
l4 = specimen4(88:blah,:);
l5 = specimen5(88:blah,:);
l6 = specimen6(88:blah,:);



%% raw Data
FlexLoad = [l1(:,13),l2(:,13),l3(:,13),l4(:,13),l5(:,13),l6(:,13)];
FlexExten = [l1(:,11),l2(:,11),l3(:,11),l4(:,11),l5(:,11),l6(:,11)];

for i =1:6
p = polyfit(FlexExten(120:170,i),FlexLoad(120:170,i),1);
f = polyval(p,FlexExten(120:170,i));

 figure(3)
plot(FlexExten(:,1),FlexLoad(:,1),'o',FlexExten(120:170,1),f,'r-')

Toecorrection = -p(2)/p(1);

FlexExten(:,i) = FlexExten(:,i) - Toecorrection;
end
% Average Data
AvgLoad_11 = sum(FlexLoad,2)/6;
AvgExten_11 = sum(FlexExten,2)/6;

%% Weight
Avgweight = data(28+botlayer,21+toplayer);    %lbs
Weight1 = Avgweight/(specimen1(10,2)*8);
```

```
Weight2 = Avgweight/(specimen2(10,2)*8);
Weight3 = Avgweight/(specimen3(10,2)*8);
Weight4 = Avgweight/(specimen4(10,2)*8);
Weight5 = Avgweight/(specimen5(10,2)*8);
Weight6 = Avgweight/(specimen6(10,2)*8);
Density = (Weight1+Weight2+Weight3+Weight4+Weight5+Weight6)/6; %lbs/in^3


%% Max Values
K = sum(stiffness)/length(stiffness);
P = sum(max(FlexLoad))/length(FlexLoad(1,:));
Ex = sum(FlexExten(location))/length(FlexLoad(1,:));


% Calculate Stress
% Panel Dimensions
d =
sum(specimen1(4,2)+specimen2(4,2)+specimen3(4,2)+specimen4(4,2)+specimen5(4,2
)+specimen6(4,2))/6; % Thickness [in]
c = 0.375;          % core thickness [in]
b =
sum(specimen1(3,2)+specimen2(3,2)+specimen3(3,2)+specimen4(3,2)+specimen5(3,2
)+specimen6(3,2))/6; % width [in]
facethick = d-c;  %[in]
t1 = toplayer/(toplayer+botlayer)*facethick; % Top face thickness
t2 = botlayer/(toplayer+botlayer)*facethick; % Bottom face thickness


% ASTM C393
% Core Shear Ultimate Stress
% For 3pt Mid-Span Loading
F = P/((d+c)*b);   % [psi]

% Facing Stress
% NOTE: only reference, use ASTM D7249 for facing ultimate stress
S =6;   % Support Span
sigma = FlexLoad*S./((d-c)*(d+c)*b);
sigmault = P*S/((d-c)*(d+c)*b);

% ASTM D7249/D7249M - Long Beam Facing Properties
% Facing Ultimate Stength
% For 3pt Mid-Span Loading
S = 6;    % Support Span
L = 0;    % Loading Span
sigmatop = FlexLoad*(S-L)./(2*(d+c)*b*t1);
sigmabot = FlexLoad*(S-L)./(2*(d+c)*b*t2);
sigmatopult = P*(S-L)/(2*(d+c)*b*t1);   % facing 1 ultimate stress, [psi]
sigmabottomult = P*(S-L)/(2*(d+c)*b*t2);   % facing 2 ultimate stress, [psi]


% ASTM D7250/D7250M
% Beam Flexural and Shear Stiffness
% #top layers = # bottom layers

E = 8.5E6                     ; % FAcing prop NEEDS TO CHANGE
```

```
D = E*(d^3-c^3)*b/12;                              % Flexural Stiffness, [lb-
in^2]
U = P*(S-L)./(4*(P*Ex-P*(2*S^3-3*S*L^2+L^3)./96*D));   % transverse shear
rigidity [lb]
G = U./(c*b);                                        % Core shear Modulus [psi]

% Changes Values if top and bottom face sheets are not equal
if string(1) == string(2)
sigma1ult = sigmault;
sigma2ult = sigmault;
D = D;
U = U;
G = G;
else

sigma1ult = sigmatopult;
sigma2ult = sigmabottomult;
D = K;
U = 0;
G = 0;
F = 0;
end


%% Standard Deviations

% Max Load
Pstd = std(max(FlexLoad));
% Max Extension
Exstd = std(max(FlexExten));
% Extension at 200lb
Ex200std = std(Exten100avg);
% Stiffness
Kstd = std(stiffness);


% List of Mechanical Properties of Sandwich Properties
MechProps_11 = [P Ex D U G F sigma1ult sigma2ult Exten100avg];  % [UltForce
UltExten FlexStiff TranShearRig CoreShearMod CoreShearStress TopfaceStress
Botface Stress]

%% extension at 100lbs
for i = 1:length(FlexLoad(1,:))
[value200(1,i) location200(1,i)] = find(FlexLoad(:,i)>100,1);
Exten200(1,i) = FlexExten(value200(1,i),i);
end
Exten100avg = mean(Exten200);
Exten100std = std(Exten200);

% List of Mechanical Properties of Sandwich Properties
MechProps_44 = [P Ex D U G F sigma1ult sigma2ult ];  % [UltForce UltExten
FlexStiff TranShearRig CoreShearMod CoreShearStress TopfaceStress Botface
Stress]

% Writes to XLS Sandwich Diaries file
```

```
Ex = sum(FlexExten(location)/length(FlexLoad(1,:)));
Exmaxstd = std(FlexExten(location)/length(FlexLoad(1,:)));
Pstd = std(max(FlexLoad));
Kstd = std(stiffness);

MatPropsall = ['E:\Dropbox\Classes\Year 5\JJJ Theses\Data\Sandwich
beams\Second Sets\Matprop.mat'];
load(MatPropsall);
temp(botlayer,toplayer) = sigma1ult;
temp(botlayer+5,toplayer)  = sigma2ult;
temp(botlayer+10,toplayer)  = P;
temp(botlayer+15,toplayer)  = Ex;
temp(botlayer+20,toplayer)  = U;
temp(botlayer+25,toplayer)  = G;
temp(botlayer+30,toplayer)  = F;
temp(botlayer+35,toplayer)  = D;
temp(botlayer+40,toplayer)  = Exten100avg;
temp(botlayer+45,toplayer)  = Pstd;
temp(botlayer+50,toplayer)  = Exmaxstd;
temp(botlayer+55,toplayer)  = Exten100std;
temp(botlayer+60,toplayer)  = Kstd;
temp(botlayer+65,toplayer)  = t1;
temp(botlayer+70,toplayer)  = t2;
save (MatPropsall, 'temp')

%% Saves .mat file with Average Data

l11=['E:\Dropbox\Classes\Year 5\JJJ Theses\Data\Sandwich beams\Second
Sets\Mechanical Properties\11.mat'];
save(l11,'MechProps_11')



%% Plots Figures
figure (1)
hold on
plot(FlexExten,FlexLoad)
xlabel('Flexure Extension (in)')
ylabel('Flexure Load (lbf)')
legend('Specimen 1','Specimen 2','Specimen 3','Specimen 4','Specimen
5','Specimen 6')

figure (2)
hold on
plot(FlexExten,sigmatop,'LineWidth',2)
plot(FlexExten,sigmabot)
xlabel('Flexure Extension (in)')
ylabel('Flexure Stress (ksi)')
legend('Specimen 1','Specimen 2','Specimen 3','Specimen 4','Specimen
5','Specimen 6')
```

A.8.9. Plots Experimental Graphs for Varying Face Sheet Thickness's

```
% Josh Lister
% Thesis - Sandwich composites
clear all
close all
clc


% Inputs
% Max deflection, Load Values

% Outputs
% Graphs

set(0,'DefaultFigureVisible','on');

%% Read in Data from Excel File

datafilename = ['E:\Dropbox\Classes\Year 5\JJJ Theses\Data\Sandwich
beams\Second Sets\TheSandwichDiaries.xls'];
 data = xlsread(datafilename); %Load the data file based on its number
top = 1:5;
bottom = 1:5;
weight = data(29:33,22:26)*6/8;

% Loads Mechanical Properties of specimens calculated in Datacode.m files
load 'E:\Dropbox\Classes\Year 5\JJJ Theses\Data\Sandwich beams\Second
Sets\Matprop.mat'


% Assigns Mechanical Properties to variables
Sigma1ult = temp(1:5,:);
Sigma2ult = temp(6:10,:);
Load = temp(11:15,:);
Exten = temp(16:20,:);
U = temp(21:25,:);
G = temp(26:30,:);
F = temp(31:35,:);
D = temp(36:40,:);
strtoweight = Load./weight;
Exten200 = temp(41:45,:);
Pstd = temp(46:50,:);
Exstd = temp(51:55,:);
Exten100std = temp(56:60,:);
Kstd = temp(61:65,:);

% Load Theoretical Deflections @ 100lbs
load 'TheodeflectoinVaryTs.mat'
load 'TheodeflectoinVaryTssame.mat'


%% Plots max deflection with respect to Layer numbering
```

```
% Max Load Plot
figure
surf(bottom*0.0114,top*0.0114,temp(11:15,:));
ylabel('Bottom facesheet thickness (in)')
xlabel('Top facesheet thickness (in)')
zlabel('Max Load (lbf)')

% Exten at 100lbf Plot
figure
surf(bottom*0.0114,top*0.0114,Exten200);
ylabel('Bottom facesheet thickness (in)')
xlabel('Top facesheet thickness (in)')
zlabel('Exten at 100lbf (lbf)')

% Max Extension Plot
figure
surf(bottom*0.0114,top*0.0114,temp(16:20,:));
ylabel('Bottom facesheet thickness (in)')
xlabel('Top facesheet thickness (in)')
zlabel('Max Extension (in)')

% % Top Layer Stress Plot
% figure
% surf(bottom*0.0114,top*0.0114,temp(1:5,:));
% ylabel('Bottom facesheet thickness (in)')
% xlabel('Top facesheet thickness (in)')
% zlabel('Top Layer Stress (ksi)')

% Bottom Layer Stress Plot
figure
surf(bottom*0.0114,top*0.0114,temp(6:10,:));
ylabel('Bottom facesheet thickness (in)')
xlabel('Top facesheet thickness (in)')
zlabel('Bottom Layer Stress (ksi)')



%% Top layer constant - Max Load
figure
hold on
plot(bottom*0.0114,Load(:,1),bottom*0.0114,Load(:,2),bottom*0.0114,Load(:,3),
bottom*0.0114,Load(:,4),bottom*0.0114,Load(:,5))
plot(bottom*0.0114,def(:,1),bottom*0.0114,def(:,2),bottom*0.0114,def(:,3),bot
tom*0.0114,def(:,4),def*0.0114,def(:,5))
xlabel('Bottom Layers (#)')
ylabel('Max Load (lbf)')
%legend('1','2','3','4','5')
 h = legend('1','2','3','4','5');
    v = get(h,'title');
    set(v,'string','Top Layer Count');

errorbar(bottom*0.0114,Load(:,1),Pstd(:,1),'b')
errorbar(bottom*0.0114,Load(:,2),Pstd(:,2),'green')
```

```
errorbar(bottom*0.0114,Load(:,3),Pstd(:,3),'red')
errorbar(bottom*0.0114,Load(:,4),Pstd(:,4),'cyan')
errorbar(bottom*0.0114,Load(:,5),Pstd(:,5),'magenta')
set(gca,'xtick',[0.0114 0.024 0.036 0.048 0.06])


%% Top layer constant - Max Extension
figure
plot(bottom,Exten(:,1),bottom,Exten(:,2),bottom,Exten(:,3),bottom,Exten(:,4),
bottom,Exten(:,5))
xlabel('Bottom Layers (#)')
ylabel('Max Exten (in)')
legend('1','2','3','4','5')
set(gca,'xtick',[1:5])


%% Bottom layer constant - Max Extension
figure
plot(bottom,Exten(1,:),bottom,Exten(2,:),bottom,Exten(3,:),bottom,Exten(4,:),
bottom,Exten(5,:))
xlabel('Top Layers (#)')
ylabel('Max Exten (in)')
legend('1','2','3','4','5')
set(gca,'xtick',[1:5])


%% Strength to Weight Ratio Plot
figure
surf(bottom*0.0114,top*0.0114,strtoweight);
xlabel('Top Layer (#)')
ylabel('Bottom Layers (#)')
zlabel('Strength to Weight Ratio (lbf)')

%% Stiffness at failure
figure
Stifffail = Load./Exten;
surf(bottom*0.0114,top*0.0114,Stifffail);
ylabel('Top Layer (#)')
xlabel('Bottom Layers (#)')
zlabel('Stiffness  ()')

%% normalised Stiffness at failure to Weight Ratio Plot
figure
Stifftoweightfail = Load./Exten./weight/42677.6085320418;
surf(bottom*0.0114,top*0.0114,Stifftoweightfail);
ylabel('Top Layer (#)')
xlabel('Bottom Layers (#)')
zlabel('Stiffness to Weight Ratio ()')

%% normalised Stiffness to Weight Ratio Plot @100lb
figure
Stifftoweight100 = 100./Exten200./weight/43053.0294559308;
surf(bottom*0.0114,top*0.0114,Stifftoweight100);
ylabel('Top Layer (#)')
xlabel('Bottom Layers (#)')
```

```
zlabel('Stiffness to Weight Ratio ()')

%% Normalised Stiffness to Weight Ratio Plot @ faliure
Stiff100 = Load./Exten./weight/56903.4780427224;
y2 = Stiff100(1,1);
y3 = [Stiff100(2,1) Stiff100(1,2) ];
y4 = [Stiff100(3,1) Stiff100(2,2) Stiff100(1,3) ];
y5 = [Stiff100(4,1) Stiff100(3,2) Stiff100(2,3) Stiff100(1,4) ];
y6 = [Stiff100(5,1) Stiff100(4,2) Stiff100(3,3) Stiff100(2,4) Stiff100(1,5)
];
y7 = [Stiff100(5,2) Stiff100(4,3) Stiff100(3,4) Stiff100(2,5) ];
y8 = [Stiff100(5,3) Stiff100(4,4) Stiff100(3,5) ];
y9 = [Stiff100(5,4) Stiff100(4,5) ];
y10 = [Stiff100(5,5)];

NMaxLoadtoweight = [y2 y3(2) y4(3) y5(4) y6(5);
                    y3(1) y4(2) y5(3) y6(4) y7(4);
                      y4(1) y5(2) y6(3) y7(2) y8(3);
                      y5(1) y6(2) y7(2) y8(2) y9(2);
                      y6(1) y7(1) y8(1) y9(1) y10];

figure
h1 =plot([2],y2,'bx');
hold on
h2 =plot([3 3],y3,'r');
h3 = plot([4 4 4],y4,'b');
h4 = plot([5 5 5 5],y5,'y');
h5 = plot([6 6 6 6 6],y6,'m');
h6 = plot([7 7 7 7 ],y7,'g');
h7 = plot([8 8 8],y8,'black');
h8 = plot([9 9],y9,'cyan');
h9 = plot([10 ],y10,'mx');
xlabel('Total layer count (#)')
ylabel('Normalized Stiffness at 100lbf/(Weight.Extension at 100lbf
(lbf/lbf.in)')
% h = legend([h1 h2 h3 h4 h5 h6 h7 h8
h9],'1','1.2','1.43','1.65','1.88','2.09','2.09','2.3','2.52','2.72');
%    v = get(h,'title');
%    set(v,'string','Normalised Weight');
 axis([1 11 1 1.4])
% axis([1 11 100 1200])

% Point text

text(2.1, y2(1), '1/1', 'Color', 'black');
text(3.1, y3(1), '1/2', 'Color', 'black');
text(3.1, y3(2), '2/1', 'Color', 'black');
text(4.1, y4(1), '1/3', 'Color', 'black');
text(4.1, y4(2), '2/2', 'Color', 'black');
text(4.1, y4(3), '3/1', 'Color', 'black');
text(5.1, y5(1), '1/4', 'Color', 'black');
text(5.1, y5(2), '2/3', 'Color', 'black');
text(5.1, y5(3), '3/2', 'Color', 'black');
text(5.1, y5(4), '4/1', 'Color', 'black');
text(6.1, y6(1), '1/5', 'Color', 'black');
text(6.1, y6(2), '2/4', 'Color', 'black');
```

```
text(6.1, y6(3), '3/3', 'Color', 'black');
text(6.1, y6(4), '4/2', 'Color', 'black');
text(6.1, y6(5), '5/1', 'Color', 'black');
text(7.1, y7(1), '2/5', 'Color', 'black');
text(7.1, y7(2), '3/4', 'Color', 'black');
text(7.1, y7(3), '4/3', 'Color', 'black');
text(7.1, y7(4), '5/2', 'Color', 'black');
text(8.1, y8(1), '3/5', 'Color', 'black');
text(8.1, y8(2), '4/4', 'Color', 'black');
text(8.1, y8(3), '5/3', 'Color', 'black');
text(9.1, y9(1), '4/5', 'Color', 'black');
text(9.1, y9(2), '5/4', 'Color', 'black');
text(10.1, y10(1), '5/5', 'Color', 'black');

%% Normalised Stiffness to Weight Ratio Plot @100lb
Stiff100 = 100./Exten200./weight/43053.0294559308;
y2 = Stiff100(1,1);
y3 = [Stiff100(2,1) Stiff100(1,2) ];
y4 = [Stiff100(3,1) Stiff100(2,2) Stiff100(1,3) ];
y5 = [Stiff100(4,1) Stiff100(3,2) Stiff100(2,3) Stiff100(1,4) ];
y6 = [Stiff100(5,1) Stiff100(4,2) Stiff100(3,3) Stiff100(2,4) Stiff100(1,5)
];
y7 = [Stiff100(5,2) Stiff100(4,3) Stiff100(3,4) Stiff100(2,5) ];
y8 = [Stiff100(5,3) Stiff100(4,4) Stiff100(3,5) ];
y9 = [Stiff100(5,4) Stiff100(4,5) ];
y10 = [Stiff100(5,5)];

NMaxLoadtoweight = [y2 y3(2) y4(3) y5(4) y6(5);
                    y3(1) y4(2) y5(3) y6(4) y7(4);
                      y4(1) y5(2) y6(3) y7(2) y8(3);
                      y5(1) y6(2) y7(2) y8(2) y9(2);
                      y6(1) y7(1) y8(1) y9(1) y10];

figure
h1 =plot([2],y2,'bx');
hold on
h2 =plot([3 3],y3,'r');
h3 = plot([4 4 4],y4,'b');
h4 = plot([5 5 5 5],y5,'y');
h5 = plot([6 6 6 6 6],y6,'m');
h6 = plot([7 7 7 7 ],y7,'g');
h7 = plot([8 8 8],y8,'black');
h8 = plot([9 9],y9,'cyan');
h9 = plot([10 ],y10,'mx');
xlabel('Total layer count (#)')
ylabel('Normalized Stiffness at 100lbf/(Weight.Extension at 100lbf
(lbf/lbf.in)')
% h = legend([h1 h2 h3 h4 h5 h6 h7 h8
h9],'1','1.2','1.43','1.65','1.88','2.09','2.09','2.3','2.52','2.72');
%    v = get(h,'title');
%    set(v,'string','Normalised Weight');
 axis([1 11 1 1.4])
% axis([1 11 100 1200])

% Point text
```

```
text(2.1, y2(1), '1/1', 'Color', 'black');
text(3.1, y3(1), '1/2', 'Color', 'black');
text(3.1, y3(2), '2/1', 'Color', 'black');
text(4.1, y4(1), '1/3', 'Color', 'black');
text(4.1, y4(2), '2/2', 'Color', 'black');
text(4.1, y4(3), '3/1', 'Color', 'black');
text(5.1, y5(1), '1/4', 'Color', 'black');
text(5.1, y5(2), '2/3', 'Color', 'black');
text(5.1, y5(3), '3/2', 'Color', 'black');
text(5.1, y5(4), '4/1', 'Color', 'black');
text(6.1, y6(1), '1/5', 'Color', 'black');
text(6.1, y6(2), '2/4', 'Color', 'black');
text(6.1, y6(3), '3/3', 'Color', 'black');
text(6.1, y6(4), '4/2', 'Color', 'black');
text(6.1, y6(5), '5/1', 'Color', 'black');
text(7.1, y7(1), '2/5', 'Color', 'black');
text(7.1, y7(2), '3/4', 'Color', 'black');
text(7.1, y7(3), '4/3', 'Color', 'black');
text(7.1, y7(4), '5/2', 'Color', 'black');
text(8.1, y8(1), '3/5', 'Color', 'black');
text(8.1, y8(2), '4/4', 'Color', 'black');
text(8.1, y8(3), '5/3', 'Color', 'black');
text(9.1, y9(1), '4/5', 'Color', 'black');
text(9.1, y9(2), '5/4', 'Color', 'black');
text(10.1, y10(1), '5/5', 'Color', 'black');

%% Normalised Max Load/Weight
layer2 = Load(1,1);
layer3 = [Load(2,1) Load(1,2) ];
layer4 = [Load(3,1) Load(2,2) Load(1,3) ];
layer5 = [Load(4,1) Load(3,2) Load(2,3) Load(1,4) ];
layer6 = [Load(5,1) Load(4,2) Load(3,3) Load(2,4) Load(1,5) ];
layer7 = [Load(5,2) Load(4,3) Load(3,4) Load(2,5) ];
layer8 = [Load(5,3) Load(4,4) Load(3,5) ];
layer9 = [Load(5,4) Load(4,5) ];
layer10 = [Load(5,5)];

weightavg2 = weight(1,1);
weightavg3 = [weight(2,1) weight(1,2) ];
weightavg4 = [weight(3,1) weight(2,2) weight(1,3) ];
weightavg5 = [weight(4,1) weight(3,2) weight(2,3) weight(1,4) ];
weightavg6 = [weight(5,1) weight(4,2) weight(3,3) weight(2,4) weight(1,5) ];
weightavg7 = [weight(5,2) weight(4,3) weight(3,4) weight(2,5) ];
weightavg8 = [weight(5,3) weight(4,4) weight(3,5) ];
weightavg9 = [weight(5,4) weight(4,5) ];
weightavg10 = weight(5,5);

Normalisedweight = [weightavg2 weightavg3 weightavg4 weightavg5 weightavg6
weightavg7 weightavg8 weightavg9  weightavg10]./weightavg2;

% Calculates Normalised (to weakest 1/5) Load at failure/weight

weak =layer6./weightavg6; %1/5 is weakest

y2 =layer2./weightavg2./weak(1);
y3 =layer3./weightavg3./weak(1);
```

```
y4 =layer4./weightavg4./weak(1);
y5 =layer5./weightavg5./weak(1);
y6 =layer6./weightavg6./weak(1);
y7 =layer7./weightavg7./weak(1);
y8 =layer8./weightavg8./weak(1);
y9 =layer9./weightavg9./weak(1);
y10 =layer10./weightavg10./weak(1);

NMaxLoadtoweight = [y2 y3(2) y4(3) y5(4) y6(5);
                    y3(1) y4(2) y5(3) y6(4) y7(4);
                      y4(1) y5(2) y6(3) y7(2) y8(3);
                      y5(1) y6(2) y7(2) y8(2) y9(2);
                      y6(1) y7(1) y8(1) y9(1) y10];

figure
h1 =plot([2],y2,'bx');
hold on
h2 =plot([3 3],y3,'r');
h3 = plot([4 4 4],y4,'b');
h4 = plot([5 5 5 5],y5,'y');
h5 = plot([6 6 6 6 6],y6,'m');
h6 = plot([7 7 7 7 ],y7,'g');
h7 = plot([8 8 8],y8,'black');
h8 = plot([9 9],y9,'cyan');
h9 = plot([10 ],y10,'mx');
xlabel('Total layer count (#)')
ylabel('Load at failure/Weight (lbf/lbf)')
% h = legend([h1 h2 h3 h4 h5 h6 h7 h8
h9],'1','1.2','1.43','1.65','1.88','2.09','2.09','2.3','2.52','2.72');
%    v = get(h,'title');
%    set(v,'string','Normalised Weight');
 axis([1 11 1 3])
% axis([1 11 100 1200])

% Point text

text(2.1, y2(1), '1/1', 'Color', 'black');
text(3.1, y3(1), '1/2', 'Color', 'black');
text(3.1, y3(2), '2/1', 'Color', 'black');
text(4.1, y4(1), '1/3', 'Color', 'black');
text(4.1, y4(2), '2/2', 'Color', 'black');
text(4.1, y4(3), '3/1', 'Color', 'black');
text(5.1, y5(1), '1/4', 'Color', 'black');
text(5.1, y5(2), '2/3', 'Color', 'black');
text(5.1, y5(3), '3/2', 'Color', 'black');
text(5.1, y5(4), '4/1', 'Color', 'black');
text(6.1, y6(1), '1/5', 'Color', 'black');
text(6.1, y6(2), '2/4', 'Color', 'black');
text(6.1, y6(3), '3/3', 'Color', 'black');
text(6.1, y6(4), '4/2', 'Color', 'black');
text(6.1, y6(5), '5/1', 'Color', 'black');
text(7.1, y7(1), '2/5', 'Color', 'black');
text(7.1, y7(2), '3/4', 'Color', 'black');
text(7.1, y7(3), '4/3', 'Color', 'black');
text(7.1, y7(4), '5/2', 'Color', 'black');
text(8.1, y8(1), '3/5', 'Color', 'black');
```

```
text(8.1, y8(2), '4/4', 'Color', 'black');
text(8.1, y8(3), '5/3', 'Color', 'black');
text(9.1, y9(1), '4/5', 'Color', 'black');
text(9.1, y9(2), '5/4', 'Color', 'black');
text(10.1, y10(1), '5/5', 'Color', 'black');

figure

surf(bottom*0.0114,top*0.0114,NMaxLoadtoweight);
xlabel('Top Layer (#)')
ylabel('Bottom Layers (#)')
zlabel('Normalised Failure Load/Weight Ratio (1/lbs)')

%% Constant Bottom Layer

figure
h1 =plot([2 3 4 5 6],Load(1,:),'cyan');
hold on
h2 =plot([3 4 5 6 7],Load(2,:),'r');
h3 = plot([4 5 6 7 8],Load(3,:),'b');
h4 = plot([5 6 7 8 9],Load(4,:),'y');
h5 = plot([6 7 8 9 10],Load(5,:),'black');
xlabel('Total layer count (#)')
ylabel('Max Load Range (lbf)')
h= legend([h1 h2 h3 h4 h5 ],'1','2','3','4','5');
   v = get(h,'title');
   set(v,'string','# Bottom Layers');
axis([1 11 250 1200])

% Point text

text(2.1, layer2(1), '1/1', 'Color', 'black');
text(3.1, layer3(1), '1/2', 'Color', 'black');
text(3.1, layer3(2), '2/1', 'Color', 'black');
text(4.1, layer4(1), '1/3', 'Color', 'black');
text(4.1, layer4(2), '2/2', 'Color', 'black');
text(4.1, layer4(3), '3/1', 'Color', 'black');
text(5.1, layer5(1), '1/4', 'Color', 'black');
text(5.1, layer5(2), '2/3', 'Color', 'black');
text(5.1, layer5(3), '3/2', 'Color', 'black');
text(5.1, layer5(4), '4/1', 'Color', 'black');
text(6.1, layer6(1), '1/5', 'Color', 'black');
text(6.1, layer6(2), '2/4', 'Color', 'black');
text(6.1, layer6(3), '3/3', 'Color', 'black');
text(6.1, layer6(4), '4/2', 'Color', 'black');
text(6.1, layer6(5), '5/1', 'Color', 'black');
text(7.1, layer7(1), '2/5', 'Color', 'black');
text(7.1, layer7(2), '3/4', 'Color', 'black');
text(7.1, layer7(3), '4/3', 'Color', 'black');
text(7.1, layer7(4), '5/2', 'Color', 'black');
text(8.1, layer8(1), '3/5', 'Color', 'black');
text(8.1, layer8(2), '4/4', 'Color', 'black');
text(8.1, layer8(3), '5/3', 'Color', 'black');
text(9.1, layer9(1), '4/5', 'Color', 'black');
text(9.1, layer9(2), '5/4', 'Color', 'black');
text(10.1, layer10(1), '5/5', 'Color', 'black');
```

```
%% Constant Top Layer

figure
h1 =plot([2 3 4 5 6],Load(:,1),'cyan');
hold on
h2 =plot([3 4 5 6 7],Load(:,2),'r');
h3 = plot([4 5 6 7 8],Load(:,3),'b');
h4 = plot([5 6 7 8 9],Load(:,4),'y');
h5 = plot([6 7 8 9 10],Load(:,5),'black');
xlabel('Total layer count (#)')
ylabel('Max Load Range (lbf)')
h = legend([h1 h2 h3 h4 h5 ],'1','2','3','4','5');
v = get(h,'title');
set(v,'string','# Top Layers');
axis([1 11 250 1200])
axis([1 11 250 1200])

% Point text

text(2, layer2(1)+20, '1/1', 'Color', 'black');
text(3, layer3(1)+20, '1/2', 'Color', 'black');
text(3, layer3(2)+20, '2/1', 'Color', 'black');
text(4, layer4(1)+20, '1/3', 'Color', 'black');
text(4, layer4(2)+20, '2/2', 'Color', 'black');
text(4, layer4(3)+20, '3/1', 'Color', 'black');
text(5, layer5(1)+20, '1/4', 'Color', 'black');
text(5, layer5(2)+20, '2/3', 'Color', 'black');
text(5, layer5(3)+20, '3/2', 'Color', 'black');
text(5, layer5(4)+20, '4/1', 'Color', 'black');
text(6, layer6(1)+20, '1/5', 'Color', 'black');
text(6, layer6(2)+20, '2/4', 'Color', 'black');
text(6, layer6(3)+20, '3/3', 'Color', 'black');
text(6, layer6(4)+20, '4/2', 'Color', 'black');
text(6, layer6(5)+20, '5/1', 'Color', 'black');
text(7, layer7(1)+20, '2/5', 'Color', 'black');
text(7, layer7(2)+20, '3/4', 'Color', 'black');
text(7, layer7(3)+20, '4/3', 'Color', 'black');
text(7, layer7(4)+20, '5/2', 'Color', 'black');
text(8, layer8(1)+20, '3/5', 'Color', 'black');
text(8, layer8(2)+20, '4/4', 'Color', 'black');
text(8, layer8(3)+20, '5/3', 'Color', 'black');
text(9, layer9(1)+20, '4/5', 'Color', 'black');
text(9, layer9(2)+20, '5/4', 'Color', 'black');
text(10, layer10(1)+20, '5/5', 'Color', 'black');

%% Max Load vs Weight


weightavg2 = weight(1,1);
weightavg3 = [weight(2,1) weight(1,2) ];
weightavg4 = [weight(3,1) weight(2,2) weight(1,3) ];
weightavg5 = [weight(4,1) weight(3,2) weight(2,3) weight(1,4) ];
```

```
weightavg6 = [weight(5,1) weight(4,2) weight(3,3) weight(2,4) weight(1,5) ];
weightavg7 = [weight(5,2) weight(4,3) weight(3,4) weight(2,5) ];
weightavg8 = [weight(5,3) weight(4,4) weight(3,5) ];
weightavg9 = [weight(5,4) weight(4,5) ];
weightavg10 = weight(5,5);

Normalisedweight = [weightavg2 weightavg3 weightavg4 weightavg5 weightavg6
weightavg7 weightavg8 weightavg9  weightavg10]./weightavg2;


figure
h1 =plot(weightavg2,layer2,'bx');
hold on
h2 =plot(weightavg3,layer3,'r');
h3 = plot(weightavg4,layer4,'b');
h4 = plot(weightavg5,layer5,'y');
h5 = plot(weightavg6,layer6,'m');
h6 = plot(weightavg7,layer7,'g');
h7 = plot(weightavg8,layer8,'black');
h8 = plot(weightavg9,layer9,'cyan');
h9 = plot(weightavg10,layer10,'mx');
xlabel('Weight of specimen (lbs)')
ylabel('Max Load Range (lbf)')
h = legend([h1 h2 h3 h4 h5 h6 h7 h8
h9],'2','3','4','5','6','7','8','9','10');
   v = get(h,'title');
   set(v,'string','Total # of Layers');
axis([0.06 0.2 0 12])


% Point text

text(weightavg2, layer2(1), '1/1', 'Color', 'black');
text(weightavg3(1), layer3(1), '1/2', 'Color', 'black');
text(weightavg3(2), layer3(2), '2/1', 'Color', 'black');
text(weightavg4(1), layer4(1), '1/3', 'Color', 'black');
text(weightavg4(2), layer4(2), '2/2', 'Color', 'black');
text(weightavg4(3), layer4(3), '3/1', 'Color', 'black');
text(weightavg5(1), layer5(1), '1/4', 'Color', 'black');
text(weightavg5(2), layer5(2), '2/3', 'Color', 'black');
text(weightavg5(3), layer5(3), '3/2', 'Color', 'black');
text(weightavg5(4), layer5(4), '4/1', 'Color', 'black');
text(weightavg6(1), layer6(1), '1/5', 'Color', 'black');
text(weightavg6(2), layer6(2), '2/4', 'Color', 'black');
text(weightavg6(3), layer6(3), '3/3', 'Color', 'black');
text(weightavg6(4), layer6(4), '4/2', 'Color', 'black');
text(weightavg6(5), layer6(5), '5/1', 'Color', 'black');
text(weightavg7(1), layer7(1), '2/5', 'Color', 'black');
text(weightavg7(2), layer7(2), '3/4', 'Color', 'black');
text(weightavg7(3), layer7(3), '4/3', 'Color', 'black');
text(weightavg7(4), layer7(4), '5/2', 'Color', 'black');
text(weightavg8(1), layer8(1), '3/5', 'Color', 'black');
text(weightavg8(2), layer8(2), '4/4', 'Color', 'black');
text(weightavg8(3), layer8(3), '5/3', 'Color', 'black');
text(weightavg9(1), layer9(1), '4/5', 'Color', 'black');
text(weightavg9(2), layer9(2), '5/4', 'Color', 'black');
```

```
text(weightavg10(1), layer10(1), '5/5', 'Color', 'black');



%% Maximum Extension of an Average american male (100lbs)

layer2 = Exten(1,1);
layer3 = [Exten(2,1) Exten(1,2) ];
layer4 = [Exten(3,1) Exten(2,2) Exten(1,3) ];
layer5 = [Exten(4,1) Exten(3,2) Exten(2,3) Exten(1,4) ];
layer6 = [Exten(5,1) Exten(4,2) Exten(3,3) Exten(2,4) Exten(1,5) ];
layer7 = [Exten(5,2) Exten(4,3) Exten(3,4) Exten(2,5) ];
layer8 = [Exten(5,3) Exten(4,4) Exten(3,5) ];
layer9 = [Exten(5,4) Exten(4,5) ];
layer10 = [Exten(5,5)];


figure
h1 =plot([2],layer2,'bx');
hold on
h2 =plot([3 3],layer3,'r');
h3 = plot([4 4 4],layer4,'b');
h4 = plot([5 5 5 5],layer5,'y');
h5 = plot([6 6 6 6 6],layer6,'m');
h6 = plot([7 7 7 7 ],layer7,'g');
h7 = plot([8 8 8],layer8,'black');
h8 = plot([9 9],layer9,'cyan');
h9 = plot([10 ],layer10,'mx');
xlabel('Total layer count (#)')
ylabel('Max Exten Range (lbf)')
h = legend([h1 h2 h3 h4 h5 h6 h7 h8
h9],'1','1.2','1.43','1.65','1.88','2.09','2.09','2.3','2.52','2.72');
   v = get(h,'title');
   set(v,'string','Normalised Weight');
axis([1 11 0.07 0.2])


% Point text

text(2.1, layer2(1), '1/1', 'Color', 'black');
text(3.1, layer3(1), '1/2', 'Color', 'black');
text(3.1, layer3(2), '2/1', 'Color', 'black');
text(4.1, layer4(1), '1/3', 'Color', 'black');
text(4.1, layer4(2), '2/2', 'Color', 'black');
text(4.1, layer4(3), '3/1', 'Color', 'black');
text(5.1, layer5(1), '1/4', 'Color', 'black');
text(5.1, layer5(2), '2/3', 'Color', 'black');
text(5.1, layer5(3), '3/2', 'Color', 'black');
text(5.1, layer5(4), '4/1', 'Color', 'black');
text(6.1, layer6(1), '1/5', 'Color', 'black');
text(6.1, layer6(2), '2/4', 'Color', 'black');
text(6.1, layer6(3), '3/3', 'Color', 'black');
text(6.1, layer6(4), '4/2', 'Color', 'black');
text(6.1, layer6(5), '5/1', 'Color', 'black');
text(7.1, layer7(1), '2/5', 'Color', 'black');
```

```
text(7.1, layer7(2), '3/4', 'Color', 'black');
text(7.1, layer7(3), '4/3', 'Color', 'black');
text(7.1, layer7(4), '5/2', 'Color', 'black');
text(8.1, layer8(1), '3/5', 'Color', 'black');
text(8.1, layer8(2), '4/4', 'Color', 'black');
text(8.1, layer8(3), '5/3', 'Color', 'black');
text(9.1, layer9(1), '4/5', 'Color', 'black');
text(9.1, layer9(2), '5/4', 'Color', 'black');
text(10.1, layer10(1), '5/5', 'Color', 'black');



%% Extension to face thickness ratio.
top = [ 1 2 3 4 5]';
bottom = [1;2;3;4;5]';
ratio = (top*(1./bottom));

figure
h1 = plot(ratio(1,:),Exten(1,:),'blue');
hold on
h2 = plot(ratio(2,:),Exten(2,:),'red');
h3 = plot(ratio(3,:),Exten(3,:),'cyan');
h4 = plot(ratio(4,:),Exten(4,:),'black');
h5 = plot(ratio(5,:),Exten(5,:),'green');
xlabel('hb/ht')
ylabel('Max Extension (in)')
h= legend([h1 h2 h3 h4 h5 ],'1','2','3','4','5');
   v = get(h,'title');
   set(v,'string','# Bottom Layers');
axis([0 6 0.12 0.25])
hold off
```

A.8.10. Comparison of FEA, Theoretical and Experimental Deflections at 100lbf

```
%% Theoretical Vs Experimental vs FEA
% bottom thickness of 0.0114in (1 layer)

figure
hold on
plot(bottom*0.0114,Exten200(1,:))
plot(bottom*0.0114,def_beam3(1,:),'r')
plot(bottom*0.0114,def_plate3(1,:),'black')
plot(bottom*0.0114,FEA3(1,:),'green')
xlabel('Top facing thickness (in)')
ylabel('Extension at 100lbf (in)')
title('1 Bottom Layers')
 h = legend('Experimental','Theoretical (Beam)','Theoretical (Plate)','FEA');
errorbar(bottom*0.0114,Exten200(1,:),Exten100std(1,:),'b')

%% Theoretical Vs Experimental vs FEA
% bottom thickness of 0.024in (2 layer)

% Error between Theoretical and FEA
```

```
ErrorFT = (def_plate3-FEA3)./def_plate3*100;   % Percentage Error
ErrorET = (def_plate3-Exten200)./def*100; % Percentage error Exp-TH
ErrorEF = (FEA3-Exten200)./FEA3*100; % percentage error Exp-FEA


figure
hold on
plot(bottom*0.0114,Exten200(2,:))
plot(bottom*0.0114,def_beam3(2,:),'r')
plot(bottom*0.0114,def_plate3(2,:),'black')
plot(bottom*0.0114,FEA3(2,:),'green')
xlabel('Top facing thickness (in)')
ylabel('Extension at 100lbf (in)')
title('2 Bottom Layers')
 h = legend('Experimental','Theoretical (Beam)','Theoretical (Plate)','FEA');
errorbar(bottom*0.0114,Exten200(2,:),Exten100std(2,:),'b')
%% Theoretical Vs Experimental vs FEA
% bottom thickness of 0.036in (3 layer)

figure
hold on
plot(bottom*0.0114,Exten200(3,:))
plot(bottom*0.0114,def_beam3(3,:),'r')
plot(bottom*0.0114,def_plate3(3,:),'black')
plot(bottom*0.0114,FEA3(3,:),'green')
xlabel('Top facing thickness (in)')
ylabel('Extension at 100lbf (in)')
title('3 Bottom Layers')
 h = legend('Experimental','Theoretical (Beam)','Theoretical (Plate)','FEA');
errorbar(bottom*0.0114,Exten200(3,:),Exten100std(3,:),'b')
%% Theoretical Vs Experimental vs FEA
% bottom thickness of 0.048in (4 layer)

figure
hold on
plot(bottom*0.0114,Exten200(4,:))
plot(bottom*0.0114,def_beam3(4,:),'r')
plot(bottom*0.0114,def_plate3(4,:),'black')
xlabel('Top facing thickness (in)')
ylabel('Extension at 100lbf (in)')
plot(bottom*0.0114,FEA3(4,:),'green')
title('4 Bottom Layers')
 h = legend('Experimental','Theoretical (Beam)','Theoretical (Plate)','FEA');
errorbar(bottom*0.0114,Exten200(4,:),Exten100std(4,:),'b')
%% Theoretical Vs Experimental vs FEA
% bottom thickness of 0.060in (5 layer)

figure
hold on
plot(bottom*0.0114,Exten200(5,:))
plot(bottom*0.0114,def_beam3(5,:),'r')
plot(bottom*0.0114,def_plate3(5,:),'black')
plot(bottom*0.0114,FEA3(5,:),'green')
xlabel('Top facing thickness (in)')
ylabel('Extension at 100lbf (in)')
```

```
title('5 Bottom Layers')
 h = legend('Experimental','Theoretical_(beam)','Theoretical_(Plate)','FEA');
errorbar(bottom*0.0114,Exten200(5,:),Exten100std(5,:),'b')
```

A.8.11. Minimum and Maximum Core weight for Optimum Strength with respect to minimum weight

```
%% Minimum and Maximum Core weight for Optimum Strength with respect to
minimum weight
clear all
close all
clc


syms w W rhoc rhof Ef b Ec tft
%w = 0.375*0.00289351852/W;
tfb = 01;%(1-w)*W/(2*rhof)-tft;% 0.012;
tft = (1-w)*W/(2*rhof)-tfb;
c = w*W/rhoc;
d = c+ (tft+tfb)/2;
Gl = 10.4427*1000;     %Core shear modulus-Ribbon direction
Ec = Gl.*(2.*(1+0.8036));
D = Ef*((tft+tfb)*((d+(tft+tfb)/2)/2)^2)%Ef*t*b*d^2/2
Ef*b*(tft+tfb)/2*d^2/2;
diff = diff(D,w)
solve = collect(solve(diff,w))
%W = rhoc*d +2*t*rhof;
minmax = vpa(subs(solve,[rhoc,rhof  Ec Ef w W],[0.00289351852 0.057
0.375*0.00289351852/W 0.00289351852*0.375+ 0.057*tft+0.057*0.012
12.936e6]),3)
%W = (rhoc*0.375+ tft*rhof+tfb
coretoWratio = rhoc*c/(rhoc*c+rhof*tft+rhof*tfb)


%% Variables
mu = 0.027; %Poissins Ratio of CF-face material
vc = mu;
P = 100;  %Applied Load (lbs)
l = 6;    %Beam span (in)
b = 3;    %Beam width (in)
nu_l = 0.8036; %Poissons of Honeycomb in Transverse
vh = nu_l;
nu_t = 0.4113; %Poissons of Honeycomb in Longitudinal
c = 0.375;
rhoc = 0.00289351852; %lbs/in^3
rhof = 0.057; %lbs/in^3

tft =linspace(.1,5,500)*0.0114;
tfb =linspace(.1,5,500)*0.0114;

tc = 0.375;       %thickness of core (in)

Gl = 10.4427*1000;     %Core shear modulus-Ribbon direction
Gh= Gl;
Gw = 5.8015*1000;      %Core shear modulus-Transverse direction
```

```
h= zeros(length(tft),length(tft));
for i = 1:length(tft)
    for j = 1:length(tft)
Gc = Gw;          %Core shear modulus-in direction of applied load
%h = tft/2 +tfb/2 + tc ;      %Distance between facing skin centres
h(i,j) = tft(j)+tfb(i)+tc;

%% Composites analytical approach

%CORE STUFF

E_cf_Tens = [12.936e6 ];
Ec = E_cf_Tens;
%Modulus of elasticity of facing skin (psi)
theta = 0;
r = 1;
x = 0;
 %Finding E for CORE
EL = Gl.*(2.*(1+nu_l));
Eh =EL;
ET = Gw.*(2.*(1+nu_t));
L = EL;%*(cosd(theta(j))).^2+ET.*(sind(theta(j)))^.2;
T = ET ;%.*(cosd(theta(j))).^2+EL.*-(sind(theta(j)))^.2;


Q11 = L./(1-(nu_l.*nu_t));
Q12 = (nu_l.*T)./(1-(nu_l.*nu_t));
Q22 = T./(1-(nu_l.*nu_t));
Q66 = L./(2.*(1+nu_l));

c4=(cosd(theta(r))).^4;
c3=(cosd(theta(r))).^3;
c2=(cosd(theta(r))).^2;

s4=(sind(theta(r))).^4;
s3=(sind(theta(r))).^3;
s2=(sind(theta(r))).^2;

Q11new=Q11.*c4+2*(Q12+2*Q66)*s2*c2+Q22*s4;

Lnew(1) = Q11new.*(1-(nu_l.*nu_t));

Q22new=Q11.*s4+2*(Q12+2*Q66)*s2*c2+Q22*c4;

Tnew(1) = Q22new.*(1-(nu_l.*nu_t));

Q12new=(Q11+Q22-4*Q66)*s2*c2+Q12*(s4+c4);
Q66new=(Q11+Q22-2*Q12-2*Q66)*s2*c2+Q66*(s4+c4);
Q16new=(Q11-Q12-2*Q66)*c3*sind(theta(1))-(Q22-Q12-2*Q66)*cosd(theta(1)).*s3;
Q26new=(Q11-Q12-2*Q66)*s3*cosd(theta(1))-(Q22-Q12-2*Q66)*sind(theta(1)).*c3;

Q_core = [Q11new Q12new Q16new;Q12new Q22new Q26new;Q16new Q26new Q66new];
```

```
% Thicknesses of core and fiber
h0(i,j) = -(h(i,j)/2); %Distance from middle axis to top of top layer
h1(i,j) = -(h(i,j)-tft(j)-h(i,j)/2); %Distance from middle axis to top of
core
h2(i,j) = h(i,j)/2-tfb(i); %Symmetric distance from middle axis to bottom of
core
h3(i,j) = h(i,j)/2; %Distance from middle axis to bottom of bottom layer

%Carbon Fiber [Q]
E_cf_Comp = 12.936e6;
CF_Q11_Comp = E_cf_Comp/(1-(mu)^2);
CF_Q12_Comp = (mu*E_cf_Comp)/(1-(mu^2));
CF_Q22_Comp = E_cf_Comp/(1-(mu)^2);
CF_Q66_Comp = E_cf_Comp/(2*(1+mu));


CF_Q_Comp = [CF_Q11_Comp CF_Q12_Comp 0;CF_Q12_Comp CF_Q22_Comp 0;0 0
CF_Q66_Comp];

CF_Q11_Tens = E_cf_Comp/(1-(mu)^2);
CF_Q12_Tens = (mu*E_cf_Comp)/(1-(mu^2));
CF_Q22_Tens = E_cf_Comp/(1-(mu)^2);
CF_Q66_Tens = E_cf_Comp/(2*(1+mu));


CF_Q_Tens = [CF_Q11_Tens CF_Q12_Tens 0;CF_Q12_Tens CF_Q22_Tens 0;0 0
CF_Q66_Tens];

%[A] matrix
A(i,j) = ((CF_Q_Comp(1,1))*(h1(i,j)-h0(i,j))) + (Q_core(1,1)*(h2(i,j)-
h1(i,j))) + ((CF_Q_Tens(1,1))*(h3(i,j)-h2(i,j)));

%[D] matrix
D(i,j) = (3/3).*(((CF_Q_Tens(1,1)).*(h1(i,j).^3-h0(i,j).^3)) +
(Q_core(1,1)*(h2(i,j).^3-h1(i,j)^3)) + ((CF_Q_Tens(1,1))*(h3(i,j)^3-
h2(i,j)^3)));

% Shear Rigidity
U(i,j) = Gl.*(h(i,j)+c).^2*b./(4*c);

% Midspan Deflection
ds1(i,j) = P*l^3./(48*D(i,j)); % Deflection due to facings
ds2(i,j) = P*l./(4*U(i,j));                % Deflection due to shear
def_beam3(i,j) = ds1(i,j)+ds2(i,j);

W(i,j) = (rhoc*c+rhof*tft(j)+rhof*tfb(i))*b*l;

    end
end

% Core to weight ratio
CtoW = rhoc*c*b*l./W;
[ValueC,IndC]=find(CtoW(:)==0.6623)
[MC,NC]=ind2sub(size(CtoW),IndC)
```

```
figure
surf(tfb,tft,CtoW)


% Rigidity
rigidity2 = P./def_beam3;
[Value,Ind]=max(rigidity2(:));
[M,N]=ind2sub(size(rigidity2),Ind);

figure
surf(tfb,tft,rigidity2./W/35483.723831087)
xlabel('Bottom Face Sheet Thickness (in)')
ylabel('Top Face Sheet Thickness (in)')
zlabel('Normalized Stiffness/Weight (lbf/lbs.in)')
axis([0 0.0114*5 0 0.0114*5 0 4])

rigval=rigidity2./W/35483.723831087;
[Value,Ind]=max(rigval(:));
[M,N]=ind2sub(size(rigval),Ind)
tfb(M)
tft(N)


normrigidity2 = rigidity2/60904.7047057812;
rigidity = 1./((l^3./48*D)+(l./4*U))./W;
normrigidity = rigidity./8.55131721958186e-06;

% Plots the Norm Rigidigty
figure
surf(tfb,tft,normrigidity)
xlabel('Bottom Face Sheet Thickness (in)')
ylabel('Top Face Sheet Thickness (in)')
zlabel('Stiffness/Weight (lbf/lbs.in)')
axis([0 0.0114 0 0.0114 0 200])
%diff = diff(rigidity,D)




%%
%% Plate Theory Theoretical Approach

Ec = 12.936e6;        % Youngs moduli of 6376 A280h carbon fibre
vc = 0.027;          % Youngs moduli of 6376 A280h carbon fibre
Gc = Ec/(2*(1+vc)); % Core Shear of Aluminium 1018
vh = 0.8036;
Gh = 10.2e3;
Eh = Gh.*(2.*(1+vh));
c = 0.375;
P = 100;
b = 3;
L = 6;
count= 500;
blah = linspace(.1,5,count)*0.0114;
clear tfb tft
```

```
for i = 1:count
tfb(i,:) = blah';
tft(i,:) = blah;


end
tft = linspace(.1,5,count)*0.0114;
tfb = linspace(.1,5,count)*0.0114;


for i =1:length(tfb)
    for j = 1:length(tfb)
        d(i,j) = tfb(i)+tft(j)+c;     % Sandwich height
Aft(i,j) = b.*tft(j);      % area of top facing
Afb(i,j) = b.*tfb(i);       % area of bottom facing
Ac = b*c;       % area of core
Cf1(i,j) = tfb(i)./2;     % centroid of bottom facing
Cf2(i,j) = tfb(i)+c+tft(j)./2;% centroid of top facing
Cc(i,j) = tfb(i)+c/2;    % centroid of core

% Centroid of Complete Steel Bar
C(i,j) =
(Afb(i,j).*Cf1(i,j)+Aft(i,j).*Cf2(i,j)+Ac.*Cc(i,j))./(Aft(i,j)+Afb(i,j)+Ac);

% Moment of Inertia
I1(i,j) = (1/(12*(1-vc^2)))*b.*tfb(i).^3;     % moment of inertia of bottom
facing
I2(i,j) = (1/(12*(1-vh^2)))*b*c^3;      % moment of inertia of core
I3(i,j) = (1/(12*(1-vc^2)))*b.*tft(j).^3;     % moment of inertia of top
facing

If1(i,j) = (I1(i,j)+ Afb(i,j).*(tfb(i)./2-C(i,j)).^2);          % Inertia of
bottom facing
Ic(i,j) =(I2(i,j)+ Ac*((tfb(i)+c/2)-C(i,j)).^2) ;       % Inertia of core
If2(i,j) = (I3(i,j)+ Aft(i,j).*(((tft(j)./2)+c+tfb(i))-C(i,j)).^2);   %
Inertia of top facing

EI(i,j) = Ec.*If1(i,j)+Eh.*Ic(i,j)+Ec.*If2(i,j);

% Shear Rigidity
U(i,j) = Gh.*(d(i,j)+c).^2*b./(4*c);
Un(i,j) = (Gc.*Aft(i,j)+Gh.*Ac+Gc.*Afb(i,j))*b;

% Midspan Deflection
ds1(i,j) = P*L^3./(48*EI(i,j)); % Deflection due to facings
ds2(i,j) = P*L./(4*U(i,j));                % Deflection due to shear
ds2n(i,j) =P*L./(4*Un(i,j));
def_plate3(i,j) = ds1(i,j)+ds2(i,j);
def_plate3n(i,j) = ds1(i,j)+ds2n(i,j);

    end
end
```

```
RigidityEI = P./def_plate3./W;
[Value,Ind]=min(RigidityEI(:))
[Mmin,Nmin]=ind2sub(size(RigidityEI),Ind)
[Value,Ind]=max(RigidityEI(:))
[Mmin,Nmin]=ind2sub(size(RigidityEI),Ind)
tfb(Mmin)
tft(Nmin)


figure
surf(tfb,tft,RigidityEI./40458.2582782153)
xlabel('Bottom Face Sheet Thickness (in)')
ylabel('Top Face Sheet Thickness (in)')
zlabel('Normalized Stiffness/Weight (lbf/lbs.in)')
axis([0 0.0114*5 0 0.0114*5 0 3])
```

A.8.12. Theoretical Beam and Plate Theory values for varying facing thickness

```
%% Theoretical Beam and Plate Theory values for varying facing thickness
% Josh Lister
% runs through theoretical mid span deflections
% for all facing thicknes's


clear all
close all
clc

load 'E:\Dropbox\Classes\Year 5\JJJ Theses\Data\Sandwich beams\Second
Sets\Matprop.mat'
%Constants
P = 100;            % Load (lbf)
Ec = 12.936e6;        % Youngs moduli of 6376 A280h carbon fibre
vc = 0.027;          % Youngs moduli of 6376 A280h carbon fibre
Gc = Ec/(2*(1+vc)); % Core Shear of Aluminium 1018
vh = 0.8036;
Gh = 10.2e3;
Eh = Gh.*(2.*(1+vh));
% Beam Dimension
c = 0.375;          % Core Height
tft =[1 2 3 4 5;1 2 3 4 5;1 2 3 4 5;1 2 3 4 5;1 2 3 4 5]*0.0114;
%temp(66:70,:);         % Facesheet height
tfb = [1 1 1 1 1;2 2 2 2 2 ;3 3 3 3 3;4 4 4 4 4;5 5 5 5 5]*0.0114;
%temp(71:75,:);
 tft = temp(66:70,:);
 tfb = temp(71:75,:);
b = 3;            % sandwich width
L = 6;              % Sandwich Length

% 5/2 says 0.2809-e2
```

```
%% Theoretical Complete Steel Beam
for i =1:5
    for j = 1:5
        d(i,j) = tfb(i,j)+tft(i,j)+c;     % Sandwich height
Aft(i,j) = b.*tft(i,j);      % area of top facing
Afb(i,j) = b.*tfb(i,j);       % area of bottom facing
Ac = b*c;       % area of core
Cf1(i,j) = tfb(i,j)./2;     % centroid of bottom facing
Cf2(i,j) = tfb(i,j)+c+tft(i,j)./2;% centroid of top facing
Cc(i,j) = tfb(i,j)+c/2;    % centroid of core

% Centroid of Complete Steel Bar
C(i,j) =
(Afb(i,j).*Cf1(i,j)+Aft(i,j).*Cf2(i,j)+Ac.*Cc(i,j))./(Aft(i,j)+Afb(i,j)+Ac);

% Moment of Inertia
I1(i,j) = (1/12)*b.*tfb(i,j).^3;     % moment of inertia of bottom facing
I2(i,j) = (1/12)*b*c^3;      % moment of inertia of core
I3(i,j) = (1/12)*b.*tft(i,j).^3;     % moment of inertia of top facing

If1(i,j) = (I1(i,j)+ Afb(i,j).*(tfb(i,j)./2-C(i,j)).^2);          % Inertia
of bottom facing
Ic(i,j) =(I2(i,j)+ Ac*((tfb(i,j)+c/2)-C(i,j)).^2) ;       % Inertia of core
If2(i,j) = (I3(i,j)+ Aft(i,j).*(((tft(i,j)./2)+c+tfb(i,j))-C(i,j)).^2);   %
Inertia of top facing

EI(i,j) = Ec.*If1(i,j)+Eh.*Ic(i,j)+Ec.*If2(i,j);

% Shear Rigidity
U(i,j) = Gh.*(d(i,j)+c).^2*b./(4*c);

% Midspan Deflection
ds1(i,j) = P*L^3./(48*EI(i,j)); % Deflection due to facings
ds2(i,j) = P*L./(4*U(i,j));                % Deflection due to shear
def_beam3(i,j) = ds1(i,j)+ds2(i,j);

    end
end

%% Plate Theory Theoretical



for i =1:5
    for j = 1:5
        d(i,j) = tfb(i,j)+tft(i,j)+c;     % Sandwich height
Aft(i,j) = b.*tft(i,j);      % area of top facing
Afb(i,j) = b.*tfb(i,j);       % area of bottom facing
Ac = b*c;       % area of core
Cf1(i,j) = tfb(i,j)./2;     % centroid of bottom facing
Cf2(i,j) = tfb(i,j)+c+tft(i,j)./2;% centroid of top facing
Cc(i,j) = tfb(i,j)+c/2;    % centroid of core

% Centroid of Complete Steel Bar
```

```
C(i,j) =
(Afb(i,j).*Cf1(i,j)+Aft(i,j).*Cf2(i,j)+Ac.*Cc(i,j)).(Aft(i,j)+Afb(i,j)+Ac);

% Moment of Inertia
I1(i,j) = (1/(12*(1-vc^2)))*b.*tfb(i,j).^3;     % moment of inertia of bottom
facing
I2(i,j) = (1/(12*(1-vh^2)))*b*c^3;      % moment of inertia of core
I3(i,j) = (1/(12*(1-vc^2)))*b.*tft(i,j).^3;     % moment of inertia of top
facing

If1(i,j) = (I1(i,j)+ Afb(i,j).*(tfb(i,j)./2-C(i,j)).^2);          % Inertia
of bottom facing
Ic(i,j) =(I2(i,j)+ Ac*((tfb(i,j)+c/2)-C(i,j)).^2) ;       % Inertia of core
If2(i,j) = (I3(i,j)+ Aft(i,j).*(((tft(i,j)./2)+c+tfb(i,j))-C(i,j)).^2);   %
Inertia of top facing

EI(i,j) = Ec.*If1(i,j)+Eh.*Ic(i,j)+Ec.*If2(i,j);

% Shear Rigidity
U(i,j) = Gh.*(d(i,j)+c).^2*b./(4*c);
Un(i,j) = (Gc.*Aft(i,j)+Gh.*Ac+Gc.*Afb(i,j))*b

% Midspan Deflection
ds1(i,j) = P*L^3./(48*EI(i,j)); % Deflection due to facings
ds2(i,j) = P*L./(4*U(i,j));                % Deflection due to shear
ds2n(i,j) =P*L./(4*Un(i,j));
def_plate3(i,j) = ds1(i,j)+ds2(i,j);
def_plate3n(i,j) = ds1(i,j)+ds2n(i,j);

    end
end


ern = (def_plate3-def_plate3n)./def_plate3*100;
```

A.8.13. Polyfit Plots for Experimental, FEA Data

```
% Josh Lister
% Thesis
% Poly fits Experimental and FEA
%
% Functions Requires
% polyfitn.m

datafilename = ['E:\Dropbox\Classes\Year 5\JJJ Theses\Data\Sandwich
beams\Second Sets\TheSandwichDiaries.xls'];
 data = xlsread(datafilename); %Load the data file based on its number
% Load = data(1:18,14);
% Exten = data(1:18,15);
% Top = data(1:18,1);
% Bottom = data(1:18,2);
%weight = data(1:18,15);
top = 1:5;
bottom = 1:5;
```

```
% Load1 = data(11:15,22:26);
% Exten1 = data(20:24,22:26);
weight = data(29:33,22:26)*6/8;
% strtoweight = Load1./weight1;


% Loads Mechanical Properties of specimens calculated in Datacode.m files
load 'E:\Dropbox\Classes\Year 5\JJJ Theses\Data\Sandwich beams\Second
Sets\Matprop.mat'
datafilename = ['E:\Dropbox\Classes\Year 5\JJJ Theses\Data\Sandwich
beams\Second Sets\TheSandwichDiaries.xls'];
data = xlsread(datafilename); %Load the data file based on its number
weight = data(29:33,22:26)*6/8;

% Assigns Mechanical Properties to variables

Exten200 = temp(41:45,:);
Pstd = temp(46:50,:);
Exstd = temp(51:55,:);
Exten100std = temp(56:60,:);
Kstd = temp(61:65,:);


%% Poly Fit Experimental

Exppolydef =
[Exten200(:,1);Exten200(:,2);Exten200(:,3);Exten200(:,4);Exten200(:,5)];
Exppolydef(1) = 0.0242;
weightpoly =
[weight(:,1);weight(:,2);weight(:,3);weight(:,4);weight(:,5)]*6/8;
ExpStifftoweight = 100./Exppolydef./weightpoly/76538.7190327658;
tft =[1; 2; 3; 4; 5;1; 2; 3; 4; 5;1; 2; 3; 4; 5;1; 2; 3; 4; 5;1 ;2 ;3 ;4;
5]*0.012;
tfb = [1; 1 ;1; 1; 1;2; 2 ;2 ;2 ;2 ;3; 3; 3; 3; 3;4; 4 ;4 ;4 ;4;5 ;5 ;5; 5;
5]*0.012;

% some 3d points
data =[tfb tft ExpStifftoweight];

% best-fit plane
C = [data(:,1) data(:,2) ones(size(data,1),1)] \ data(:,3);    % coefficients

% evaluate it on a regular grid covering the domain of the data
[xx,yy] = meshgrid(.0114:.005:5*0.012, 0.0114:.005:5*0.012);
zz = C(1)*xx + C(2)*yy + C(3);

% or expressed using matrix/vector product
%zz = reshape([xx(:) yy(:) ones(numel(xx),1)] * C, size(xx));

% best-fit quadratic curve
C = [ones(25,1) data(:,1:2) prod(data(:,1:2),2) data(:,1:2).^2] \ data(:,3);
zz = [ones(numel(xx),1) xx(:) yy(:) xx(:).*yy(:) xx(:).^2 yy(:).^2] * C;
zz = reshape(zz, size(xx));
```

```
C = x2fx(data(:,1:2), 'quadratic') \ data(:,3);
zz = x2fx([xx(:) yy(:)], 'quadratic') * C;
zz = reshape(zz, size(xx));

model = polyfitn(data(:,1:2), data(:,3), 2);
zz = polyvaln(model, [xx(:) yy(:)]);
zz = reshape(zz, size(xx));

% plot points and surface
figure('Renderer','opengl')
line(data(:,1), data(:,2), data(:,3), 'LineStyle','none', ...
    'Marker','.', 'MarkerSize',25, 'Color','r')
surface(xx, yy, zz, ...
    'FaceColor','interp', 'EdgeColor','b', 'FaceAlpha',0.2)
grid on;

view(9,9);
xlabel ('Bottom Face Sheet Thickness (in)');
ylabel ('Top Face Sheet Thickness (in)');
zlabel ('Normalised stiffness by weight at 100 lbf');
colormap(cool(64))

hold on

zzexp = zz;
%% Polyfit FEA data
tft =[1; 2; 3; 4; 5;1; 2; 3; 4; 5;1; 2; 3; 4; 5;1; 2; 3; 4; 5;1 ;2 ;3 ;4;
5]*0.012;
tfb = [1; 1 ;1; 1; 1;2; 2 ;2 ;2 ;2 ;3; 3; 3; 3; 3;4; 4 ;4 ;4 ;4;5 ;5 ;5; 5;
5]*0.012;

rhof = 0.057;
rhoc = 0.00289351852;
c = 0.375;
b = 3;
l = 6;
weightFEA = (tft.*rhof+tfb.*rhof+c*rhoc).*b*l;

FEApoly = [FEA3(:,1);FEA3(:,2);FEA3(:,3);FEA3(:,4);FEA3(:,5)];
FEApolystiff=100./FEApoly./weightFEA/60513.3050559903;

% some 3d points
data =[tfb tft FEApolystiff];

% best-fit plane
C = [data(:,1) data(:,2) ones(size(data,1),1)] \ data(:,3);    % coefficients

% evaluate it on a regular grid covering the domain of the data
[xx,yy] = meshgrid(.012:.005:5*0.012, 0.012:.005:5*0.012);
zz = C(1)*xx + C(2)*yy + C(3);

% or expressed using matrix/vector product
%zz = reshape([xx(:) yy(:) ones(numel(xx),1)] * C, size(xx));
```

```
% best-fit quadratic curve
C = [ones(25,1) data(:,1:2) prod(data(:,1:2),2) data(:,1:2).^2] \ data(:,3);
zz = [ones(numel(xx),1) xx(:) yy(:) xx(:).*yy(:) xx(:).^2 yy(:).^2] * C;
zz = reshape(zz, size(xx));

C = x2fx(data(:,1:2), 'quadratic') \ data(:,3);
zz = x2fx([xx(:) yy(:)], 'quadratic') * C;
zz = reshape(zz, size(xx));

model = polyfitn(data(:,1:2), data(:,3), 2);
zz = polyvaln(model, [xx(:) yy(:)]);
zz = reshape(zz, size(xx));

% plot points and surface
%figure('Renderer','opengl')
line(data(:,1), data(:,2), data(:,3), 'LineStyle','none', ...
    'Marker','.', 'MarkerSize',25, 'Color','r')
surface(xx, yy, zz, ...
    'FaceColor','interp', 'EdgeColor','b', 'FaceAlpha',0.2)
grid on;

view(9,9);
xlabel ('Bottom Face Sheet Thickness (in)');
ylabel ('Top Face Sheet Thickness (in)');
zlabel ('Normalised stiffness by weight) at 100 lbf');
colormap(cool(64))

zzfea = zz;

% Error between FEA and Experimental
error = (zzfea-zzexp)./zzfea*100;
sum(error,10);

norm(error)/10
```

A.8.14. 3D Polyfit function for Data Points

```
function polymodel = polyfitn(indepvar,depvar,modelterms)
% polyfitn: fits a general polynomial regression model in n dimensions
% usage: polymodel = polyfitn(indepvar,depvar,modelterms)
%
% Polyfitn fits a polynomial regression model of one or more
% independent variables, of the general form:
%
%   z = f(x,y,...) + error
%
% arguments: (input)
%  indepvar - (n x p) array of independent variables as columns
%        n is the number of data points
%        p is the dimension of the independent variable space
%
%        IF n == 1, then I will assume there is only a
```

```
%       single independent variable.
%
%  depvar   - (n x 1 or 1 x n) vector - dependent variable
%       length(depvar) must be n.
%
%       Only 1 dependent variable is allowed, since I also
%       return statistics on the model.
%
%  modelterms - defines the terms used in the model itself
%
%       IF modelterms is a scalar integer, then it designates
%          the overall order of the model. All possible terms
%          up to that order will be employed. Thus, if order
%          is 2 and p == 2 (i.e., there are two variables) then
%          the terms selected will be:
%
%             {constant, x, x^2, y, x*y, y^2}
%
%          Beware the consequences of high order polynomial
%          models.
%
%       IF modelterms is a (k x p) numeric array, then each
%          row of this array designates the exponents of one
%          term in the model. Thus to designate a model with
%          the above list of terms, we would define modelterms as
%
%          modelterms = [0 0;1 0;2 0;0 1;1 1;0 2]
%
%       If modelterms is a character string, then it will be
%          parsed as a list of terms in the regression model.
%          The terms will be assume to be separated by a comma
%          or by blanks. The variable names used must be legal
%          matlab variable names. Exponents in the model may
%          may be any real number, positive or negative.
%
%          For example, 'constant, x, y, x*y, x^2, x*y*y'
%          will be parsed as a model specification as if you
%          had supplied:
%          modelterms = [0 0;1 0;0 1;1 1;2 0;1 2]
%
%          The word 'constant' is a keyword, and will denote a
%          constant terms in the model. Variable names will be
%          sorted in alphabetical order as defined by sort.
%          This order will assign them to columns of the
%          independent array. Note that 'xy' will be parsed as
%          a single variable name, not as the product of x and y.
%
%       If modelterms is a cell array, then it will be taken
%          to be a list of character terms. Similarly,
%
%          {'constant', 'x', 'y', 'x*y', 'x^2', 'x*y^-1'}
%
%          will be parsed as a model specification as if you
%          had supplied:
%
%          modelterms = [0 0;1 0;0 1;1 1;2 0;1 -1]
%
```

```
% Arguments: (output)
%  polymodel - A structure containing the regression model
%        polymodel.ModelTerms = list of terms in the model
%        polymodel.Coefficients = regression coefficients
%        polymodel.ParameterVar = variances of model coefficients
%        polymodel.ParameterStd = standard deviation of model coefficients
%        polymodel.R2 = R^2 for the regression model
%        polymodel.AdjustedR2 = Adjusted R^2 for the regression model
%        polymodel.RMSE = Root mean squared error
%        polymodel.VarNames = Cell array of variable names
%           as parsed from a char based model specification.
%
%        Note 1: Because the terms in a general polynomial
%        model can be arbitrarily chosen by the user, I must
%        package the erms and coefficients together into a
%        structure. This also forces use of a special evaluation
%        tool: polyvaln.
%
%        Note 2: A polymodel can be evaluated for any set
%        of values with the function polyvaln. However, if
%        you wish to manipulate the result symbolically using
%        my own sympoly tools, this structure can be converted
%        to a sympoly using the function polyn2sympoly.
%
%        Note 3: When no constant term is included in the model,
%        the traditional R^2 can be negative. This case is
%        identified, and then a more appropriate computation
%        for R^2 is then used.
%
%        Note 4: Adjusted R^2 accounts for changing degrees of
%        freedom in the model. It CAN be negative, and will always
%        be less than the traditional R^2 values.
%
% Find sympoly toolbox here:
%
http://www.mathworks.com/matlabcentral/fileexchange/loadFile.do?objectId=9577
&objectType=FILE
%
% See also: polyvaln, polyfit, polyval, polyn2sympoly, sympoly
%
% Author: John D'Errico
% Release: 2.0
% Release date: 2/19/06

if nargin<1
  help polyfitn
  return
end

% get sizes, test for consistency
[n,p] = size(indepvar);
if n == 1
  indepvar = indepvar';
  [n,p] = size(indepvar);
end
[m,q] = size(depvar);
```

```
if m == 1
  depvar = depvar';
  [m,q] = size(depvar);
end
% only 1 dependent variable allowed at a time
if q~=1
  error 'Only 1 dependent variable allowed at a time.'
end

if n~=m
  error 'indepvar and depvar are of inconsistent sizes.'
end

% Automatically scale the independent variables to unit variance
stdind = sqrt(diag(cov(indepvar)));
if any(stdind==0)
  warning 'Constant terms in the model must be entered using modelterms'
  stdind(stdind==0) = 1;
end
% scaled variables
indepvar_s = indepvar*diag(1./stdind);

% do we need to parse a supplied model?
if iscell(modelterms) || ischar(modelterms)
  [modelterms,varlist] = parsemodel(modelterms,p);
  if size(modelterms,2) < p
    modelterms = [modelterms, zeros(size(modelterms,1),p -
size(modelterms,2))];
  end
elseif length(modelterms) == 1
  % do we need to generate a set of modelterms?
  [modelterms,varlist] = buildcompletemodel(modelterms,p);
elseif size(modelterms,2) ~= p
  error 'ModelTerms must be a scalar or have the same # of columns as
indepvar'
end
nt = size(modelterms,1);

% check for replicate terms
if nt>1
  mtu = unique(modelterms,'rows');
  if size(mtu,1)<nt
    warning 'Replicate terms identified in the model.'
  end
end

% build the design matrix
M = ones(n,nt);
scalefact = ones(1,nt);
for i = 1:nt
  for j = 1:p
    M(:,i) = M(:,i).*indepvar_s(:,j).^modelterms(i,j);
    scalefact(i) = scalefact(i)/(stdind(j)^modelterms(i,j));
  end
end
```

```
% estimate the model using QR. do it this way to provide a
% covariance matrix when all done. Use a pivoted QR for
% maximum stability.
[Q,R,E] = qr(M,0);

polymodel.ModelTerms = modelterms;
polymodel.Coefficients(E) = R\(Q'*depvar);
yhat = M*polymodel.Coefficients(:);

% recover the scaling
polymodel.Coefficients=polymodel.Coefficients.*scalefact;

% variance of the regression parameters
s = norm(depvar - yhat);
if n > nt
  Rinv = R\eye(nt);
  Var(E) = s^2*sum(Rinv.^2,2)/(n-nt);
  polymodel.ParameterVar = Var.*(scalefact.^2);
  polymodel.ParameterStd = sqrt(polymodel.ParameterVar);
else
  % we cannot form variance or standard error estimates
  % unless there are at least as many data points as
  % parameters to estimate.
  polymodel.ParameterVar = inf(1,nt);
  polymodel.ParameterStd = inf(1,nt);
end

% R^2
% is there a constant term in the model? If not, then
% we cannot use the standard R^2 computation, as it
% frequently yields negative values for R^2.
if any((M(1,:) ~= 0) & all(diff(M,1,1) == 0,1))
  % we have a constant term in the model, so the
  % traditional %R^2 form is acceptable.
  polymodel.R2 = max(0,1 - (s/norm(depvar-mean(depvar)) )^2);
  % compute adjusted R^2, taking into account the number of
  % degrees of freedom
  polymodel.AdjustedR2 = 1 - (1 - polymodel.R2).*((n - 1)./(n - nt));
else
  % no constant term was found in the model
  polymodel.R2 = max(0,1 - (s/norm(depvar))^2);
  % compute adjusted R^2, taking into account the number of
  % degrees of freedom
  polymodel.AdjustedR2 = 1 - (1 - polymodel.R2).*(n./(n - nt));
end

% RMSE
polymodel.RMSE = sqrt(mean((depvar - yhat).^2));

% if a character 'model' was supplied, return the list
% of variables as parsed out
polymodel.VarNames = varlist;

% ====================================================
% ============== begin subfunctions ==============
```

```
% ================================================
function [modelterms,varlist] = buildcompletemodel(order,p)
%
% arguments: (input)
%  order - scalar integer, defines the total (maximum) order
%
%  p     - scalar integer - defines the dimension of the
%          independent variable space
%
% arguments: (output)
%  modelterms - exponent array for the model
%
%  varlist - cell array of character variable names

% build the exponent array recursively
if p == 0
  % terminal case
  modelterms = [];
elseif (order == 0)
  % terminal case
  modelterms = zeros(1,p);
elseif (p==1)
  % terminal case
  modelterms = (order:-1:0)';
else
  % general recursive case
  modelterms = zeros(0,p);
  for k = order:-1:0
    t = buildcompletemodel(order-k,p-1);
    nt = size(t,1);
    modelterms = [modelterms;[repmat(k,nt,1),t]];
  end
end

% create a list of variable names for the variables on the fly
varlist = cell(1,p);
for i = 1:p
  varlist{i} = ['X',num2str(i)];
end



% ================================================
function [modelterms,varlist] = parsemodel(model,p);
%
% arguments: (input)
%  model - character string or cell array of strings
%
%  p     - number of independent variables in the model
%
% arguments: (output)
%  modelterms - exponent array for the model

modelterms = zeros(0,p);
if ischar(model)
  model = deblank(model);
end
```

```
varlist = {};
while ~isempty(model)
  if iscellstr(model)
    term = model{1};
    model(1) = [];
  else
    [term,model] = strtok(model,' ,');
  end

  % We've stripped off a model term. Now parse it.

  % Is it the reserved keyword 'constant'?
  if strcmpi(term,'constant')
    modelterms(end+1,:) = 0;
  else
    % pick this term apart
    expon = zeros(1,p);
    while ~isempty(term)
      vn = strtok(term,'*/^. ,');
      k = find(strncmp(vn,varlist,length(vn)));
      if isempty(k)
        % its a variable name we have not yet seen

        % is it a legal name?
        nv = length(varlist);
        if ismember(vn(1),'1234567890_')
          error(['Variable is not a valid name: ''',vn,''''])
        elseif nv>=p
          error 'More variables in the model than columns of indepvar'
        end

        varlist{nv+1} = vn;

        k = nv+1;
      end
      % variable must now be in the list of vars.

      % drop that variable from term
      i = strfind(term,vn);
      term = term((i+length(vn)):end);

      % is there an exponent?
      eflag = false;
      if strncmp('^',term,1)
        term(1) = [];
        eflag = true;
      elseif strncmp('.^',term,2)
        term(1:2) = [];
        eflag = true;
      end

      % If there was one, get it
      ev = 1;
      if eflag
```

```
        ev = sscanf(term,'%f');
        if isempty(ev)
            error 'Problem with an exponent in parsing the model'
        end
      end
      expon(k) = expon(k) + ev;

      % next monomial subterm?
      k1 = strfind(term,'*');
      if isempty(k1)
        term = '';
      else
        term(k1(1)) = ' ';
      end

    end

    modelterms(end+1,:) = expon;

  end

end

% Once we have compiled the list of variables and
% exponents, we need to sort them in alphabetical order
[varlist,tags] = sort(varlist);
modelterms = modelterms(:,tags);
```

A.8.15. Theoretical Maximum Bending Strength With Respect to Minimum Weight

```
%%% Theoretical Flexural Strength

clear all
close all
clc


Ef=12.936e6; % face Young's modulus (Longitudinal) [psi]
Ec_L=3.679e4; % core Young's modulus (Longitudinal) [psi]
% Ef_W=12.7e6; % face Young's modulus (Transverse) [psi]
Ec_W=1.5242e4; % core Young's modulus (Transverse) [psi]
tf=linspace(0.012,0.06);%[0 1 2 3 4 5]*0.012; % face thickness [in]
tb = linspace(0.012,0.06);
tc=0.375; % core thicknessm [in]
P=301/1.5; % Central load per unit width [lbf/in]
L=6; % span [uin]
Xf=127e3; % Face Compressive Strength
Sc_L=325; % Core Longitudinal Shear Yield Strength (175 for transverse)
Sc_W= 175; % "  "
Xc=700; % Core Compressive Streng100
b = 3;
```

```
% Ef=Ef_L.*(cosd(theta(i))).^2+Ef_W.*(sind(theta(i))).^2;
Ec=Ec_L;
Sc=Sc_L;
Gc = Ec/(2*(1+0.8113));
for i=1:length(linspace(0.012,0.06))
    for j = 1:length(linspace(0.012,0.06))
d=(tf(i)+tb(j))/2+tc;% distance between the centroids of the faces

Df=Ef.*((tf(i)+tb(j))/2).^3./12; % Bending stiffness of faces about their
individual neutral axis
Dc=Ec.*tc.^3./12; % Bending Stiffness of core
Do=Ef.*tf(i).*d.^2./2; % Bending stiffness of faces about the middle axis
D=Df+Dc+Do; % Flexural Rigidity

%%% Deflection and Moment
k=Ec./tc;
beta=(k./(4.*Df)).^(1/4);


%%% Maximum Loads per unit width for each failur modes

Pmax_f_compressive_failure=Xf./((L./(4.*tf(i).*d))+(6./(4.*(tf(i).^2).*beta))
); % Face compressive failure load
Pmax_c_shear_yield=2.*Sc.*d; % core shear yield load
Pmax_c_compressive_yield=2.*Xc./beta; % core compressive yield load
Pmax_f_Microbuckling = 4*tf(i).*d*(Xf)./L;  % Microbuckling face yield
Pmax_Indentation = tf(i).*((pi^2*Ef*d*Xc^2)/(3*L))^(1/3); % indentation with
face buckling (plastic)

Load(j,i) = min([Pmax_f_compressive_failure Pmax_c_shear_yield
Pmax_c_compressive_yield Pmax_f_Microbuckling Pmax_Indentation]);
end
end

i=linspace(0.012,0.06);
   j = linspace(0.012,0.06);
figure
surf(j,i,Load)
xlabel('Top Face Sheet Thickness (in)')
ylabel('Bottom Face Sheet Thickness (in)')
zlabel('Predicted Failure/Yield Load (lbf)')
hold on
text(0.04, 0.04,300,'Core Shear Yield','Color','white')
text(0.02, 0.025,250,'Core Compression Yield','Color','white')
text(0.00, 0.04,150,'Face Compressive Failure','Color','white')


%% Bending Stiffness with minimum weight
m = ones*i;
for w = 1:length(i)
    for q = 1:length(i)
weight1(w,q) = m(w)+m(q);
    end
end
weight = (weight1*0.057+0.375*0.00289)*6;
```

```
LtoW = Load./weight;
figure
surf(j,i,Load./weight./min(LtoW(:)))
xlabel('Top Face Sheet Thickness (in)')
ylabel('Bottom Face Sheet Thickness (in)')
zlabel('Normalised Strength/Weight (lbf)')
hold on
text(0.04, 0.04,6,'Core Shear Yield','Color','white')
text(0.02, 0.025,7,'Core Compression Yield','Color','white')
text(0.00, 0.04,4,'Face Compressive Failure','Color','white')



[ValueC,IndC]= max(LtoW(:));
[MC,NC]=ind2sub(size(Load./weight),IndC)
```